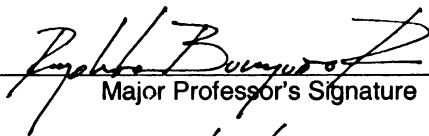This is to certify that the
thesis entitled

EXPERIMENTAL EVALUATION AND FIELD MONITORING
OF SELF-CONSOLIDATING CONCRETE PRESTRESSED
BOX BEAMS IMPLEMENTED IN A DEMONSTRATION
BRIDGE

presented by

David A. Bendert

has been accepted towards fulfillment
of the requirements for the

_____M.S._____ degree in _____Civil Engineering_____

_____
Major Professor's Signature

_____05/07/2007_____
Date

PLACE IN RETURN BOX to remove this checkout from your record.
TO AVOID FINES return on or before date due.
MAY BE RECALLED with earlier due date if requested.

DATE DUE	DATE DUE	DATE DUE

6/07 p:/CIRC/DateDue.indd-p.1

EXPERIMENTAL EVALUATION AND FIELD MONITORING OF SELF-
CONSOLIDATING CONCRETE PRESTRESSED BOX BEAMS
IMPLEMENTED IN A DEMONSTRATION BRIDGE

By

David A. Bendert

A THESIS

Submitted to
Michigan State University
In partial fulfillment of the requirements
For the degree of

MASTER OF SCIENCE

Department of Civil and Environmental Engineering

2007

ABSTRACT

EXPERIMENTAL EVALUATION AND FIELD MONITORING OF SELF-CONSOLIDATING PRESTRESSED BOX BEAMS USED IN A DEMONSTRATION BRIDGE

By

David A. Bendert

Self Consolidating Concrete (SCC) is a tailorable concrete with superior fresh properties that can lead to reduced production times and costs in precast/prestressed element production. Concerns from Departments of Transportation about the use of SCC in highway bridges have prevented these potential benefits from being fully realized in the production of precast/prestressed bridge beams. A demonstration bridge utilizing SCC was built to allow the Michigan Department of Transportation (MDOT) to evaluate the use of SCC in bridge beams including the beam production process and short and long term performance of SCC beams. Experimental evaluations were used to find the flexural and shear capacities of the SCC beams, while long-term evaluations included continuous strain and temperature monitoring of the beams in the demonstration bridge. Reduced production times of 60% and reduced labor requirements of nearly 50% were realized during the production of the bridge beams. The flexural and shear capacities of the SCC beams were very similar to the capacities of the NCC beams with all beams surpassing design requirements. Similar trends have been realized in the continuous strain readings of the demonstration bridge. While monitoring of the demonstration bridge continues, the results of the evaluation have shown that SCC can by successfully utilized in precast prestressed bridge beams for highway bridges.

This thesis is dedicated to my wife, Allison.
For her unending dedication, unbridled love,
and willingness to stand by me as I pursued my dream.

ACKNOWLEDGEMENTS

TABLE OF CONTENTS

LISTS OF TABLES

LIST OF FIGURES

1 PROJECT OVERVIEW AND INTRODUCTION

1.1 Summary

Self-consolidating concrete (SCC) is a recent development in the concrete industry that offers many benefits to both producers and consumers of concrete structures, including government Departments of Transportation. The benefits of SCC are almost entirely related to its fresh properties. Its ability to flow through dense steel reinforcing schemes and fill intricate formwork without the aid of vibration make SCC a popular alternative to normally consolidated concrete (NCC). Properly proportioned SCC can consolidate under its own weight while remaining homogenous through all phases of the construction process. When SCC is used effectively, the end result is a high quality product that performs as well as its NCC counterpart. However, the mix design modifications that are required to produce the benefits of SCC have led to questions about the hardened performance of the finished products. Because of this, the Michigan Department of Transportation (MDOT) was interested in assessing the feasibility of using SCC in highway bridges. The research project reported in this thesis was developed to investigate the complete construction process using SCC, including the development of representative SCC mix designs, evaluation of the bond of the prestressing strand with SCC, evaluation of the production process, and finally the production and construction of a demonstration bridge using beams cast with SCC.

The M-50/US-127 bridge over the Grand River in Summit Township south of Jackson Michigan was selected as the right candidate for its replacement with a demonstration bridge utilizing SCC in the bridge beams. The demonstration bridge,

shown in Figure 1, consists of six simply supported 27 in. x 36 in. spread box beams with

a span of 50 ft. A schematic of the bridge is shown in Figure 2.
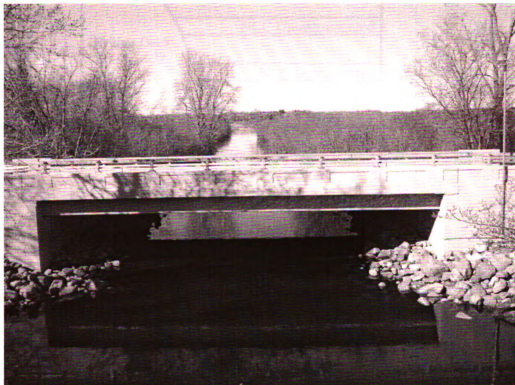
Figure 1. M 50/US 127 Demonstration Bridge using SCC Beams

```
|◄————— Effective Span = 50' ——————►|
┌────────────────────────────────────────┐  ┌─
│        \                                │  ┬
│         \        NCC Uninstrumented     │  │
│          \┌─────────────────────────┐   │  │
│           \        NCC Uninstrumented   │  │
│ Bridge Deck \┌────────────────────┐   │  │
│ Width = 49'  \      NCC Instrumented    │  │  5 @ 8'-½"
│               \┌──────────────────┐    │  │
│                \    SCC 1 Instrumented  │  │
│                 /┌─────────────────┐   │  │
│                /    SCC 2 Instrumented  │  │
│               /┌──────────────────┐    │  │
│              /     SCC 3 Instrumented   │  ┴
│             /────────────────────────   │  └─
└────────────────────────────────────────┘
|◄————— Beam Length =  52' ——————►|
```
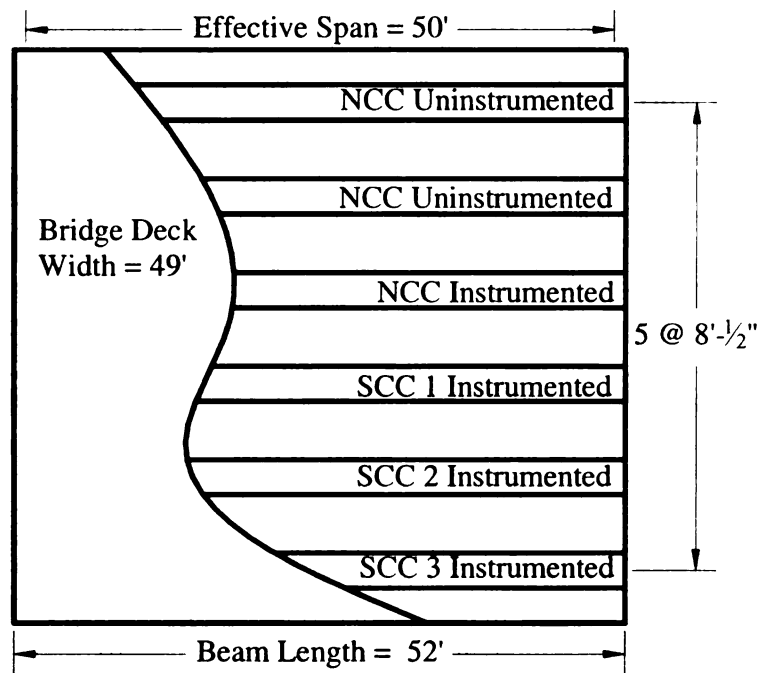
Figure 2. Schematic of Demonstration Bridge

Three SCC mix designs, which attempt to bound current SCC mix design practice, were developed for this project. A fourth mix design, an NCC mix, was used as an experimental control. Three identical box beams were cast from each of the four mix designs. Of the three beams from each mix design, one was instrumented for long term monitoring of strain and temperature and was placed in the demonstration bridge. The remaining two beams from each mix design were instrumented for experimental evaluation. The experimental evaluation of the full-scale prestressed beams was done at Michigan State University's (MSU) Civil Infrastructure Laboratory prior to the construction of the demonstration bridge. Two four-point bending tests were conducted for these evaluations. The two tests evaluated the flexural and shear performance of the beams. An additional five NCC beams were cast without any instrumentation. Two of these beams were used in the construction of the demonstration bridge. The remaining three NCC beams were cast to replace the SCC beams in the event that their laboratory

3

performance was inadequate. A total of 17 beams, 8 NCC and 9 SCC, were cast for this project at the Fabricator's precast plant in Michigan in the months of June and July of 2005.

1.2 Research Objectives

There were three objectives to this research project. Each objective was designed to help MDOT determine the feasibility of using SCC in highway bridges. The objectives were:

- To evaluate the short term performance of SCC beams,

- To evaluate the long term performance of SCC beams, and

- To evaluate the production process and quality control for the manufacturing of SCC beams.

The short-term evaluation of SCC beams through full-scale tests of replica bridge beams was done to ensure that the capacity demands in the bridge system were safely met by these members. Both the shear and flexural capacities were experimentally determined through structural testing to evaluate the short-term performance of the SCC beams with respect to the baseline NCC beams. The long-term evaluation of SCC beams includes monitoring strain and temperature from the demonstration bridge. The collected data is providing important information about any prestressing force losses in the beams that could be attributed to different creep and shrinkage behavior of SCC. Finally the production process evaluation included assessment of the mix design development, and quality monitoring of the concrete production and finished beams. Also included in this

research effort was an evaluation of the production process of SCC prestressed beams to define any necessary changes in order to better use SCC.

1.3 Scope and Organization

This thesis presents the research work related to the implementation of SCC in bridge beams of a demonstration bridge for MDOT through a Federal Highway Administration (FHWA) Innovative Bridge Research Construction (IBRC) project. The thesis is divided into 7 chapters. Chapter 2 presents research on SCC technology including the historical development of SCC, the effect of various materials on the fresh properties of SCC, current status and recent developments using SCC, the use of SCC in precast facilities, and finally outstanding issues regarding the use of SCC. Chapter 3 presents the methods used to produce the mix designs for this project. This chapter includes information on fresh property evaluations and results from three separate mix development processes. Chapter 4 looks at the production and quality control of prestressed box beams using SCC and provides a discussion on production changes that were necessary to effectively used SCC in the beam production. The experimental component to the research, consisting of flexural and shear evaluations of SCC and NCC beams is presented in Chapter 5. Chapter 6 presents the field-monitoring program and representative results for the long-term evaluation of the SCC box beams in the demonstration bridge. Finally, Chapter 7 presents the conclusions reached from this research project.

2 SELF-COMPACTING CONCRETE TECHNOLOGY

2.1 Historical Overview

SCC was developed in Japan in the early 1980's by Okamura and his colleagues in response to the decline in the skilled labor force in Japan [14]. The inability to find adequate labor was leading to durability problems in concrete structures caused by either over or under consolidation. In developing SCC, Okamura wanted to create a durable concrete that was easy to place and finish independent of the quality of the labor [9] [38]. If successful, Okamura believed SCC would produce products of consistently superior quality than NCC.

Like all new products, SCC was slow in gaining popularity. SCC was first successfully produced in 1988 and the first presentation on SCC was at the 2nd East Asia and Pacific Conference on Structural Engineering and Construction in 1989 [14][23]. However, the first large-scale commercial use of SCC did not occur until 1998. In that year SCC was used in the anchorages for the Akashi-Kaikyo Bridge in Japan [37]. In this project, SCC was pumped 600 ft from the on site batching plant to the casting area. The reduction of the construction period from an estimated 2.5 years with NCC to 2 years with SCC showed the significant time savings that could be achieved when SCC was used [14][37]. By the year 2000, 10,800,000 ft^3 of SCC was being used annually in Japan. This volume of concrete was split nearly equally between ready mix applications and precast production [40].

As knowledge of SCC became more available, its use began spreading from Japan through Asia and into Europe. Countries such as Korea, Thailand, Sweden, the Netherlands, and Canada began to research and use SCC in the mid 1990's [14].

According to Daczko and Vachon [14], the spread of SCC in Europe did not develop because of concerns about the quality of conventional concrete, but instead was spurred mainly by the economic benefits of SCC recognized by large construction and precast companies. As the use of SCC became more popular in the mid 1990's, several European-wide research projects and committees were formed to help the development process. One such committee, specifically for the study of SCC, was formed by the International Union of Laboratories and Experts in Construction Materials, Systems, and Structures (RILEM from the French name) [18][40]. One project that developed from these groups was a bridge in Sweden cast completely of SCC. This project differed from the use of SCC in the bridge in Japan in that the entire bridge was made using SCC. The use of SCC in this project resulted in a cost savings and a reduction in pollution during the bridge construction [18][40]. According to Goodier [18] nearly all of Europe was using or studying SCC by 2003. As the use of SCC became more prevalent in Europe many countries began adopting guidelines for the use of SCC. By the year 2003 guidelines, or a draft of guidelines, were in place in Austria, Finland, France, Germany, Italy, Netherlands, Norway, Sweden, and for Europe in general [18].

SCC has developed slower in the United States than in Europe. Beginning around the year 2000, US precast/prestressed product producers as well as admixture companies began to push for the ability to use SCC in their projects. According to Daczko and Vachon [14], and Ouchi et. al. [40] the spread of SCC in the US was motivated by economic interests similar to those seen in Europe. Research on SCC in the US grew quickly as was evidenced by the first North American Conference on Self-Consolidating Concrete, held at Northwestern University in 2002 [18]. Goodier [18] reports in his

survey of the growth of SCC that estimated volumes of 108,000-135,000 ft^3 per day of SCC were being used at precast plants in North America in 2003. Because of the rapid growth of SCC in the US, a FAST team was created by PCI (Precast/Prestressed Concrete Institute) with the intention of developing a guideline for the use of SCC. Interim Guidelines for the Use of SCC in Precast/Prestressed Construction was published by PCI in 2003 [23].

2.2 Theoretical Considerations

SCC is unique because of its fresh, or plastic, behavior. The ability to fill formwork and consolidate under its own weight, without external energy, not only defines SCC, but governs the proportioning of SCC mix designs as well. Concrete in general can be tailored to achieve performance standards. When developing a traditional NCC mix design, most of the focus is placed on tailoring the mix design to satisfy the hardened property requirements. Factors such as the water to cement ratio (*w/c*), coarse aggregate content (*CAC*), sand to past ratio (*s/pt*), and admixtures (mineral and chemical) use are adjusted to control the strength, stiffness or the durability of the finished product. In the case of SCC, these same factors are varied to *additionally* control the fluidity and segregation resistance of the fresh concrete. However, tailoring SCC mix designs to achieve specified hardened properties, while still necessary, is no longer the primary driving force of an SCC mix design selection.

The widely known benefits of SCC come from the fresh property performance of the concrete. The fresh properties are governed by three factors: filling ability, passing ability, and segregation. The filling ability of SCC is its ability to fully fill formwork without the use of vibration. This includes flowing around obstacles including dense

8

reinforcing steel schemes and form block outs. The passing ability of SCC is its ability to flow around and through obstacles without segregating or experiencing aggregate blocking. The segregation resistance of SCC is defined as the ability to resist segregation of its coarse aggregate components through all phases of the construction process including transportation from the batching plant to casting site, placement in the formwork, and finishing of the product [23].

The successful development of these three factors can lead to an increase in productivity and product quality while reducing the cost of production. The high workability of SCC and the fact that vibration is unnecessary leads to a reduction in labor required to produce concrete elements as well as a reduction in the time of production. The self-consolidating nature of SCC can lead to a higher quality finished product than can be achieved with NCC. While SCC generally has higher material costs, these costs are more than compensated for by reductions in labor and increased productivity that result from using SCC [18][23].

The benefits of SCC do not always come easily or immediately. Like with all new products, there is a learning curve for using SCC [36]. One of the challenges associated with proportioning SCC is that there are many different ways to achieve the desired fresh property performance. Compounding this problem is the difference in behavior that SCC shows depending on the materials used. SCC is said to be extremely sensitive to small changes in mix design components and quantities [18][36]. When different methods are used to develop SCC in research, different results often ensue. Domone [16] reports that research has shown that caution is required when comparing data from individual mix designs. The practice of reporting results of one SCC mix

9

design for SCC in general can be misleading, as the data presented in these projects only accurately represent the specific mix design studied. The results may not be extrapolated to all SCC mixes in general. To obtain general information on SCC, multiple mix designs representing multiple proportioning methods need to be analyzed.

Currently there is no commonly accepted procedure to proportion SCC mix designs [9]. However, according to Khayat [26], the balance that is achieved in creating SCC is always the same. This balance involves satisfying two opposing parameters.

On one side of this balance is the need to make concrete fluid enough to flow easily around obstacles without becoming obstructed [26]. This high level of fluidity must be maintained for the duration of the manufacturing process, including placement and finishing of the concrete. The amount of fluidity required depends on the specific project being completed. If intricate formwork with a dense reinforcing steel scheme is used, the fluidity must be relatively high, but if the reinforcing steel is not densely arranged a lower fluidity can be used.

While maintaining the desired level of fluidity, a quality SCC must also resist segregation [26]. In order to be effective and useful in practice, the fluid SCC mixture must remain stable through all phases of the construction process, including transporting and placing of the concrete. If allowed to segregate, aggregate will settle through the fluid concrete mixture and collect at the bottom. This non-uniform distribution can lead to production problems during casting of members, and quality problems with the cured member.

There is a tradeoff between the fluidity and segregation resistance of the fresh concrete [26][39]. In general, as the fluidity of concrete is increased, cohesion and the

10

related ability to resist segregation is decreased. At some point both the requirements for fluidity and segregation resistance can be met. This tradeoff is further illustrated in Figure 3. Consistently achieving this balance adds to the difficulty of producing high quality SCC.

Fluidity/Deformability

A. Increase paste deformability
  * use of HRWR
  * balanced w/c ratio

B. Reduce inter-particle friction
  * low coarse aggregate volume
  * use cont. graded powder

Easy Flow/Low Blockage

A. Enhance cohesiveness
  * low w/c ratio
  * use of VMA

B. Compatible flow space and
   aggregate size
  * low coarse aggregate volume
  * low max. size aggregate

Fluidity/Stability Trade-off

Low Viscosity, High Fluidity

Deformability

High Viscosity, Low Fluidity

Viscosity

Homogeneity/Stability

A. Reduce solids separation
  * limit aggregate content
  * reduce max. size aggregate
  * increase cohesion & viscosity
    - low w/c ratio
    - use of VMA

B. Minimize bleeding
  * low w/c ratio
  * use of high-area powder
  * increase VMA

Figure 3.   Fluidity, Stability Tradeoff in SCC Mix Designs

There are many ways to increase the fluidity of the concrete. Perhaps the easiest way is to add water to the mix [26]. The end result of this process though, is a concrete with a high *w/c* ratio and low cohesiveness. Furthermore, a concrete with a high *w/c* ratio is often less durable and weaker, which can lead to early deterioration of the concrete structure.

A second way to increase the fluidity of the concrete is to remove a portion of the coarse aggregate from the mix. With fewer large particles, less energy is required to deform the fluid concrete mixture as it flows around obstacles without blocking.

However, fewer coarse aggregates also means the ability of the hardened concrete to resist crack propagation is limited. As coarse aggregate is generally much stronger than the cement paste, a crack will develop at the interface between the cement paste and the aggregate. The random arrangement of the coarse aggregate through the cement paste creates a tortuous path for a crack to propagate through a concrete element. If fewer aggregates are present in the concrete, the crack will require less energy to propagate, as it will have fewer obstacles to avoid.

The segregation resistance of the concrete can be achieved through an increase of the s/pt ratio. Having more fine aggregate in the concrete mixture raises the viscosity of the fluid portion of the mixture. This increased viscosity will result in better suspension of the coarse aggregate. However, a mix using a poor aggregate gradation can lead to problems with the water demand and workability of the concrete. A mix with a high fine aggregate content is also more likely to experience drying shrinkage [36].

It can be seen that every change made to a concrete mix design to produce a desired result may lead to negative consequences as well. To properly proportion a concrete mix, the effect of altering all of the parameters must be considered together. SCC generally cannot be efficiently made by merely altering a NCC mix design. To effectively achieve the desired benefits of SCC, more ingredients need to be considered than are in the NCC mix design.

Several additional ingredients in SCC make achieving the balance between fluidity and segregation resistance easier. Among them are chemical admixtures including high range water reducers (HRWRs) and viscosity modifying admixtures (VMAs). Traditional mineral admixtures including silica fume, fly ash, blast furnace

slag, and limestone powder also make the balance between fluidity and cohesion possible [36]. When the effects of these ingredients are considered along with the other parameters discussed above, high quality concrete that exhibits the benefits of SCC can be produced consistently.

2.2.1 High Range Water Reducers (HRWRs)

HRWRs are very important to the production of SCC [38][39]. These chemicals act to increase the fluidity of the concrete while maintaining a reasonable w/c ratio. This is accomplished by more effectively using the water added to the mixture. HRWRs are made of organic molecules that adsorb on the solid particle surfaces. Naturally, the cement particles dispersed in the water have mixed charges causing some particles to be attracted to each other through electrostatic forces. This attraction causes flocculation of the particles, which traps a significant portion of the water. Because this water is trapped it is not utilized in the cement paste, as it cannot come into contact with unhydrated cement. Over time this water evaporates from the concrete leaving behind pores. Because this water is not utilized in the cement paste the viscosity of the paste is higher than it theoretically could be. The molecules of HRWRs neutralize the surface charge of the cement particles so that all of the particles have the same charge. This causes the particles to repel each other throughout the mix water. As the particles are more evenly dispersed through the water, more of the water is used to hydrate the cement producing a less viscous paste that can flow much easier than before. The proper use of HRWRs allows SCC to be developed with a reasonably low w/c ratio leading to a higher strength, more durable concrete [26][32].

2.2.2 Viscosity Modifying Admixtures (VMAs)

VMAs directly affect the mix water of the concrete [36]. These chemicals work to increase the viscosity of the cement paste, which in turn helps suspend the coarse aggregate in the fluid cementitious mixture. Using a VMA results in a more stable and cohesive concrete mixture. The molecules that make up VMAs are high molecular weight, water-soluble polymers that act to raise the viscosity of the water. These admixtures work to prevent segregation through increased cohesion as well as prevent bleeding [32]. The use of VMAs achieves the desired increase in viscosity without leading to an increased susceptibility to drying shrinkage as other methods would [36].

2.2.3 Mineral Admixtures

Partial cement replacement by silica fume, fly ash, blast furnace slag, or limestone powder is a common practice in NCC, but it can also help to produce SCC as well. The use of these admixtures influences the fluidity of SCC by reducing inter-particle friction. The shape of these particles is spherical when compared to the irregular shape of the cement particles [36]. As mineral admixtures are less reactive than cement, their inclusion will slow down the hydration reaction. This slower reaction increases the time that the mixture remains in its fluid state. The longer the reaction takes, the longer the concrete remains a fluid and preserves the beneficial fresh properties that define SCC. There is also a cost benefit when using fly ash, as these particles are by-products of other industries and they are thus widely available and cheap thus reduce the total cost [32].

2.3 Status and Recent Developments in SCC

It has been nearly twenty years since the development of SCC. Since its creation in Japan, the use of SCC has spread around the world and has been used in many projects. Committees in major industry and research organizations such as the American Concrete Institute (ACI), the American Society of Testing Materials (ASTM), PCI, and RILEM continue to evaluate the use of SCC [23].

In the United States the precast industry and admixture companies continue to push for the widespread use of SCC in many facets of civil engineering construction. However, some consumers of concrete technology including state Departments of Transportation (DOTs) have been slow to accept SCC as a viable alternative to NCC [35][41]. These groups have concerns about SCC related to quality control and long-term performance. These concerns keep SCC as a popular research topic in the US, but limit its implementation in construction projects.

A survey of research and case studies using SCC published in 2006 [16] shows that the spread of research on SCC has shifted from its center in Asia during 1993-1999 to Europe from 2000-2003, with the USA increasing the number of research and commercial projects through 2003. In 68 published case studies, 57 were uses of SCC in ready mix projects and only 11 were in precast facilities. However, Domone noted [16] that the number of reports of SCC being used in precast plants was increasing at the time of the survey. A large majority of the cases were in commercial projects; just 25% of the case studies were for demonstration or large scale testing projects. A summary of the mix designs used in these case studies shows that all mixes follow the same guideline in general:

15

- Low coarse aggregate content

- Increased paste content

- High powder content

- Low water/powder ratio

- High superplasticizer dose

- Viscosity modifying agent.

Also, 90% of the mixes had a spread flow of 23"-29" [16].

2.3.1 Recent SCC Research

Research on SCC continues to evaluate issues related to the mix design development, fresh properties, and hardened properties. Many research projects look at the effect of mix design components including admixtures, on the fresh and hardened properties of SCC [25][28]. Still others try to develop schemes for developing mix designs [50]. Many papers have focused on the effect that SCC has on formwork pressure. These projects are important to the continued advancement of SCC as they increase the understanding of how SCC works. However, these projects do not address significant areas of concern regarding the use of SCC. SCC can only be used successfully if structural elements produced with it perform at a satisfactory level. Paramount to this is the successful use of SCC in the production of prestressed products.

Limited research on the structural behavior of SCC has been published. The published projects focus on topics such as the bond of prestressing strand to the concrete and the shear strength of SCC members. Full scale testing of structural elements cast with SCC or long term monitoring of SCC structures is rarely reported in the literature.

2.3.2 Performance of Beams Made With SCC

Multiple projects investigating the performance of both reinforced and unreinforced beams made with SCC have produced somewhat conflicting results. One project looking at the load displacement response reinforced beams cast with SCC reports that the SCC beams behave similarly to regular concrete, with the only differences in cracking pattern being attributed to differences in the compressive strengths of the concretes [45]. Das et. al. [15] found that reinforced concrete beams cast with SCC had higher shear strength than those cast with regular concrete. Wilson and Kiousis [53] on the other hand found that SCC beams had a reduced shear strength when compared to NCC. Limited information was provided on their SCC mix design. They reported only that "the tested strength of this mix was 10 ksi and the mix uses a large volume of smaller aggregates to assist in uniform stratification [53]." They reported that the ACI Building Code equations for the shear strength of reinforced concrete beams did not always yield conservative results when SCC was used to cast beams. Lachemi et al tested beams made of SCC without shear reinforcement to analyze the shear strength of SCC. They concluded that the reduced coarse aggregate content of SCC lowered the post shear cracking resistance of the beam [27]. The confusion that follows these results has made the widespread acceptance of SCC difficult.

2.3.3 Prestressing Strand Concrete Bond

In prestressed concrete applications the bond between the prestressing strand and the concrete plays a major role in the adequate behavior of the structural element. Several research projects have studied strand bond performance on SCC beams again with conflicting results being reported. The bond strength and transfer length of

17

pretensioned SCC bridge girders was investigated by Girgis and Tuan, who found that SCC has higher bond strength and therefore lower transfer lengths at 28 days than conventional concrete [33]. Their research did not include full scale testing of the bridge girders, rather they took measurements for transfer length on full scale prestressed bridge beams that were to be implemented in a bridge. Hegger and Kommer [21] found that the ACI Building Code yielded unconservative predictions for the transfer length of prestressed beams cast with SCC. Larson, Peterman and Esmaeily investigated the transfer length, and flexural capacity of prestressed SCC beams and found that ACI and AASHTO codes were conservative in the predictions of both parameters [29]. Burgueño and Haq [10] reported that ACI equations conservatively predicted transfer lengths in SCC beams, but the equations for development length did not produce conservative results for high-fine SCC mix designs. Like the shear resistance of reinforced beams, the confusion that results from the reports raises questions about the acceptability of SCC.

2.3.4   Prestressed Beams Made With SCC

While the bond between prestressing steel and concrete is an important factor in prestressed concrete beams, the absolute capacities of these sections is the ultimate parameter of importance. Several projects have investigated the flexural and shear capacities of prestressed beams cast with SCC through large-scale testing. Choulli and Mari [12] found that even though the shear capacity of prestressed girders cast with SCC was lower than NCC, applicable codes conservatively predicted the performance. Naito [35] analyzed the use of SCC for bridges in Pennsylvania. In doing so he tested 45-inch deep 35 foot long Bulb-T beams to failure. The response of the SCC beams and the NCC beams were very similar with both exceeding the AASHTO design capacities. The

Virginia DOT investigated using SCC in bridge girders [41] by conducting tests on Bulb-T beams for transfer and development length. Tests on flexural and shear capacities are also being conducted but the results reports have not been published yet. Larson et. al. [30] monitored prestressed I-girders in a bridge for one year to evaluate prestress losses due to creep and shrinkage. They reported that the SCC beams had a smaller prestress losses than the NCC beams, however, these losses were within the PCI recommendations. The results of these studies show that the capacities of SCC beams are in line with building code requirements and with the performance of NCC beams.

2.3.5 Standardization of SCC Fresh Property Testing

In 2003 PCI published the "Interim Guidelines for the use of Self-Consolidating Concrete in Precast/Prestressed Applications" [23]. This report was the first guideline published in the United States. In the guideline, PCI identified nine common test methods to evaluate the fresh properties of SCC. These methods were:

- Slump Flow/Inverted Slump Flow, includes Visual Stability Index (VSI) and T_{50} test methods
- J-Ring Test method
- V-Funnel Test method
- L-Box Test Method
- U-Box Test Method
- Filling Vessel Test Method
- GTM Screen Stability Test Method
- Orimet Test Method
- Bleeding Test Method (French) [23].

19

The tests were chosen for their common use in both commercial and research arenas. In the 2006 edition of the ASTM testing methods three tests for SCC were standardized. These tests include the J-Ring test for passing ability, the Slump Flow test for flow ability, and the Column technique for segregation resistance [48][49]. The standardization of these tests by ASTM provides a unified model from which SCC fresh properties should be measured. A complete discussion of the fresh property tests used for this project is included in section 3.2.2.

2.4 SCC for Precast Construction

Precast plants have demonstrated successful uses of SCC in Japan, Europe, and the US [16][18][24][40]. Using SCC in a precast plant presents challenges that are not seen when using NCC. The mix design development of SCC is time consuming and can be difficult. Production processes used with NCC may need to be altered to use SCC effectively. Even with these potential problems, many precast plants successfully use SCC every day.

In Japan, SCC has been used in several high profile structures. The Higashi-Oozu Viaduct used precast/prestressed T beams [40]. Cost savings from using SCC in this project totaled 7%, including a 33% decrease in the labor costs and a 4% increases in the material costs. Umehara et. al [52] reported that two specific SCC products have been used to produce a total of 63,000 ft^3 of concrete for projects at 35 separate properties.

SCC is a popular alternative to NCC in Europe as well. The Netherlands, Sweden, Norway, and France are the largest producers of SCC in Europe. The largest manufacturer of precast concrete in Europe is the Consolis Group [24]. The company has 52 factories and is currently operating in 11 countries. Consolis' annual use of SCC

exceeds 100,000 m^3 and accounts for roughly 20% of the total concrete produced. In 2005 the estimated production of SCC was 261,400 cyd [24].

To date the Consolis Group has used SCC in multiple projects including the manufacture of multiple prestressed beams. Other unique projects, such as concrete sheet piles, complicated staircase elements, and an artificial reef element have all been cast using SCC in their plants. While no specifics are given, the company claims benefits from reduced labor requirements and improved work environment [24].

The precast/prestressed industry in the United States is beginning to use SCC as an alternative to NCC [40]. The introduction of SCC in precast plants has led to problems that must be resolved. The increased number of material constituents and critical reliance on quality control can make consistent production of high quality SCC in precast plants difficult [17]. Employees who have developed specific skills in working with NCC need to be retrained to effectively work with SCC. Even with these problems, SCC is becoming a common product in the US. Two published case studies regarding the use of SCC in US precast plants are reviewed next to highlight difficulties and successes with the use of SCC in precast concrete production.

At the Rocky Mountain Prestress Company, Denver, Colorado, a test program was developed to aid in the successful implementation of SCC in the plant [17]. The program consisted of three phases, a laboratory phase, a field test phase, and finally an implementation phase. The laboratory phase consisted of developing a relationship between mix design, cost, and performance. Mix design parameters were analyzed for their effect on fresh and hardened properties of the concrete as well as cost to develop an optimal mix. In the field test phase the flow properties of the concrete were evaluated in

21

conjunction with the plants mixing and placing equipment. Once satisfactory performance in these preliminary phases was established, the implementation phase was conducted to assess the performance of the concrete through the production of several mock-up of double T elements. The company encountered problems with the transportation of the concrete from the batching plant to the casting area and with the slope of the double-T formwork. Working through these problems they were able to successfully introduce the SCC mixes into their daily operations. The results of tests show that the SCC mixes used in the plant have decreased the concrete placement time by 20% compared to the use of NCC [17].

A second example of the use of SCC in the US precast/prestressed industry is at High Concrete Structures, Inc., Denver, Pennsylvania. At this plant SCC was used to help cast twice as many Double T beams in one casting bed than was possible with NCC [43]. To accomplish this, the company had to develop SCC mixes that could obtain 3500 psi in six to seven hours and 7000 psi at 28 days. The use of this new process in one of 4 casting beds led to a 25% increase in production per day for that bed. The company projected a total increase in production of 75% if all four casting beds were double cycled in a similar manner [43].

2.5 Outstanding Issues

Concerns about the use of SCC remain, even as it becomes more common in everyday practice. If SCC is approved for use by state DOTs, use will increase significantly. However, it is yet to be seen how SCC will be fully utilized by producers and consumers of SCC technology. Professional organizations globally have begun producing specifications for the use of SCC. In Europe, the European Concrete Standard

EN206-1, is being modified to specifically include SCC. This modification could include standardization of test methods for SCC and the development of a specification for the use of SCC [20].

Further research on long term properties of SCC such as creep and prestress losses will take time to be conducted and published. Only with continued use and increased experience will the behavior of structures cast with SCC become better known. The more SCC is used the better its behavior will be understood.

The use of SCC is currently being hindered by the lack of standards and codes for the use of SCC. While guidelines have been published, they must be updated so that they represent the state of the art in the industry. Finally, long term data from research projects must be collected and presented to fully understand how SCC behaves over long periods of times.

3 MIX DESIGN DEVELOPMENT AND PERFORMANCE

3.1 Overview

The general lack of experience in working with SCC leads to difficulties in developing SCC mix designs that consistently produce high quality SCC. While many methods have been discussed for such a development, mixes are heavily dependent on locally available materials and processes [9][26][39][50]. SCC mix design development requires trial and error procedures that iterate on desired out comes from a specific fresh property or a combination of fresh properties. Upon satisfactory achievement of these properties, the mix must be evaluated and refined for hardened performance.

3.2 SCC Mix Design Development and Evaluation

3.2.1 SCC Mix Design Development Methods

With all of the possible changes that can be made to produce SCC it is often challenging to develop a quality SCC mix that is reliable and easy to recreate. Many SCC mix designs have been proposed by researchers. However, the use of a single mix design in a research project leads to difficulties when interpreting and comparing the published data. While the results reported from research accurately represent the specific SCC mix design studied they may not represent all SCC mix designs. This problem could be alleviated if a range of mix designs are studied in a project. This would allow researchers to see how mix design modifications affect research results.

Among all of the proposed SCC mix designs, there seems to exist two approaches that bound most current SCC mix designs. These two limiting concepts have been identified in the research by Khayat [26] and Bonen and Shah [9]. Bonen and Shah [9]

referred to them as powder-type SCC and VMA (Viscosity Modifying Admixture)-type SCC, while Khayat describes them more generally. The first method described by Khayat achieves the fluidity requirements through the reduction of the coarse aggregate volume and the use of HRWR (High Range Water Reducer). The stability comes from a low w/c ratio with a high s/pt (sand to past) ratio. No VMA is required in this mix. The second method uses a high w/c ratio with little to no HRWR to achieve the fluidity requirements, allowing for a moderate volume of coarse aggregate, while the stability is achieved through the use of VMA and moderate s/pt ratios. Table 1 details the relative proportions of the w/c ratio, amount of HRWRs, VMAs, CAC (Coarse Aggregate Content), and s/pt ratio for the two methods.

In general, powder-type SCC uses HRWRs to increase the fluidity of the cement paste while maintaining a low *w/c* ratio and a decreased CAC. Larger amounts of fine aggregates are necessary to resist segregation in the mix as the VMA level is low. VMA-type SCC has a higher *w/c* ratio and uses less HRWR for its fluidity. The viscosity and segregation resistance are controlled by the use of VMAs while maintaining moderate to low s/pt ratio and level of CAC. Either of these methods, or a combination of the two has been shown to produce high quality SCC [9][26].

Table 1.   Mix Design Experimental Matrix

Mix Design	w/c	HRWR	VMA	CAC	S/Pt
Powder SCC	Low	High	Low	less	More
Combination SCC	Moderate	Moderate	Moderate	Moderate	Moderate
VMA SCC	High	Low	High	Moderate	Less
NCC	Moderate	As needed	None	Moderate	Moderate

3.2.2 SCC Mix Design Evaluations

As previously discussed, the performance of SCC is most often characterized by its fresh properties. The ability of the concrete to fill formwork, flow around obstacles, and resist segregation determines the usefulness of the mix for a given application. In the 2006 edition of the ASTM standards for Concrete and Aggregates [48][49], two tests related to the fresh properties of SCC were included. These tests are the Slump Flow and the J-Ring. While there are many other tests that commonly used to measure relevant parameters [9][23], only four were chosen to characterize the SCC mixes for this project. They are:

A. Inverted Slump Flow Test

B. Visual Stability Index

C. J-Ring

D. L-Box

3.2.2.1 Inverted Slump Flow Test

Slump flow is a measure of the concrete's ability to flow under its own weight. It is analogous to a standard concrete slump test for NCC. For this test a standard Abrahm's cone is inverted on a flat surface. As shown in Figure 4, concrete is placed in the cone without any form of vibration or tamping. Excess water or concrete is removed from the flat surface around the cone as its presence can affect test results. As the cone is lifted vertically in a slow and even motion, the SCC flows into a circular concrete patty, as shown in Figure 5. The average diameter of the patty is obtained by taking two orthogonal measurements. This average value represents the slump flow for the SCC.

An SCC mix that has a high value of slump flow will have an easier time filling formwork under its own weight [23].

Prior to conducting this test the acceptable range of the SCC slump flow must be defined. It is important that the acceptable range be relevant to the project for which the concrete will be used. A larger vale would be required on a project with more intricate formwork or dense steel reinforcing schemes. Bonen and Shah [9] suggest a minimum value for the inverted spread of 23 inches. According to the Special Provision for the Production of Prestressed Beams with Self-Consolidating Concrete [11] written for this project and included as APPENDIX A, a slump flow diameter of 27 in. plus or minus 1 in. (26 in. – 28 in.) was prescribed as a satisfactory range of slump flow.

Figure 4.   Inverted Slump Flow Test
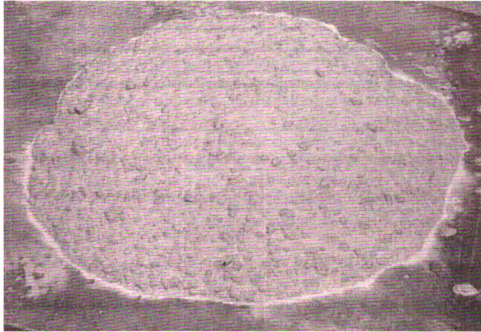
Figure 5. Concrete Patty from Inverted Slump Flow Test

3.2.2.2 Visual Stability Index

While adequate flow is generally the main parameter used to assess SCC, a highly flowable concrete may not always be acceptable. To be of high quality, SCC must not only fill formwork and consolidate under its own weight, it must also remain homogenous throughout the entire construction process. The visual stability index (VSI) is a qualitative measure of the concretes ability to resist segregation. While no single property of the concrete can be quantified using the VSI, it can be used as a measure of the relative quality control of the concrete [23].

Table 2. VSI Ratings Criteria [23]

Rating	Criteria
0	No evidence of segregation in the slump flow patty or sampling wheelbarrow
0.5	No mortar halo or aggregate pile in the slump flow patty, but very slight evidence of bleed or air popping on the surface of the SCC in the sampling wheelbarrow
1	No mortar halo or aggregate pile in the slump flow patty but some slight bleed or air popping on the surface of the concrete in the sampling wheelbarrow
1.5	Just noticeable mortar halo and/or a just noticeable aggregate pile in the slump flow patty and noticeable bleeding in the sampling wheelbarrow
2	A slight mortar halo and /or aggregate pile in the slump flow patty, and highly noticeable bleeding in the wheelbarrow
3	Clearly segregating by evidence of a large mortar halo and/or large aggregate pile in the center of the concrete patty and a thick layer of paste on the surface of the resting concrete in the wheelbarrow

The VSI can be recorded from the previously described inverted slump flow test. Once the test has been conducted, a rating is given to the concrete based on criteria such as the amount of water bleeding from the edge of the concrete patty, the amount of aggregate piled in the center of the patty, or the presence of an aggregate free mortar halo at the edge of the patty. This test is subjective and is best used to relatively compare several similar SCC mixes.

A perfect VSI rating of 0 would be obtained by a mix that produces a concrete patty with aggregate dispersed to the edge of the concrete with no visible free water bleeding beyond the edge of the patty. The ratings increase in increments of 0.5 and vary from 0 to 3. Table 2 lists the rating evaluation guide as taken from PCI's "Interim Guidelines For the Use of SCC" [23]. For this project a VSI of 1.0 or lower was required for a qualifying test.

3.2.2.3 J-Ring

While the slump flow is an adequate measures of the concrete's ability to flow, it does not measure the ability of the concrete to flow around obstacles. As the concrete flows through obstacles such as reinforcing steel, the entire mixture must travel together. If the coarse aggregate were to be blocked by the obstacles as the paste continues through, the mix would have to be reevaluated. The J-Ring test can assess this "passing ability" of SCC [23].

The J-Ring test is very similar to the inverted slump flow test. It uses an inverted Abrahm's cone placed inside a ring of evenly spaced vertical bars as shown in Figure 6. The spacing and diameter of the bars in the J-Ring should reflect the reinforcing scheme of the element being cast and the maximum aggregate size used in the SCC mix design. The test is executed exactly like the inverted slump flow test with the result shown in Figure 7.

Important information on the passing ability is not only found in the average diameters of the concrete patty but in the depth of the concrete inside and outside the ring. These values are obtained by measuring from the top of the J-Ring to the top of the concrete and subtracting this value from the full height of the J-Ring. The measurements are taken at four locations along the two orthogonal diameters as shown in the schematic drawing of the J-Ring test in Figure 8 and Figure 9. In an ideal situation the concrete would be able to flow without any resistance from the obstacles. This would be seen by a small difference between the level of concrete inside the J-ring and the level of the concrete on the outside of the J-ring. In addition, the coarse aggregate would still remain evenly dispersed to the edge of the concrete patty.
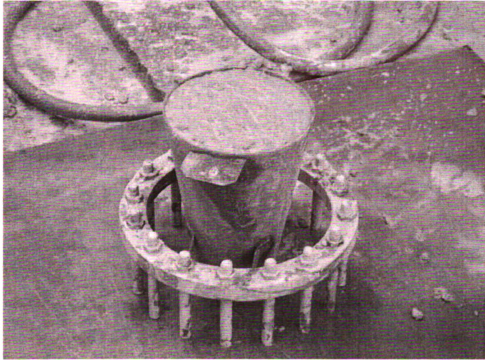
Figure 6. J-Ring Test Set Up

Calculating the J-Ring test value is done by taking the median value of the four depth measurements of the concrete inside and outside the J-ring. The changes in depth from the center of the concrete patty to the inside of the J-Ring and from the inside of the J-Ring to the outside of the J-Ring are used to calculate the J-Ring value. Equation (1) is used to calculate the J-Ring Value:

$$(1) \quad J - Ring = 2(h_{am} - h_{bm}) - (h_{1m} - h_{am})$$

where h_{am} is the median inside depth, h_{bm} is the median outside depth and h_{1m} is the depth at the center of the patty. According to the PCI Interim Guidelines for SCC a value of 0.6 in. shows excellent passing ability and a value of 0.4 in. is acceptable [23]. According to the Special Provision for the Production of Prestressed Beams with Self-Consolidating Concrete [11] (APPENDIX A), the state requirements for this project area J Ring value between 0.5 and 0.6.
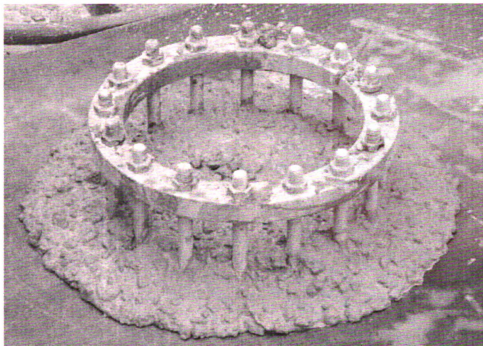
Figure 7. Result of J-Ring Test
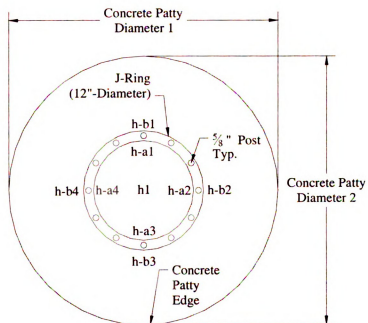
Figure 8. Schematic of J-Ring Test
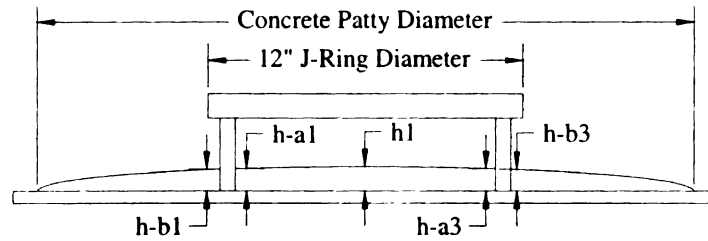
Figure 9. J-Ring Test Apparatus Profile

3.2.2.4 L-Box

The L-box test is another measure of the passing ability of SCC. The apparatus for this test is shown in Figure 10. It consists of two rectangular chambers arranged in the shape of an L. The vertical chamber is separated from the horizontal chamber by a vertical sliding gate. To obstruct the flow of the concrete from the vertical camber into the horizontal chamber, vertical bars are placed just out side the gate. The test is conducted by filling the vertical chamber and allowing the concrete to rest for one minute. At the end of one minute, the gate is lifted up to the height of the horizontal chamber and the concrete flows through the horizontal chamber as shown in Figure 11. The time the concrete flow takes to reach the halfway point and the end of the horizontal chamber are recorded. Once the concrete comes to rest the height of the concrete in each chamber is measured. If the obstacles provided little resistance to the passing ability of the concrete, the ratio of these heights would equal one [23]. For this test a value from 0.5 to 1.0 is considered acceptable. According to the Special Provision [11] (APPENDIX A) for this project the state requirement is a L-Box value greater than 0.8.

33
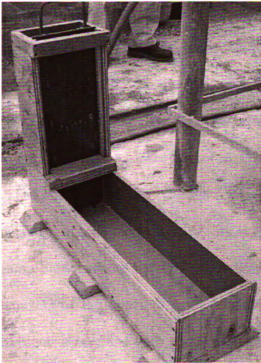
Figure 10. L-Box Test Apparatus   **Figure 11.   L-Box Test**

3.2.2.5 Fresh Property Test Discussion

It is commonly accepted that the battery of tests just described, while important in research, may not be practical in a production facility.   Results of these tests are extremely time sensitive, as the plastic properties of SCC decay rapidly as the concrete curing process progresses.   The tests also require more equipment than a standard slump test, which makes transporting them to and around a job site difficult.   Also, the results of the L-Box and J-Ring test require calculations that cannot be easily done in the field.   However, this does not mean these tests have no value.   When developing an SCC mix design these tests can provide important information about the fresh property behavior of the concrete.   The performances of the concrete can lead directly to changes in the mix designs.   The use of tests with overlapping scopes provides multiple points of reference on which to base changes to the mix proportioning.

As mentioned previously, the 2006 edition of the Annual Book of ASTM Standards [48][49] includes two standards specifically for the use of SCC. These standards include the Slump Flow Test Method [49], and the J-Ring Test Method [48]. Some differences exist between the methods published by ASTM and those in PCI's "Interim Guidelines for the Use of SCC [23]." The most significant difference is that the ASTM standard for the J-ring test does not include a calculation based on the depth of the concrete. Instead the passing ability is calculated by finding the difference between the Slump Flow and the J-Ring Flow, where both values are the average of two orthogonal diameters of the concrete patty. According to ASTM a difference of 1 inch or less represents a concrete with good passing ability while a difference of 2 inches or greater represents a concrete with poor passing ability [48]. As the ASTM standards were not available at the time of this project, the test methods presented in the PCI guidelines were followed.

3.2.3 SCC Mix Design Development

The SCC mix designs used for this project were developed to bound the current practices of SCC mix proportioning. These mixes were intended to lie at the extremes of possible SCC mixes. The concept was that any effects produced by these mixes would bound the results from mixes that would be commonly developed to somewhere in between these extremes.

All of the mix designs developed for this project used 700 lbs of Type III cement. The target 28-day compressive strength of all of the mixes was 5,500 psi with at least 5,000 psi required to release the prestressing strands. Local natural aggregates, which met MDOT specifications for use in prestressed bridge elements, were used, namely

natural coarse aggregate 17A and natural sand 2NS. The level of entrained air was to be 6%. The specific quantities for each SCC mix design and the process used to obtain them are discussed below.

Three SCC mix designs were developed for this project to bound current practices of SCC mix design proportioning. One of the mix designs, SCC 1, used a powder based approach while a second mix, SCC 3, used a VMA-based approach, both similar to the mix designs described by Khayat [26] and Bonen and Shah [9], to achieve the SCC fresh property behavior. The final SCC mix design, SCC 2, used a combination of the two approaches.

The project mix designs were developed by the fabricator based on baseline mix designs provided by MSU through the project's special provisions [11]. These baseline mix designs, presented in Table 3, were previously used in an MSU research project that studied the bond of prestressing strand and SCC and had an intended compressive strength of 7000 psi at 28 days. Degussa Admixtures Inc. (now BASF Admixtures) provided technical assistance in the development of the mix designs.

Development of the final SCC mixes for use in the project required numerous trial batches and adjustments to the baseline mix designs in Table 3. Performance of the mix designs was assessed through the following tests: inverted slump flow, J-Ring, L-Box and Visual Stability Index [23]. Adjustments were made to the mix designs based on the test results until satisfactory fresh performance was consistently produced.

Table 3. Baseline SCC Mix Designs

	NCC	SCC 1	SCC 2	SCC 3
Constituent (lbs/yd^3)				
Cement – Type III	700	700	700	700
Fine Aggregate	1216	1519	1426	1275
Coarse Aggregate (17A)	1580	1380	1380	1435
Water	280	245	280	315
Air	6%	6%	6%	6%
w/c ratio	0.4	0.35	0.4	0.45
Admixtures (oz/cwt)				
Air Entraining	1	0.5	0.5	0.5
High Range Water Reducer	2	6.29	7	8
Viscosity Modifier	0	0	1	9
Set Retardant	6	6.14	6.69	6

3.2.3.1 SCC 1

The SCC 1 mix was intended to imitate a powder-type SCC, as described by Bonen and Shah [9] and Khayat [26]. This means that the concrete fluidity is achieved by using a relatively high amount of HRWR and a reduced amount of coarse aggregate, while the segregation resistance comes from an increased amount of fine aggregate. The high amount of HRWR allowed the w/c ratio to be kept to a relatively low 0.35.

Table 4 shows the mix design evolution for SCC 1 with the results of the fresh property and compressive strength tests in Table 5. The first attempt at creating SCC 1 resulted in a slump flow value of 24 in., which was less than the 27 in. requirement specified in the project special provisions [11]. However, the mix showed good resistance to segregation with a VSI of 0. To raise the spread value of the concrete, HRWR was added to the mix for the second trial. Although this change increased the fluidity of the concrete, it lowered the segregation resistance of the mix. In order to maintain the fluidity but improve the stability of the concrete, the fine aggregate content was reduced while the amount of water added to the mix was increased. The result of

37

this was a slightly less fluid mix, with a perfect VSI rating. While the spread did not fall in the required range, the mix design was adopted as small adjustments to the fluidity could be made at the time of casting. The final mix design was able to meet the strength requirement as 5000 psi was obtained in less than one day.

Table 4.   SCC 1 Mix Development

	SCC 1-1	SCC 1-2	SCC 1-3
Constituents (lb/yd^3)			
Cement	700	700	700
Fine Aggregate	1,612	1,612	1591
Coarse Aggregate (17A)	1350	1350	1350
Water	248	248	256
Air	6.00%	6.00%	6.00%
w/c ratio	0.35	0.35	0.37
Admixtures (oz/ cwt)			
Air Entraining	1	1	1
HRWR	14	15	15
VMA	1	1	1

Table 5.   SCC 1 Test Results

	SCC 1-1	SCC 1-2	SCC 1-3
Slump Flow (in.)	24	26.5	25
VSI	0	.5	0
f'$_c$ (psi)			
<1 day	1294	4754	4953
7 day	7630	8677	6265

3.2.3.2 SCC 2

The SCC 2 mix represented a balanced combination of a powder and VMA-type SCC mixes as described Bonen and Shah [9] and Khayat [26]. The target w/c ratio for this mix was 0.4. As the amount of cement in each mix was fixed at 700 lbs/yd^3, the higher w/c ratio was achieved by using more water than was used in the SCC 1 mix

design. Because of the increased amount of water in this mix design a lower amount of HRWR was used than in the SCC 1 mix. Compared to SCC 1, the SCC 2 mix design had a larger CAC and a reduced amount of fine aggregates, resulting in a lower s/pt ratio.

Table 6 shows the evolution of the SCC 2 mix design and the results for fresh property and compressive strength tests are shown in Table 7. The spread value and the VSI rating for the first SCC 2 mix design attempt fell short of the special provision requirements [11]. To compensate for this, coarse aggregate was removed from the mix and the fine aggregate content was increased. HRWR was also added to ensure that good flow was obtained. While the second mix of SCC 2 met the required slump flow value, the mix showed some segregation with a VSI rating of 1. To improve the segregation resistance, a portion of the fine aggregate was removed and VMA was added. Water was also added to the mix design, slightly raising the w/c ratio, to maintain the desired spread value. The test results showed that the final SCC 2 mix met the requirements for both the slump flow and VSI rating. The flow was within 1 in. of the 27 in. requirement and the VSI was 0.5. The strength requirement was also met by this mix design as 5000 psi was obtained in 2 days

Table 6.   SCC 2 Mix Development

	SCC 2-1	SCC 2-2	SCC 2-3
Constituents (lbs)			
Cement	700	700	700
Fine Aggregate	1,457	1,527	1513
Coarse Aggregate (17A)	1420	1350	1350
Water	280	280	285
Air	6.00%	6.00%	6.00%
W/c Ratio	0.4	0.4	0.41
Admixtures (oz/cwt)			
Air Entraining	1	1	1
HRWR	11	12	12
VMA	0	0	2

Table 7.   SCC 2 Results

	SCC 2-1	SCC 2-2	SCC 2-3
Spread (in.)	25.5	27.5	26
VSI	2	1	.5
f'_c (psi)			
<1 days	2873	5012	4294
2 days	5252	-	5614
7 days	6511	6262	6281
14 days	6360	6520	6078

3.2.3.3 SCC 3

The SCC 3 mix was modeled after a VMA type SCC mix described by Bonen and Shah [9] and Khayat [26]. The target w/c ratio of the SCC 3 mix was the highest of the four project mix designs at 0.45. The larger amount of water used in this mix required that the amount of HRWR used in the mix design to be the lowest of the SCC mixes. To ensure adequate segregation resistance of this mix design, a relatively large amount of VMA was used. The higher amount of VMA meant that segregation could be controlled with fewer fine aggregates and a higher CAC than in the previous SCC mix designs.

Table 8 shows the mix design evolution for SCC 3. As can be seen from the results shown in 0, the first SCC 3 mix design did not meet the slump flow requirement, but had an acceptable segregation resistance with a VSI rating of 1. Both parameters were improved by increasing the amount of HRWR and VMA. While test results were not provided by the fabricator, the second batch of the SCC 3 mix design met the performance standards from the special provisions, and the mix design was adopted without further alterations.

Table 8. SCC 3 Mix Design Development

	SCC 3-1	SCC 3-2
Constituents (lbs/yd^3)		
Cement	700	700
Fine Aggregate	1,320	1,320
Coarse Aggregate (17A)	1450	1450
Water	320	320
Air	6.00%	6.00%
W/c Ratio	0.46	0.46
Admixtures (oz/cwt)		
Air Entraining	1	1
HRWR	10	10.7
VMA	5	6

Table 9. SCC 3 Results

	SCC 3-1	SCC 3-2
Spread (in.)	25	-
VSI	1	-
F'$_c$ (psi)		
<1 day	5780	-
7 day	6316	-

3.2.3.4 Final mix Designs

The final mix designs for each concrete type are given in Table 10. The three SCC mix designs were the result of the mix development process presented in the previous sections. The NCC mix design was the standard fabricator mix used for bridge beams. These mixes were chosen for their ability to perform adequately in both the plastic and hardened states.

Table 10. Project Mix Designs

	SCC 1	SCC 2	SCC 3	NCC
Constituents (lb/yd³)				
Cement	700	700	700	564
Fine Aggregate	1,591	1,513	1,320	1,354
Coarse Aggregate (17A)	1,350	1,350	1,450	1,883
Water	256	285	320	151
Air	6.00%	6.00%	6.00%	6.00%
W/c Ratio	0.35	0.4	0.46	0.27
Admixtures (oz/cwt)				
Air Entraining	1	1	1	1.9
HRWR	15	12	10.7	11.3
VMA	1	2	6	

3.2.4 Discussion

From the mix design process just described it can be seen that SCC mixes can be produced using opposing methods. The mix designs developed for this project were intended to be at the extremes of the various mix design methods and may not represent a "good mix" to use in practice. This implies that the mixes used in this project could have been improved to more easily satisfy production requirements such as finishing and placing of the concrete. However, as an objective of this project was to investigate a

range of SCC mix design by developing and using mixes that lie at the extremes of current mix design development practice, these mix designs were selected for their research potential. SCC mixes that use a combination of these procedures and lie in the middle of the range represented by the project mix designs may produce high quality concrete with more consistency and ease.

As these mixes were developed, significant collaboration between the three parties involved was necessary and extremely beneficial. The combined knowledge and experience of the admixture, precast, and research representatives was highly valuable in the development of mixes that satisfied both production and research objectives. Without this collaboration these mix designs would not have been developed.

The ability to economically introduce SCC to local precast plants depends on the feasibility of using locally available materials and equipment commonly available to the plants. The mix design development process conducted for this research confirmed that materials and equipment commonly used in local precast plants is acceptable for use in the production of SCC. This includes many of the procedures common to local precast plants, such as methods of concrete mixing and transportation of the concrete from the mixing equipment to the casting area.

3.3 Strand Bond Evaluation

The ability to effectively use prestressed concrete depends on the quality of the bond between the concrete and the prestressing strand. The length over which the strand must be bonded in order for the concrete to achieve the full strand strength depends on many factors including the arrangement of the strands, the condition of the strands, the method of release of the strand, and the concrete. The length required to develop full

strand stress in the concrete, the transfer length and the development length, are defined by long-standing equations in the AASHTO Specifications[2][3]. However, research has shown that this equation may not be conservative for all sources of strand [31] or types of concrete. Unconservative values lead to longer transfer and development lengths, which manifest themselves as reduced flexural and shear strength of the prestressed concrete beam near the ends. Since concrete tensile strength and density impact its ability to bond to strand, there were concerns that this problem could be further complicated when using SCC. The concern is that the mix design modifications that lead to the beneficial properties of SCC may have a negative influence on the bond between the concrete and the prestressing strand. This uncertainty led MDOT to include a requirement for the evaluation of the strand bond for the SCC mix designs in the project special provisions [11]. The PCI guidelines [23] suggest using a flexural development length test or a direct load test to evaluate the bond between the prestressing stand and an SCC mix. While several tests have been proposed for the purpose of evaluating the strand bond, the modified Moustafa test proposed by Logan [23] and recommended by the PCI interim guidelines on SCC was chosen for this project [31]. The use of direct structural tests to determine the flexural development length was not considered for this project due to constraints on production time and cost. The Large Block Pull-Out test (LBPT) described by Logan [23] was chosen to evaluate strand bond because it requires only small amounts of material and it's simple to execute with equipment found at the precast plant.

3.3.1 Large Block Pull-Out Test (LBPT) Overview

Logan analyzed the bond between concrete and prestressing strand from seven different manufacturers to see if different strand manufacturing processes affected the bond [31]. A second objective of Logan's work was to set a benchmark for the pullout capacity of the strand that could predict the transfer and development lengths. The testing program included pull out tests conducted on unstressed samples of 0.5-inch diameter prestressing strand embedded 18 inches in concrete and three-point bending tests on prestressed beams to measure the required development length [31].

The development lengths Logan found by experiment were compared to the development lengths predicted by the ACI-318 code equations [1]. It was found that strands that exceeded an ultimate pullout strength of 36 kips in the large block pullout test (LBPT) had a development length which was conservatively predicted by the ACI code. However there were significant differences between the measured and predicted development length when the pull out force did not exceed 12 kips [31]. From the results it was determined that the minimum acceptable average pull out capacity for 0.5-in. strand was 36 kips, the minimum acceptable average for the first slip of the strand during the pull out test is 16 kips.

All of Logan's test specimens were cast with a specific NCC mix. Thus, the focus of his study was on evaluating the prestressing strand, and the concrete was not a variable in the test. However, the modifications made to the SCC mix designs have raised concerns about whether proper bond will develop when SCC mixes are used. Specifically, whether the increased levels of HRWR and VMA in SCC mix designs

would lower the ability of the cement paste to develop adequate bond with the strand [33].

The LBPT described by Logan included pullout tests on embedded unstressed prestressing strand samples. The 0.5-inch strands were embedded 18 inches into concrete blocks. The blocks had dimensions of 6 feet 8 inches long, by 2 feet deep, by 2 feet high. Each block included 18 strands spaced at 8 inches in two rows 12 inches apart. A 2-inch tube was included around each strand at the top surface of the block to debond the concrete from the strand. To test the pull out strength, the strand were pulled vertically from the block using a hydraulic ram bearing against the concrete block. The rate of loading was 20 kips per minute. The tests were conducted on the morning after casting [31].

Because of the relative newness of SCC, the issue of prestressing strand is a widely discussed problem. Research using Logan's LBPT has been done with SCC. Morgan-Girgis and Tuan [33] analyzed the bond of 0.6 in. prestressing strand in SCC using an approach similar to Logan's. LBPT's were conducted on the strand and compared with results from beam tests to assess the transfer and development lengths. Morgan-Girgis and Tuan found that lower bond between SCC and the strand was seen at early age. This was shown with longer transfer lengths from beam tests, however the same trend was not seen in the pull out tests. At 28-days, the SCC showed higher bond strength than NCC in both the beam tests and the LBPT [33].

For this project the LBPT proposed by Logan was used to evaluate the *relative* bond characteristics of the four different concrete mix designs with the prestressing strand to be used in the bridge beams. Blocks were cast of each concrete mix design: 24

in. tall by 36 in. wide and 24 in. deep. Six 0.6 in. diameter unstressed prestressing strand samples, with an ultimate capacity of 270 ksi, were embedded 18 inches in the blocks and were arranged as shown in Figure 12, and schematically in Figure 13. The strands were pulled out of the block 48 hours after casting using a hydraulic ram as shown in Figure 14. Values of first slip and ultimate load were recorded using the dial gage on the ram control. The accuracy of the gage was limited to 500 lbs. For safety, the upper limit on the jacking load used on each test was 47,000 lb, or 80% of the ultimate strand capacity.

An additional block was cast using a mix design that was as close as possible to the one recommended by Logan. The suggested mix design is included in Table 11 while the modified mix design used for this project, is in Table 12. Other than slight variations on the mix quantities the modified mix was very similar to the suggested mix design. This test served to qualify the strand, as it is the main purpose of the test. The rest of the blocks were cast with the different project SCC and NCC mixes. These tests allowed a *relative* evaluation of bond performance on the different types of concrete.

Two rounds of tests were conducted to verify the results. The test used in this project differed from Logan's test in the following ways:

- The diameter of the prestressing strands was 0.6 in. instead of 0.5 in.

- The rate of loading was estimated using a stop watch - there is possible error in this value due to the manual control of the hydraulic ram

- The ultimate load of the test was set at 47,000 lbs or 80% of the ultimate strand capacity due to safety

Table 11. Suggested LBPT Mix Design

	LBPT Mix Design
Constituents (per yd^3)	
Cement (lbs)	660
Fine Aggregate (lbs)	1,100
Coarse Aggregate (lbs)	1,900
Water (lbs)	292
Admixtures (oz/cwt)	
Air Entraining	0
Normal Range Water Reducer	26
VMA	0

The test results were valuable even with these potential limitations. The PCI guidelines state, "that the bond with SCC is equivalent or better than with a conventional concrete of similar design when using similar strand [23]" suggesting a relative performance rather than a direct comparison to Logan's benchmark levels. It will be discussed later, that results from this and other research projects indicate that the direct pullout strength of strand on SCC is lower than on NCC. Recommendations have been provided to PCI [19] to modify their recommendations to more realistic expectations as discussed in Section 3.3.3.

Table 12. Modified LBPT Mix Design

	Modified LBPT Mix Design
Constituents (per yd³)	
Cement (lbs)	660
Fine Aggregate (lbs)	1,031
Coarse Aggregate (lbs)	1,850
Water (lbs)	291
Admixtures (oz/cwt)	
Air Entraining	0
Normal Range Water Reducer	0
VMA	0

The benchmark described by Logan was developed for 0.5 in. diameter strand. Logan has suggested a modified benchmark for the use of 0.6 in. diameter strand [31]. The modified benchmark uses a modified block geometry as well. Instead of the 18 in. embedment used with the 0.5 in. diameter strand, Logan proposed a 20 in. embedment with the 0.6 in. diameter strand. Maintaining the bond stress for the 0.5-inch. benchmark at 1.27 ksi, the benchmark for the 0.6 in. strand becomes 48 kips. This benchmark proposed by Logan for 0.6-inch diameter strands requires the same stress as the 0.5-inch strand but increases the embedment length to balance the increase in diameter. Logan's modified recommendations for 0.6-inch strand were not available until after the tests were complete, and the embedment length used in this project was 18 inch. The benchmark level for the 0.6 in. strand with an 18 in. embedment, assuming the same constant bond stress from the 0.5 in. strand of 1.27 ksi, can be calculated as 43.1 kips. Similarly, the first slip level was altered such that the bond stress was maintained at a consistent value. The 16 kip benchmark level represents a stress of 0.565 ksi with 0.5-

inch strand embedded in 18-inches of concrete. When this benchmark is modified for the

0.6-inch diameter strand with an embedment of 18 inches, it increases to 19.2 kips.
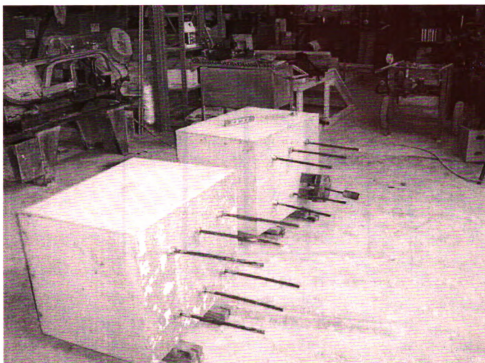
Figure 12. Pull-out Test Specimen Prior to Testing
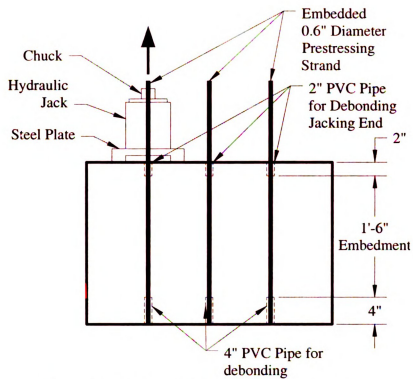
Figure 13. Schematic of Pull-Out Test Specimen
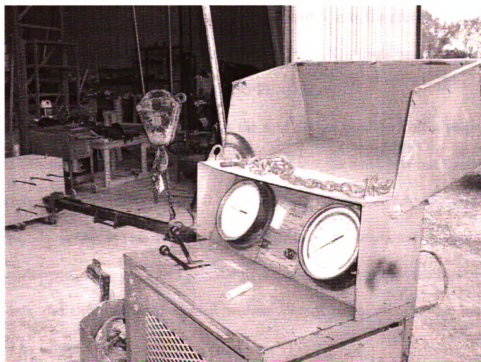
Figure 14. Test Set-up For Pull Out Test

3.3.2 Observations and Results

The ultimate load test is used to show the strength of the bond developed between the strand and the concrete. It is used in this project to qualify the different concrete mix designs. The results of both rounds of tests are shown in Table 13 and graphically in Figure 15. For each test the concrete was 48 hours old. Each test was conducted 48 hours after the casting of the block. Each result is the average of 6 tests for each mix design. The mix design emulating the one by Logan to verify the strand bond was used with success here. The bond exceeded the 47,000 lbs limit of the test. This surpasses the 43.1 kip benchmark value that qualifies the strand for adequate bond. Logan's concrete mix was not used in the second round of tests (see Table 13). Once the strand is qualified to have good bond quality, a *relative* evaluation of the effect of concrete type, i.e., SCC versus NCC, can be made. The first movement values are shown in Table 14 and graphically in Figure 16. Each result is the average of 6 tests for each mix design. The requirements from the Special Provision state that the SCC strands must achieve 67% of the bond strength of the NCC strands [11] (APPENDIX A).

From Table 13 it can be seen that the mix design used by Logan surpassed the modified benchmark level of 43.1 kips. This means that the bond between the strand and the concrete was adequate to achieve the development lengths predicted by the ACI-318 Building Code equations [1]. It is unclear whether this benchmark can be applied to the other mix designs. Because of this uncertainty, only the *relative* performances of the four project mix designs will be discussed without regard to the benchmark load levels proposed by Logan.

52

In general, it can be seen that the values of ultimate load in the second test were lower than the values of ultimate load obtained in the first test. Part of the reason for this may have been inconsistencies in the test procedure in the first test. The hydraulic ram used to test the specimen was controlled manually and the loading rate was estimated using a stopwatch. In the second tests the rate of loading was observed to be more consistent and lower than in the first test. A higher loading rate may be the cause of the higher ultimate loads shown in the first round of tests.

Regardless of the value, the relative performance of the four mix designs is consistent in the first and second series of tests. For the SCC concrete mix designs, the SCC 1 mix design had the highest ultimate load in both rounds of tests, the SCC 2 mix design had the second highest load and the SCC 3 mix had the least bond strength of all of the mixes. Comparing results from the more consistent second round of tests, the SCC 1 mix design performed better than the NCC mix design by 13 percent, while the SCC 2 and SCC 3 mixes showed ultimate loads 3 and 30 percent lower than the NCC mix, respectively.

Table 13. Ultimate Loads from LBPT

Mix Design	Ultimate Load Test 1 (lbs)	Standard Dev. (lbs)	% difference from NCC	Ultimate Load Test 2 (lbs)	Standard Dev. (lbs)	% difference from NCC
NCC	47,000	0	-	34,500	4,212	-
SCC 1	47,000	0	0	39,000	1,530	13.04
SCC 2	37,000	5,562	-21.28	33,500	4,212	-2.90
SCC 3	30,000	2,690	-36.17	24,000	3,216	-30.43
Logan	47,000	0	-	-	-	-
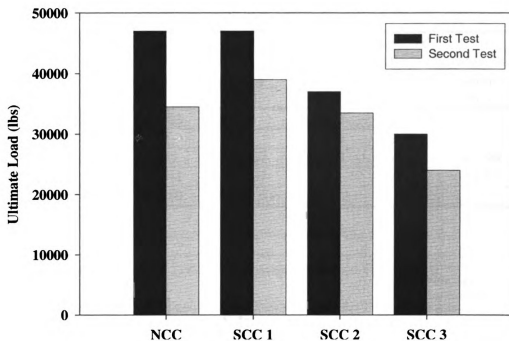
Figure 15. Ultimate Load of LBPT for all Mix Designs

From the data for the first slip load it can be seen that during the first round of tests the SCC 1 and NCC mix designs had average values above the benchmark level of 19.2 kip. However, during the second round of tests, none of the concretes had average values that met this benchmark. Again, it is unknown whether these benchmarks can be used given the modifications made to the testing procedure. What can be seen from this data is that the relative performance of the four study mix designs for the first slip load is similar to the relative performance of the ultimate load. In terms of the load at first slip, the SCC 1 mix design had the highest average, but was only slightly higher than the NCC mix design. SCC 1 also had the highest average of the three SCC mix designs. The SCC 3 mix design produced the lowest average value.

Table 14. First Slip Loads for LBPT

Mix Design	1st Slip Load Test 1 (lbs)	Standard Dev. (lbs)	% difference from NCC	1st Slip Load Test 2 (lbs)	Standard Dev. (lbs)	% difference from NCC
NCC	30,000	2,683	-	15,500	3,061	-
SCC 1	28,500	2,739	-5	15,000	1,291	-3.23
SCC 2	11,500	895	-61.67	13,500	681	-12.90
SCC 3	11,500	1,441	-61.67	7,500	612	-51.61
Logan	27,500	3,650	-	-	-	-
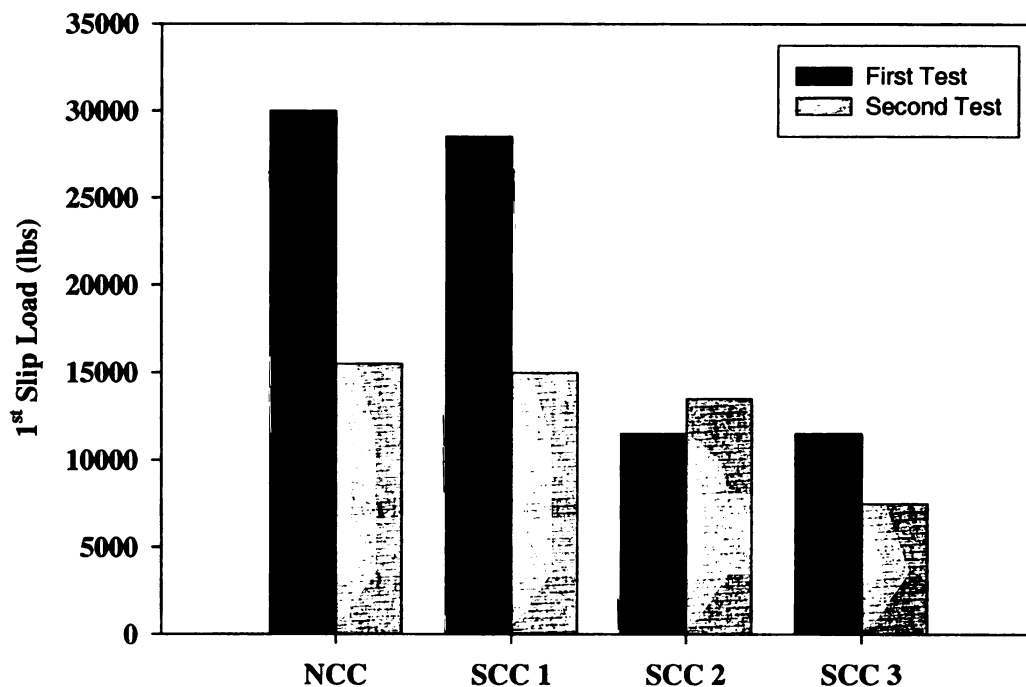
Figure 16. 1st Slip Loads for LBPT.

3.3.3   Discussion

The results of the pullout test may be related to the mix designs. Specifically, the use of chemical admixtures in the concrete may affect the bond of the concrete with the prestressing strand. The amount of VMA varies from 0 oz/cwt in the NCC mix to 6 oz/cwt in the SCC 3 mix. As the SCC 3 mix has the lowest bond strength, the VMA may be responsible for the poor bond. This may be due to the fact that the SCC 1 mix had the

least amount of VMA of all three SCC mixes and it showed the highest bond strength of the three mix designs.

The pull out tests served to confirm the relative performance of the different SCC mix designs. While the pullout performance of the three SCC mixes was different, testing that is outside the scope of this project would be required to fully understand why. However, even with the range of results obtained in these tests, the size of the elements cast for the bridge are large enough such that slightly increased transfer and development lengths will not negatively affect the overall performance and safety of the bridge.

Other studies done on the bond performance of SCC using the pull out test have found that SCC mixes have lower bond strengths than NCC. Burgueño and Haq [10] and Morgan-Girgis and Tuan [33] have all shown reduced pullout strengths for SCC mix designs. The reasons for these reduced strengths are not yet fully understood.

3.4 Mix Development and Performance Conclusions

The SCC mix design development and evaluation led to the following conclusions:

- Three SCC mix designs were developed to bound current mix design development approaches. The mixes represent a range of acceptable SCC mix designs.

- The mixes were developed through trial and error iterations using fresh property test evaluations.

- The mixes were developed through the collaboration of representatives from the admixtures company, the precast company, and the research group.

- The mix design process showed that locally available products and equipment were suitable for producing SCC.

- Fresh property tests including the slump flow, VSI, J-Ring, and L-Box were used to develop the mix designs.

- The fresh property tests also helped to assess and determine consistent quality control of the mixes from batch to batch.

- The LBPT provided values that were used to relatively compare the bond between the prestressing strand and the different project concrete types.

- SCC 1 had the highest pull-out bond strength, and SCC 3 had the lowest of the three SCC mixes. However, these values were not considered critical for this project.

4 PRODUCTION OF SCC PRESTRESSED BOX BEAMS

4.1 Technical Considerations

SCC is considered an acceptable alternative to NCC in some projects because of its superior performance in the fresh or plastic state. Generally, SCC is used in projects with dense reinforcing schemes or complicated formwork. In these cases it is often difficult to consolidate the concrete, making SCC an alternative. The use of SCC can also make some casting processes faster and less complicated.

The production of box beams often used for highway bridge construction is one situation where SCC is considered a viable option. The cross section of the box beam contains a Styrofoam void that blocks out the center of the beam over specified lengths. The void is included to block out concrete where it does not add much resistance to the section and reduce the self-weight of the beam. For practical reasons, the void in the beam cross-section is obtained by a stay-in-place Styrofoam block. The creation of the void through the Styrofoam block makes casting the beam both time and labor intensive, as the process requires several steps. The use of SCC could reduce these steps. However, implementing SCC is not as easy as simple as just changing the concrete. One main challenge is to determine the pressure generated by the flowable concrete onto the formwork. For the production of box beams it further implied holding the Styrofoam block in the correct position as the concrete is poured into the formwork. The Styrofoam block must be restrained against the force of the rising concrete and the restraints should not affect the finished process.

During the production of the beams for this project these tests offered important information on the consistency and quality control of the concrete. All three tests were

conducted on the first SCC batch of the day. The results of these tests determined whether that the SCC batch just mixed was adequate for placement in the beams. Subsequent batches were subjected only to the inverted slump flow test to verify the flow parameters of the concrete. If substantial differences in the slump flow value were observed from batch to batch throughout the day, adjustments were made to the mix designs to bring the flow into an acceptable range.

Current precast/prestressed industry practice for producing box beams requires four stages, making it both time and labor intensive. This process includes putting the prestressing strand, bottom stirrups, and metallic straps (ties to secure the Styrofoam block) in place on the casting bed during the first stage. The top reinforcing steel cage, including stirrups and longitudinal reinforcement, are assembled and set aside. Figure 17 shows a casting bed that was prepared to cast an NCC beam for this project. In the second stage the bottom flange of the beam is cast. As the concrete is poured into the form it is vibrated with mechanical vibrators. The level of the concrete in the bottom flange is checked to ensure that proper thickness of the bottom flange was achieved. Figure 18 shows the bottom flange of the NCC beam being poured. Once the bottom flange is poured, consolidated, and leveled, the Styrofoam block and the pre-tied top-reinforcing cage are secured in place during the third stage of the production process. Figure 19 shows the concrete poured in the bottom flange with the void in place. This step must be done as fast as possible to ensure that the concrete in the bottom flange remains plastic so that a homogeneous joint can be made upon casting the webs of the box section. Figure 20 shows the amount of activity required for the crew to secure the pre-tied top portion of the reinforcing steel. In the fourth and final stage of the process

the webs, or sidewalls, and top flange are cast. During the fourth stage, the concrete is poured directly on top of the Styrofoam block and manually distributed throughout the formwork. This process is shown in Figure 21. Sufficient vibration is used in the sidewalls to ensure that a cold joint does not develop between the bottom flange and the sidewalls.

Figure 17. NCC Casting Bed Prior to Casting
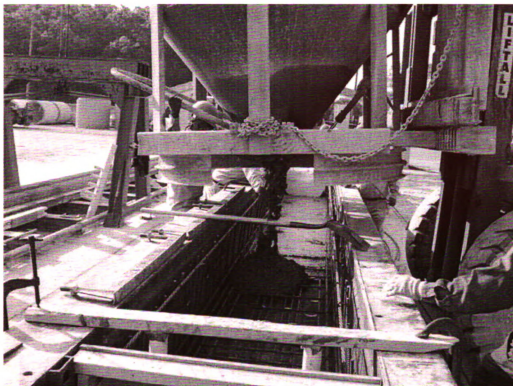
Figure 18.   Casting NCC Beam

Figure 19. The Bottom Flange of The NCC Beam

Figure 20. Installing Top Reinforcement On NCC
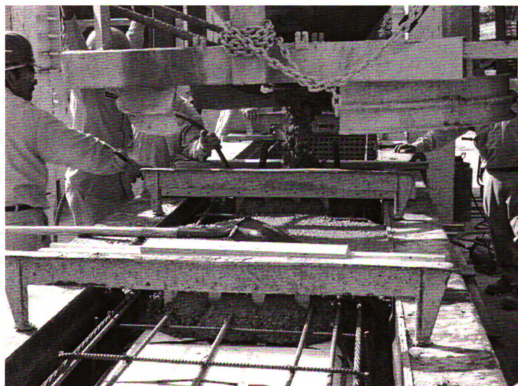
Figure 21. Casting Top Flange and Side Walls In NCC Beam

One advantage of using SCC to cast the box beams is the elimination some of the labor-intensive steps that occur during the conventional casting process with NCC. With SCC the box beam production process can be reduced to two steps. In the first step for producing the SCC box beams for this project, all of the reinforcing steel and Styrofoam blocks were put in place. Plastic spacers were used to ensure the correct vertical and horizontal location of the Styrofoam block, and were left inside the concrete. The void was tied to the prestressing strands in the bottom flange of the beam with metallic straps to ensure that it did not rise with the rising level of concrete. Figure 22 shows an SCC mock-up beam with all reinforcement and voids in place before casting.
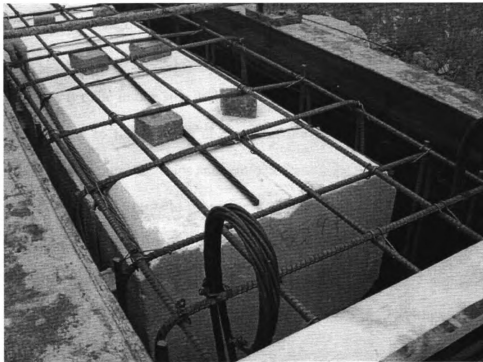
Figure 22. SCC Beam Ready to Be Cast
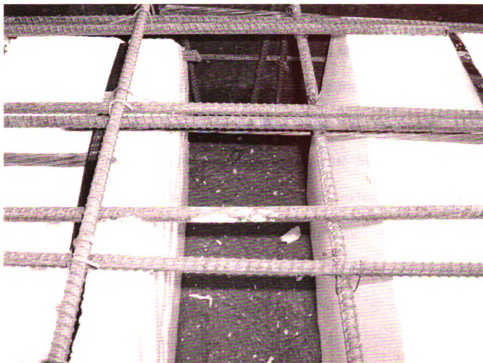
Figure 23. Rising Concrete in SCC Beam

In the second stage of the production process using SCC, the concrete is placed in the forms. This is done in one step without any vibration. The high flowability of SCC allows the concrete to flow around obstacles in the formwork. Figure 23 shows the concrete as it flows around the voids and reinforcement.

There are multiple ways to place the SCC in the formwork. The location where the concrete is poured into the form can play a role in the performance of SCC. One option is to pour the concrete at one end of the form and allow it to flow along the length of the beam. If the concrete does not have sufficient fluidity it would not be able to successfully flow along the entire length of the beam and the pouring location would have to be moved. A second option is to pour the concrete between the void and the side of the formwork. When added to the form in this manner, the concrete is able to flow under the void and begin to flow up the other side of the formwork. The discharge point

can be moved along the length of the beam so that the concrete can fill the entire form evenly. Figure 24 shows the concrete being discharged into the sidewall of the beam formwork. After the concrete reaches the top level of the formwork, the concrete can be poured on top of the void, and the concrete can flow along the void to cast the top flange.

A production plan was developed to ensure that SCC was suitable for the production of box beams. This process included the production of mock-up beams similar to the beams being cast for the bridge construction. The following sections discuss this production process, including results and observations from the casting operations.
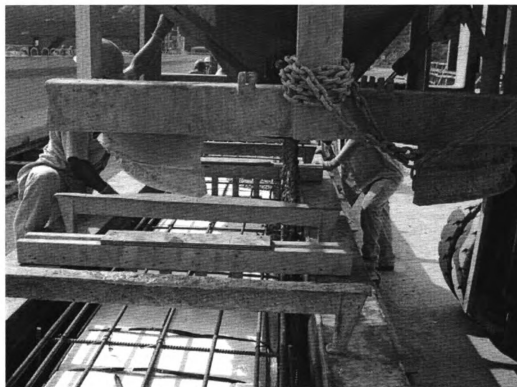
Figure 24.   Casting SCC Beam

4.1.1 Specimen Mock-up

To ensure that box beams could be produced in reduced steps using SCC, a mock up trial was conducted on May 16th and 18th of 2005. The purpose of the mock ups was two fold: (1) the process of filling the formwork with fewer steps needed to be verified, ensuring that the Styrofoam void could be properly restrained; and (2) experience needed to be gained from batching continuous SCC to ensure the ability to consistently produce high quality SCC.

One mock-up beam was cast for each of the four project mix designs, SCC 1, SCC 2, SCC 3, and NCC. The plan and cross-section of the beams are shown in Figure 25 and Figure 26. Each mock-up beam had a length of 20' and cross section dimensions of 27" x 36". The bottom and side flanges were 4.5" thick and the top flange was 5" thick. Five 0.6" diameter prestressing strands reinforced the bottom flanges of the beams. Each strand was prestressed to 43.8 kips. Five #4 reinforcing bars spaced at six inches were included in the top flange of the beam and U-shaped #4 stirrups were spaced evenly along the length of the beam in both the top and bottom flanges for shear reinforcement. One 14-inch diaphragm was located at the center of each beam and a 2-foot solid end block was cast at each end. The design 28-day compressive strength of the concrete was 5,500 psi, with a minimum of 4,000 psi required to release the strands.
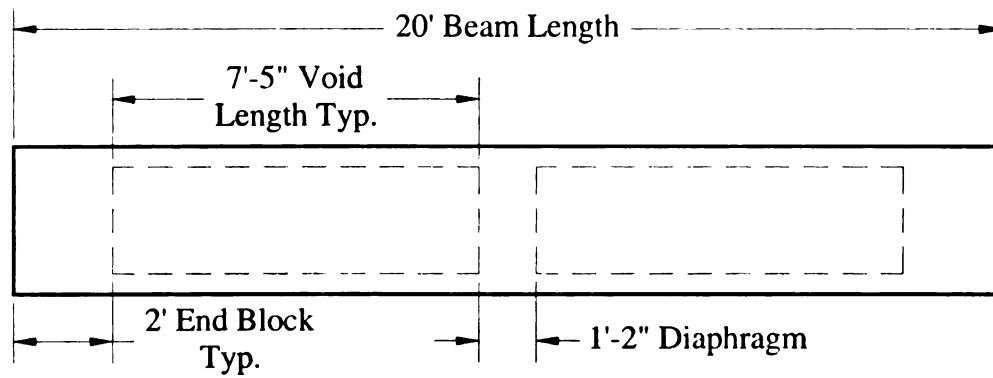
Figure 25. Mock-Up Beam Plan

During the construction of the mock-up beams, concrete was mixed in 2 yd^3 batches. The Inverted Spread Flow, J-Ring, and L-Box tests were conducted on the first batch from each mix design to verify the quality of the SCC used in the mock-ups. Subsequent batches were tested only with the Inverted Slump Flow to verify that the SCC was being produced consistently. The results of the initial tests are presented in Table 15. The concrete was transported from the batching area to the casting bed using one discharge bucket carried on a fork truck. The concrete was placed in the forms by discharging it from the bucket at multiple locations along the forms. The location and speed of the discharge were varied throughout the production of the mock-up beams to determine the effect this would have on the filling ability of the SCC.
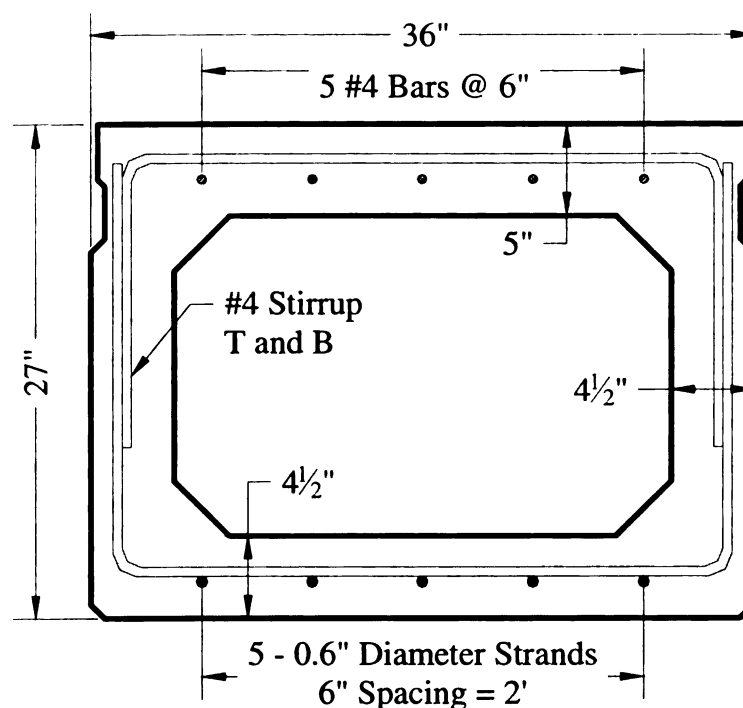
Figure 26. Mock-up Cross Section

Table 15. Mock-Up Fresh Property Test Results

	SCC 1	SCC 2	SCC 3
Inverted Spread Flow Test			
Spread (in.)	26	28.5	27
VSI	0.5	1.0	0.5
J-Ring Test			
Spread (in.)	21.75	27.5	23
J-Ring Value	0.75	0.375	1
L-Box Test			
L-Box	0.56	0.56	0.66

4.1.2 NCC Observations

The process described above used to cast the NCC mock-up beam took an hour or more to complete. However, it is important to note that some of this time was spent waiting for concrete to be delivered from the mixing area to the casting bed. In one instance a batch of concrete was thrown away as it did not meet quality control standards,

significantly adding to the total casting time. Still the casting process with NCC is cumbersome and difficult, as it requires significant amounts of labor and time. By reducing the number of steps in the process, the production cost and throughput can be improved.

4.1.3 SCC Observations

4.1.3.1 SCC 1 Observations

To cast the SCC 1 mock-up beam, the concrete was poured along the side of the beam between the edge of the form and the Styrofoam block. The fluidity of the concrete allowed it to flow under the void and rise up on the opposite side. The concrete flowed along the length of the beam and around all obstacles. The discharge location was moved to several locations along the beam. Like the NCC mock-up beam, this process took approximately one hour to complete. Again significant time was spent waiting for concrete to be transported to the casting area. In addition, two SCC 1 batches were discarded due to poor test performances. The number of workers helping with the casting process was reduced by half compared to the NCC beam.

After the casting of this beam was completed, it was discovered that the Styrofoam void was not adequately restrained. The hydraulic force from the concrete filling the form pushed the Styrofoam void against the steel straps that were supposed to hold it in place. The force was large enough to cause the Styrofoam to crush locally at the straps allowing the void to rise 1" or more along the entire length of the beam. Even though the void rose significantly, a flat top surface was achieved on the beam as can be seen in Figure 27.

Figure 27. Finished SCC 1 Mock-Up Beam

4.1.3.2   SCC 2 Observations

The process of casting the SCC 2 mock-up beam was altered slightly to assess the effect of discharge location on the ability of the concrete to fill the formwork. For the SCC 2 beam, the concrete was discharged into the end block to see if the concrete could flow the entire length of the beam. The concrete was successful in flowing along the beam length as is evidenced in Figure 28, where the edge of the concrete flow can be seen emerging from under the void.

After the first batch of concrete was discharged into the form, the concrete self-leveled along the length of the beam. This showed that the SCC 2 concrete was able to flow well along the length of the beam. The second batch of SCC 2 was discharged into the diaphragm at the center of the beam. The rate of the discharge was increased to see

the effect of the discharge rate on the flow properties of the concrete. The resulting hydraulic force caused the Styrofoam block to rise significantly. As the block rose, the reinforcing cage was lifted to such a degree that a flat top surface could not be achieved on the beam. The reinforcing steel can be seen above the top edge of the formwork in Figure 29 and Figure 30. The number of workers required to cast the SCC 2 beam was comparable to the number of workers used in the SCC 1 beam. The time that was spent in casting the SCC 2 beam was also comparable to the SCC 1 and NCC beams. Again time was spent waiting for the concrete to be delivered to the casting bed.

Edge of
Concrete Flow
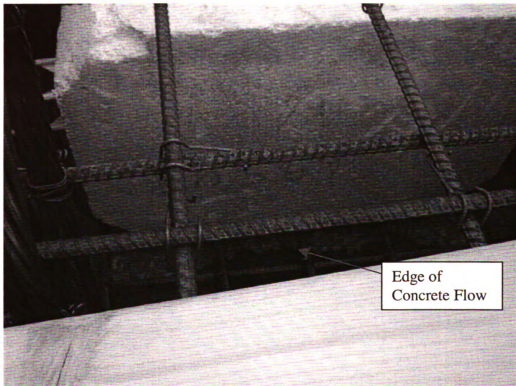
Figure 28. SCC Flowing to End of Formwork

Figure 29. Finished SCC 2 Beam With Exposed Reinforcing Steel
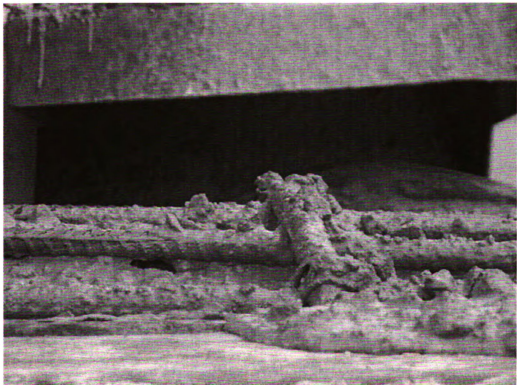
Figure 30. Result of Void Movement in SCC 2 Beam

4.1.3.3   SCC 3 Observations

During the casting of the SCC 3 mock-up beam care was taken to prevent any movement of the Styrofoam block and the reinforcing steel. The concrete was discharged along the side of the void as was done previously in the SCC 1 beam. The rate of discharge was also minimized to reduce the force of the flowing concrete on the block. In the end, even with the precautionary measures, the Styrofoam block raised similarly to the SCC 1 beam. A flat top surface was obtained on the beam as can be seen in Figure 31. However, it is clear that the reinforcement had been vertically shifted due to the uplift of the Styrofoam block. The casting time of the SCC 3 beam was lower than the previous beams as the concrete was mixed more efficiently.
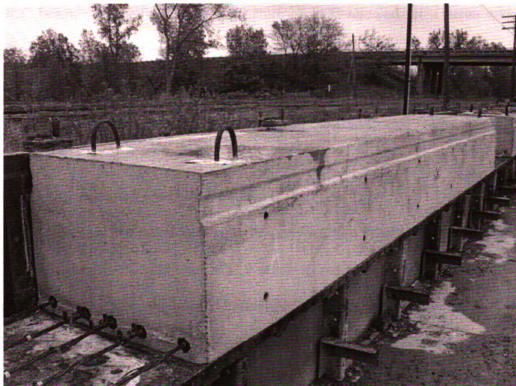
Figure 31. Finished SCC 3 Mock-Up Beam

4.1.4 Discussion

While the production of the mock-up beams confirmed that SCC was able to flow along the length of the beam and around all of the obstacles in the formwork, the performance was hampered because of the inability to properly restrain the Styrofoam block. The reduction in time that was expected from the reduced steps required to cast the SCC beams was not realized as any time improvements were counteracted by the increased time to mix and test the SCC. Inefficiencies in the mixing process caused down time at the casting bed. However, a reduced labor force was used to cast the SCC beams. Approximately half of the workers used to cast the NCC beams were needed to cast the SCC beams. Another result observed in the production of the mock-up beams was the improved surface quality that was evident in the SCC beams when compared to the NCC beam. The self-consolidating nature of SCC allowed for a better and more complete compaction of the concrete, which was evident by the presence of fewer and smaller deformities on the concrete surface, or "bug holes." A discussion of the conclusions reached during the mock-up beam production follows.

4.1.4.1 Styrofoam Void Hold Downs

As a result of the failed attempt to properly restrain the Styrofoam void in any of the three SCC beams an additional SCC 2 mock-up beam was produced two days after the initial attempt. The concrete used in the additional mock-up beam had a spread flow of 25 in., and a VSI rating of 0.5. The remaining fresh property values were not provided by the fabricator. To further restrain the void in this additional mock-up, wood restraints were constructed and placed along the length of the beam as shown in Figure 32. The restraints were bolted to the side metal formwork to keep them in the proper location as

shown in Figure 33. A full view of the Styrofoam block restraints is shown in Figure 34. The restraints consisted of two 2 in. x 4 in. cross beams separated by a 2 in. x 2 in. spacer. Four 2 in. x 2 in. legs extended from the cross beams to hold the block at the proper height. A 1/8-inch masonite plate was placed under the restraints to prevent the legs of the restraint from punching through the Styrofoam block. The masonite plate remained embedded in the concrete after the concrete cured. Once the concrete was in place and before it began to set the restraints were removed, as shown in Figure 35. Figure 36 shows the scar left on the surface of the beam after the restraint was removed. This scar was smoothed over by traditional finishing of the beams.

The additional restraints were successful in keeping the Styrofoam block in place during the casting of the final mock-up beam. No movement of the block was observed after the concrete was placed. Importantly, the concrete was able to flow through the legs of the restraints without blocking. The finished product, seen in Figure 37, shows the result of the improved production process.
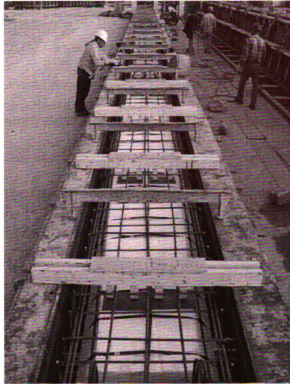
Figure 32. Void Restraints Spaced Along Beam Length
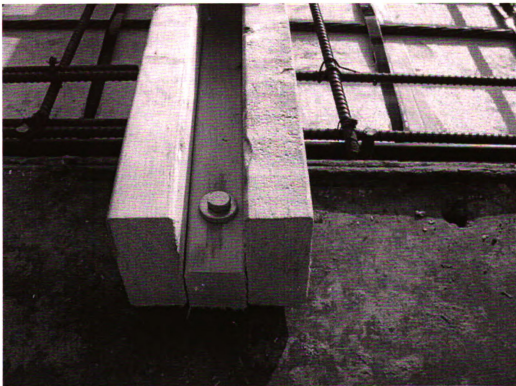
Figure 33. Void Restraint Bolted to Formwork
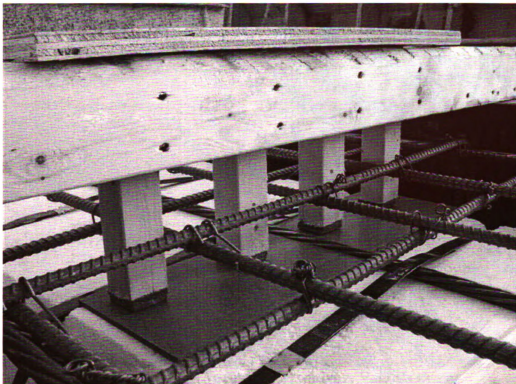
Figure 34. Close up of Void Restraint

Figure 35. Removing Void Restraint From Finished Beam
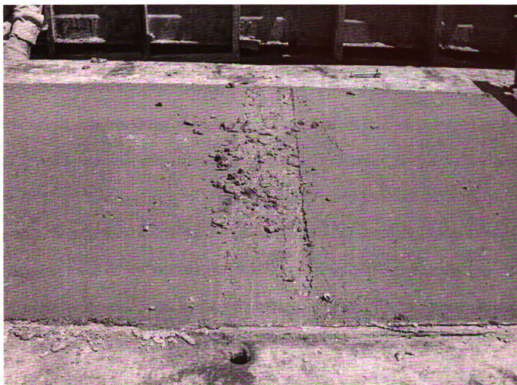
Figure 36. Scar On Surface of Beam from Void Restraint
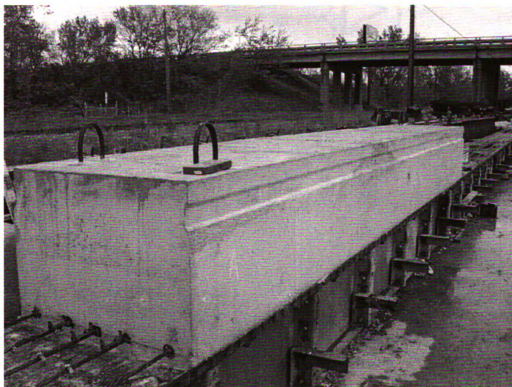
Figure 37. Finished SCC 2 Beam Cast With Additional Void Restraints

4.1.4.2   Surface Finish Quality

The improved surface quality of SCC is evidenced by a reduction in the size and number of visible surface imperfections. The ability of the concrete to consolidate under its own weight removes many of the surface imperfections that are common with NCC. The SCC mock-up beams showed fewer and smaller "bug holes" on the surface than seen on the NCC mock-up. Figure 38, Figure 39, and Figure 40 show this clearly. While some marks were present on the surface of the SCC 1 specimen they are not as numerous, or as large, as those on the NCC beam. The SCC 2 beam had better appearance than the SCC 1 beam, with even fewer surface imperfections. The SCC 3 beam (not pictured) also had an improved surface quality compared to the NCC beam.

Figure 38. SCC 1 Surface Quality

Figure 39. SCC 2 Surface Quality

Figure 40. NCC Surface Quality

4.1.4.3   Mixing and Batching Process

Even though the production of a box beam using SCC requires only two steps, the time to cast the SCC beams was equal to that required for the NCC beams. Much of the time that it took to cast the beams was spent waiting for concrete to be delivered to the casting bed from the mixing area because concrete was not being mixed efficiently. A new batch of concrete was not started until the bucket returned from the casting bed, so nothing could happen at the casting bed while the concrete was being mixed and tested. If the fresh performance of the concrete was adequate then the batch would be taken to the casting bed. If it was not adequate, modifications were made to the concrete and a second round of tests was conducted. It was learned that the use of two discharge buckets carried by two fork trucks and continuous mixing of concrete would allow concrete to be poured into the formwork continuously thus eliminating the time where the crew at the casting bed was waiting for concrete. As one discharge bucket was being discharged at the casting bed the second would be being filled at the mixing plant. This batch could be tested and the fork truck could take the next batch to the casting bed as the first bucket was returned to receive the next batch. This continuous flow could save time in the process. Given the experimental nature of the mock-up beams, the time required to cast the SCC beams was reasonable, however this time did not reflect the reduced cycle times possible when using SCC.

In the casting of all three SCC mock-up beams, some batches of the SCC had to be thrown away as they were improperly mixed. To have an efficient flow of concrete from the mixing area to the casting bed, the mixes need to be of consistent quality. Significant time was wasted as batches had to be altered to achieve acceptable fresh

property performance. On a given day it may take several attempts to produce consistent concrete as the mix design is modified for factors such as moisture content of the aggregate and humidity. These same modifications are made to NCC with greater success as the concrete producer has more experience working with NCC. With time and experience concrete producers can produce SCC of a consistent quality without significant added time for adjusting batch properties.

4.1.4.4 Strand Draw –in Measurements

When the prestressing force is transferred to the box beams the prestressing strands retreat into the beams a small amount. The amount the strands move into the beam is controlled by the bond strength between the prestressing stand and the concrete. In an attempt to quantify the bond strength through this "draw-in" value, measurements of an arbitrary length were taken on selected strands before and after the release of the prestressing force. The measurement was taken between a reference point on the strand and the face of the beam using a digital caliper. The reference point was determined by connecting a 1 in. wide section of a steel channel to the prestressing strand with hose clamps. The measurement was taken from the leg of the channel farthest from the face of the beam.

The measurements from the mock-up beams are shown in Table 16. In this table negative values have been removed. Negative values would imply that the distance between the face of the beam and the reference point got larger after transferring the prestressing force to the beam. This is not possible as the strand draws into the beam. It is more likely that the reference point moved. The process of transferring the prestressing force to the beam by fire cutting the strand causes a very violent expansion

of the strand. This expansion is so great that it sometimes plastically deformed the hose clamps. After the completion of the mock-up beams the measurement of the strand draw in using steel channel and hose clamps was deemed unreliable. A second method of creating a reference point directly on the prestressing strand by means of a gouge or notch was ruled out for safety reasons. Therefore, these measurements were not taken during the production of the project beams.

Table 16. Strand Draw-in Measurements

Mix	End A				End B			
	Strand	Draw-in	Avg.	Std Dev	Strand	Draw-in	Avg.	Std Dev
SCC 1	1	0.0060	0.0060	-	1	0.0538	0.0357	0.017
	2	-			2	0.0332		
	3	-			3	0.0200		
SCC 2	1	0.0762	0.0762	-	1	-	-	-
	2	-			2	-		
	3	-			3	-		
SCC 3	1	0.0137	0.0538	0.0805	1	-	0.0070	0.0028
	2	0.1465			2	0.0090		
	3	0.0013			3	0.0050		
NCC	1	-	0.0310	-	1	0.0267	0.0375	0.0151
	2	-			2	0.0310		
	3	0.0310			3	0.0548		
SCC 2-2	1	-	0.0172	0.0019	1	-	0.0283	0.0354
	2	0.0158			2	0.0032		
	3	0.0185			3	0.0533		

4.2 Beam Production

4.2.1 Overview

Once mock-up beams were produced with satisfactory results, the actual bridge beams could be made. Four casts were needed to produce the 17 beams. All of the beams were cast in late June and early July of 2005. At each of the first three castings,

five beams were cast in a 300-foot casting bed. At these times, three of the beams cast were of one SCC mix design type and two were of the NCC mix design. A fourth cast was conducted to complete the final two NCC beams.

For each concrete mix design three beams were cast to play a specific role in this project. One of these beams was instrumented to monitor strain and temperature in the demonstration bridge; this beam is referred to as the field beam. Two of the beams were instrumented for laboratory evaluations. The laboratory evaluations consisted of two four point bending tests to evaluate the shear and flexural performance of the beams. These beams are referred to as the shear beam and flexure beam respectively. Two additional bridge beams, were cast using NCC and were included in the bridge but not instrumented. Finally three extra beams were cast using NCC. These beams were available to replace any SCC beam in the demonstration bridge that did not perform satisfactorily in laboratory evaluations. Figure 41 shows the casting sequence for the four casting days.

Cast #1 (6-21-05)

|← —————————— 300' Casting Bed —————————— →|

| SCC 1
Flexure Beam | SCC 1
Shear Beam | SCC 1
Field Beam | NCC
Flexure Beam | NCC
Shear Beam |

|← ———————————— 5 Beams @ 52' ———————————— →|

Cast #2 (6-24-05)

|← —————————— 300' Casting Bed —————————— →|

| SCC 2
Shear Beam | SCC 2
Flexure Beam | SCC 2
Field Beam | NCC
Field Beam | NCC
Bridge Beam |

|← ———————————— 5 Beams @ 52' ———————————— →|

Cast #3 (6-29-05)

|← —————————— 300' Casting Bed —————————— →|

| SCC 3
Shear Beam | SCC 3
Flexure Beam | SCC 3
Field Beam | NCC
Bridge Beam | NCC
Extra Beam |

|← ———————————— 5 Beams @ 52' ———————————— →|

Cast #4 (7-1-05)

|← —————————— 300' Casting Bed —————————— →|

| | | NCC
Extra Beam | NCC
Extra Beam | |

|← 2 Beams @ 52' →|

Figure 41. Casting History

4.2.2 Beam Geometry

The box beams were 36 in. wide by 27 in. deep. The top flange was 5 in. thick while the bottom and side flanges were 4.5 in. thick. The Styrofoam void cross section was 27 in. wide by 17.5 in. deep. Each beam was 52 ft long with a 2-ft solid block on each end. An 8-in. wide diaphragm was located at the center of each beam. The

Styrofoam void between the end block and the diaphragm is 23 ft - 8 inches long. The beam plan and cross section are shown in Figure 42 and Figure 43. The beams had a non composite concrete area of 509.4 square in. and a moment of inertia of 47,223 in^4. The neutral axis for the beams was found to be 13.6 in. from the bottom of the beam, or 13.4 in. from the top of the beam. The composite beam, with the deck considered, had a concrete area of 1,373 square in. and a moment of inertia of 155,789 in^4. The neutral axis of the beam with the deck moves to 24.86 in. from the bottom of the beam. This information is summarized in Table 17.

Table 17. Untransformed Section Properties

Time Step	Area (in^2)	I (in^4)	y (in.)
Non Composite	509.40	47,223	13.60
Composite	1,373	155,789	24.86

The beam's main reinforcement consisted of 16 - 0.6" diameter prestressing strands arranged in three rows in the bottom flange of the beam as shown in Figure 43. Two of the strands in the bottom row were debonded 4 ft from the end of the beam. An additional two 0.6" diameter prestressing stands were included in the top flange of the beams. These strands were debonded 13 ft in either direction from the center of the beam. The prestress jacking force for all 18 of the strands was 43,900 pounds. Other reinforcing steel consisted of 5 - #4 bars in the top flange with six-inch spacing, and #4 U-shaped shear stirrups in the top and bottom of the beam. The stirrups were spaced in the following way: two spaces at 2.25 in., 12 spaces at 6 in. then 12 in. spaces. The shear stirrups are not shown in Figure 43. All 17 beams were identical in size and reinforcing details. The only exception was that the beams produced for laboratory testing did not include slab ties

86

Figure 42. Beam Plan

▣ Debonded 4' from end
◈ Debonded 13' in each direction
from the center of the beam
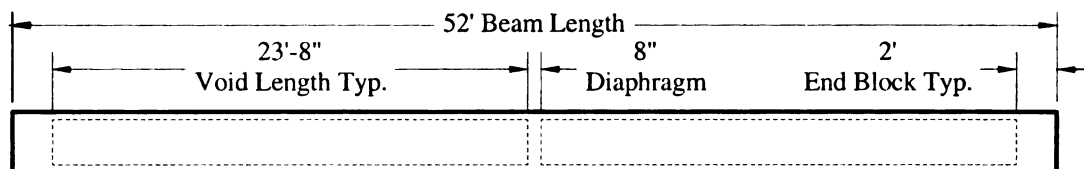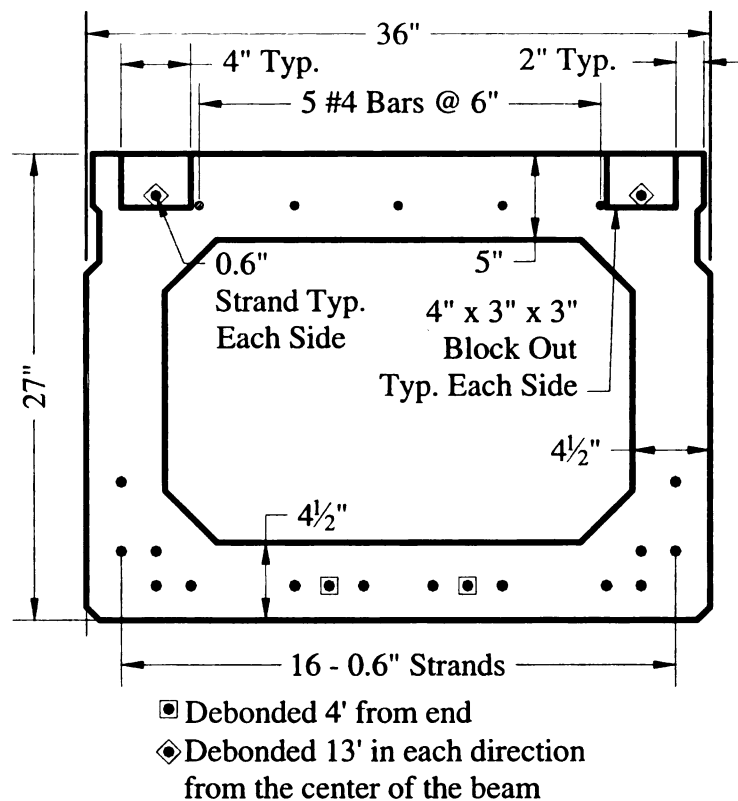
Figure 43. Typical Beam Cross Section

4.2.3   Casting Process

The casting of these beams required extensive collaboration between the MSU research team and the fabricator's work crew. This was due in part to the instrumentation that was installed in the beams and to the use SCC. Two days of work were required before the actual casting could take place.

87

The work prior to casting included preparing the formwork at the casting bed and arranging the prestressing strand. An initial force of 5,000 lbs was placed on the strands to pull them taught. The MSU research team then applied the foil strain gages to the strands in the necessary locations. Then the strands were loaded to the required prestressing force. With the strands in place the fabricator's crew could begin attaching the reinforcing cages. In the case of the two NCC beams, only the bottom stirrups and metallic void ties were put in place. For the three SCC beams the entire reinforcing cage and voids were placed in the beds. During this process the MSU research team installed the instruments in the field beams. Once the instruments were installed, the instrument wires were bundled together in a debonding strip, run along the length of the beam and out the south bulkhead of the formwork. Foil strain gage wires from the laboratory test beams were routed up the nearest stirrup and through a piece of debonding strip at the top face of the beam.

In all four casts, the NCC beams were cast first. SCC is more sensitive than NCC to the moisture content of both the mixing drum and aggregate. By mixing NCC in the mixer before SCC, the mixer was "primed". The 2 cubic yard batches of concrete were transported to the casting bed in discharge buckets carried by fork trucks. Instead of using one bucket and fork truck in the casting process as was done during the production of mock-up beams, two buckets were used in the production of the project beams. This was done so that there was no delay at the beds waiting for concrete. As one bucket was being emptied into the formwork the second bucket was being filled at the mixing plant.

For the SCC beams, the concrete was poured along one edge of the beam formwork between the Styrofoam void and the formwork. The SCC was able to flow

under the void in all directions and began to come up the other side of the formwork. The dumping location moved down the beam until approximately half of the beam was poured. Once this was accomplished the concrete was dumped on top of the void starting at the farthest end.

4.2.4 First Cast (6/21/05)

The beams cast on the first day included the two NCC laboratory evaluation beams, and the three SCC 1 beams. All of the instruments were put in place before the morning of the cast. Initial readings from the instruments were recorded on the morning of the cast. The entire casting process took approximately 5 hours to complete. During this time the temperature ranged from the 70 °F at the start of the cast to the 85 °F at the end of the cast. For the entire day the average temperature was 71 °F with a maximum temperature of 85 °F and an average relative humidity of 71%. The day was mostly cloudy.

4.2.4.1   NCC Beams

In total, eight – 2 yd^3 and one – 1.5 yd^3 batches of NCC were produced for a total of 17.5 yd^3. The actual and target average values for the NCC mix design are shown in Table 18. These values are shown for information only as a representation of all of the concrete mixes produced during this cast. This is not the mix design that was used to cast this beam. Any significant deviations from the expected mix design were made by the fabricator without the knowledge of the researchers. The specific values for each of the 9 NCC batches are listed in APPENDIX B.

The first NCC beam casting began at 8:30 am. The bottom flange was finished 15 minutes later at 8:45 am. The top reinforcing steel cage placement began at 8:50 am. The sides and top flange of the beam began at 9:20 am and the beam was finished at 9:50 am, 1 hour and 20 minutes after the casting began.

The second NCC beam casting began at 9:45 am and the bottom flange was finished at 10:00 am. The void and top reinforcing steel were in place in the second NCC beam by 10:30 am and the beam was finished by 11:00 am. The second NCC beam took 1 hour and 15 minutes to cast. These times are summarized in Table 19.

Table 18. Average NCC Mix Design

	Target Value	Actual Value
Constituents (lbs/yd³)		
Cement	564	566
Fine Aggregate	1353	1347
Coarse Aggregate	1877	1882
Total water	219	218
w/c	0.39	0.39
Admixture (oz/yd³)		
Air Entraining	11	10
VMA	20	20
HRWR	64	63

Table 19. NCC Beam Casting Time

Event	NCC-1	NCC-2
Start of Casting Bottom Flange	8:30 am	9:45 am
End of Casting bottom flange	8:45 am	10:00 am
End of placing voids and top reinforcement	9:20 am	10:30 am
End of casting beam	9:50 am	11:00 am
Total Time	1 hr 20 min	1 hr 15 min

The average time between NCC batches during the first casting was 18 minutes 19 seconds and the average mixing time was 5 minutes 20 seconds. The time between batches is representative of how much time was spent without concrete being cast. This average includes relatively short times when concrete is being poured in the forms, but it also includes time spent putting the void and reinforcement in place. From Table 19 it can be seen that the time between the end of the casting of the bottom flange and the end of placing the voids and top reinforcement was 35 and 30 minutes. During this time no concrete was being poured into the formwork. If this time becomes too long the concrete poured into the bottom flange could begin to set. If this occurs, a cold joint could form between the sidewall and bottom flange.

During the casting of the NCC beams anywhere from 10 to 18 members of the fabricator's work crew were working on the beam. The greatest work force was required in the second stage of the casting process when the reinforcing cage had to be completed. This process is shown in Figure 20.

4.2.4.2   SCC 1 Beams

During the casting of the SCC 1 beams, 13 - 2 yd^3 and one – 1 yd^3 batches were produced for a total of 27 yd^3. The average actual and target values for the SCC 1 mix design are shown in Table 20. These values are shown for information only as a representation of all of the concrete mixes produced during this cast. This is not the mix design that was used to cast this beam. Any significant deviations from the expected mix design were made by the fabricator without the knowledge of the researchers. For the first SCC 1 batch of the day, the Slump Flow, J-Ring, and L-Box tests were all conducted. These values, along with the air content, unit weight, and concrete

temperature are reported in Table 21. For the remaining batches, only the Slump Flow test was conducted. The results of these tests are shown in Table 22. The average Slump Flow value was over 26 inches within the 27 inch plus or minus 1 inch range specified in the project special provisions. The mix designs for all of the SCC 1 batches produced during the first cast are listed in APPENDIX C.

Table 20. Average SCC 1 Mix Design

	Target Value	Actual Value
Constituents (lbs/yd^3)		
Cement	700	705
Fine Aggregate	1656	1651
Coarse Aggregate	1350	1357
Total water	260	262
w/c	0.37	0.37
Admixture (oz/yd^3)		
Air Entraining	12	12
VMA	21	21
HRWR	105	105

Table 21. SCC 1 Fresh Properties

Test	SCC 1
Slump Flow (in.)	27
J-Ring Flow	26
J-Ring Value	0.75
L-Box Ratio	0.79
Air (%)	6.58
Conc Temp (F)	77.7
Unit Wt (lb/yd^3)	142

Table 22. SCC 1 Slump Flow Values

Batch	Average Slump Flow (in.)
1	27
2	26.75
3	26.5
4	25.75
5	27.75
6	26.5
7	28.5
8	28.25
9	23.5
10	25.75
Average	26.6

The time it took to cast the three SCC 1 beams is shown in Table 23. The beams took an average of 31 minutes to cast. This is compared to over 1 hour 15 minutes in the NCC beams. The average time between SCC 1 batches was approximately 8 minutes. This is much faster than the 18 minutes between the NCC batches. The average mixing time for the SCC 1 was batches 6 minutes 51 seconds, which was approximately 1 minute longer than for the NCC batches.

Not only is the total time to produce the batches significantly reduced, the number of people required to cast these beams was also significantly reduced. There were only three people required to cast the SCC 1 beams. Two people were needed to drive the two fork trucks carrying the discharge buckets from the batching plant to the casting bed. The third person was required only to discharge the concrete into the formwork.

Table 23. SSCC 1 Beam Casting Times

	SCC 1-1	SCC 1-2	SCC 1-3
Start	11:50 am	12:30 pm	12:54 pm
End	12:30 pm	12:50 pm	1:27 pm
Total Time (min)	40	20	33

4.2.5   Second Cast (6/24/05)

The second cast occurred on the 24th of June, three days after the first cast. The beams cast during this time included two NCC bridge beams including the instrumented demonstration beam, and the three SCC 2 beams. As in the first cast, all of the instruments were put in place before the morning of the cast. Initial readings from the instruments were recorded on the morning of the cast.

The weather for the second cast was very hot. During the approximately 5-hour casting period the temperature ranged from approximately 75 °F at 6:00 am to approximately 85 °F at 11 am. The average temperature for the day was 83 °F with a maximum temperature of 92 °F. The average relative humidity was 58% with sunny skies throughout the day.

4.2.5.1   NCC

A total of 16.6 yd^3 of NCC were produced for the second cast. The average values from the eight 2 yd^3 and one 0.6 yd^3 batches are shown in Table 24. These values are shown for information only as a representation of all of the concrete mixes produced during this cast. This is not the mix design that was used to cast this beam. Any significant deviations from the expected mix design were made by the fabricator without the knowledge of the researchers. The values for each batch are shown in APPENDIX D.

The time it took to cast each beam is shown in Table 25. The total time spent producing the NCC beams was 2 hours 31 minutes. The average casting time for both of the NCC beams was approximately 1 hour 15 minutes. The first NCC beams took 59 minutes to cast. It took approximately 20 minutes to complete each of the steps in the casting process. This included 20 minutes to pour the concrete for the bottom flange, 20 minutes to install and secure the voids and top reinforcing steel, and 20 minutes to pour the remaining concrete in the top flange and side wall. The second NCC beam took 1 hour 32 minutes to cast due to time spent routing instrument cables in the second beam. Once the top reinforcing steel was secured in place, the instrument cables had to be routed from their location near the center of the beam to the end of the beam. This took additional time that was not included in casting the other NCC beams. The average mixing time for the NCC batches was 10 minutes 40 seconds with an average of more than 19 minutes between each batch.

Table 24. Average NCC Mix Design

	Target Value	Actual Value
Constituents (lbs/yd^3)		
Cement	564	571
Fine Aggregate	1352	1368
Coarse Aggregate	1883	1889
Total water	221	221
w/c	0.39	0.39
Admixture (oz/yd^3)		
Air Entraining	11	10
VMA	14	13
HRWR	64	64

Table 25. NCC Beam Casting Times

Event	1st NCC Beam	2nd NCC Beam
Start casting beam	6:10 am	7:10 am
Finish casting bottom flange	6:30 am	7:17 am
Finish placing voids and top reinforcement	6:50 am	7:24 am
Finish casting beam	7:09 am	8:42 am
Total Time	59 min	1 hr 32 min

4.2.5.2 SCC 2

A total of 24 yd^3 of SCC 2 were produced in 12 - 2 yd^3 batches to cast all three of the SCC 2 beams. The average target and actual values for the SCC 2 mix design are shown in Table 26 with all of the batches being listed in APPENDIX E. These values are shown for information only as a representation of all of the concrete mixes produced during this cast. This is not the mix design that was used to cast this beam. Any significant deviations from the expected mix design were made by the fabricator without the knowledge of the researchers. From the mix design values, it can be seen that no major deviations from the target values occurred. SCC 2 was a combination type SCC, which means that the mix had a moderate amount of HRWR and VMA, a higher amount of fine aggregate, and a reduced amount of coarse aggregate when compared to NCC.

Table 26. Average SCC 2 Mix Design

	Target Value	Actual Value
Constituents (lbs/yd^3)		
Cement	700	709
Fine Aggregate	1488	1483
Coarse Aggregate	1438	1442
Total water	274	276
w/c	0.39	0.39
Admixture (oz/yd^3)		
Air Entraining	12	11
VMA	21	21
HRWR	84	84

The results of the fresh property tests conducted on the first SCC 2 batch are shown in Table 27. Slump flow values from 9 other batches (as measured by the fabricator) are shown in Table 28. The average slump flow from these 9 tests was 27 inches. This value shows that SCC could be produced within a reasonable range of the target slump flow. The 27-inch J-Ring flow indicates that the SCC 2 concrete had excellent passing ability. There was no change between the obstructed flow and the free flow. Values of air content, concrete temperature, and unit weight compare well with NCC.

Table 27. SCC 2 Fresh Properties

Test	SCC 2
Slump Flow (in.)	27
J-Ring Flow	27
J-Ring Value	0.25
L-Box Ratio	0.64
Air (%)	6.8
Conc Temp (F)	77.7
Unit Wt (lb/yd^3)	144

Table 28. SCC 2 Slump Flow Values

Batch	Average Slump Flow (in.)
1	28.25
2	28
3	27
4	27.75
5	25.5
6	27
7	27.5
8	26
9	26
Average	27

The times required to cast the SCC 2 beams are shown in Table 29. The total time to cast all three beams was 1 hour 16 minutes. On average it took 25 minutes to cast each of the three SCC 2 beams. The average time between SCC 2 batches being produced was 5 minutes 19 seconds. The SCC 2 batches mixed for an average of 3 minutes 42 seconds.

Table 29. SCC 2 Beam Casting Times

	SCC 2-1	SCC 2-2	SCC 2-3
Start	9:45 am	10:18 pm	10:36 pm
End	10:18 pm	10:33 pm	11:04 pm
Total Time (min)	33	15	28

4.2.6 Third Cast (6/29/05)

The third cast occurred on the 29th of June, five days after the second cast (including two weekend days). The beams cast during this time included the final two uninstrumented NCC bridge beams, and the three SCC 3 beams. As in the first and second casts, all of the instruments were put in place before the morning of the cast. Initial readings from the instruments were recorded on the morning of the cast.

The weather for the third cast was not as hot as the second cast. The temperature was between 70 °F and 80 °F during the 5-hour casting period from 5:30 am to 10:30 am. The average temperature for the entire day was 80 °F and the maximum temperature was 90 °F. The average relative humidity was 69% and the sky was mostly cloudy during the day.

4.2.6.1 NCC

A total of 18 yd^3 of NCC were produced for the third cast. The mix design, which is nearly identical to the NCC mix designs used in the previous two casts, is shown in Table 30. These values are shown for information only as a representation of all of the concrete mixes produced during this cast. This is not the mix design that was used to cast this beam. Any significant deviations from the expected mix design were made by the fabricator without the knowledge of the researchers. . From each mix design listed in APPENDIX F it is possible to see that some mixes contained no VMA while others had amounts consistent with that used in the previous casts.

Table 30. Average NCC Mix Design

	Target Value	Actual Value
Constituents (lbs/yd^3)		
Cement	564	567
Fine Aggregate	1354	1349
Coarse Aggregate	1885	1888
Total water	220	221
w/c	0.39	0.39
Admixture (oz/yd^3)		
Air Entraining	9	8
VMA	5	5
HRWR	64	64

The times required to cast each beam were not recorded for the third cast. From the information provided by fabricator regarding the production of concrete batches it can be seen that concrete was produced from 5:30 am to 7:45 am. This is consistent with the two previous casting operations. In cast one and two, the production of the NCC beams took approximately 2 hours and 30 minutes to complete. The average time between batches was 17 minutes 43 seconds and the average mixing time was 2 minutes 49 seconds.

4.2.6.2   SCC 3

The total volume of SCC 3 produced for the third cast was 28 yd^3. This was done in 14-2 yd^3 batches. The average target and actual mix designs used for all 14 batches are shown in Table 31. These values are shown for information only as a representation of all of the concrete mixes produced during this cast. This is not the mix design that was used to cast this beam. Any significant deviations from the expected mix design were made by the fabricator without the knowledge of the researchers. The amounts used in all 14 batches are included in APPENDIX G.

The results of the fresh property tests on the first SCC 3 batch are shown in Table 32. The 23.25 inch slump flow value is below the target of 27 inches. From Table 33 the average slump flow was 23.45 inches. The fabricator had difficulty in producing concrete at the high flow value desired. However, the concrete was still able to flow around the obstacles in the formwork. A 23-inch slump flow was sufficient to fill the forms for this project. Even though the concrete did not meet the requirements for this project it was selected because it was able to adequately fill the formwork without sacrificing the quality of the product.

Table 31. Average SCC 3 Mix Design

	Target Value	Actual Value
Constituents (lbs/yd^3)		
Cement	700	709
Fine Aggregate	1374	1369
Coarse Aggregate	1458	1461
Total water	310	310
W/c	0.44	0.44
Admixture (oz/yd^3)		
Air Entraining	8	8
VMA	21	21
HRWR	56	55

Table 32. SCC 3 Fresh Properties

Test	SCC 3
Slump Flow (in.)	23.25
J-Ring Flow	22.25
J-Ring Value	1
L-Box Ratio	0.56
Air (%)	6.3
Conc Temp (F)	80
Unit Wt (lb/yd^3)	140.72

The total time to cast all three SCC beams was 1 hour 40 minutes. The average time for the three beams was 33 minutes. The average mixing time was 2 minutes 45 seconds and on average 6 minutes 41 seconds elapsed between each batch being produced.

Table 33. SCC 3 Slump Flow Values

Batch	Slump Flow (in.)
1	22.5
2	23.75
3	23.25
4	23
5	23.25
6	23.25
7	23.75
8	23.75
9	25
10	23
Average	23.45

4.2.7   Fourth Cast (7/1/05)

The fourth and final cast occurred on the 1st of July. The beams cast during this time included the two additional NCC bridge beams that served as back ups in case any of the SCC mix designs beams did not perform satisfactorily in the laboratory evaluations. No instrumentation was included in these beams.

The weather during the fourth cast was much milder than the first three. The casting took 3 hours and began at 5:30 am. The temperature did not vary significantly during the day as the temperature remained in the 70's for the duration of the cast. The average temperature on this day was 64 degrees with a maximum temperature of 74 degrees. There were scattered clouds in the sky during the casting and the average relative humidity for the day was 67%.

4.2.7.1   NCC

A total of 16.6 yd3 of NCC was produced in six - 2 yd3, four - 1yd3, and one - 0.6 yd3 and batches. The average values of the target and actual mix designs are shown in

Table 34. These values are shown for information only as a representation of all of the concrete mixes produced during this cast. This is not the mix design that was used to cast this beam. Any significant deviations from the expected mix design were made by the fabricator without the knowledge of the researchers. The target and actual values for each batch are listed in APPENDIX H.

Table 34. Average NCC Mix Design

	Target Value	Actual Value
Constituents (lbs/yd^3)		
Cement	564	568
Fine Aggregate	1354	1349
Coarse Aggregate	1888	1883
Total water	219	219
w/c	0.39	0.39
Admixture (oz/yd^3)		
Air Entraining	7	7
VMA	6	6
HRWR	64	63

While specific times were not recorded regarding the casting of each of the two NCC beams, concrete was produced from 5:30 am to 8:30 am. This implies that the NCC beams took 1.5 hours to complete on average. The average mixing time for the concrete batches was 4 minutes 25 seconds while there was an average of 19 minutes 57 seconds between batches.

4.2.8 Beam Production Discussion

The beam casting times show that SCC requires significantly less production time compared to NCC. Table 35 summarizes the production times for all of the casting

operations. Time savings of 50 - 70% are seen when using SCC. The average time savings was 61% for all three SCC mixes. This time savings is a direct result of being able to cast the SCC beams in one step without any vibration required to consolidate the concrete.

Table 35. Production Time Savings Using SCC

Cast	Concrete	Total Time (min/beam)	SCC Time Reduction	Average Mixing Time (min)	Average Time Between Batches (min)
1	NCC	77.5	60 %	5.33	18.32
	SCC 1	31		6.85	8.00
2	NCC	79	72 %	10.67	19.32
	SCC 2	25		3.70	5.32
3	NCC	67.5	51 %	2.87	17.72
	SCC 3	33		2.74	6.68
4	NCC	60	-	4.42	19.95

The average time between batches was less than 10 minutes for the three SCC mixes during beam production - SCC was being produced almost constantly during the production process. The average mixing time results show that the majority of the time between pouring batches of SCC was spent mixing the next batch, while for NCC there would be down time for the production crew while they waited for the batch to be mixed. This is a more efficient use of labor as the people producing the concrete work more constantly when producing SCC than when they produce NCC.

Not only does the use of SCC save time, it also resulted in a savings on labor during the casting operations. For the NCC beams anywhere from 10-18 people were working on the beam at a given time. The largest number of people was required when the reinforcing steel and voids were being installed after the bottom flange had been poured. Casting the SCC beams required only 4 people.

The time savings seen when casting with SCC are for the day of casting only. Some of the time saved during the day of casting is canceled out due to the increased amount of time spent preparing to cast. However, part of the reason the time between each casting was so long was because of tasks related to the research project. Time had to be spent installing instruments as well as taking instrument readings. It is unclear how much time these research tasks added to the overall preparation. As production experience is gained in the use of SCC, the actual time savings can be defined with more precision. These values will vary depending on the project size and type.

The release of the SCC 1 beams was delayed because adequate strength was not obtained by the time the fabricator's crew would normally release the strands. It took an additional hour to reach the required strength compared to the normal practice. This was the only concrete that did not reach the required strength before the normal time to release the strands. Adjustments to the SCC 1 mix design could result in a more rapid early strength gain.

The constant quality control monitoring during the casting process allowed for changes to be made to the mix design to adjust for the conditions at the time. This step was important, as the SCC mixes were more sensitive to small changes in factors such as the ambient temperature and moisture content of the aggregate.

4.3 Material Properties

The properties of the materials used in this project are important in the testing and analysis work for this research. Concrete material properties were measured at various times throughout the project. These were taken at times when they were needed for the project. The two properties that were measured were the compressive strength and the

tensile strength of the concrete. The properties of the prestressing steel were given by the strand manufacturer.

4.3.1 Compressive Test

The concrete compressive strength, f'_c, was measured by testing 4 in. by 8 in. cylinders in compression according to ASTM Specification C39-05 [46] on four occasions. The first test was conducted before the prestressing strands were released. A minimum of 5,000 psi was required to transfer the prestressing force. The next two tests were conducted in conjunction with the structural tests, one each for the flexural and shear tests. The final value was taken in April of 2006 in conjunction with other material property tests not included in this project.

The cylinders tested in compression were moist cured for 24 hours and then placed in a curing room until they were tested. The cylinders tested in compression were capped with Sulfur to reduce friction between the steel testing apparatus and the concrete cylinder. This friction can introduce tension into the test resulting in a reduced compressive strength.

The results of the tests for the four concrete mix designs are shown in Table 36 through Table 39, and in Figure 44. Each value represents an average of at least three tests. The standard deviations of the multiple test values are shown in the tables. The first value in each table was provided by the fabricator with out a standard deviation, thus none is provided in the table.

The general trends followed by the compressive strength gain are as would be expected. All mixes, except the SCC 3 mix, showed significant strength gains in the beginning of the project. The majority of the strength gains for the NCC, SCC 1, and

SCC 2 concretes occurred by the time the flexural tests were conducted approximately 40 days after the concretes were produced. The SCC 3 concrete showed a similar rate of strength gain throughout the entire length of the project. One anomaly is in the reduced strength seen for the third strength test conducted on the SCC 1 concrete. It is unclear why this reduction occurred. However, similar results were obtained in all three cylinders tested as can be seen by the relatively low standard deviation value. By the time the fourth test was conducted, the SCC 1 concrete showed the highest strength of all the mixes.

Table 36. NCC Compressive Strength

Age (days)	F'$_c$ (psi)	Std. Dev (psi)	Event
0.79	6,207	-	transfer of prestressing force
41	8,196	437	flexure test
55	8,560	134	shear test
287	9,106	435	April 2006

Table 37. SCC 1 Compressive Strength

Age (days)	F'$_c$ (psi)	Std. Dev (psi)	Event
0.88	6,338	-	transfer of prestressing force
43	8,290	300	flexure test
58	7,519	158	shear test
310	10,133	937	April 2006

Table 38. SCC 2 Compressive Strength

Age (days)	F'$_c$ (psi)	Std. Dev (psi)	Event
3	6,572	-	transfer of prestressing force
42	6,754	290	flexure test
66	7,711	430	shear test
298	7,980	296	April 2006

Table 39. SCC 3 Compressive Strength

Age (days)	F'$_c$ (psi)	Std. Dev (psi)	Event
0.79	5,062	-	transfer of prestressing force
40	6,685	236	flexure test
54	6,953	118	shear test
288	7,556	163	April 2006
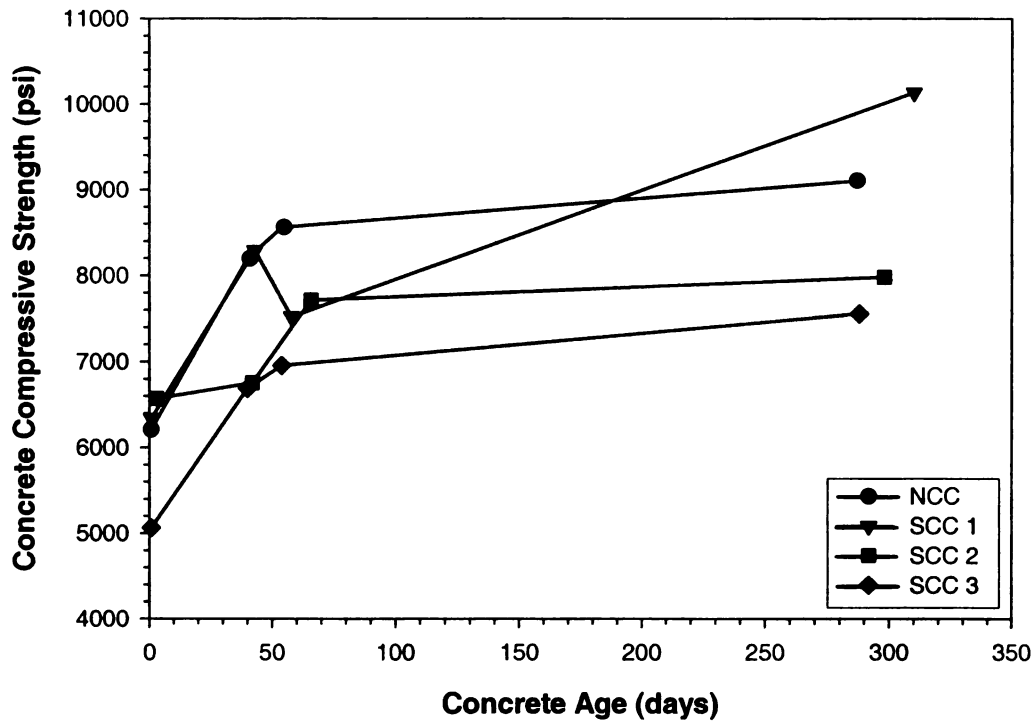
Figure 44. Concrete Compressive Strength

4.3.2 Tensile Strength

Split tensile tests were conducted according to ASTM Standard C496-04 [47] at the time of the shear test. The results of the test are shown in Table 40. All values are the results of at least three tests except for NCC, which is the result of only two tests.

The results of these tests follow the predicted trend. The strongest concrete in compression at this point in time was the NCC concrete. It follows logically that it would also have the highest tensile strength. The SCC 3 compressive strength was the lowest as is the case for the tensile strength. The SCC 1 and SCC 2 mixes had similar compressive strengths and also show similar tensile strengths.

Table 40. Split Tensile Test Results

	Age (days)	f'_t (psi)	Std. Dev. (psi)
NCC	55	646	105
SCC 1	58	609	56
SCC 2	66	576	38
SCC 3	54	514	73

4.3.3 Prestressing Strand Properties

The properties of the prestressing steel are listed in Table 41. Two spools of strand were used to produce the beams used in this project. The properties listed include the area of the strand, modulus of elasticity of the strand, and the yield and ultimate strengths of the strand.

Table 41. Prestressing Steel Properties

	Spool No. 9003098001	Spool No 9003085202
Strand Area (in^2)	0.2268	0.2279
Modulus of Elasticity (psi)	29,030,000	28,940,000
Yield Stress (psi)	242,292.769	245,936.814
Ultimate Stress (psi)	266,463.845	265,427.819

4.4 Production Conclusions

The production of the box beams for the demonstration project allowed for the evaluation of several SCC mixes in an actual production setting. From this experience the following conclusions could be drawn:

- The use of SCC in the production of box beams reduced the production time an average of 61% compared to using NCC.

- The number of people required to produce the SCC beams was lower than the number to produce NCC beams. The NCC production crew was 15 workers compared to a maximum of five for the production of the SCC beams.

- In order to successfully produce box beams using SCC some modifications to the production process were required. Specifically, the use of void hold downs were required to maintain the desired cross section dimensions.

- Due to the improved flow properties of SCC, surface quality of box beams was improved compared to the NCC beams.

- Because the beam casting process was so much faster with SCC, concrete batches needed to be produced nearly continuously. With NCC, the slower casting process meant that there was significant down time between batches..

- The constant quality control during the production of the SCC batches allowed for necessary adjustments to maintain consistent fresh property behavior throughout the beam production process.

5 FLEXURAL AND SHEAR PERFORMANCE OF SCC AND NCC PRESTRESSED BOX BEAMS

5.1 Testing Program Overview

Two test beams were produced for each concrete mix design. One of the beams was used in an evaluation of the flexural capacity, and the other was evaluated for shear capacity. The beams were replicas of the beams to be used in the M-50/US-127 Bridge, (B02 of 38071) specifically: 52-ft long 27 in. by 36 in. prestressed box beams. A typical cross section of the box beam through the Styrofoam void with reinforcement details was previously shown in Figure 43. The test beams were not provided with slab ties since the beams were not going to be provided with a slab and the inclusion of the slab ties would have complicated the application of loads in the test setup.

Evaluation of the beam's flexural capacity was assessed through a four-point bending flexural test. For the test, the beams were simply supported with a span of 50-ft and loaded at two points spaced 8 ft from each other. Shear capacity was also evaluated through a four-point bending test but with a shortened supported span. Loading conditions in the shear test were also at two points 8-ft apart and centered about the beam. For the shear tests, the shear span for the NCC beam was 8 ft – 7 in., while the shear span for the SCC beams was 6 ft – 7 in.. The change in shear span was made after testing the NCC beam to increase the shear force demands in the section. The shear test setups had overhanging cantilevers at both ends of the supported span. Further details on the test setup and instrumentation are given later. The information herein is part of a research report on the experimental evaluation of the beams for SCC demonstration bridge [6].

5.2 Theoretical Considerations

The calculations of design shear and flexural capacities of prestressed concrete beams involved well-known approaches. The formulation of these approaches is thoroughly described in the literature and building codes, for example Naaman [34] describes the ACI building code 318 formulations in his textbook, while AASHTO presents two methods in the 2nd Edition LRFD Specification and in the 17th Edition of the Standard Specifications [2][3]. Common among these formulations are the simplifying assumptions that [34]:

- Plane sections remain plane

- Strain is linearly distributed across the cross section

- Concrete and steel experience perfect bond.

The design shear and flexural capacities for the test beams were calculated using the equations from the 17th Edition of the American Association of State Highway and Transportation Officials (AASHTO) Bridge Standard Specifications [2] since these were the guidelines used by MDOT for the design of the M-50/US-127 Bridge. The shear capacities were also analyzed using the 2nd Edition of the AASHTO-LRFD Bridge Design Specifications [3] since the model for shear resistance in this design code are more comprehensive and realistic. For the analyses, the voided cross section of the box beams was simplified to an I-beam whose web thickness was the width of the two box sidewalls. This section was then analyzed as a flanged section given that the neutral axis of the cross section lies below the depth of the top flange of the beam.

5.2.1 Flexural Capacity

The moment resistance of a simply supported beam loaded in the direction of gravity is found from the internal couple between the compressive force in the top flange of the beam and the tensile force in the bottom flange. The compressive force acting at the top of the beam is primarily carried by the concrete in the top flange, while the tensile forces at the bottom of the beam is taken by the reinforcing steel, either prestressed or non prestressed. In the design of concrete structures the tensile strength of concrete is neglected such that the entire tensile force is carried by the reinforcing steel. If the section is under-reinforced such that sudden compression failures are avoided, the flexural capacity of the section is assumed to be reached when the reinforcing steel in the tension flange yields. Additional assumptions necessary to produce the commonly accepted simplified formulas for flexural capacity include the use of the Whitney equivalent stress block. This idealized compressive stress distribution approximates the compressive stress distribution as a rectangle. Improvements on this assumption could be made through the use of a parabolic or trapezoidal stress distribution.

The moment resistance can be defined by defining section moment equilibrium about either the compressive force in the concrete or the tensile force in the steel. As the flexural capacity of the beam is determined to be the point when the tensile steel yields, the maximum compressive force in the concrete bust be equal to this tensile force. Due to the internal couple the maximum compressive force must equal the force in the reinforcement at yield, this is given in the ACI code for a flanged cross section is given as Equation (2):

$$(2) \qquad 0.85 f_c'(b - b_w) h_f + 0.85 f_c' b_w a = A_{ps} f_{ps} + A_s f_y$$

where b is the width of the flange, bw is the width of the web, hf is the thickness of the flange, a is the depth of the equivalent compressive stress block, Aps is the area of the prestressing steel, fps is the stress in the prestressing strand at ultimate load, As is the area of the non prestressed steel in the tension zone, and fy is the yield strength of the non prestressed steel. The factor of 0.85 in equation (2) is used to correct for the assumed stress distribution (Whitney stress block). The moment resistance of the section can be obtained from the compressive force in the section by Equation (3):

$$(3) \qquad M_n = 0.85 f_c'(b - b_w) h_f \left(d - \frac{a}{2} \right) + 0.85 f_c' b_w a \left(d - \frac{a}{2} \right) \qquad \text{(in- lb)}.$$

where d is the distance from the extreme compression fiber to the centroid of the prestressing steel. The moment arm of this couple is the distance between the location of the compressive force and the tensile force. The compressive force acts at the centroid of the assumed compressive stress distribution while the tensile force acts at the centroid of the prestressing steel. In equation (3) this distance is given as the difference between the depth to the centroid of the prestressing steel, d, and half the depth of the assumed compressive stress block, a. These variables are shown in Figure 45.
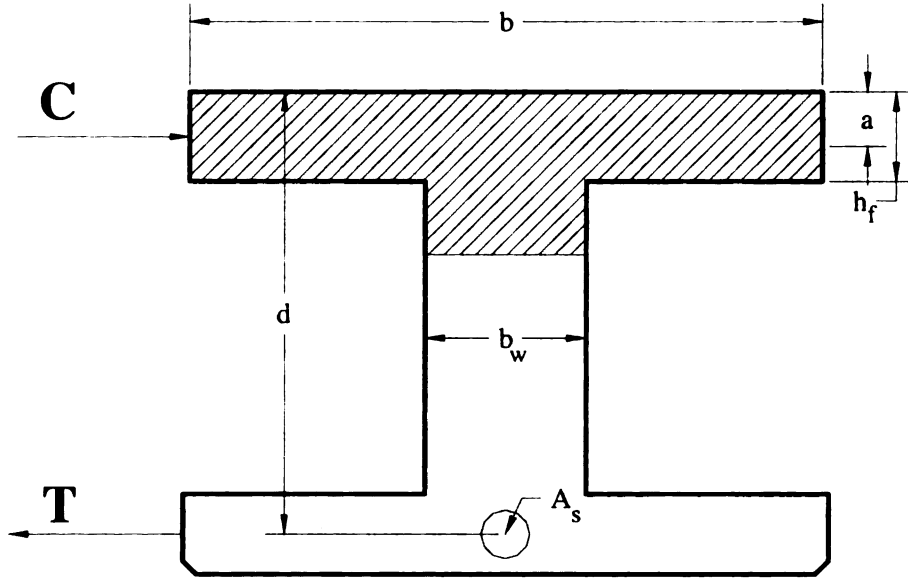
Figure 45. Moment Resistance Variable Definitions

In equation (3) the values of M_n and a are unknown. The depth a can be found from equation (2) assuming that the value of f_{ps} is known. In the ACI 318-05 Building Code [1] an estimate for f_{ps} is given for members with bonded tendons as Equation (4):

$$(4) \quad f_{ps} = f_{pu}\left(1 - 0.5\rho_p \frac{f_{pu}}{f_c'}\right) \quad \text{(psi)},$$

with f_{pu} equal to the ultimate stress of the prestressing strand, and ρ_p is given by equation (5):

$$(5) \quad \rho_p = \frac{A_{ps}}{bd}.$$

Thus, the only unknown value, a, can be directly solved for from equation (2) as given by Equation (6):

$$(6) \quad a = \frac{A_{ps}f_{ps} + A_s f_y - 0.85f_c'(b - b_w)h_f}{0.85f_c'b} \quad \text{(in.)}.$$

For the case where there is no non-prestressed steel included in the tensile flange of the cross section the values pertaining to this steel can be set to zero. To find the equations for a rectangular cross section the value b_w can be taken equal to b.

5.2.1.1 17th Edition AASHTO Standard Specifications Flexural Capacity

The AASHTO Standard [2] presents the following equations given that the beam designed for this project has no non-prestressed steel in the tensile flange and behaves as a flanged beam.

The average steel stress at the ultimate load is given by Equation (7):

$$(7) \quad f_{su}^* = f_s'\left[1 - \left(\frac{\gamma^*}{\beta_1}\right)\left(\frac{p^* f_s'}{f_c'}\right)\right] \quad \text{(psi)},$$

where f_s' is the ultimate stress of the prestressing steel, γ^* is a factor depending on the type of prestressing steel, it is taken as 0.28 for the low-relaxation steel used in this project, β_1 is a factor that depends on concrete strength, and p^* is the ratio of prestressing steel. The value for f_{su}^* cannot exceed f_{py} which is the yield stress of the prestressing steel. β_1 depends on the compressive strength of the concrete and can be taken as 0.85 if f_c' is less than 4000 psi or 0.65 if f_c' is greater than 8000 psi. If f_c' is between 4000 and 8000 psi β_1 is to be obtained by using Equation (8):

$$(8) \quad \beta_1 = 1.05 - 0.05\frac{f_c'}{1000}.$$

116

The moment resistance of the section is given by Equation (9):

$$(9) \quad M_n = A_{sr} f_{su}^* \left[1 - 0.6 \left(\frac{A_{sr} f_{su}^*}{b_w d f_c'} \right) \right] + 0.85 f_c' (b - b_w) h_f \left(d - 0.5h \right) \quad \text{(in.-lb)},$$

where A_{sr} is the area of the prestressing steel, and h is the overall height of the member.

5.2.1.2 2nd Edition AASHTO LRFD Specification Flexural Capacity

The AASHTO-LRFD Specifications [3] recommends using a different set of equations to determine the flexural capacity of prestressed sections. The average stress in the prestressing steel is estimated using Equation (10):

$$(10) \quad f_{ps} = f_{pu} \left(1 - k \frac{c}{d_p} \right) \quad \text{(psi)},$$

where c is distance from the extreme compression fiber to the neutral axis of the beam and is given by Equation (11):

$$(11) \quad c = \frac{A_{ps} f_{pu} + A_s f_y - A_s' f_y' - 0.85 \beta_1 f_c' (b - b_w) h_f}{0.85 f_c' \beta_1 b_w + k A_{ps} \dfrac{f_{pu}}{d_p}} \quad \text{(in.),}$$

and k is given by the Equation (12):

$$(12) \quad k = 2 \left(1.04 - \frac{f_{py}}{f_{pu}} \right).$$

The moment resistance is given by Equation (13):

117

$$(13) \quad M_n = A_{ps}f_{ps}\left(d_p - \frac{a}{2}\right) - A_s'f_s'\left(d_s' - \frac{a}{2}\right) + 0.85f_c'(b - b_w)\beta_1 h_f\left(\frac{a}{2} - \frac{h_f}{2}\right), \text{ in lb}$$

where d_s is the depth of the compressive reinforcement and a is again the depth of the equivalent stress block given by Equation:

$$(14) \quad a = c\beta_1 \quad \text{(in.)}$$

5.2.2 Shear Capacity

Determining the shear resistance of a reinforced or prestressed concrete section is more complicated than determining flexural resistance. Despite the numerous research efforts and the many proposed approaches, the problem of shear in concrete beams is still being debated and no theory has been developed that applies to all types of concrete structures [34]. Still, through many years of study, applicable (under a set of assumptions and limitations) theories for the behavior of reinforced concrete beams in shear have been developed.

Shear stresses cause cracks to develop in concrete in two ways: flexural-shear cracks and web-shear cracks. Both of these crack types occur when principal tensile stresses in the concrete exceed its cracking strength. In general, cracks develop perpendicular to the direction of the principal compressive stresses.

Flexural-shear cracks develop from a combination of flexural and shear loading. Flexural cracks develop in a concrete beams normal to the beam longitudinal axis. If the diagonal tension at the crack tip reaches the tensile strength of the concrete, the direction of the crack will begin to change to an incline. The development of these inclined cracks could then lead to failure of the beam (shear failure) before the full flexural resistance has

118

been developed. These types of cracks can also lead to secondary cracks that occur along the longitudinal reinforcement causing a loss of bond that can lead to a failure in the anchorage zone of the beam [34].

Web-shear cracks occur in beams with narrow webs. These cracks develop when the principal tensile stresses in a region reach the concrete's tensile strength before the flexural stress. The failures associated with web-shear cracking are similar to those in beams with flexural-shear cracks.

Prestressed concrete behaves differently in shear than reinforced concrete. The diagonal tension stress in the concrete beam is reduced by the compressive prestressing force. This force also leads to a smaller angle of inclination of the cracks that develop due to diagonal tension. This consequently reduces the required number and size of shear reinforcing steel [34].

Transverse, or shear, reinforcement is thus provided in reinforced concrete beams to ensure that the beam fails in flexure. Flexural failures are more ductile then shear failures and are the preferred method of failure. Once a beam is cracked in shear its ability to carry tensile stress is significantly reduced. The inclusion of steel transverse to the longitudinal axis of the beam allows additional tensile stress to be carried by the steel. A beam is said to be at its shear capacity once the concrete has cracked and the steel has yielded [34]. Sufficient reinforcing steel is included to ensure that the flexural capacity of the beam is achieved before the shear capacity.

5.2.2.1 17th Edition AASHTO Standard Specification Shear Capacity Equations

The approach used in the of the AASTHO Standard Specifications [2] to calculate the shear capacity of a prestressed concrete beam are essentially the same as that

recommended by the ACI-318 Building Code [1]. The nominal shear strength of a prestressed concrete beam is given by Equation (15):

$$(15) \quad V_n = V_c + V_s \quad \text{(lbs)},$$

where V_c is the shear strength provided by the concrete and V_s is the shear strength provided by the steel. The component V_c is taken to be the lesser of the force required to cause flexural-shear cracks or web-shear cracking. The AASHTO Standard Specifications defines Equation (16) to approximate the shear required to cause web-shear cracking.

$$(16) \quad V_{CW} = \left(3.5\sqrt{f_c'} + 0.3 f_{pc}\right) b' d + V_p \quad \text{(lbs)}$$

where f_{pc} is the compressive stress in the concrete at the extreme fiber due to the effective prestress force, b' is the width of the beam web or flange, d is the depth from the extreme compressive fiber to the centroid of the prestressing force, and V_p is the vertical component of the prestressing force. For beams with straight tendon profiles only, as is the case for the beams in this project, V_p is neglected.

Equation (17) below is used in the AASHTO Standard Specifications [2] to predict the shear at which flexural-shear cracking will occur. The development of this equation is complicated by the fact that the shear distribution in a cracked beam is not known.

$$(17) \quad V_{ci} = 0.6\sqrt{f_c'} b' d + V_d + \frac{V_i M_{cr}}{M_{max}} \quad \text{(lbs)}$$

120

In Equation (17) V_d is the shear force due to the dead load, V_i is the factored shear force due to externally applied loads, M_{cr} is the cracking moment as calculated with Equation (18) below, and M_{max} is the maximum factored moment at a section due to the externally applied loads.

$$(18) \qquad M_{cr} = \frac{I}{Y_t} \left(6\sqrt{f_c'} + f_{pc} - f_d \right) \qquad \text{(in-lbs)}$$

In Equation (18) I is the moment of inertia if the cross section, Y_t is the distance from the centroidal axis of the cross section to the extreme tension fiber, and f_d is the stress due to the unfactored dead load.

The shear strength provided by the steel reinforcement is given by Equation (19)

$$(19) \qquad V_S = \frac{A_v f_{sy} d}{s} \qquad \text{(lbs)},$$

where A_v is the area of shear reinforcement, and s is the spacing of the shear reinforcement.

The method presented by the Standard Specifications [2] to calculate the shear resistance of a reinforced concrete beam is often conservative [13]. First, it assumes that the cracked concrete carries no tensile stress. A second assumption is that the angle of crack inclination in a reinforced concrete beam is 45 degrees. As cracked concrete carries a small amount of tensile stress, and cracks in prestressed concrete beams are inclined at angles less than 45 degrees, the shear resistance of a reinforced concrete beam is often higher than that predicted by the ACI or Standard Specifications method.

5.2.2.2 2nd Edition AASHTO LRFD Specification Shear Capacity Equations

The shear equations presented in the AASHTO-LRFD Specifications [3] are based on the modified compression field theory (MCFT). This theory improves the shear resistance calculation for a reinforced concrete beam by accounting for a reduced angle of crack inclination and the amount of tensile stress carried by the cracked concrete. The theory was developed by Collins and Vechio and is presented in reference [13].

The procedure required to implement the MCFT is not as straight forward as the ACI method since it requires iterations to find the answer. The general expression for shear resistance in Equation (15) still applies. However, the shear strength provided by the concrete is now given by Equation (20):

$$(20) \qquad V_c = 0.0316 \beta \sqrt{f_c'} b_w d_v \qquad \text{(kips)},$$

where β is a factor that indicates the diagonally cracked concretes ability to transmit tensile stresses. The shear resistance of the transverse steel reinforcement is given by Equation (21)

$$(21) \qquad V_s = \frac{A_v f_y d_v \cot \theta}{s} \qquad \text{(kips)},$$

where θ is the angle of inclination of diagonal stresses. The values of β and θ are found analytically. It can be seen, that under the format of Equations (20) and (21) the ACI method conservatively assumes β and θ to have values of 2 and 45 degrees, respectively. However, the MCFT provides a way to obtain more realistic values for these parameters. The AASHTO LRFD specifications adopt a *simplified* method to determine the values of β and θ according to the MCFT. The method is still iterative, but it is simplified by using

an average axial strain value rather than a more sophisticated sectional analysis. The simplified procedure begins with an estimated value of the longitudinal strain, ε_x, in the beam element. Using this value and the ratio of the average shear stress (υ_b) to the compressive strength of the concrete ($f'c$), values of β and θ can be read from Table 42, which is taken from the AASHTO LRFD Specifications [3]. The value of strain must then be re-calculated to see if the assumed starting value was correct. The longitudinal strain can be calculated using Equation (22):

$$(22) \quad \varepsilon_X = \frac{\dfrac{M_u}{d_v} + 0.5 N_u + 0.5 \left(V_u - V_p \right) \cot \theta - A_{ps} f_{po}}{2 \left(E_s A_s + E_p A_{ps} \right)},$$

where M_u is the factored moment, N_u is the factored axial load, and V_u is the factored shear force, applied by external loads. If the calculated value and the chosen value of the axial strain do not match, a second estimation of ε_x is made and the process is repeated. When the estimated and calculated strains are equal, the shear capacity can be calculated using Equation (15), (20), and (21).

Several assumptions are made to calculate the shear capacity using this method. First the concrete shear stresses are assumed to be uniformly distributed over the shear area of the beam. Secondly, the angle of the principal compressive stress is held constant over the shear area. Finally, that the shear strength of the section can be determined from one location in the web. Nonetheless, the method provides a considerable improvement in determining realistic shear capacities while permitting the evaluation of the *complete* shear force-deformation response, something that is not possible with the limit-state equations in the ACI method. Furthermore, the MCFT method explicitly takes into

account the interaction of bending and shear forces in the resulting effective strain in the beam as given in Equation (22). This equation, together with equilibrium of along a beam section along a flexural crack can be used to formulate the interaction between flexure and moment capacities of a reinforced concrete section [13]. This is discussed further in the next section.

Table 42. Values of θ and β for Sections With Transverse Reinforcement [3]

$\frac{\nu}{f_c'}$	$\varepsilon_x \times 1000$										
	≤ −0.20	≤ −0.10	≤ −0.05	≤ 0	≤ 0.125	≤ 0.25	≤ 0.50	≤ 0.75	≤ 1.00	≤ 1.50	≤ 2.00
≤ 0.075	22.3 / 6.32	20.4 / 4.75	21.0 / 4.10	21.8 / 3.75	24.3 / 3.24	26.6 / 2.94	30.5 / 2.59	33.7 / 2.38	36.4 / 2.23	40.8 / 1.95	23.9 / 1.67
≤ 0.100	18.1 / 3.79	20.4 / 3.38	21.4 / 3.24	22.5 / 3.14	24.9 / 2.91	27.1 / 2.75	30.8 / 2.50	34.0 / 2.32	36.7 / 2.18	40.8 / 1.93	43.1 / 1.69
≤ 0.125	19.9 / 3.18	21.9 / 2.99	22.8 / 2.94	23.7 / 2.87	25.9 / 2.74	27.9 / 2.62	31.4 / 2.42	34.4 / 2.26	37.0 / 2.13	41.0 / 1.90	43.2 / 1.67
≤ 0.150	21.6 / 2.88	23.3 / 2.79	24.2 / 2.78	25.0 / 2.72	26.9 / 2.60	28.8 / 2.52	32.1 / 2.36	34.9 / 2.21	37.3 / 2.08	40.5 / 1.82	42.8 / 1.61
≤ 0.175	23.2 / 2.73	24.7 / 2.66	25.5 / 2.65	26.2 / 2.60	28.0 / 2.52	29.7 / 2.44	32.7 / 2.28	35.2 / 2.14	36.8 / 1.96	39.7 / 1.71	42.2 / 1.54
≤ 0.200	24.7 / 2.63	26.1 / 2.59	26.7 / 2.52	27.4 / 2.51	29.0 / 2.43	30.6 / 2.37	32.8 / 2.14	34.5 / 1.94	36.1 / 1.79	39.2 / 1.61	41.7 / 1.47
≤ 0.225	26.1 / 2.53	27.3 / 2.45	27.9 / 2.42	28.5 / 2.40	30.0 / 2.34	30.8 / 2.14	32.3 / 1.86	34.0 / 1.73	35.7 / 1.64	38.8 / 1.51	41.4 / 1.39
≤ 0.250	27.5 / 2.39	28.6 / 2.39	29.1 / 2.33	29.7 / 2.33	30.6 / 2.12	31.3 / 1.93	32.8 / 1.70	34.3 / 1.58	35.8 / 1.50	38.6 / 1.38	41.2 / 1.29

5.2.3 Shear-Moment Interaction

The shear capacity predicted by the AASHTO Standard Specifications [2] will be larger than the true shear capacity as evaluated from a flexural test. This is due to the fact that the development of the equation for the shear capacity assumes that the section undergoes pure shear loading with out any bending. The inclusion of flexural stresses at a section reduces the shear capacity of the beam as evidenced by Equation (22). Thus, there is a trade-off between the shear capacity and the flexural capacity of the beam. If a test is conducted in pure flexure, with no shear, the flexural capacity can be achieved. This is what is typically pursued in a typical flexural test, where the section of interest is located under constant moment demands. Clearly, if the beam could be tested in pure shear the full shear capacity would be achieved. However, the test setup to introduce this kind of loading is very complicated. Rather, most shear demands are unavoidably accompanied by flexural demands, as was the case in the shear evaluation experiments in this project. The critical shear section was thus in a region experiencing both shear and flexural stresses.

The reduction of the shear capacity by flexural actions is caused by the increase of the longitudinal strain in the steel reinforcement when shear is applied. This can be seen from Equation (22). This increase of the strain reduces the amount of strain available to resist the flexural forces. As the capacity of a section is defined at the yield point of the steel, additional strain in the longitudinal steel will bring the steel closer to yield.

The MCFT can be used to predict the affects of the interaction between shear and flexure. From the AASHTO-LRFD [3] Equations (20) and (22) can be used to produce a flexure-shear interaction diagram. The longitudinal strain ε_x is changed through a range

of values and the shear capacity and moment capacity are found using Equations (20) and (22). In this project, this evaluation was done using the program Response 2000 [8], which is a sectional analysis program that incorporates MCFT in its full form [13] rather than in the simplified approach outlined by the AASHTO-LRFD Specifications.

5.3 Flexural Experimental Evaluation

5.3.1 Test Setup, Instrumentation and Protocol

The flexural capacity of the box beams was assessed through four-point bending tests. The four-point bending setup was chosen to create a region of constant moment without shear to assess pure flexural response. An overview drawing of the test setup is given in Figure 46. The 52-ft beams were simply supported 1-ft from the ends on top of reinforced concrete support blocks. A 3-inch thick laminated elastomeric pad was used between the beam and the reinforced concrete block to avoid stress concentrations and allow for beam end rotations. The beam was symmetrically loaded at midspan at two locations spaced 8 feet apart. Loading was applied by a pair of servo-controlled hydraulic actuators attached to a gravity reaction frame. To avoid local loading on top of the box beam upper flange, the load was distributed by means of a spreader steel beam that straddled the beam transversely. A 1-in. thick glass-reinforced elastomeric pad was used between the spreader steel beam and the top of the box beam to minimize stress concentrations. A picture of the test setup is shown in Figure 47.
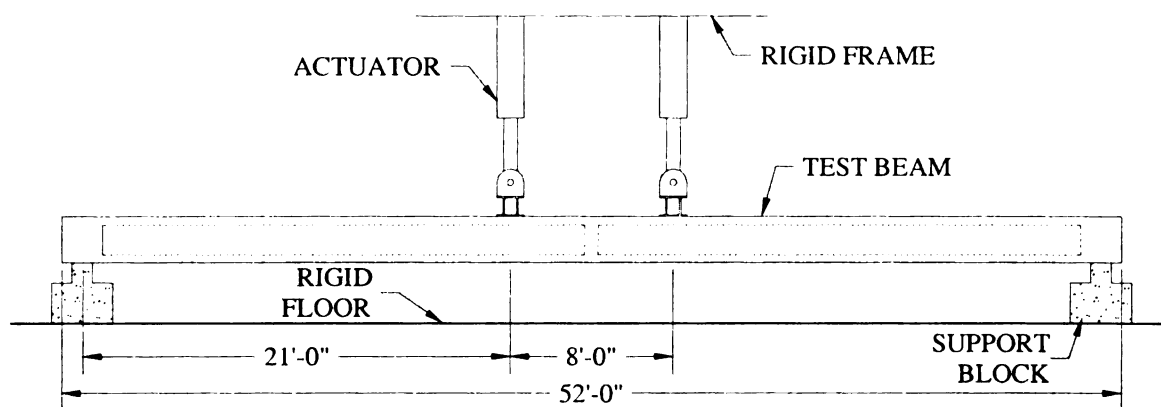
Figure 46. Flexural Test Setup – Overall Features and Dimensions

The material properties for the prestressing steel and each of the four project mix designs are state in section 4.3 in Table 36 through Table 41. The compressive strength at the time of the flexure test for each mix design is restated in Table 43 for reference.

Table 43. Flexure Test Concrete Compressive Strengths

Mix Design	Age at day of flexure test (days)	f'c (psi)	Standard Dev. (psi)
NCC	41	8,196	437
SCC 1	43	8,290	200
SCC 2	42	6,754	290
SCC 3	40	6,685	236

The flexural tests were provided with diverse instrumentation to monitor overall performance and test setup control. The provided instrumentation was:

- Displacement transducers to measure vertical motion of the beam at midspan, point of load application, and support locations.

- Rotation transducer at the beam end to measure beam rotation at the support.

- Rotation transducer perpendicular to the beam at midspan to evaluate any torsion effects.

128

- Displacement transducers at 10 prestressing strands on one end of the beam to monitor any relative slip between the strand and face of the concrete beam.

- Strain gages in selected bottom-row prestressing strands and at selected locations. A schematic of strain gage locations is given in Figure 48, Figure 49, and Figure 50.

- Strain gages on the concrete surface at the top of the compression flange at beam midspan. A schematic of strain gage locations is given in Figure 48, Figure 49, and Figure 50.
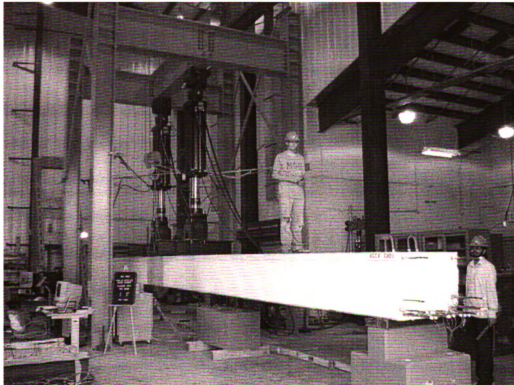
Figure 47. Overall View of Flexural Test Setup

The flexural tests were conducted by monotonically loading the beam up to failure. The beams were initially loaded in force control in increments of 10 kips at a rate of 0.01 kip/sec. The system response was carefully monitored to evaluate the onset of significant section cracking. Once the section started to show significant nonlinear behavior, the loading was applied in displacement control in typical intervals of 0.25 in. at a rate of 0.0025 in./sec.

5.3.2 Observations and Results

The response of the flexure test beams was very much as expected for all tests. However, it should be noted that the first two tests (NCC and SCC1) showed asymmetrical cracking indicative of torsion effects. It was found that this was due to the uneven top of one of the support blocks. This was corrected for all subsequent tests. While the torsional stresses have an effect on the first cracking load and cracking behavior of the beams, the demands on the NCC and SCC1 beams are considered negligible for the ultimate strength. As the ultimate load was the main focus of this study the effect of the torsion demands were disregarded.

The sectional capacity of the beams was smaller at midspan (center of the constant moment area) due to the presence of open pockets on the top flange with approximate dimensions of 4" in length (along the beam length), 3" in width and 3" in depth, see Figure 43. These pockets were used to flame-cut the top strands in the section. The NCC beam was tested with these pockets left un-grouted, which essentially reduced the width of the section compression flange. The pockets of the SCC2 beam had been grouted at the producer's plant and the beam was tested with these pockets filled, however all other beams were tested with the top flange pockets un-grouted.

130

The appearance of flexural cracks, their paths, and their widths for all beams was consistent with expected behavior. A photograph of the overall beam response (SCC1 unit) at near maximum capacity is shown in Figure 51. Since the beams were tested without the deck compression flange, failure of the section was thus dictated by failure of the compression flange. The failures were explosive since the concrete compressive strengths were relatively high and also due to the high strength of the prestressing strand. However, the failures were technically ductile as the prestressing strands yielded before failure.
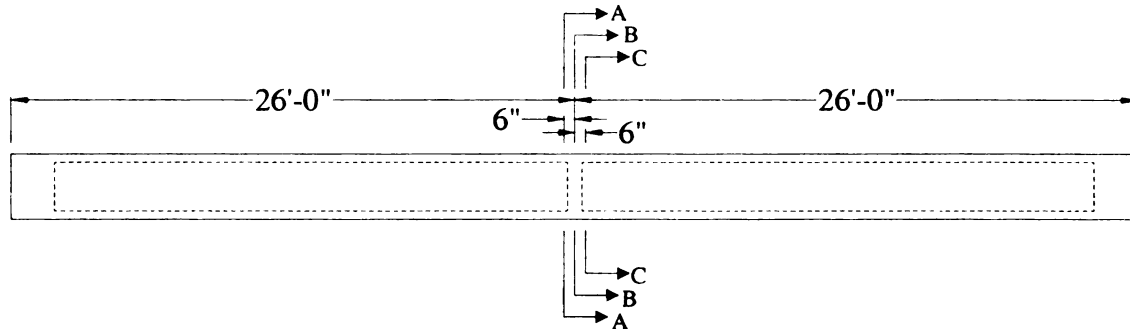
Figure 48. Plan View of Strain Gage Locations

Figure 49. Strain Gage Location Sections A-A and C-C

Figure 50. Strain Gage Location Section B-B

132

A view of the typical failure mode for all of the flexure tests is shown in Figure 52. As it can be seen in this figure, after compression failure of the top flange, the section essentially folded onto itself as internal equilibrium forces seek a balanced condition. After failure of the webs, the large rotations spalled off the concrete underneath the prestressing strands. No deformation was recorded by the transducers mounted on the prestressing strands at the beam end, indicating no signs of strand slip.
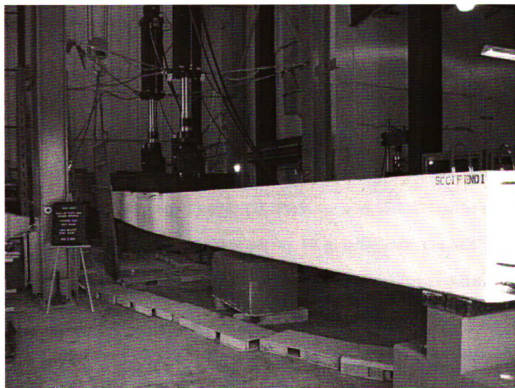
Figure 51. SCC1 Flexure Test Beam near Ultimate Capacity
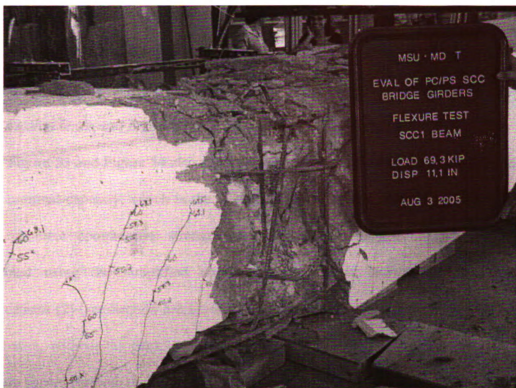
Figure 52. Failure Mode of SCC1 Flexure Beam

The results are summarized in Table 44. In this table the maximum total applied load and displacement are shown as well as the maximum moment that was achieved at the beam midspan. This maximum value is compared to the midspan moment predicted using the AASHTO Standard Specification [2]. From this comparison it can be seen that the NCC beam exceeded the design moment by 10 percent while the SCC 1 beam exceeded this value by 9 percent. The SCC 2 and SCC 3 beams both exceeded the design moment by 6 percent.

The applied force per actuator versus the beam maximum (center) displacement for all flexure beams is shown in Figure 53. The traces for each of the beams are identified by the use of different symbols. It can be seen that the overall response of all beams was essentially equal, with the NCC beam reaching a slightly higher load at failure and the SCC1 beam showing the largest deformation at failure. Figure 54 shows the

moment versus curvature response of the mid-span section for all beams. The section curvature was calculated from the strain gage readings on the top surface of the concrete compression flange and the strain gages in the first row of prestressing strands (see Figure 48, Figure 49, and Figure 50).

Figure 53 and Figure 54 also shows two response limit lines corresponding to the design nominal capacity, which is the design capacity for the bridge with the assumed design concrete compressive strength of 5,500 psi. The sectional capacity was determined using the simplified approach presented in the AASHTO Standard Specifications [2] (see Section 5.2.1). This design capacity was calculated for the girder only, that is, without the deck, in order to compare its value against test results. The limits are shown for both the full and reduced section. The full cross section refers to the section capacity neglecting the existence of the before-mentioned top flange pocket. The reduced section assumes that the compression flange reduces to an effective width of 26 in. upon subtracting the width of both pockets (3 in. each) and the strip of concrete on the outside (2 in. each), as shown in Figure 43. Clearly, the capacity of the reduced section is slightly lower than that of the full section.

Comparison of the beam's load-displacement and applied moment-curvature response against the design limits in Figure 53 and Figure 54 shows that the design limits may have not been reached in some cases. However, it should be realized that the responses in Figure 53 and Figure 54 are due to *applied* forces only, which is without considering initial self-weight demands. Self-weight demands for the 50 ft simple span are significant: a positive moment at midspan of approximately 176.6 kip-ft. Thus, the capacities achieved for the test beams should consider these initial demands for

comparison against the calculated design capacities. This was done for the load-displacement and moment-curvature traces shown in Figure 55 and Figure 56, respectively. It can be seen from these figures that the sectional capacities of all beams clearly exceed the required design capacities.

Comparison of the relative performance of the flexural beams, and particularly, the performance of the SCC beams compared to the NCC beams, can also be seen in Figure 55 and Figure 56. It can be observed that the NCC beam reached the highest section capacity and that the SCC3 had the lowest (see Table 44). As far as deformations, the SCC1 had the highest deformation at failure and the NCC beam had the lowest. Clearly, the beams had different concrete strengths at the day of test. Thus, in an attempt to compare performance while taking into account the different concrete strengths, the responses were normalized with respect to the compressive force in the top beam flange using equivalent stress block parameters. In normalizing the test values, the compressive strength from the day of test was used. The normalized force-displacement and moment-curvature responses are shown in Figure 57 and Figure 58, respectively. It should be noted that the design limit lines have also been normalized accordingly using the design concrete compressive strength of 5,500 psi.
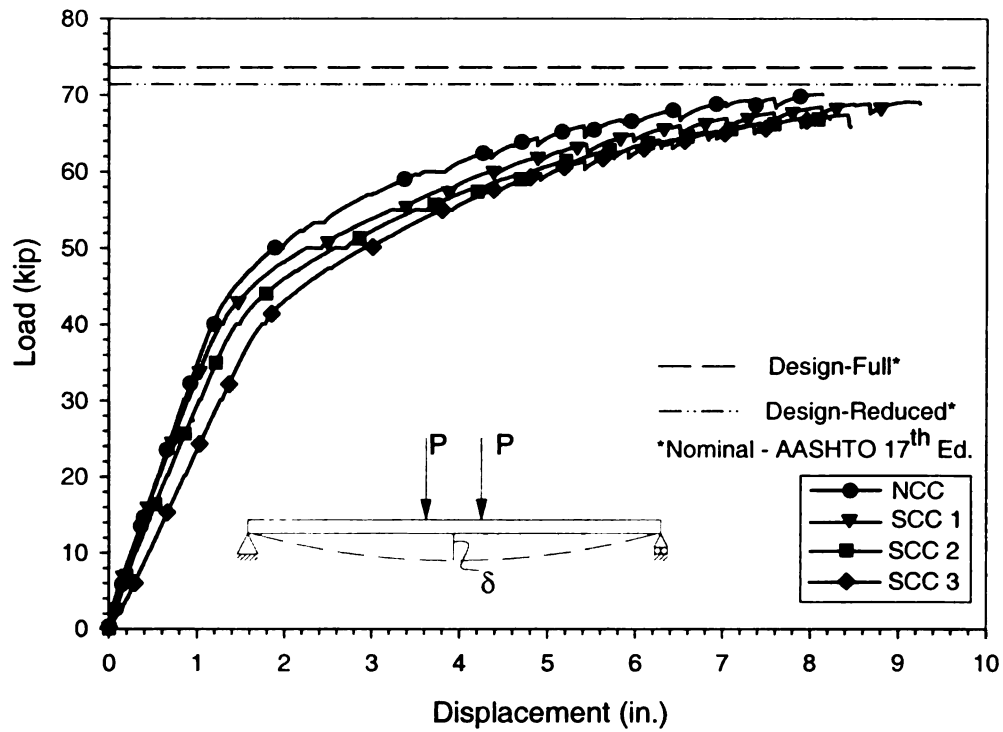
Figure 53. Applied Load vs. Displacement Response of All Flexure Beams
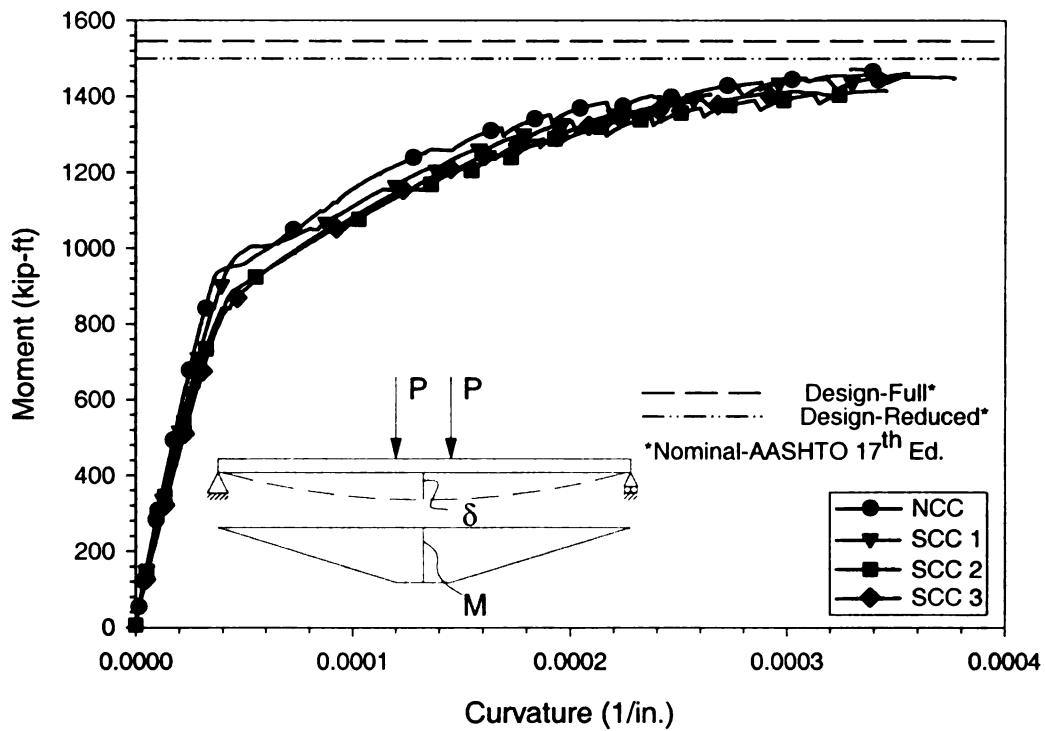
Figure 54. Applied Moment vs. Curvature Response of All Flexure Beams
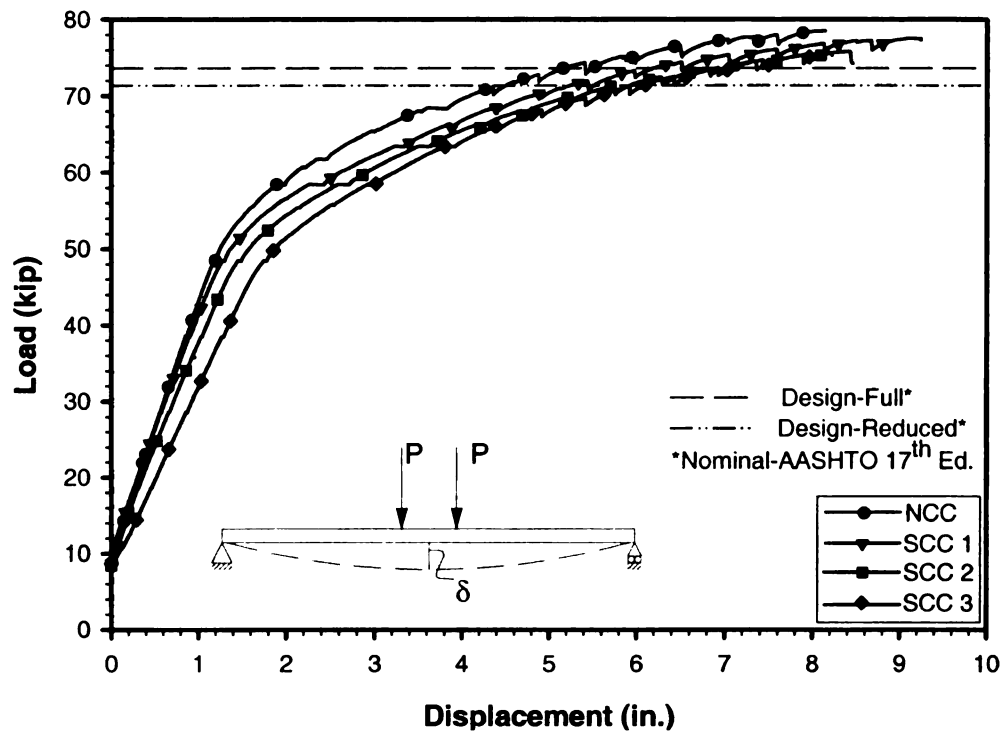
Figure 55. Total Load vs. Displacement Response of All Flexure Test Beams
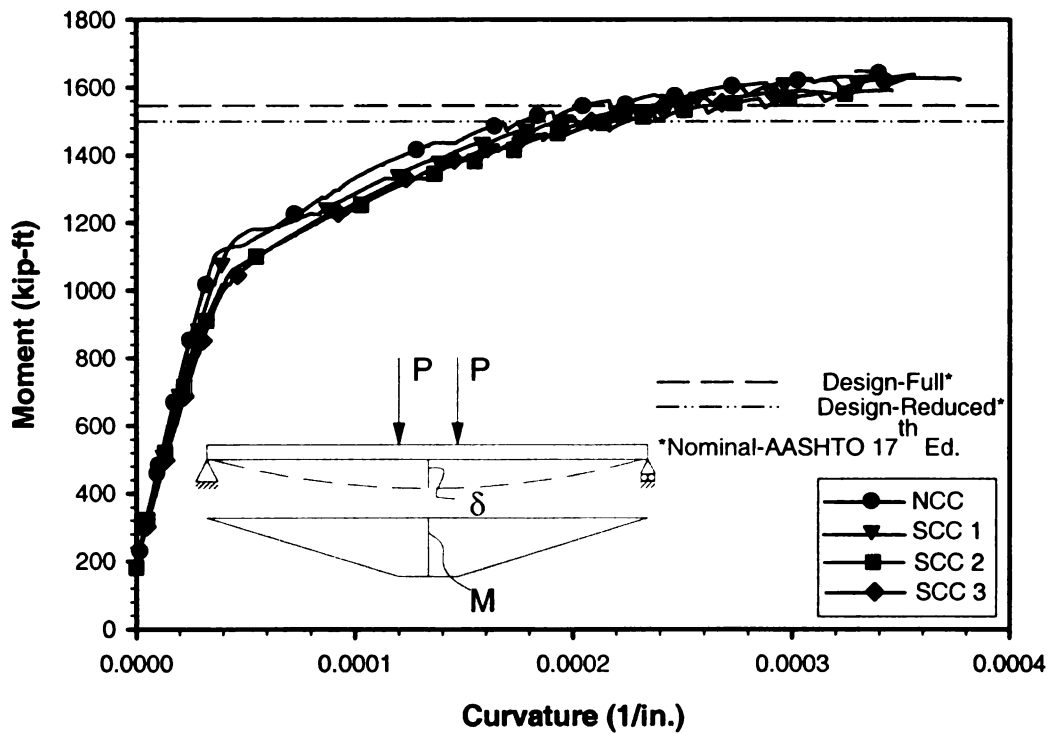
Figure 56. Total Moment vs. Curvature Response of All Flexure Test Beams
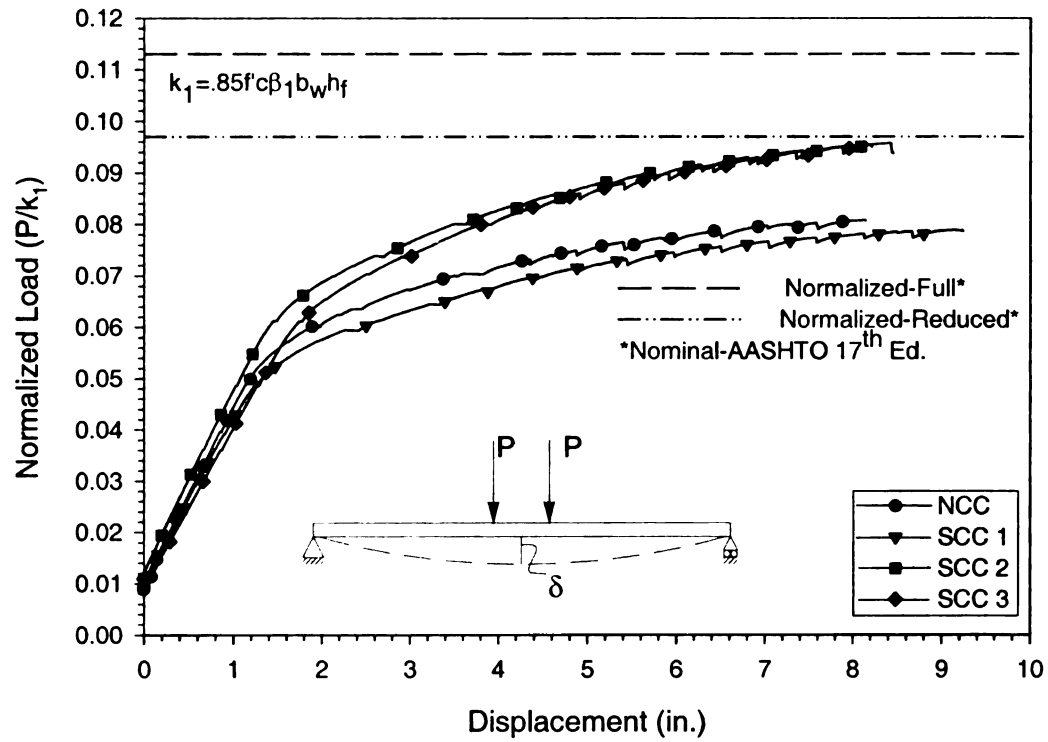
Figure 57. Normalized Total Load-Displacement Response of Flexure Beams
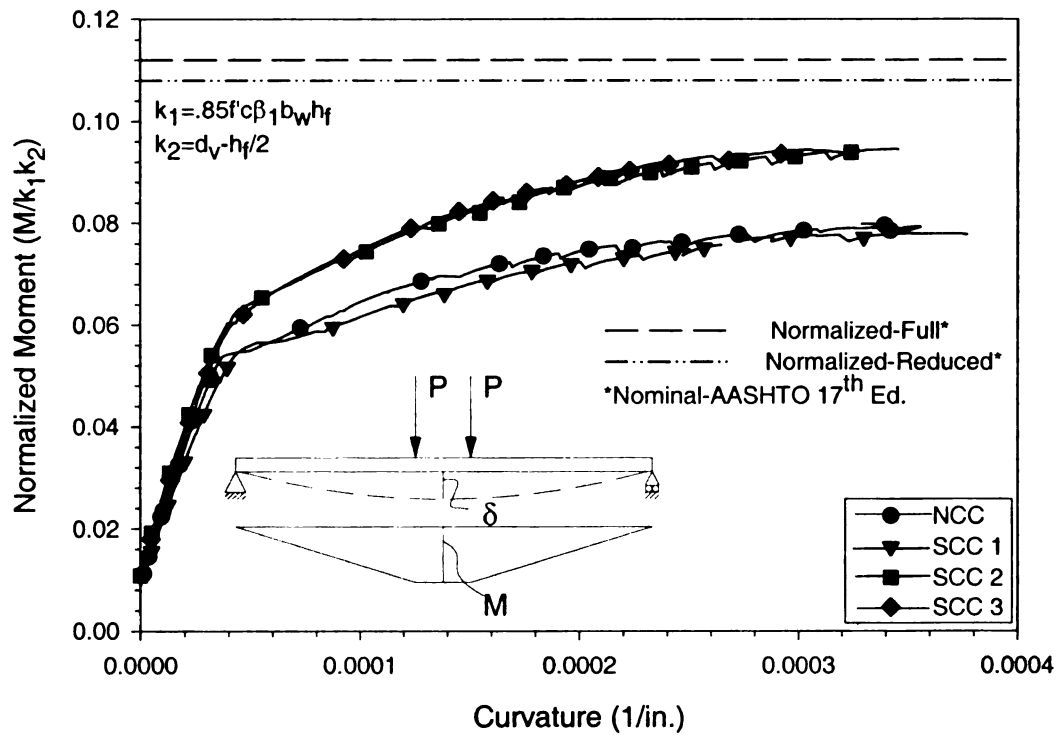
Figure 58. Normalized Total Moment-Curvature Response of Flexure Beams

Table 44. Maximum Achieved Capacities of Flexural Beams

	Maximum Total P-Load (kip)	Maximum Applied Center Disp. (in.)	Maximum Total Moment (kip-ft)	Design Moment [AASHTO] * Full/Reduced (kip-ft)	Actual to Design Ratio (Red.)
NCC	78.5	8.1	1,648.8	1,546/1,499	1.10
SCC1	77.5	9.2	1,628.4	1,546/1,499	1.09
SCC2	75.9	8.5	1,592.8	1,546/1,499	1.06
SCC3	75.7	8.2	1,590.0	1,546/1,499	1.06

* AASHTO Standard Specifications – 17th Edition [1]

In spite of the attempt at normalizing the response the comparison does not seem to be adequate in order to discriminate the beam's performance against a pre-established limit. The normalized plots essentially show the efficiency of the section with respect to the concrete compressive strength. Thus, it can be noted that the beams with the higher compressive strength (NCC and SCC1) have the lowest normalized response value, while the beams with the lower concrete strength (SCC2 and SCC3) achieve greater normalized ratios. This essentially indicates that for the under-reinforced section, the compressive strength of concrete is not a significant parameter. This is confirmed by the fact that in spite of having different concrete compressive strengths, the overall load and moment capacities of the beams as shown in Figure 55 and Figure 56 was essentially equal.

5.4 Shear Experimental Evaluation

5.4.1 Test Setup, Instrumentation and Protocol

The shear capacity of the box beams was also assessed through four-point bending tests with the same support and loading conditions previously described for the

flexure tests, however the shear spans were considerably reduced in order to increase shear force demands. A picture of the test setup is shown in Figure 59. The shear span was chosen with the goal of inducing shear failure in the beam before reaching the section flexural capacity in the center section. However, reducing the shear spans led to overhanging cantilevers beyond the simple supports of the setup causing negative moments to develop in the beam at the supports. To minimize these negative moments, and their effect on the beam behavior, the reduction of the shear spans was limited. The setup was thus determined by the need to keep the beam overhangs at a minimum and minimizing flexure-shear interaction to ensure a shear-dominated failure.

The material properties for the prestressing steel and each of the four project mix designs are state in section 4.3 in Table 36 through Table 41. The compressive strength at the time of the shear test for each mix design is restated in Table 43 for reference.

Table 45. Shear Test Concrete Compressive Strengths

Mix Design	Age at day of shear test (days)	f'c (psi)	Standard Dev. (psi)
NCC	55	8,560	134
SCC 1	58	7,519	158
SCC 2	66	7,711	430
SCC 3	54	6,953	118

An overview of the first shear test for the NCC beam is shown in Figure 60. The shear span in this setup was 11 ft. As discussed later, the flexural and shear capacities of the beam for this configuration were too close and a flexural failure was reached before inducing significant shear deformations in shear spans. Thus, the tests setup for the subsequent SCC beams was changed so that the shear span was reduced to 9 ft as shown

141

in Figure 61. Implications of this change in the test observations and in the interpretation of results are discussed later.
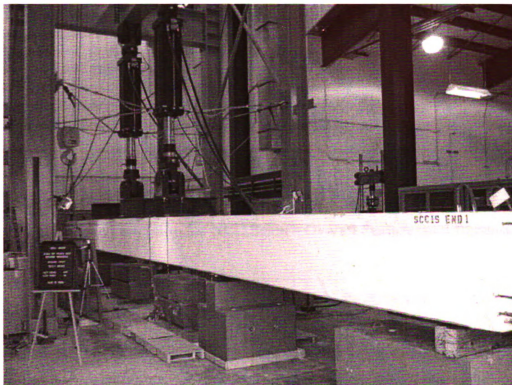
Figure 59. Overall View of Shear Test Setup

The shear tests were provided with a different instrumentation scheme than the flexural test beams. Again, instrumentation was placed to monitor performance and overall test setup control. In order to assess shear behavior, most of the instrumentation was located in what was determined as the *critical shear section*. The critical shear section was determined from sectional analyses using the program Response 2000 [8] to be located approximately 29 inches into the shear span from the points of load application (see Figure 60 and Figure 61). Since shear effects are not localized at a section but rather

distributed over the region of shear cracks, a *shear critical region* was thus defined over a distance of ± h/2 from the critical shear section.
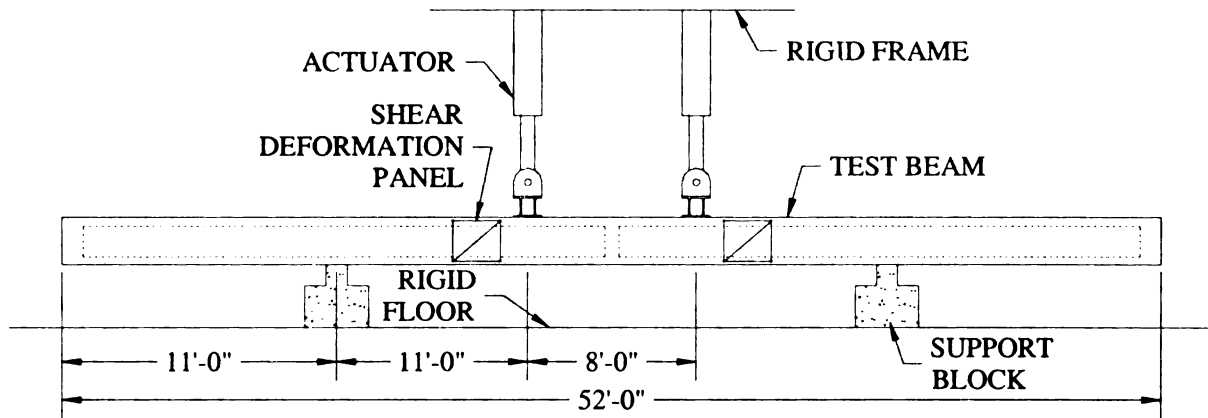
Figure 60. Shear Test Setup for NCC Beam – Overall Features and Dimensions
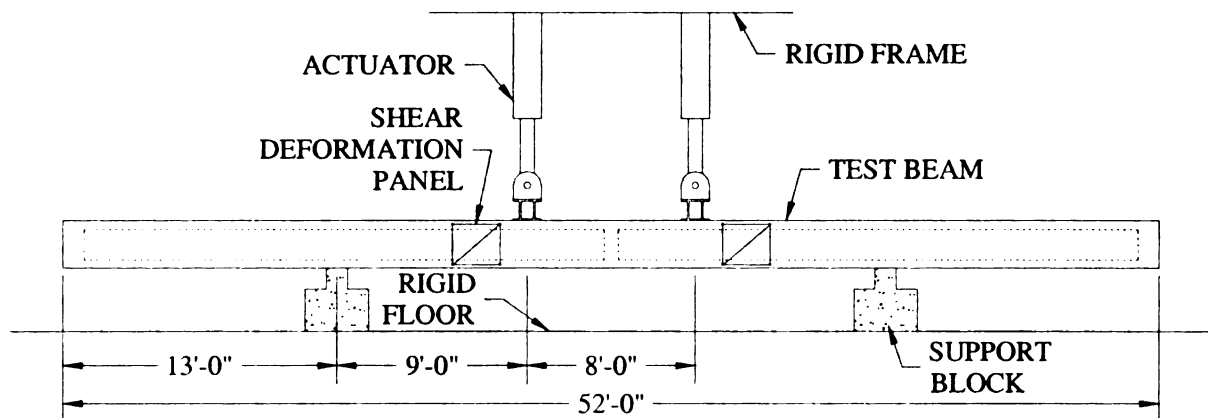
Figure 61. Shear Test Setup for SCC Beams – Overall Features and Dimensions

The instrumentation provided to the shear beams was:

- Displacement transducers to measure vertical motion of the beam at midspan, point of load application, and support locations.

- An arrangement of displacement transducers around the shear critical section named a *shear deformation panel* to measure average shear deformations in the shear critical sections (see Figure 62).

- A rotation transducer on the beam at the support section.

- A rotation transducer perpendicular to the beam at midspan to evaluate any torsion effects.

- Strain gages in selected bottom-row prestressing strands and at selected locations. A schematic of strain gage locations is given in Figure 63, Figure 64, and Figure 65.

- Strain gages along the height of selected shear stirrups in one of the shear critical sections (see Figure 63, Figure 64, and Figure 65

- Strain gages on the concrete surface at the top of the compression flange at beam midspan and at the critical shear section (see Figure 63, Figure 64, and Figure 65)

The test protocol for the shear beams was the same as that previously described for the flexural tests (see Section 5.3.1).
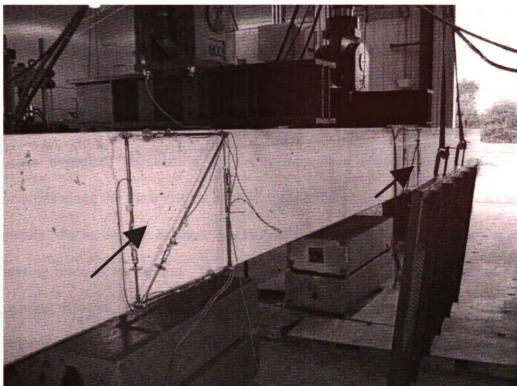
Figure 62. View of Shear Deformation Panels

5.4.2   Observations and Results

Interpretation of results from the shear tests is more intricate than for the flexure tests. This follows due to complexities from unbonded tendons along the beam length and the continuity of the beam beyond the supports as cantilever overhangs. The partially bonded/debonded strands in the top flange modified the shear and flexural capacity of the beam along its length; while the cantilever overhang continuity over the supports allowed the beam to redistribute loads beyond the supports (see Figure 66). Further discussion of these effects follows.

Shortening of the span in the four-point bending setup essentially increases the force required to reach flexural failure at the beam mid-span due to the reduced lever arm. Predictive analyses were used to identify the region along the beam expected to

have the highest shear deformation demands. For all beams, this section was approximately 29 inches from the point of loading along the shear span. As previously mentioned, shear deformation measurement panels were placed centered about this critical section (see Figure 59 and Figure 62).

As expected, degradation of the system was concentrated through shear deformations along the shear critical zone as seen in the picture of Figure 67. As seen in this picture, the inclination of shear cracks was very shallow due to the high levels of prestressing force in the section. This same prestressing level, which extended beyond the supports, allowed the beam to redistribute member demands towards the end of the beams even after the critical shear section reached its capacity. Thus, while the shear capacity of the critical section was reached, complete shear failure of the beams was not reached in all cases except for one test unit. The SCC3 beam exhibited a flexure-shear failure upon crushing of the compression zone in flexure (see Figure 68). This failure is not a typical shear failure but follows from the combined flexure and shear loading and the weakening of the beam due to shear cracking. This effect is further discussed next with reference to the measured data.

The total (corrected for self-weight) shear force versus center displacement for all of the shear test beams is shown in Figure 69. It can be seen in this figure that the response of the NCC beam was considerably different than that of the SCC beams. The reason for this difference was that the shear span for the NCC beam was 11 ft while that for the SCC beams was 9 ft. Thus, the force-displacement response for the SCC beams (with the shorter shear span) is much stiffer.
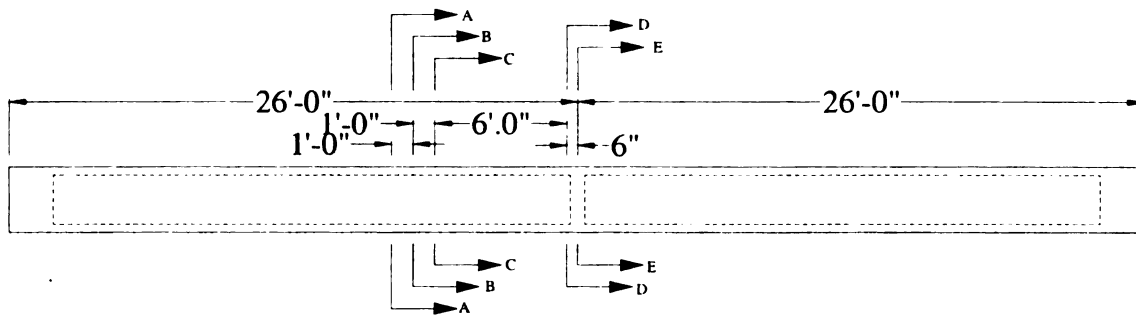
Figure 63. Strain Gage Instrumentation Location for Shear Test Beams

▼ Strain Gage Location
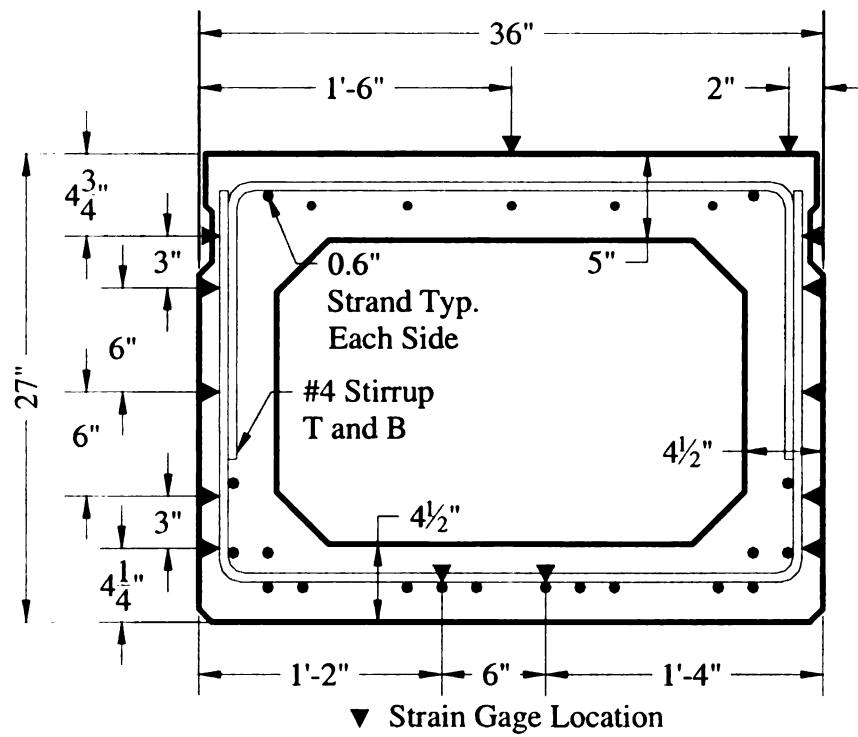
Figure 64. Strain Gage Locations Sections A-A, B-B, C-C

147
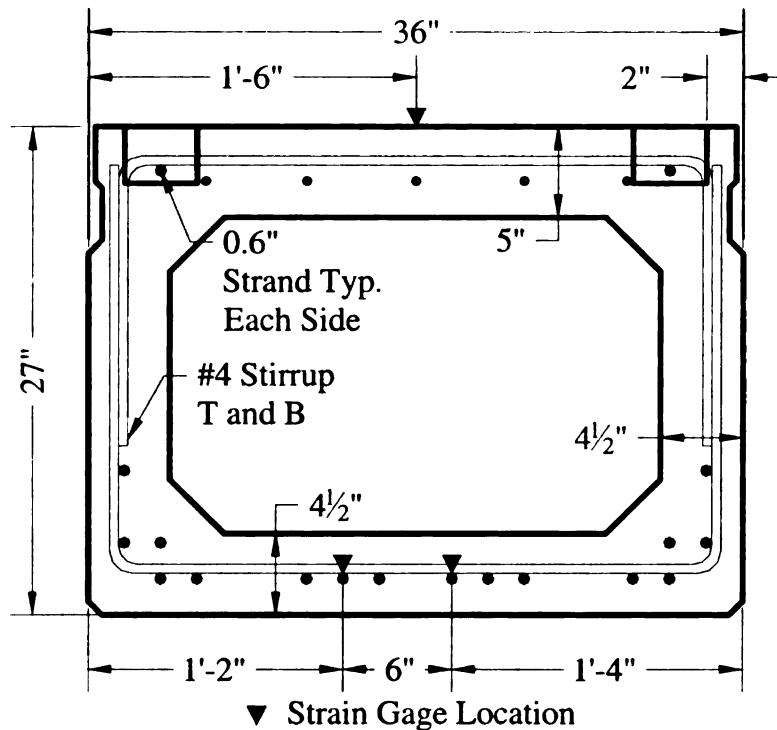
Figure 65. Strain Gage Locations Section D-D and E-E

While the effect of the shorter shear span is clearly noticeable in the overall beam force-displacement response, the shear behavior is best evaluated by studying the section response at the critical shear region. The total moment-curvature response at the critical shear section for all beams is shown in Figure 70. In this plot it can first be seen that the response of all beams is very similar. Secondly, it can also be observed that the moment-curvature response is almost elasto-plastic, with a much sharper shift towards the inelastic regime than observed in the flexural tests (see Figure 56). This indicates that the moment capacity at the critical section abruptly reaches a maximum. The additional section capacity (can think of it as the "hardening" region) is due to the redistribution of loading on to the cantilever overhang.

148
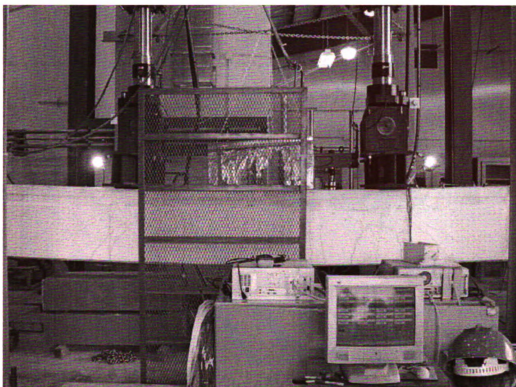
Figure 66. Response of SCC2 Shear Test Beam near Maximum Response
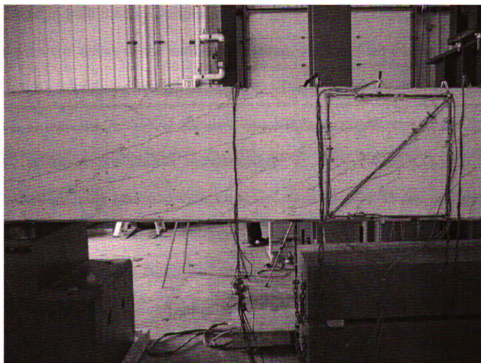
Figure 67. Typical Distress in Shear Span and Critical Shear Region

Figure 68. Flexure-Shear Failure of SCC3 Shear Test Unit

Noted in both the force-displacement (Figure 69) and moment-curvature (Figure 70) responses are values of the nominal capacities calculated for the design beam, i.e., with a design compressive strength of 5,500 psi. The nominal capacities were calculated according to both the AASHTO Standard Specifications [2] as well as the simplified sectional analysis procedures recommended in the AASHTO-LRFD Design Specifications [3]. The reason to show capacities according to both design codes is that, as seen in the figures, the values predicted by the 17th Edition Standard Specifications are much higher than observed in the test, while those obtained with the AASHTO-LRFD provisions compare much more favorably. In addition, it can be noted that the nominal capacities of the critical shear section calculated with the AASHTO-LRFD provisions compare reasonably well to the onset of significant flexural softening of the sections

(Figure 70), which is different than the behavior observed for the pure bending sections in the flexural beam tests (see Figure 56).

The reason for the reduced shear capacity of the tested beams compared to the design value from the Standard Specifications is due to flexure-shear interaction effects. The shear and flexural capacities of a section under combined moment and shear demands will be a compromise between the capacities for pure flexure and pure shear failure [13][22]. This effect is not explicitly taken into account in the Standard Specifications; however, the LRFD Specifications address this issue for the determination of shear capacities, which is based on the principles of the modified compression field theory [13]

The presence of shear in a section will also decrease the flexural capacity of a section due to the additional horizontal tensile forces created by the diagonal compressive struts in the section web. Neither code provides explicit guidelines to estimate the reduced flexural capacity of the section due to the presence of shear. However, this reduced moment capacity can be determined by considering the additional tensile strains generated in the section due to shear [13][22] (also see Section 5.2.3). These calculations were performed by making use of the program Response 2000 [8] for the sectional shear capacity equations from the AASHTO-LRFD specifications. A shear-moment interaction diagram computed by Response 2000 for the design beam (f'_c = 5,500 psi) is shown in Figure 71. In this figure, the loading line corresponds to the test setup with a shear span equal to 9 ft and the extreme ordinate and abscissa values correspond to the pure flexure and pure shear capacities.
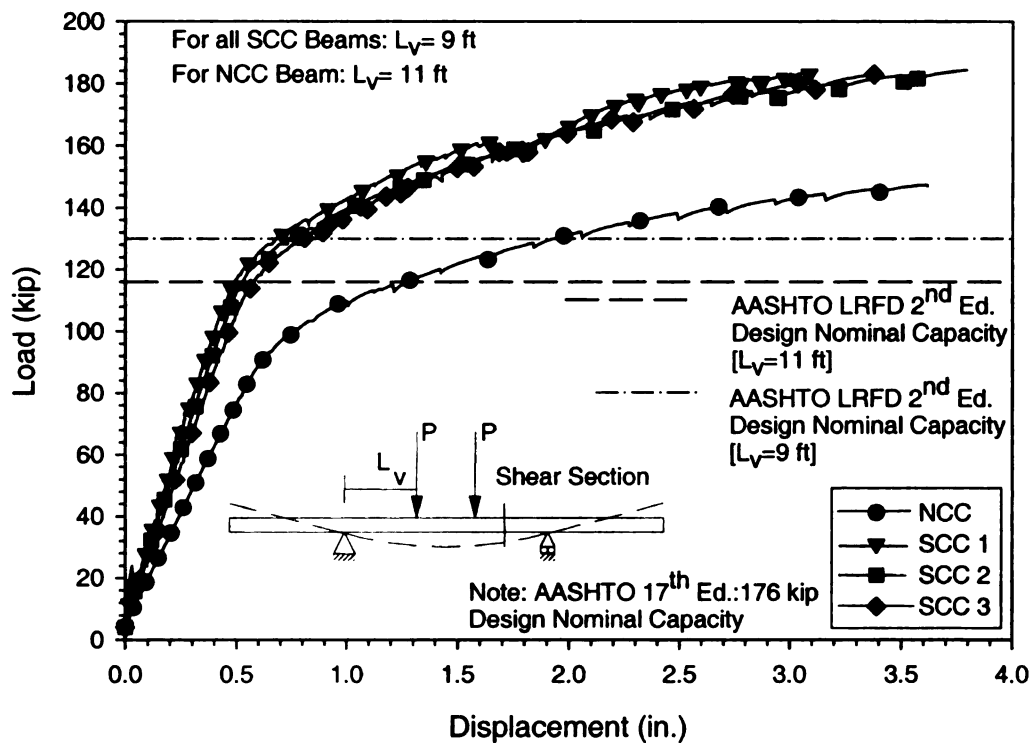
Figure 69. Total Shear Force vs. Center Displacement Response
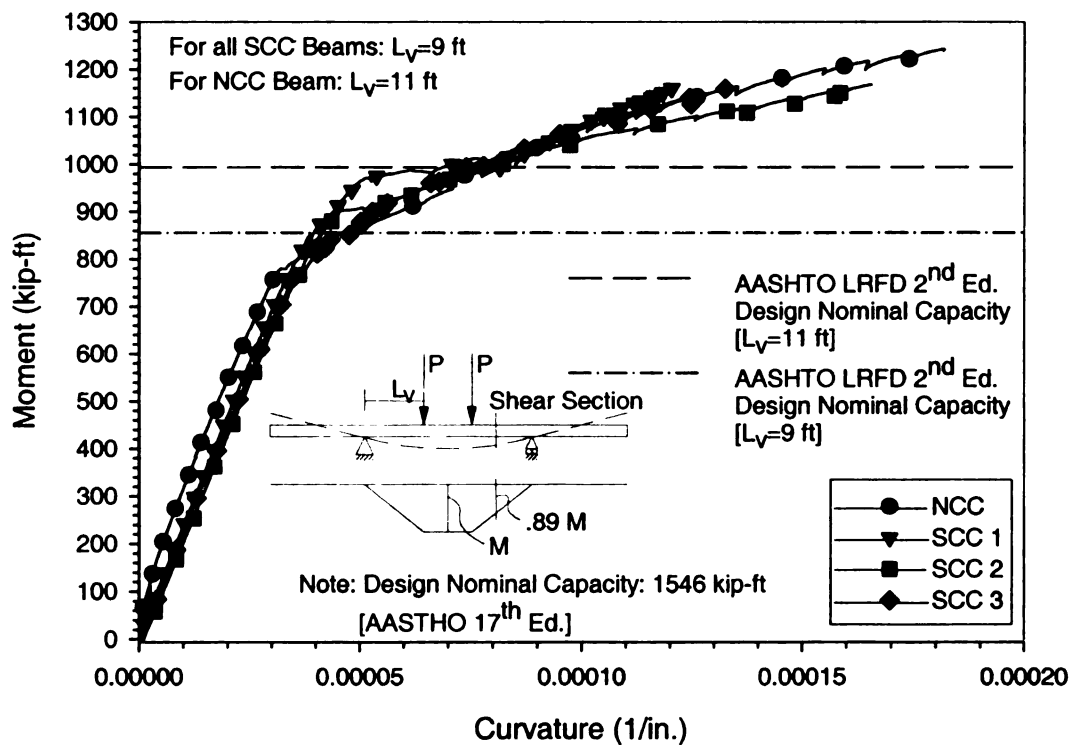
Figure 70. Total Moment vs. Curvature Response at Critical Shear Section

152
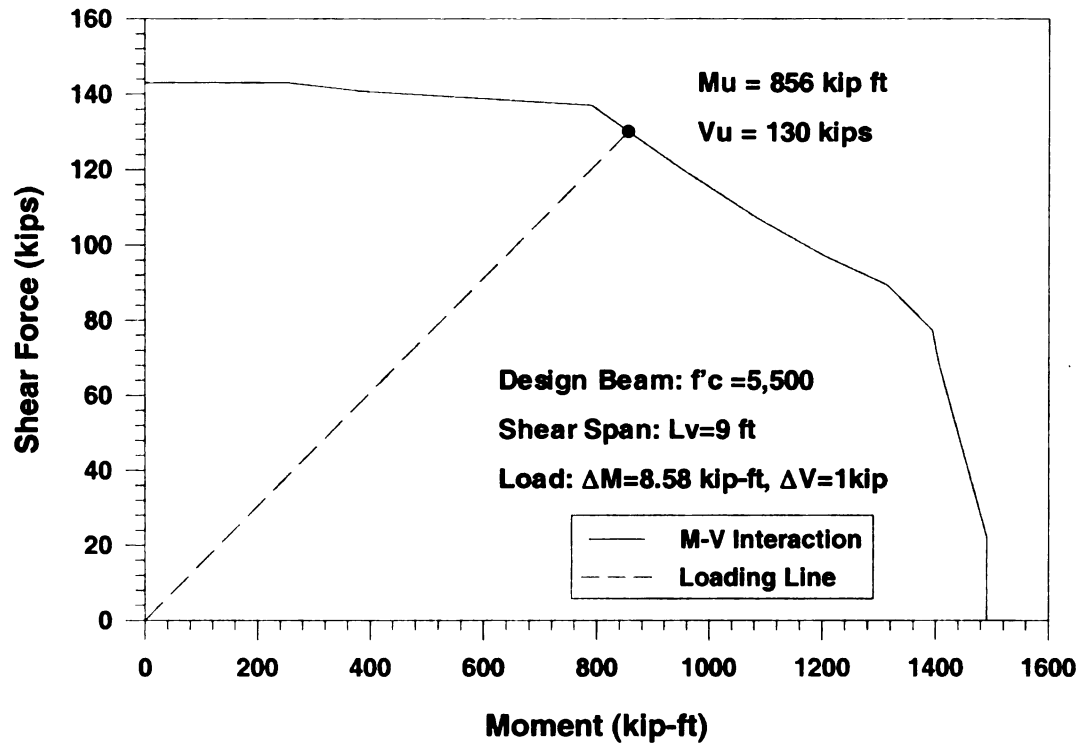
Figure 71. Moment-Shear Interaction Diagram with AASHTO-LRFD

As done for the flexural beams, the shear force-displacement and moment-curvature responses were normalized with respect to the compressive force in the flange to take into account the different concrete strengths in the beams. The normalized shear force-displacement and moment-curvature traces are shown in Figure 74 and Figure 75, respectively. It should be noted that the design limit lines have also been normalized accordingly using the design concrete compressive strength of 5,500 psi. As before, the comparison does not seem to be adequate in order to discriminate the beam's performance against a pre-established limit. The normalized plots essentially show the efficiency of the section with respect to the concrete compressive strength. Thus, it can be noted that the beams with the higher compressive strength (NCC and SCC1) have the lowest normalized response value, while the beams with the lower concrete strength (SCC2 and SCC3) achieve greater normalized ratios.

153

lowest normalized response value, while the beams with the lower concrete strength (SCC2 and SCC3) achieve greater normalized ratios.

The shear performance of the test units is best assessed by studying the shear force versus shear strain response in the critical section (29" from the loading points). This was achieved by determining the average shear strains in this region with the before-mentioned shear deformation panels (Figure 62). The average strain on each edge of the shear deformation panel as well as the diagonal are shown in Figure 72 as ζ_i. These values are derived from the deformations shown in Figure 72 as u_{ix} and u_{iy}. These deformations can be divided into the five deformation modes shown in Figure 73. Using Equations (23) and (24) the values of strain can be derived [44].
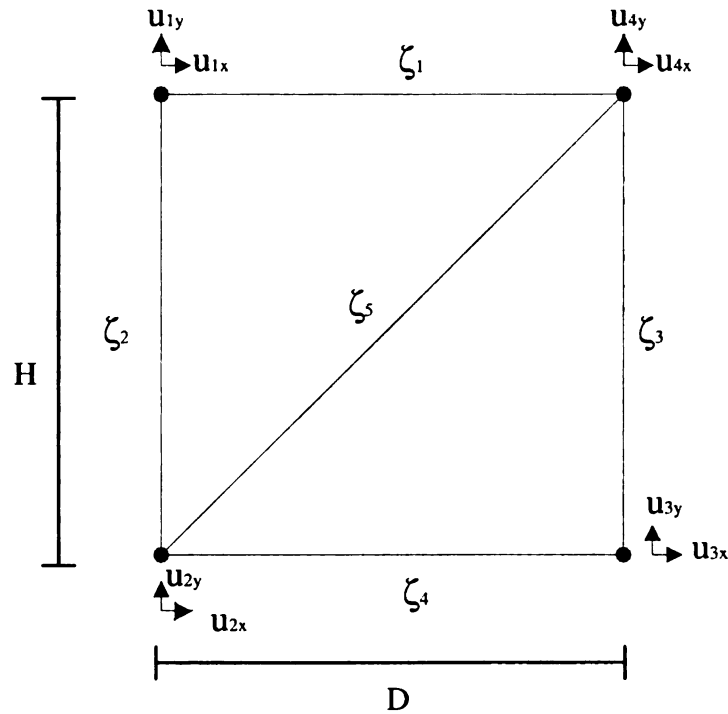
Figure 72. Shear Deformation Panel Theory

The resulting shear force vs. shear strain histories in both panels for the NCC and SCC 1 beams are shown in Figure 76 and Figure 77, respectively. The experimental

154

plots are accompanied by a threshold limit and an analytical shear force vs. shear strain prediction. Both of these analytical values were computed for the concrete strength of the beam at the day of the test. The threshold limit shown was calculated according to the AASHTO-LRFD Specifications [3] simplified sectional analysis procedure. The measured shear strain plotted in the history is an average value from the five average strains shown in Figure 72.
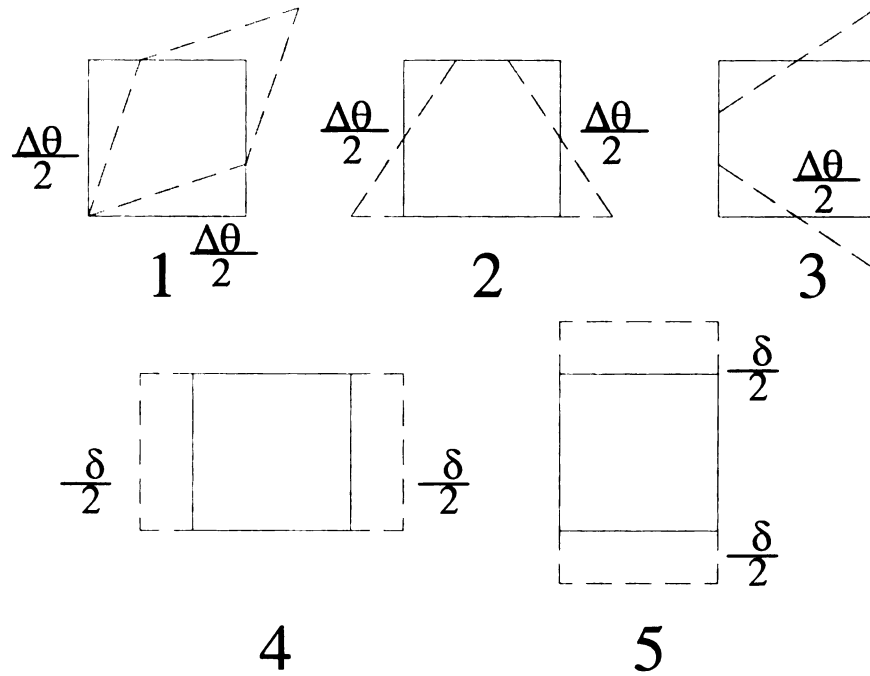
Figure 73. Shear Deformation Modes

$$
\begin{Bmatrix} \Delta\theta^{(1)} \\ \Delta\theta^{(2)} \\ \Delta\theta^{(3)} \\ \delta^{(4)} \\ \delta^{(5)} \end{Bmatrix} =
\begin{bmatrix}
\dfrac{1}{2H} & -\dfrac{1}{2D} & -\dfrac{1}{2H} & -\dfrac{1}{2D} & -\dfrac{1}{2H} & \dfrac{1}{2D} & \dfrac{1}{2H} & \dfrac{1}{2D} \\
\dfrac{1}{H} & 0 & -\dfrac{1}{H} & 0 & \dfrac{1}{H} & 0 & -\dfrac{1}{H} & 0 \\
0 & -\dfrac{1}{D} & 0 & \dfrac{1}{D} & 0 & -\dfrac{1}{D} & 0 & \dfrac{1}{D} \\
-\dfrac{1}{2} & 0 & \dfrac{1}{2} & 0 & \dfrac{1}{2} & 0 & \dfrac{1}{2} & 0 \\
0 & \dfrac{1}{2} & 0 & -\dfrac{1}{2} & 0 & -\dfrac{1}{2} & 0 & \dfrac{1}{2}
\end{bmatrix}
\begin{Bmatrix} u_{1x} \\ u_{1y} \\ u_{2x} \\ u_{2y} \\ u_{3x} \\ u_{3y} \\ u_{4x} \\ u_{4y} \end{Bmatrix}
$$

(23)

$$
(24) \quad \begin{Bmatrix} \xi_1 \\ \xi_2 \\ \xi_3 \\ \xi_4 \\ \xi_5 \end{Bmatrix} = \begin{bmatrix} -1 & 0 & 1 & 0 & 0 \\ 0 & 1 & 0 & 0 & 0 \\ 0 & 0 & 0 & 1 & 0 \\ 0 & 0 & 0 & 0 & 1 \\ 0 & 0 & \dfrac{D}{\sqrt{D^2+H^2}} & \dfrac{H}{\sqrt{D^2+H^2}} & 0 \end{bmatrix} \begin{Bmatrix} u_{1x} \\ u_{1y} \\ u_{4x} \\ u_{4y} \\ u_{3x} \end{Bmatrix}
$$

As explained earlier, the AASHTO LRFD specifications are used for comparison with the experimental data from the shear tests since the values estimated by the Standard Specifications ignore the interaction between shear and flexure, which leads to higher estimates for shear strength. The analytical response (shown with hollow symbols) was determined from a sectional analysis program based on the modified compression field theory (Response 2000) [8]. It can be seen that the calculated capacities according to the MCFT agree closely with the experimental data, as does the analytical shear force vs. shear strain response. The deviations seen between the analytical and experimental traces in the initial part of the response are attributed to limitations on the resolution of the displacement transducers used in the shear deformation panels (see Figure 62).

From the responses of the NCC and SCC1 beams (Figure 76 and Figure 77, respectively) it can be seen, first that there is a clear point at which the shear strains in the critical region increase at a very high rate and second, how this level corresponds very closely to the predicted shear capacity of the section. It can thus be concluded that the sections, both in the NCC and SCC1 beams, reached their shear capacity. From the responses it can also be observed that the "post-elastic" behavior is essentially flat, thus indicating that the section has essentially no more shear resistance.

force vs. shear strain response for all beams is given in Figure 78. In this figure, the measured strains in the deformation panels for each beam were averaged. Also in Figure 78 are threshold limits that indicate the nominal shear design capacity according to the AASHTO-LRFD specifications for the design compressive strength of 5,500 psi. Two threshold lines are shown since one corresponds to the shear span setup of the NCC beam (11 ft) and the other corresponds to the shear span of the SCC beams (9 ft).
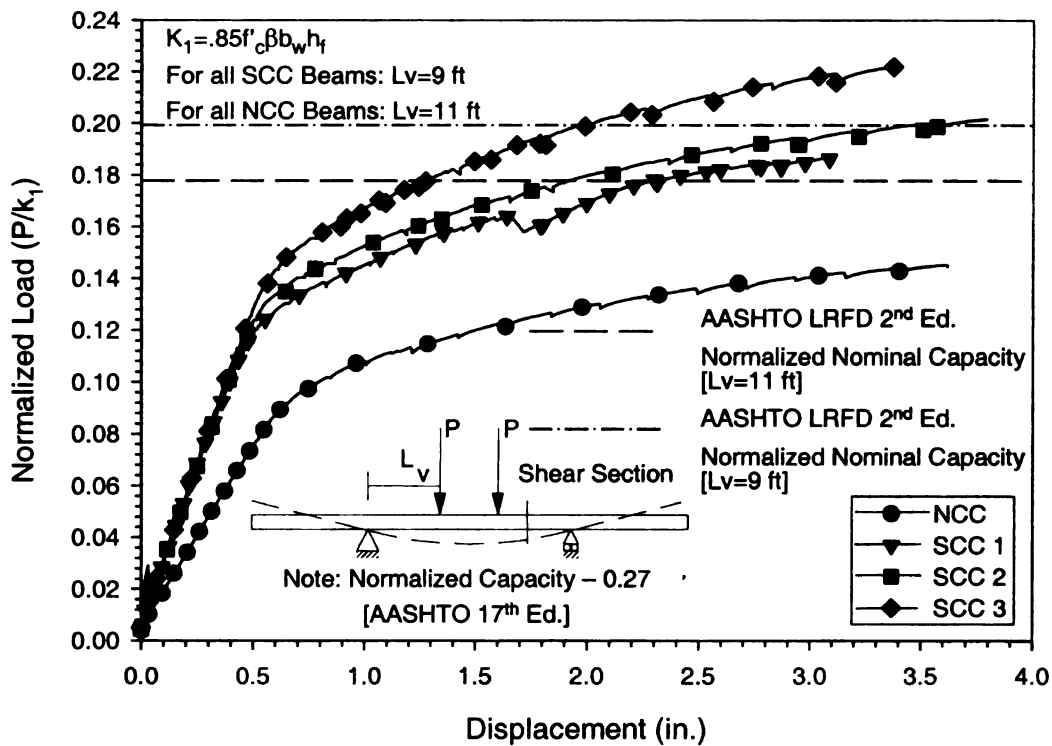
Figure 74. Normalized Shear Force vs. Displacement at Critical Shear Section

157
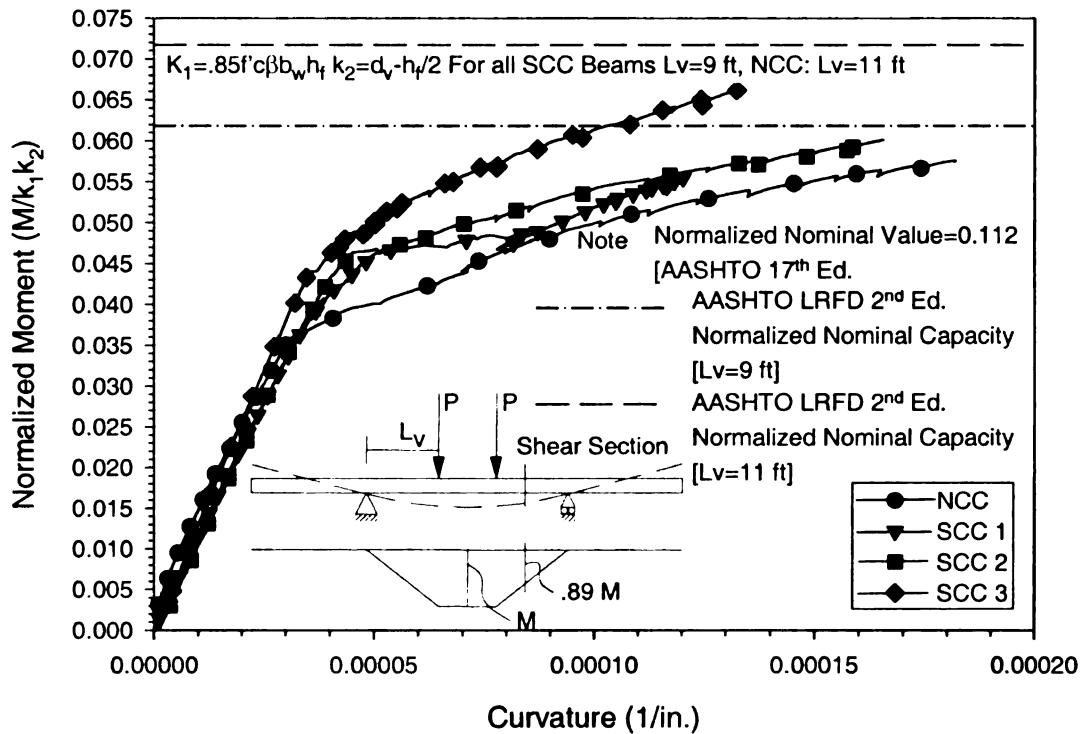
Figure 75. Normalized Moment vs. Displacement Response at Critical Shear Section
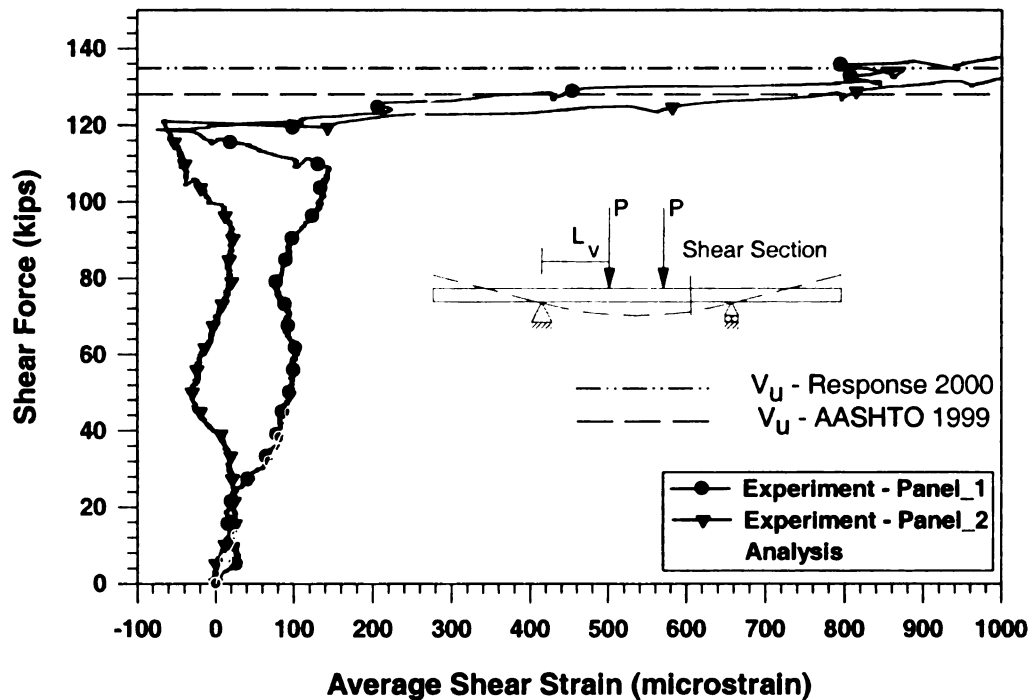
Figure 76. Total Shear Force vs. Shear Strain for NCC Beam

158
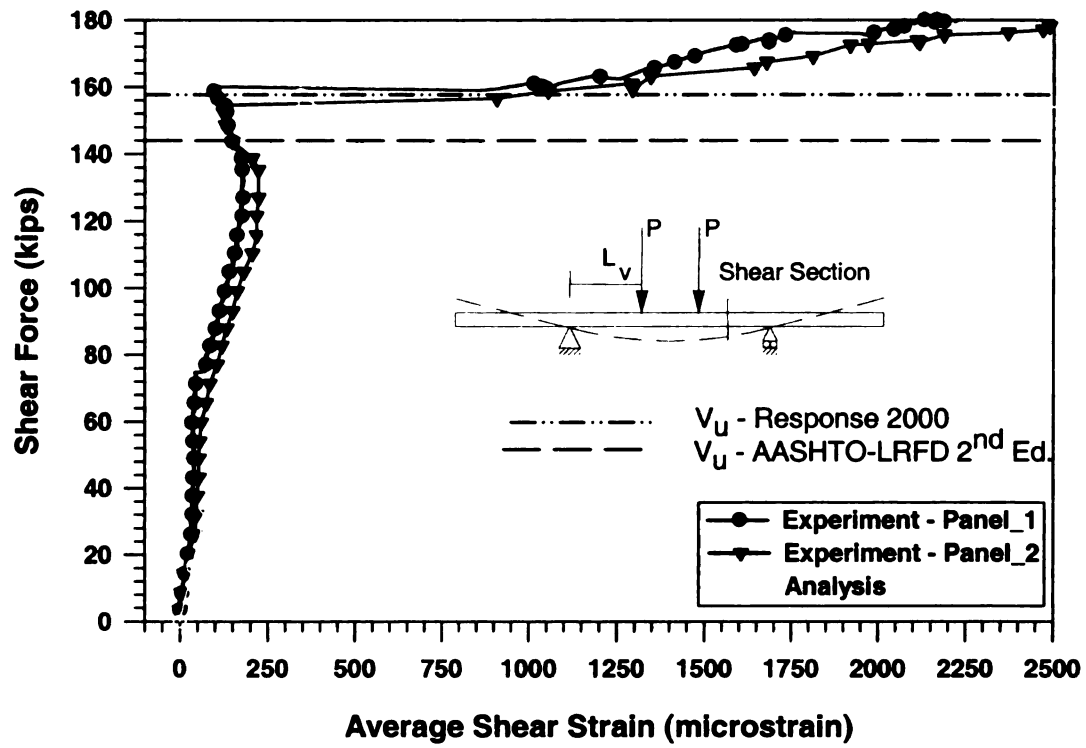
Figure 77. Total Shear Force vs. Shear Strain for SCC1 Beam
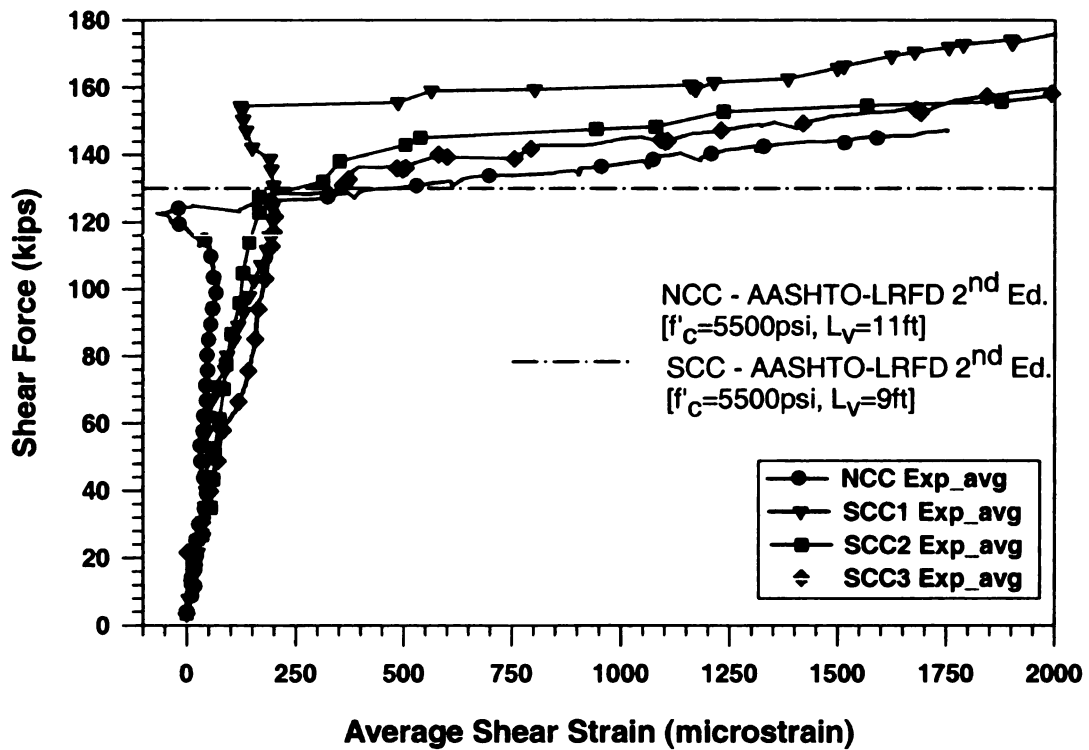
Figure 78. Total Shear Force vs. Shear Strain at Critical Section for All Beams

While only the SCC 3 beam exhibited a flexure-shear failure, all of the beams reached their shear capacities at the critical shear section. However, due to the large amount of prestressing force provided by the prestressing strand the beam was able to redistribute the shear demand beyond the supports to the overhanging portion of the beam once the shear capacity was reached. This allowed the beam to carry additional shear load as the test continued without causing a shear failure of the beam. The beams eventually failed in flexure, generally the failure was a compression failure in the top flange of the beam, as the loads were increased. This was previously shown in Figure 68. Some of the tests were stopped before this flexural failure occurred but only after it was determined that the shear capacity of the critical section had been reached.

The fact that the beams reached their shear capacities is supported by information on the shear reinforcement at the critical shear section. By showing that the shear reinforcement at the critical shear section yielded in all beams, it is possible to show that the beam was no longer capable of resisting shear loads at this point. The shear reinforcement consisted of #4 U-shaped stirrups in the top and bottom flanges of the beams (see Figure 63, Figure 64, and Figure 65). These stirrups were spaced at six inches throughout the end blocks of the beam and then at twelve inches through the remaining portion of the beam. Strain gages were installed on four stirrups near the critical shear section prior to the beams being cast. The four instrumented stirrups were spaced one foot apart starting five feet from the center line of the beam and continuing to eight feet from the center line as shown in Figure 79.
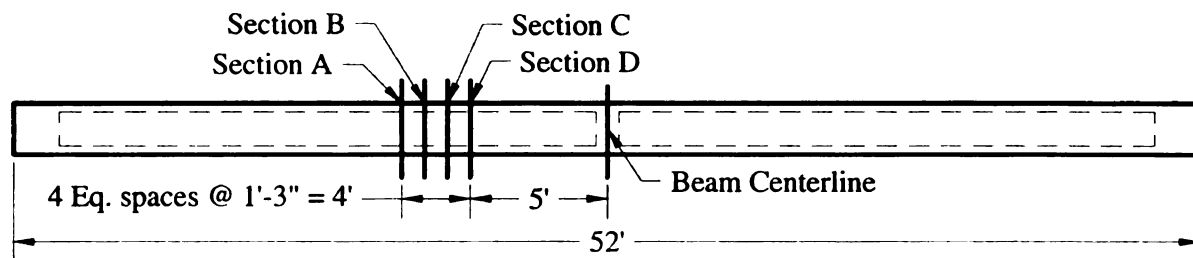
Figure 79. Instrumented Shear Stirrup Location
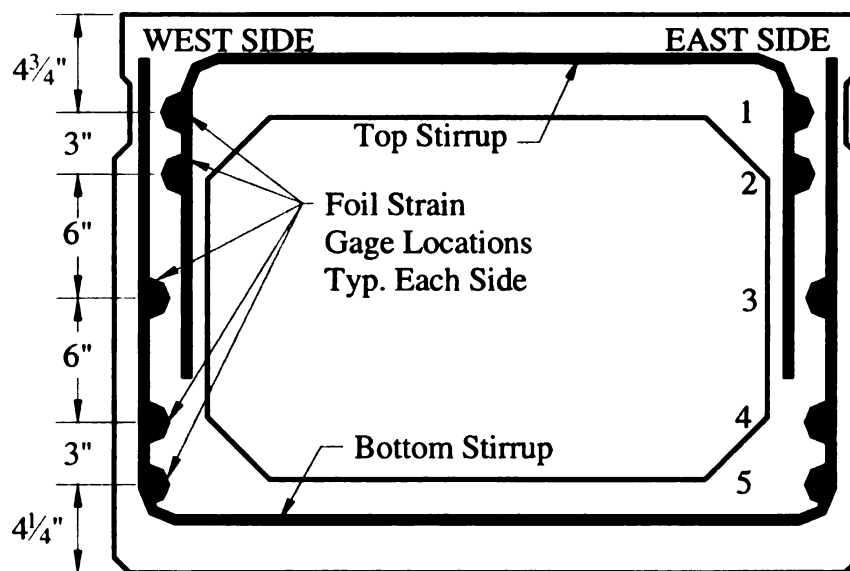
Figure 80. Strain Gage Location on Shear Stirrup

The critical shear section was found through computer analysis to be 6'-5" from the centerline of the beam or 29" from the point of load application. The gages were located along the section depth as shown in Figure 80. Five gages were installed on each side of the stirrups, east and west. The top stirrups had two gages on each leg for a total of four gages, and the bottom stirrups had three gages per leg for a total of six gages. With respect to the bottom of the beam, the gages were located at heights of 4.5, 7.25, 13.25, 19.25, and 22.25 in. on each side of the beam (see Figure 80). The gages are numbered as shown in Figure 80 from top to bottom, 1 through 5. A unique name can be

161

made for each gage using the section name, beam side, and gage number (i.e. A-E1 Section A, east side of beam, gage 1).

The role of the transverse reinforcement is to resist shear forces once the concrete in the web of the beam has cracked and to control crack opening. The tension field created by shear forces is first resisted by the concrete until its tensile strength is exceeded and cracks perpendicular to the tension stress field are formed. Steel reinforcement then resists the tensile forces required to provide a "bridge" for tensile field between concrete cracks. At the crack, increasing shear forces are then carried solely by the steel. In a region where significant cracking has occurred, shear resistance is carried by a combination of tensile forces in the transverse steel and friction along the concrete cracked surfaces. As shear demands increase the deformation demands on the transverse steel will lead to reaching yield. Once a transverse bar has yielded, the deformations become plastic and are not recoverable. Further application of load beyond the point where the steel has yielded will cause the bar to continue to deform and the shear crack to continue to open. A profile of the strain history from the instrumented stirrups (Figure 81 - Figure 84) shows that the stirrups in each beam yielded at the locations of interest. It can be seen that in all tests the load was applied beyond the yield point of the transverse reinforcement and that the strain in the stirrups increased at a much higher rate after yield was reached.

Figure 81 shows strain profiles from the second instrumented stirrup in the NCC beam, located at Section B 3'-6" from the load point along the shear span as shown in Figure 79 The strains are plotted along the height of the beam for multiple load and corresponding displacement levels. The development of strain along the beam depth

162

during the test is shown from left to right in the plot figure, with earlier loading events shown on the left side. From the figure it is possible to see that the stirrup reached the yield point of (estimated at 2000 microstrains for reinforcement with a yield point of 60 ksi.) at approximately the 132 kip load level. The first gage to record a strain beyond the yield point was that at 7.25 in. from the beam bottom. As the test progressed strains in excess of 2000 microstrains were recorded by all but the top gage at this section. The shape of the plot at the end of the test mimics a parabolic distribution of strain through the beam depth. Observing the strain profiles at the different load levels, it can be seen that very little strain was developed in the stirrup during the application of the first 90 kips of the test. However, after the stirrup yielded at 132 kips, small increments of load (5 and 6 kips) caused large increases in the strain readings. The NCC beam test ended at a load of 143 kips and a maximum midspan displacement of 3.8 in. At this loading level, a maximum strain of 6500 microstrain was recorded by gage B-E4 on the stirrup at Section B.
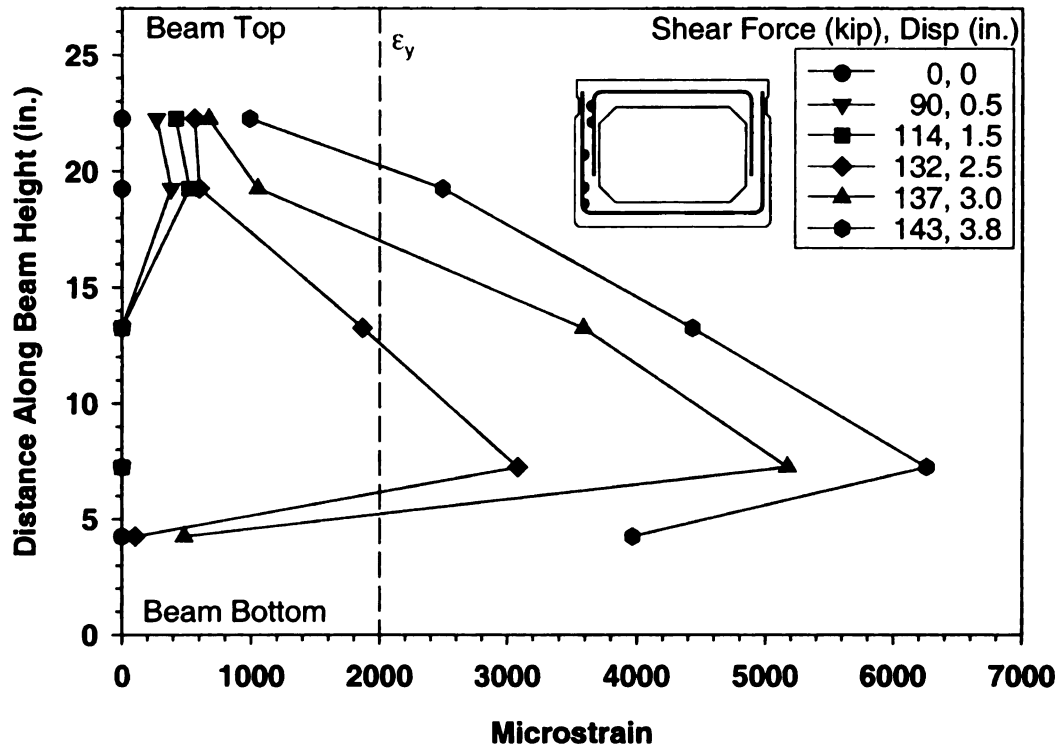
Figure 81. Strain Profiles on Shear Stirrups at Section B for NCC Beam

Strain profiles for one side of one stirrup from the SCC 1, SCC 2, and SCC 3 beams are shown in Figure 82, Figure 83, and Figure 84, respectively. Changes made to the shear test set up after the NCC test to increase the force required to cause flexure failure changed the response of the SCC beams. The most significant change was a stiffer response causing higher loads. Therefore, the stirrups in the SCC beams yielded at higher loads than the NCC beam. The plot of the SCC 1 strain profiles shows that the stirrup reached yielding before 156 kips. The critical stirrup in the SCC 2 yielded near 145 kips, and the SCC 3 critical stirrup yielded before 156 kips.

Only one side of one stirrup is shown for each beam. These representative values are presented as they are the most complete profiles from each beam. Other stirrups had gages that did not record properly through the entire test.
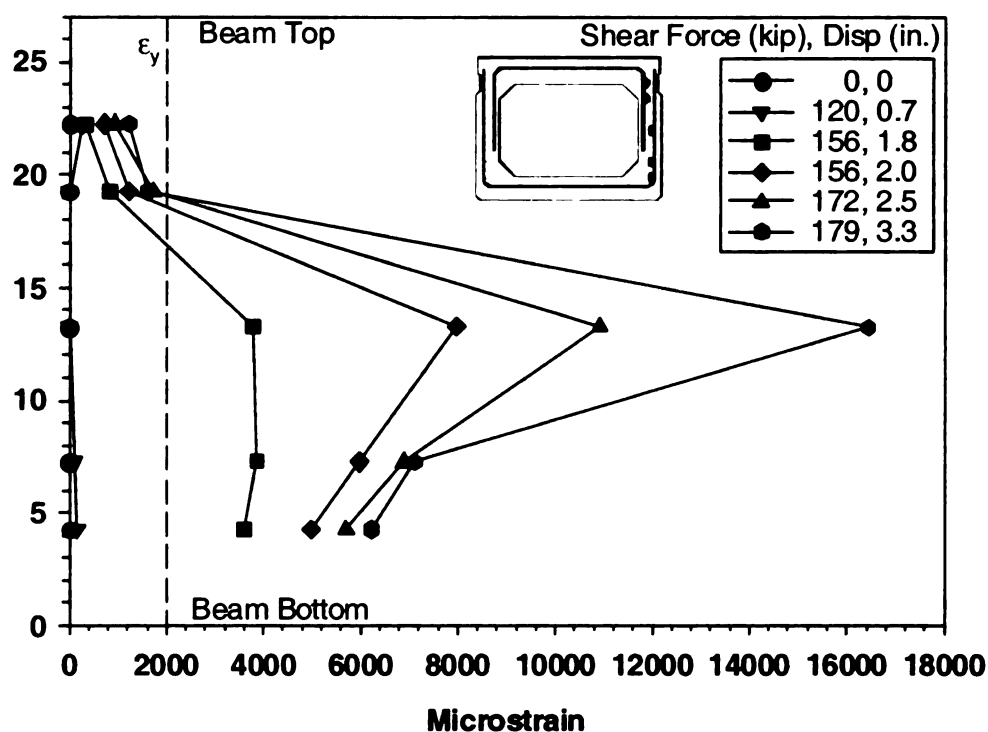
Figure 82. Strain Profiles on Shear Stirrups at Section A for SCC 1 Beam

The strain profiles from the transverse reinforcement in the critical shear region show that the stirrups were demanded well beyond yield for most of the section depth. This information, together with the shear force versus shear strain plots from Figure 78, supports the conclusion that the maximum shear capacity of the beam *section* was reached in all tests. Furthermore, the data in Figure 78 shows that the section shear capacity exceeded the design level.
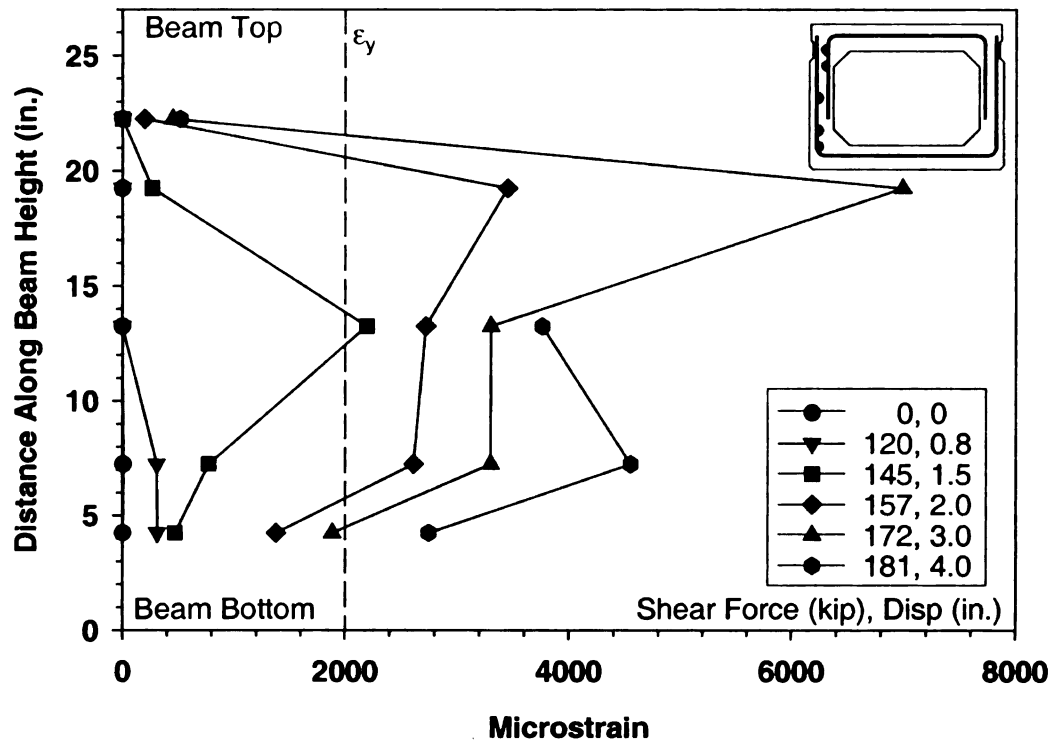
Figure 83. Strain Profiles on Shear Stirrups at Section B for SCC 2 Beam
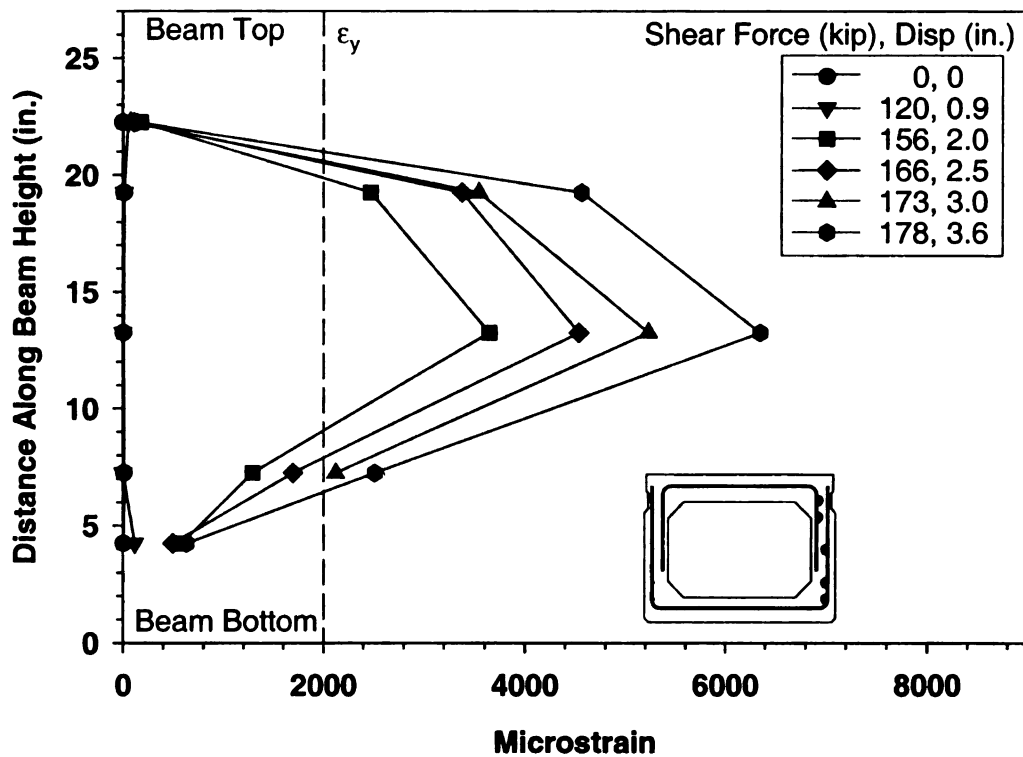
Figure 84. Strain Profiles on Shear Stirrups at Section B for SCC 3 Beam

A summary of the maximum achieved capacities, defined as the point beyond which shear strains increase at a very rapid rate, or in the "plastic" region (see Figure 78) are given in Table 46. It should be noted that the nominal design values shown in the table use the design concrete compressive strength of 5,500 psi. From the values in Table 46 and Figure 78 it can be seen that the SCC1 beam reached the maximum overall shear capacity and highest ratio (1.22) compared to the nominal strength. While the NCC beam had the lowest shear capacity, the nominal design capacity for the longer shear span is also lower due to the larger influence of flexural effects (longer shear span). Thus, the ratio of actual to nominal capacity for the NCC beam was not the lowest (see Table 46). The lowest ratio of actual capacity to nominal strength was for the SCC3 beam, which exceeded the nominal capacity by 8%.

Table 46. Maximum Achieved Capacities of Shear Beams at Critical Shear Section

	Maximum Total Shear (kip)	Maximum Total Moment (kip-ft)	Nominal Design Shear [a] (kip)	Nominal Design Moment [b] (kip-ft)	Actual to Design Ratio (Shear)
NCC	128.4	1102.3	116	994	1.11
SCC1	159.0	1046.6	130	856	1.22
SCC2	145.5	957.8	130	856	1.12
SCC3	140.3	923.3	130	856	1.08

[a] According to AASHTO LRFD [1] Simplified Section Analysis Method

[b] Based on moment-shear interaction envelope calculated using Response 2000 [8] for AASHTO-LRFD criteria.

In spite of the above-noted differences, the shear performance of all SCC beams was similar and their differences were essentially in the behavior of the "post-elastic"

region. This is consistent with the fact that all mixes had similar tensile strength but their aggregate content is different. This would imply that cracking behavior would be similar but that post-cracking response will differ.

The previous discussions have presented data showing that the shear capacity of the critical section in all beams was exceeded. The ultimate failures of the *beams*, however, were not of a pure shear failure in the critical shear region. Further, while the NCC beam failed in flexure at midspan due to the larger shear span (see Figure 60) the section response (Figure 76) and stirrup data (Figure 81 - Figure 84) supports that the shear capacity of the critical shear section was indeed reached. Analysis of this data was not available during testing thus the shear span was shortened for the SCC beam tests (see Figure 61). From Figure 78 it can be seen that all the SCC beams were tested past the point where the beams had exhibited significant "post-elastic" shear deformations but before any global failure. Thus, the critical shear sections the SCC 1 and SCC 2 beams reached their capacity even if complete failure of the beams in shear did not occur. A view of the shear distress in the critical region is shown in Figure 67. The SCC3 beam had a combined flexure-shear failure initiated in the constant moment region also after significant "post-elastic" shear deformations in the shear-critical zone (see Figure 78). A view of the shear-flexure mode for the SCC3 beam was shown in Figure 68.

As explained earlier, the reason the beams were able to continue carrying load after the shear section exceeded its capacity was due to the redistribution of forces on to the continuing beam and the large amount of prestressing in the section. Thus, even though the critical section had reached its shear capacity, the prestressing forces in the beam were large enough to keep the section prestressed and thus able to redistribute

loads. Therefore, in spite of their ultimate global flexure dominated response all beam tests allowed evaluation of the section shear capacity.

5.5 Experimental Evaluation Conclusions

This chapter presented a summary of the testing program aimed at evaluating the flexural and shear response of prestressed beams made from self-consolidating-concrete to determine their suitability for use in the M-50/US-127 demonstration bridge over the Grand River. Four flexure and four shear tests were conducted on full-scale replicas of the bridge box beams, one for each of the project mix designs, which were developed to bound the current approaches to SCC mix design.

The flexural tests showed that the overall behavior of the SCC beams was very similar to that of the conventional beam (NCC). Cracking patterns, widths, and failure levels followed predicted responses through conventional prestressed concrete theory. While the failure of the flexure test units was explosive, the beam was not over-reinforced and the strands yielded before failure, technically defining the failure mode as ductile. Consequently, variations in concrete compressive strength did not significantly modify the beam's ultimate capacity, which were very similar for all beams. The absolute capacities of the SCC beams were marginally lower than that of the NCC beam, specifically, 1.3, 3.4, and 3.5 percent lower for the SCC1, SCC2, and SCC3 beams, respectively. However, the flexural capacities of the SCC beams exceeded the required design capacity by 6 to 9 percent according to Table 44.

The shear behavior of the SCC beams was also found to be adequate and very similar to that of the NCC beam. Cracking paths and widths were consistent in all beams and the failure levels closely matched analytical predictions. The shear capacities of the

SCC beams were comparable to that of the NCC beam. The ratio of capacity to nominal strength for the SCC1, SCC2 and SCC3 beams as 1.22, 1.12, and 1.08, respectively, while that same ratio for the NCC beam was 1.11 according to Table 46. The shear capacity and response of the SCC beams is thus considered adequate.

Due to the large amount of prestressing and the extension of the beam beyond the supports, failure of the critical section in shear did not result in overall member failure. Rather, the beam was able to re-distribute demands beyond the critical shear area thus allowing the beam to resist increasing loads that in two beams eventually lead to flexure-induced failures and in two others the tests were terminates. However, even though the overall member failure was not in a pure shear mode, the shear behavior and capacity provided by the beams was successfully evaluated. This was determined by studying the shear force versus shear strain response of the critical shear areas in the beam, which showed that the *sections* reached a peak shear force beyond which shear strains would increase rapidly in an almost elastic-perfectly-plastic response. This same behavior was supported by the moment-curvature response of this sections, which had essentially a bi-linear response with a failure at a load level much below the known flexural capacity. The reduced flexural capacity of the section is thus a consequence of the shear failure of the section. In addition, evaluation of strain profiles of the steel stirrups in the critical shear areas indicated that the transverse steel had yielded through the section depth for all beams, further supporting that sections shear failure was reached.

Overall, the performance of the SCC prestressed box beams in flexure and shear was found to be essentially equal to that of the NCC beam and their behavior was well predicted by conventional prestressed concrete theory. While additional issues pertaining

to long-term behavior of SCC in prestressed elements, namely creep effects, are still to be fully evaluated, the short-term flexural and shear response evaluated through this testing program indicates that the SCC prestressed beams safely satisfy their prescribed design requirements. The results of this testing program provided sufficient evidence to believe the SCC beams could be used in the demonstration bridge as planned.

6 LONG TERM PERFORMANCE OF SCC BRIDGE BEAMS

6.1 Overview

The structural testing program described in the previous chapter assessed short-term properties of bridge members produced with SCC. Results from these tests indicated that the flexural and shear response of these members is essentially equal to that of NCC members. Furthermore, it was shown that the capacities of the SCC members exceeded the design capacity requirements for the demonstration bridge planned for this project. The experimental program, however, cannot provide answers on questions regarding differences in the long-term performance of SCC members compared to NCC members under normal exposures to vehicle loading, weather demands, and long-term material volume changes.

The performance of a bridge member over its service life is affected by many external factors. These factors include external loading (including repetitive loading) from vehicles, exposure to changes in weather, and exposure to deicing chemicals. Other factors that affect this performance are related to the materials themselves. These include concrete creep, permeability, and toughness and steel relaxation. Finally, the long-term performance of the bridge member can be affected by the overall performance of the bridge system. This includes the ability of the beams to expand and contract freely under temperature changes. All of these factors will affect the long-term performance of the beams.

The field-monitoring program for this project was designed to analyze how time dependent factors affect the structural performance of SCC members. To this end, a

172

demonstration bridge consisting of six spread box beams was built and instrumented to monitor the performance of both NCC and SCC beams.

Of the six beams composing the demonstration bridge, three were produced with SCC and three were produced using NCC. The three SCC beams and one of the NCC beams were instrumented to monitor changes in concrete strain and temperature. Two types of instruments were installed in each beam to measure these parameters. Eight Type T thermocouples were installed to record temperature, and eight vibrating wire strain gages were installed to measure strain in the concrete. The results obtained from the instruments can be used to assess the performance of the SCC beams.

The field monitoring system, including a description of the instruments and the datalogging system, are presented followed by the results taken from the system. Finally, five factors are investigated to explain the data recorded by the field monitoring system. These include:

- Prestress losses
- Presence of diaphragm
- Temperature
- Bearing stiffness, and
- Data normalization.

6.2 Field Monitoring System

The field monitoring system consists of 64 gages connected to a Campbell Scientific (Logan, Utah) datalogger. The datalogger was programmed to record data 12 times throughout the day (at equal time intervals) and store them until they can be downloaded to a personal computer. The data was then post-processed to a more useable

format. The datalogger system, including the instrumentation, is described in more detail below.

6.2.1   Instrumentation

The purpose of instrumenting the field beams was to obtain long-term information about the in-service performance of the elements cast with the different concrete mix designs. To accomplish this, each field beam was provided with eight vibrating wire strain gages (VWSG) to record changes in concrete strains and eight Type T thermocouples to record temperatures.

6.2.1.1 Vibrating Wire Strain Gages (VWSG)

The VWSG used in this project were Geokon (Lebanon, New Hampshire) model number 4200 gages, which are specially designed for embedment in concrete. They have a range of 3,000 microstrains and a temperature range of 212 °F (-4 °F to 176 °F). VWSG were selected for this project because of their rugged construction and their long-term reading stability, or resistance to reading drift. However, the VWSG are slow to respond and thus not suitable to record rapid changes in strain.

The VWSG were installed in the field beams at three sections along the length of the beam as shown in Figure 85. Two gages were installed in the top and bottom flanges at section A, and one gage was installed in each flange at sections B and C. The nomenclature used to identify the gages is as follows: the gage located in the top flange at Section C is named C-T, and likewise the gage located in the bottom flange at Section B is named B-B. To distinguish between the gages at Section A, where two gages are placed in each flange, a number 1 or 2 follows the gage name. Therefore, A-T1

174

represents the first gage located in the top flange, while A-B2 is the gage in the bottom

flange as shown in Figure 86. To secure the instruments at the proper location, each gage

was attached to two pieces of #4 reinforcing steel and suspended between the prestressing

strands in the bottom flange and the mild steel reinforcement in the top flange. An

example of the installed VWSG before the concrete was cast is shown in Figure 87.
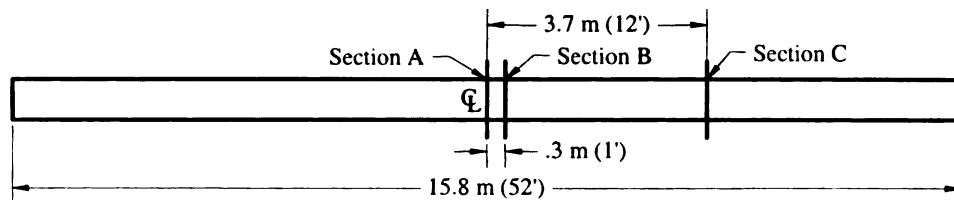
a) Instrumentation Sections Field Beam
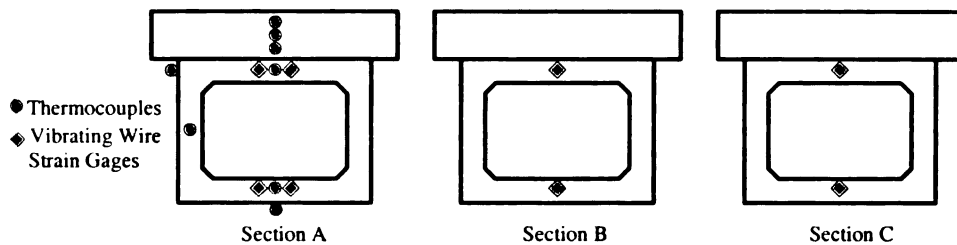
b) Instrument Locations for Field Beam

Figure 85. Field Beam Instrumentation
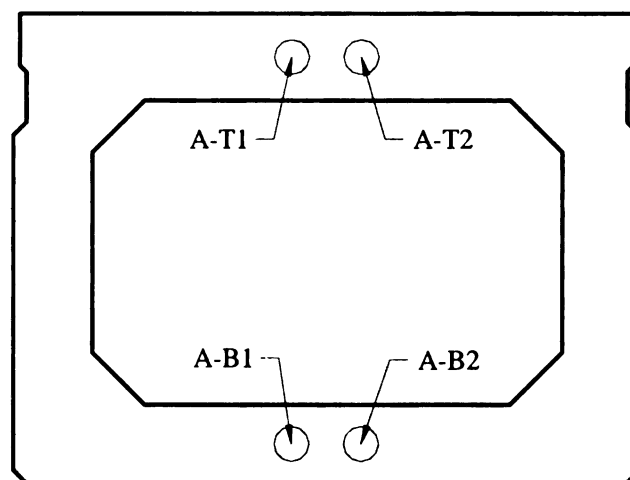
Figure 86. Naming Convention for VWSG

175
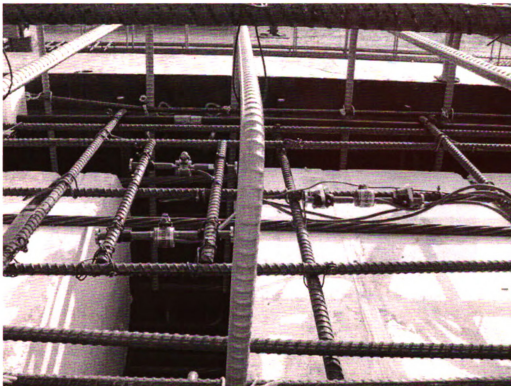
Figure 87. Vibrating Wire Strain Gages Installed in The Top Flange

The VWSG, shown schematically in Figure 88, consists of a wire suspended between two metal disks. An electromagnetic coil is attached to the gage at the midpoint of the wire. The coil is used to excite, or "pluck," the wire by inducing an electromagnetic field. As the wire is excited it vibrates. The coil can measure the frequency of the wire vibration. The coil changes the frequency of the wire vibration through a set range. In this range is the resonate frequency of the wire. The coil recognizes the resonate frequency and transmits this reading to the datalogger where this frequency is converted to a strain measure.
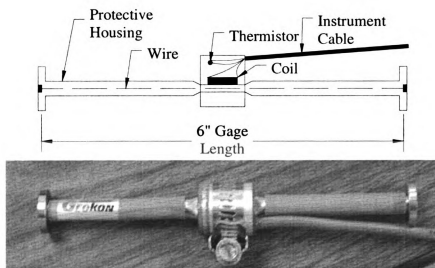
Figure 88. Schematic of Vibrating Wire Strain Gage

The VWSG measures the change in strain in the concrete by measuring the change in the wire's resonate frequency. As the strain in the concrete changes the two metal disks change position relative to each other. As this happens the tension in the wire suspended between the discs changes, causing the wire to resonate at a different frequency.

The VWSG used in this project also contain a thermistor in the coil housing. The thermistor records the temperature at the measurement location. It is important to have an accurate value of temperature because the difference between the thermal coefficient of expansion of the embedded steel wire and the concrete affects the accuracy of the strain reading. In addition, readings are to be taken over time and they need to be compensated for temperature at the time the measurement is taken.

As the temperature increases both the steel wire in the VWSG and the concrete expand. However, because the coefficient of thermal expansion of steel is larger than that of concrete, the wire will expand more than the concrete. This will appear to be a

compressive strain in the concrete, when this may not be the case. To account for this the strain should be corrected for temperature according to Equation (25):

$$(25) \quad \varepsilon = \Delta T \left(CTE_{steel} - CTE_{concrete} \right)$$

where ΔT represents the change in temperature in °F, CTE_{steel} is the coefficient of thermal expansion of steel, and $CTE_{concret}$ is the coefficient of thermal expansion of concrete both measured in microstrain/°F. The actual strain experienced by the concrete is then given by Equation (26):

$$(26) \quad \varepsilon_{actual} = \left(\varepsilon_i - \varepsilon_0 \right) B + \left(t_i - t_0 \right) \left(CTE_{steel} - CTE_{concrete} \right)$$

where ε_i and t_i are the ith reading of the strain and temperature respectively, ε_0 and t_0 are the initial readings of the strain and temperature. The constant B is a batch calibration factor that corrects for wire clamping; which results in a higher reading than the actual strain. The batch factor for the VWSG used in this project was provided by the manufacturer as a value of 0.958.

The initial strain and temperature values in the unstressed condition of the beam were recorded to be used as the reference values for future readings. These values were taken during the beam production process after the concrete was cast but before the prestressing strands were cut. To record the values, a Geokon (Lebanon, New Hampshire) GK-403 Readout Box was used. This box is capable of exciting the wire and recording the strain as well as the temperature.

The initial temperature and strain values for the gages are shown in Table 47 through Table 50. Two gages did not read properly at the time the strands were cut. The gages were A-B1 in the NCC beam and C-T in the SCC 2 beam. Fortunately, these instruments began working properly once the beams were in place at the bridge.

178

Table 47. NCC VWSG Initial Readings

Instrument	Temperature (°F)	Strain (micro strain)
A-T1	97.2	2769.3
A-T2	96.3	2613.7
A-B1	96.3	-
A-B2	97.2	2752
B-T	90.1	2875.1
B-B	94.6	2949.1
C-T	90.1	2779.8
C-B	132.0	2771.2

Table 48. SCC 1 VWSG Initial Readings

Instrument	Temperature (°F)	Strain (micro strain)
A-T1	133.9	3364.9
A-T2	133.7	3302.9
A-B1	146.1	2244.5
A-B2	145.8	2472.3
B-T	120.7	2985.3
B-B	135.7	2436.8
C-T	118.4	2691.4
C-B	131.4	2740

Table 49. SCC 2 VWSG Initial Readings

Instrument	Temperature (°F)	Strain (micro strain)
A-T1	94.1	3421.3
A-T2	94.3	3405
A-B1	102.0	2702.6
A-B2	102.0	2644.1
B-T	91.2	2815
B-B	99.3	2790.4
C-T	91.4	-
C-B	98.6	2768

Table 50. SCC 3 VWSG Initial Readings

Instrument	Temperature (°F)	Strain (micro strain)
A-T1	115.0	3214.1
A-T2	116.4	3163.2
A-B1	130.6	2581.4
A-B2	130.1	2678.2
B-T	94.6	3214.3
B-B	117.5	2746.1
C-T	91.9	2837.7
C-B	110.5	2672.6

6.2.1.2 Thermocouples

Thermocouples are used to measure temperature in their surrounding environment. The instrument is made of two wires of dissimilar metallic conductors. The choice of the materials affects the effectiveness of the thermocouple. The thermocouples used for this project were Type T from Omega Engineering (Stamford, Connecticut). Type T thermocouples are made of a positive Copper wire and negative Constantan wire. The wires are welded together at the measurement end, and left unconnected at the reference end. Figure 89 shows the measurement end of a Type T thermocouple used in this project.

Blue – Copper (+)

Red – Constantin (-)
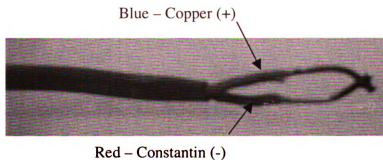
Figure 89. Measurement End of Thermocouple

The thermocouple is able to measure the difference in the temperature between the measurement end and the reference end. When the ends of two dissimilar metals are held at different temperatures a voltage develops between them. This voltage varies according to the temperature in a known and regular way such that it can be converted to temperature. The welded end of the wire is embedded into concrete to record the temperature.

The thermocouples were set in place by attaching them to the reinforcing steel as shown in Figure 90. The location of the thermocouples throughout the depth of the beam are shown in Figure 91 Three thermocouples were installed at section A of the beam (Figure 85). One thermocouple was in the top flange of the beam, the second was in the sidewall of the beam at the mid height of the beam, and the third was in the bottom flange of the beam. The remaining five thermocouples were installed once the bridge was being erected at the bridge site. Three thermocouples were located in the deck of the bridge, and two thermocouples were placed on the outside of the beam at section A of each of the four instrumented beams. One of the external thermocouples was placed on the bottom of the beam and the second was placed at the joint between the deck and the beam of each of the four instrumented beams.
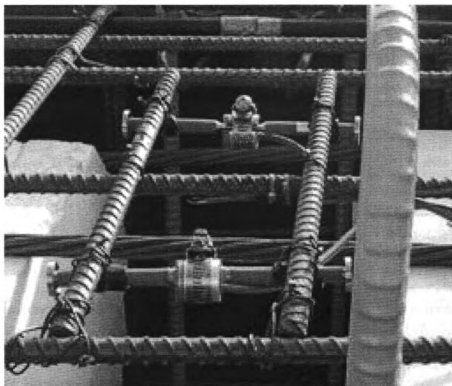
Figure 90.   Installed Thermocouple
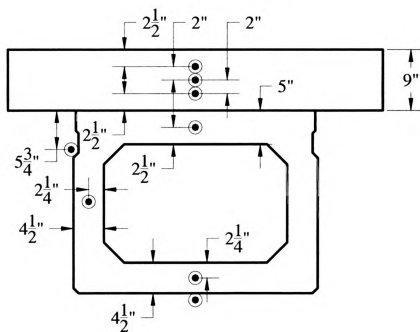
Figure 91.   Thermocouple Locations

6.2.2   Data Collection System

The automated collection system used to monitor data from the installed instruments consists of one datalogger, four multiplexers, and one vibrating wire gage interface. The system was automated to record data at specific times throughout the day. External power sources provide the necessary voltage to execute the data collection program.

The datalogger used is a Campbell Scientific (Logan, Utah) CR10x. The datalogger is powered externally by a 12-volt rechargeable deep cycle marine battery (model number SRM 29). The battery has a 100 amp-hour capacity and is recharged by a 10 W solar panel. The panel was placed atop a 12-foot pole that is attached to the eastern return wall of the bridge abutment as shown in Figure 92. The solar panel has dimensions of 16.5 in. by 10.6 in. and the voltage output from the solar panel at maximum power is 17.5 V.
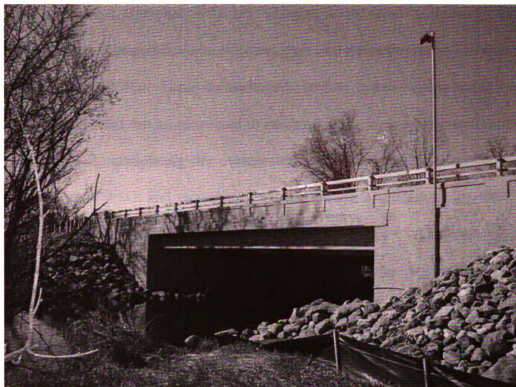
Figure 92. Full Bridge Picture Showing Solar Panel

Two types of multiplexers are used between the instruments and the dataloggers. The role of the multiplexers is to expand the number of instruments that can be read by the datalogger. Instruments connected to the multiplexers share a common channel on the datalogger. The datalogger program advances through the instruments connected to each multiplexer reading and storing each data point.

The 32 thermocouples are connected to two Campbell Scientific (Logan, Utah) AM25T solid-state multiplexers that are specifically designed for thermocouples. Each AM25T can hold 25 thermocouples. The vibrating wire strain gages are connected to two Campbell Scientific (Logan, Utah) AM 16/32 relay multiplexers capable of handling 16 four-wire gages or 32 two-wire gages. Each of the 32 VWSG used in this project has four wires thus two AM16/32 multiplexers were required. The final component of the

datalogging system is a Campbell Scientific (Logan, Utah) AVW4 vibrating wire interface. This device is placed between the datalogger and the multiplexers to enhance the reading from the VWSG. These enhancements include expanding the number of AM16/32 multiplexers that can be connected to the datalogger, removing noise from the vibrating wire signal, completing the thermistor bridge needed to measure the temperature with the VWSG, and increasing the peak-to-peak excitation of the VWSG frequency.

The datalogger functions were automated with a program written using the Campbell Scientific (Logan, Utah) datalogger support software PC208W program creator EDLOG. The program is designed to execute every two hours starting at 12:00 am for a total of 12 executions each day. Two hours is the maximum execution time allowed by the datalogger. On each execution of the program each gage is read once and its value is recorded by the datalogger. The vibrating wire strain gages record both strain and temperature. This allows the strains to be corrected for the difference between the coefficient of thermal expansion of the steel in the vibrating wire strain gage and the concrete. Accordingly each time the program executes 3 types of data are recorded: the strain from the strain gage, the temperature from the strain gage, and the temperature from the thermocouples. There are 8 strain gages per beam and 4 beams total for a total of 32 strain gages. There are also 8 thermocouples per beam for a total of 32 thermocouples. That means on each program execution 96 data points are recorded. Each day 1,152 data points are stored by the datalogger and each month nearly 35,000 data points are stored. The datalogger has a final storage capacity of 62,280 data points. Given the number of points stored every day, the system will reach its capacity after 53

days. Once the capacity of the system is reached, the earliest recorded data will begin to be overwritten by new data points. Currently the system data is collected every month. Each time the program runs it takes 1.5 minutes to cycle through all 64 instruments and record the 96 data points.

The data is downloaded from the datalogger by connecting a laptop computer to the datalogger using the PC208W software. The connection is made through a Campbell Scientific (Logan, Utah) SC32B Optically Isolated RS-232 Interface. A cable converting the 9 pin serial signal to USB is also used to retrieve the data.

The data was post-processed using a custom MATLAB (The Mathworks, Natick, Massachusetts) program. The program was designed to separate and convert the data into a more useable form. This includes correcting the strains for temperature and reducing the data to the desired times. Of the twelve readings taken each day only four are kept for analysis. These are the 12 am, 6 am, 12 pm, and 6 pm readings. The MATLAB program plots and stores these values. The rest of the data is stored separately.

To connect the instruments to the datalogger the wires from each instrument were routed to the north end of the beams and then to the datalogger location as shown in Figure 93. Once at the end of the beam the bundle of wires crosses through the bridge backwall. The wires from the NCC and SCC 1 beams and the SCC 2 and SCC 3 beams were routed to the center of the back wall between each set of two beams where the bundle of wires cross back through the back wall to the underside of the bridge. Once under the bridge the wires were routed to the datalogger box, which was mounted on the back wall underneath the bridge between the NCC and SCC 1 beams.

From the time the wires leave the beam they are encased in non-metallic schedule 40 PVC pipe so that the entire system is protected from moisture. The datalogger and power source were housed in locked weatherproof PVC cabinets. The datalogger box contains a back plate designed for connecting the system components. All components of the datalogger system box are secured in this box. Both the datalogger and battery boxes are connected to the back wall by threaded rods embedded into the concrete with a two-part construction adhesive.
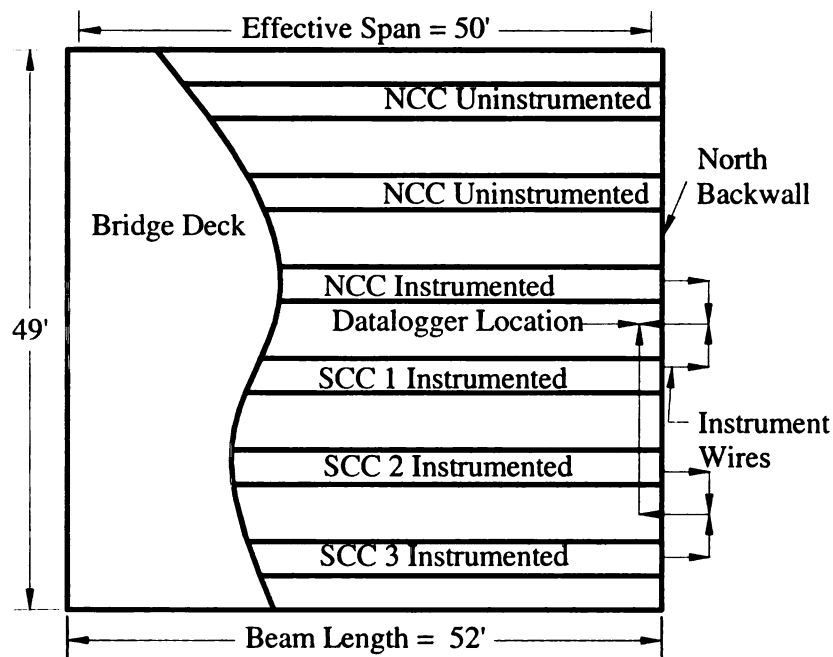
Figure 93. Wire Routing Scheme

6.2.3 Observations and Results

The data recorded from the instruments in the demonstration bridge could provide information on the performance of elements cast with SCC. Data showing similar performances between the NCC and SCC beams would indicate that the SCC does not behave differently over time when used in a prestressed bridge element. However,

differences in the concrete strain in the SCC beams could indicate problems that could ultimately lead to an early failure of a bridge element cast with SCC.

Before monitoring of the instruments in the beams could begin at the bridge site, four preliminary strain measurements were taken. Measurements were taken after transfer of the strand force, after the top strands were cut at the beam centerline, once the beams were in place at the bridge site (on top of abutment supports), and after the deck was cast in place. These events, including the date they occurred, are summarized in Table 51. The bridge was opened to traffic shortly after the deck was cast in the middle of October 2005. Monitoring of the bridge data began on December 22, 2005.

Table 51.   Preliminary Strain Measurement Events

	Event	Date
1	After strands were released	6-22-05 – 6-30-05
2	After top strand was cut	8-2-05
3	In place at bridge site	9-21-05
4	After deck was cast	10-2-05

The results of the strain measurements in the bottom flange at the midspan of the beam, section A, at 12:00 pm for all of the beams are shown in Figure 94. As discussed previously, the first four points in the plot are the initial measurements taken during the construction phase of the project. The monitoring of the instruments at the bridge site began on December 22, 2005. Gaps in the plots, such as the gap in the SCC 3 plot in Figure 94 during the month of April, are due to loose wire connections. Unfortunately, these occurred occasionally throughout the year and were corrected as soon as possible.
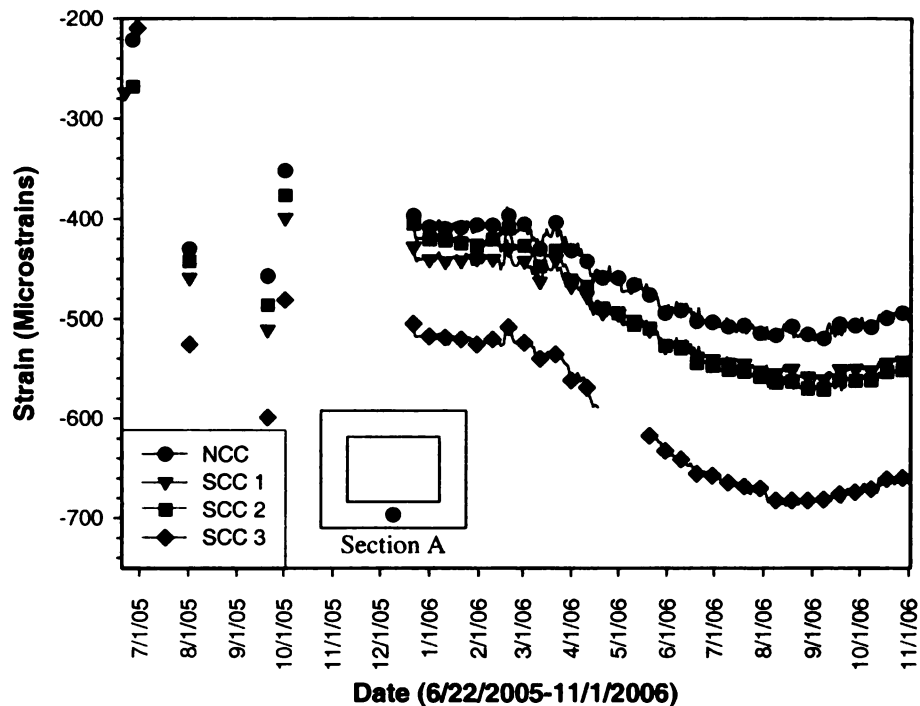
Figure 94. Strains In The Bottom Flange of Section A

The plots shown in Figure 94 show similar behavior over the period of observation. While each beam has a different starting value the overall shape of each plot is similar. As will be seen in future figures of the data from the VWSG at other locations in the beams, the strain readings in all four plots began to become more compressive, i.e., more negative, near the end of the month of February 2006. Then during the month of August 2006 the readings began to become more tensile, or less negative. The maximum decrease in strain is anywhere from 100 – 200 microstrain during these time periods.

The strain readings in the top flange of Section A are plotted in Figure 95. Again the first four points represent readings taken during the construction of the bridge. Again while the overall performance of these beams seems to be similar, with similar shapes to the responses, the starting point of these plots is different. Because of the different

starting points the scale of this plot is larger than the plot for the strain in the bottom flange. Even though the starting values of the plots are very different, the overall response is similar for the four beams. The continuous monitoring shows a decrease in strain starting in the end of February 2005, and an increase in strain beginning in September 2005. This decrease in strain is comparable to the decrease seen in the bottom flange results.
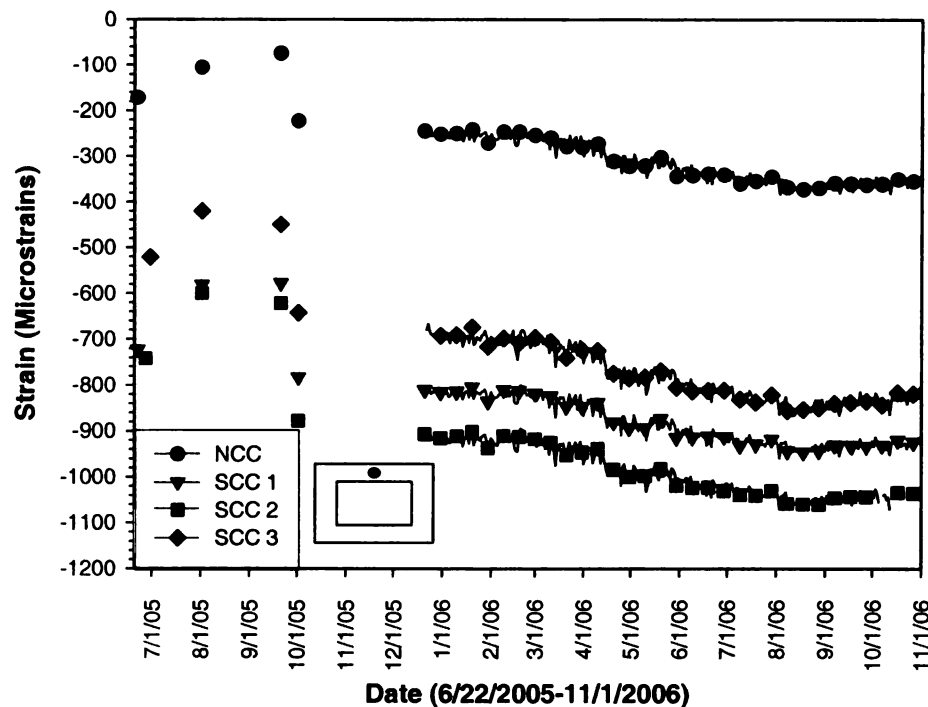
Figure 95. Strains at Top of Beam Flange Section A

The decrease in strain shown in both Figure 94 and Figure 95 seems to be related to temperature as the maximum decrease occurs during the warmest months of the year. This can be verified by examining the data recorded by the thermocouples. Figure 96 and Figure 97 show the recorded thermocouple temperatures at the top of the bridge deck and in the bottom flange of the beams at 12:00 pm each day. As expected, the temperature

increased through the summer months. Table 52 gives the maximum, minimum, and average temperatures recorded in the top of the deck for each beam. The minimum temperature recorded was approximately 14°F in the middle of February 2006, while the maximum-recorded temperature was 91 °F in August. The average temperature for all of the beams was near 56 °F at the top of the deck.

The plot of the temperature in the bottom of the flange at Section A in Figure 97 is very similar to that at the top of the deck. The maximum, minimum and average temperatures are reported in Table 53. At the bottom of the beam the maximum temperature occurred on the same day as in the top of the deck, and was found to be 86 °F. The minimum temperature in the bottom of the beam was found to be near 17 °F. to the temperatures in the top flange. The average temperature at this location was found to be near 55 °F.
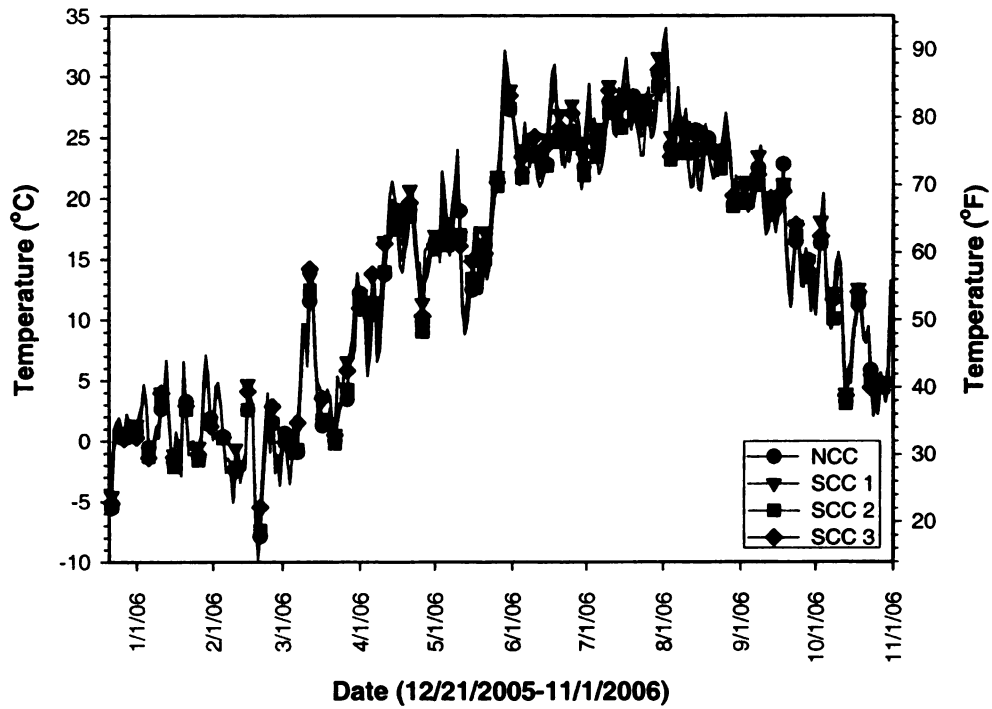
Figure 96. Temperature at Top of Bridge Deck at Section A
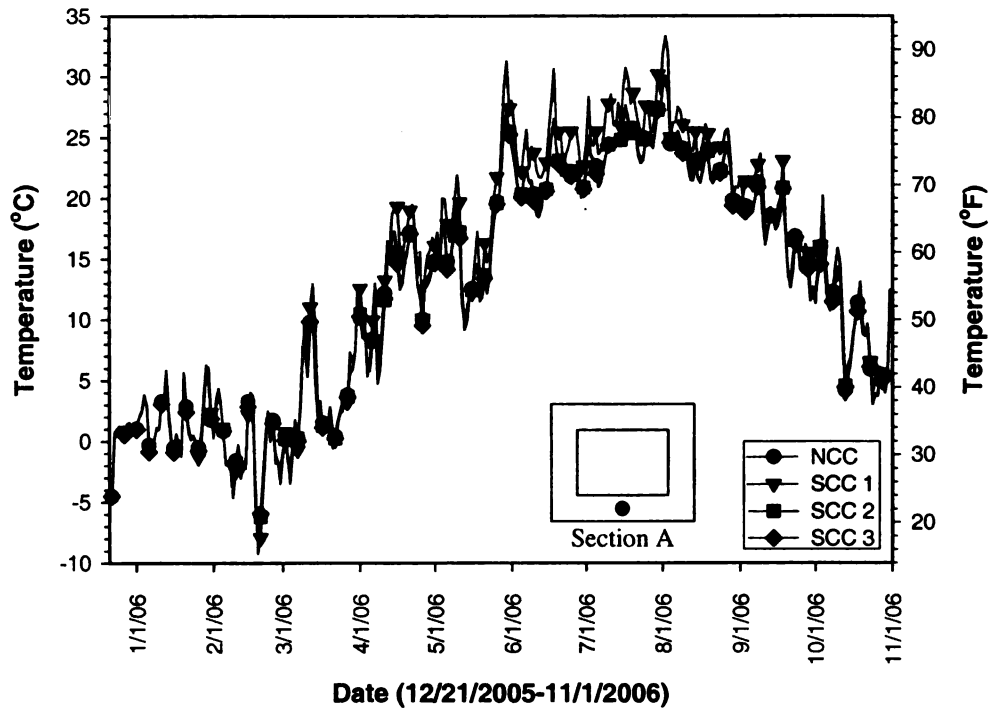
Figure 97. Temperatures in the Bottom Flange at Section A

Table 52. Maximum, Minimum, and Average Temperatures At Top of Deck

	NCC	SCC 1	SCC 2	SCC 3
Max Temp (°F)	91.6	93.1	89.1	90.6
Minimum Temp (°F)	14.5	17.2	14.8	17.7
Average Temp (°F)	56.3	58.0	55.3	56.9

Table 53. Maximum, Minimum, and Average Temperatures At Bottom of Beam

	NCC	SCC 1	SCC 2	SCC 3
Max Temp (°F)	86.1	86.4	86.1	86.0
Minimum Temp (°F)	17.1	17.5	17.7	17.7
Average Temp (°F)	54.8	54.9	57.3	54.5

Figure 98 through Figure 101 show the plots of the strains in the top and bottom flanges of sections B and C, which were located 12 inches and 12 feet from Section A, respectively. These plots are very similar to the plots of the strain at Section A, as similar trends appear in each case.
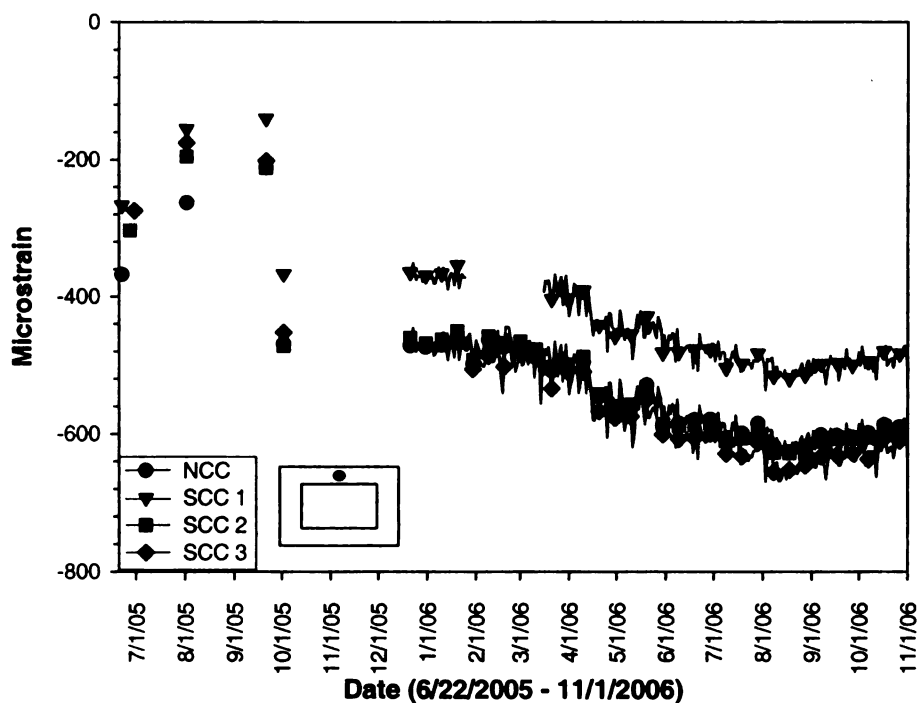
Figure 98. Strains in the Top Flange of Section B
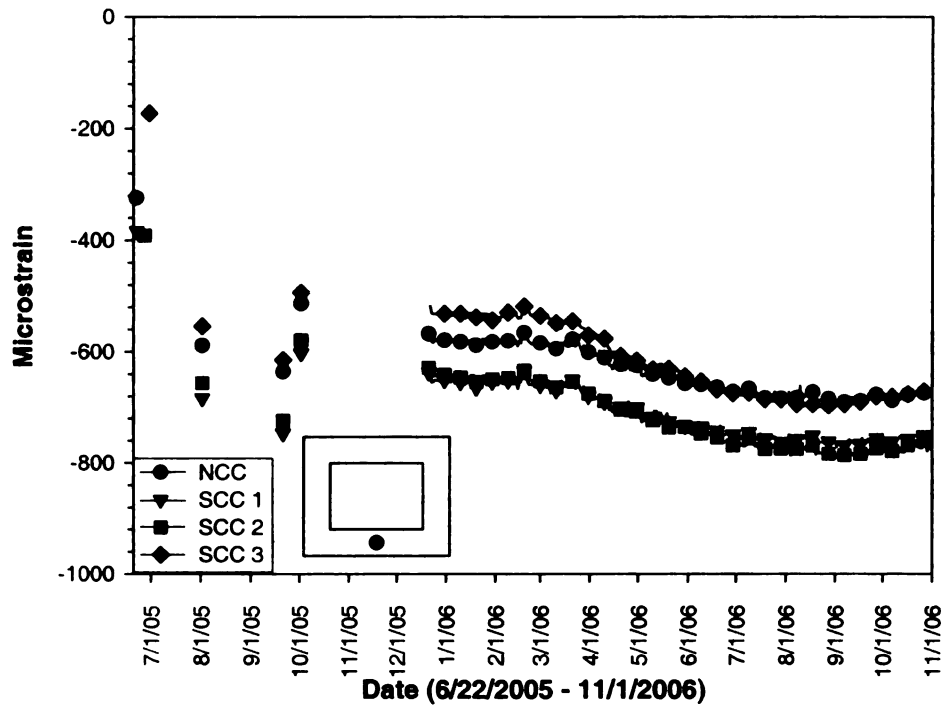
Figure 99. Strains in the Bottom Flange of Section B
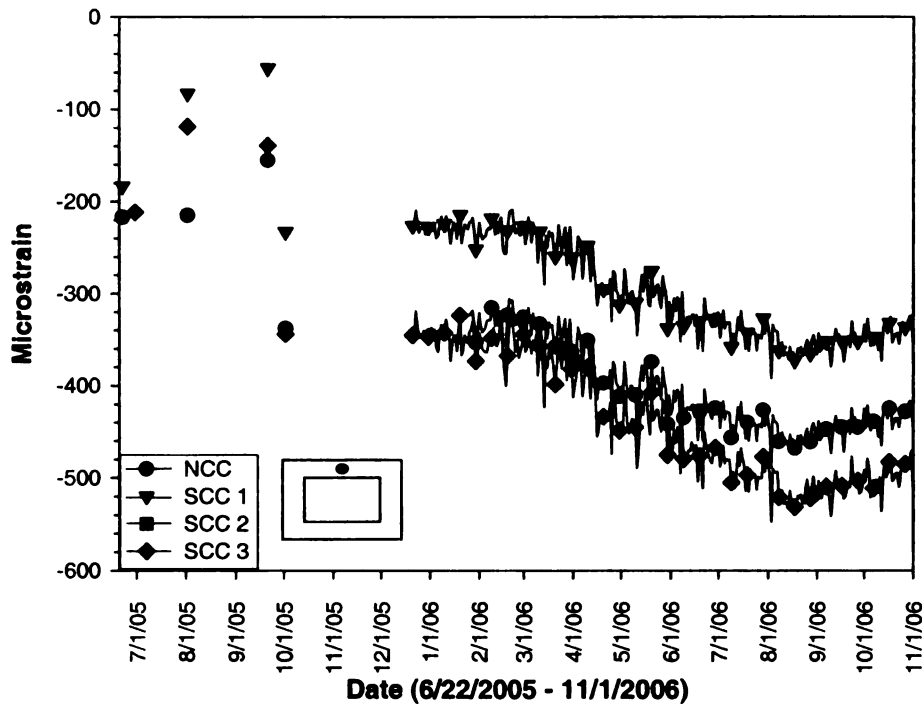
Figure 100. Strains in the Top Flange of Section C

194
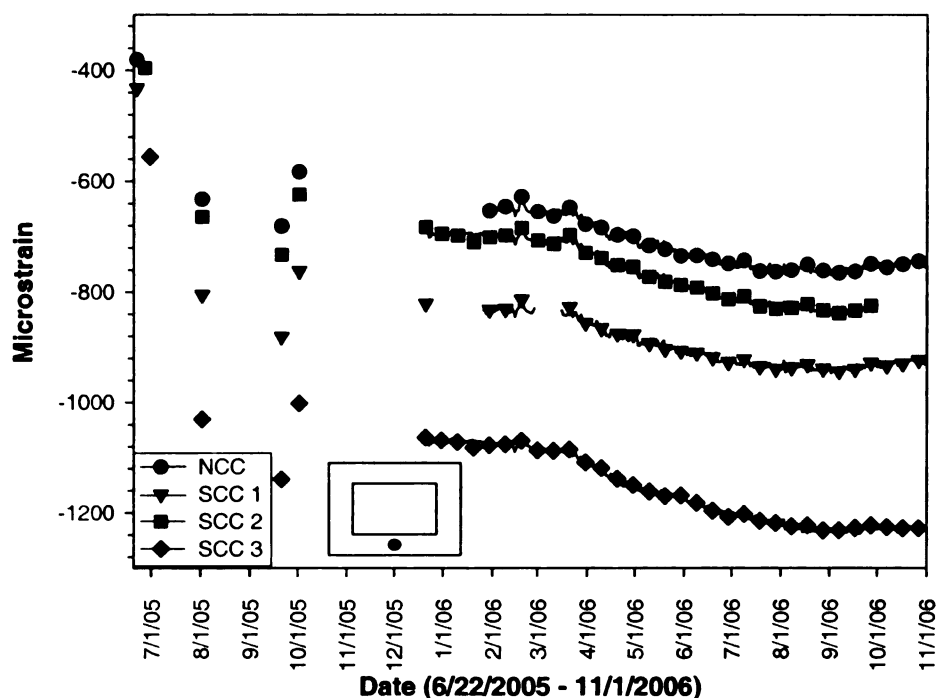
Figure 101. Strains in the Bottom Flange of Section C

6.2.4 Discussion

In order to verify the plots presented above, as well as to investigate some of the differences that exist between the responses of the beams for the four concrete mix designs, several factors that could affect this response were investigated. These include:

- Prestress loss calculations.

    o The expected prestress loss was calculated using multiple methods. These methods ranged from lump sum analysis to time dependent calculations. The plot of the strain in the section due to the prestress loss should match closely to the measured values as presented above. These calculations can act to verify that the

measured strain response is correct. The prestress loss calculations are discussed in Section 6.3.

- Influence of Diaphragm.
  - o The influence of an 8 inch diaphragm located at the center of each beam was analyzed. This analysis was conducted to see how the presence of this diaphragm could change the strain measured in the beam. The analysis and results are presented in Section 6.4.

- Influence of Temperature.
  - o The increase of temperature in the summer months could affect the strain measured in the beam. An temperature analysis looking at both uniform and gradient temperature induced strain was conducted with the results presented in Section 6.5

- Influence of Bearing Stiffness.
  - o The stiffness of the bearing, including all components of the bridge system, could affect the strain measurements in the beam by preventing the beam from expanding. The bearing stiffness is investigated to see how it could influence the measured strain response. The results of this analysis are presented in Section 6.6

- Data Normalization.
  - o The presented response of the strain in the top flange of the beams show large differences in the starting values for the four concrete mix designs. In an attempt to eliminate this discrepancy,

the data was normalized to remove the influence of the initial value. The results of this analysis are presented in Section 6.7.

6.3 Prestress Losses

The performance of the bridge beams could be negatively affected by differences in the rate of prestress loss, which could lead to larger than expected deflections and the early onset of crack formation. This could potentially lead to premature failure of the bridge members. Changes made to achieve the beneficial properties of the SCC mix designs could adversely allow these mitigating factors to produce the negative effects. Thus, field monitoring of the SCC bridge members could provide information on a developing problem.

The long-term strain readings taken from the field instrumentation need to be interpreted for any differences in performance between the SCC beams and the instrumented NCC beam. While this judgment can be made qualitatively from the measured data, it is of interest to estimate if the measured strains coincide with the expected behavior. Further, if differences do exist, it is of interest to determine what long-term effect may be causing them.

Since this project deals with prestress elements, the strains in the beam element include not only the effects due to external loading and temperature effects but the stresses introduced by the prestressing steel. Furthermore, it is well known that the large forces in the steel strands and the sustained compressive stress state in the concrete will lead to volume-related material changes in the steel and concrete. These changes will in turn change the self-equilibrating force state in the prestressed section. The manifestation of these effects is the loss of prestress in the section. This will clearly affect the readings

in the strain instruments and thus it is of interest to estimate prestress losses to better

compare the predicted and measured strain measurements in the instrumented beams.

Over time the prestressing force applied to a structural member will decrease due

to changes in the steel and the concrete. Some losses happen immediately and others

happen over the life of the bridge element. If not properly accounted for in a design, the

loss of prestressing could compromise serviceability or even cause failure of the element.

The losses that occur in prestressed elements can be attributed to four main

sources:

- elastic shortening,

- steel relaxation,

- shrinkage of concrete,

- creep of concrete.

Elastic shortening is an immediate prestress loss that occurs at the time of transfer

of the prestress force to the concrete. When the force is transferred to the concrete the

element instantaneously shortens. Since the concrete is bonded to the strand when this

shortening occurs, the strand also must shorten by the same amount. The shortening of

the prestressing strand causes the force in the prestressing strand to decrease as well. The

amount that this force decreases depends on the size of the force applied to the concrete

and the ratio of the modulus elasticity of the prestressing strand and the concrete.

Steel relaxation, or creep of steel, is a time dependent loss. This loss occurs as a

constant stress is applied to the steel. Two types of relaxation are calculated. An initial

amount of relaxation is generally calculated between the time the strand is stressed and

the time the force is transferred to the concrete. This value is important as it reduces the

amount of force transferred to the concrete. This in turn affects the amount of prestressing force lost due to elastic shortening. Relaxation is then considered from the time of transfer to the end of the bridge service life.

The prestressing force lost due to the drying shrinkage of the concrete is another time dependent loss. Concrete shrinkage occurs over time as free water evaporates from the concrete. The spaces previously occupied by water crush causing the concrete to shorten [32]. The shortening of the concrete also shortens the bonded prestressing strand, which causes a reduction on the prestressing force.

The final contribution to the loss of prestressing force is the time dependent loss due to creep of the concrete. Concrete creep occurs as a compressive stress is applied to the concrete over a period of time. The strain that occurs in the concrete as a result of this stress causes the concrete to shorten, again shortening the bonded prestressing strand, and lowering the prestress force.

Accurately estimating the amount of prestressing force lost over time depends on the ability to accurately predict the amount of strain produced due to the previously described prestressing loss sources. Many models have been produced for this purpose. Each relies on empirical evidence from research data. While differences exist between the various models, accurate results can be obtained from them.

6.3.1 Theoretical Considerations

Multiple methods have been developed to account for the prestressing losses. Each method takes into account the same parameters but may look at them with a different material model. The main differences between the methods are in the estimation of the time dependent losses. Some methods try to estimate these losses as

one lump sum value. Other methods try to predict each time dependent loss separately. The accuracy of these methods depends on the models used to predict the strains from the time dependent phenomenon. Five methods were used to analyze the prestressing loss expected for the members in the demonstration bridge. The first three methods are from the 2007 AASHTO-LRFD Specification (AASHTO-LRFD-3) [4]. A fourth method is a time-step analyses using time dependent models described by Naaman [34]. The final method comes from the 1998 version of the AASHTO-LRFD Specification (AASHTO-LRFD-2) [3].

6.3.1.1 AASHTO-LRFD-3 [4] Provisions

Three methods for calculating the total prestressing loss are presented in the AASHTO-LRFD-3 Specification [4]. These methods include two lump sum estimates where the total prestress loss is using one equation. The third method, a refined method, uses separate equations to calculate each of the time dependent losses.

The lump sum estimate presented in the AASHTO-LRFD-3 Specifications [4] was also previously presented in the AASHTO-LRFD-2 Specification [3]. This method estimates all of the time dependent values in one lump sum term. The predicted values rely on the partial prestress ratio (*PPR*), which is a weighted average of the yield stress for the prestressed steel to the yield stress of the total steal in the beam. This method applies to prestressed members that are made with:

- concrete with a strength higher than 3,500 psi,

- normal weight concrete,

- concrete that is either steam or moist cured,

200

- prestressing strands or bars.

The AASHTO-LRFD-3 Specification [4] states that for this method to be applied, the member should be constructed in average exposure conditions with average temperatures. According to the AASHTO-LRFD-3 Specification [4], this method was developed using a computerized time-step analysis of many bridges and building members designed and built with an average range of variables including creep coefficient, concrete shrinkage, relative humidity, moist or steam cured, and, *PPR* ratio. When low relaxation steel is used, as is the case for this project, the lump sum values can be reduced by 4,000 psi.

According to the lump sum method the upper bound of the total time dependent prestressing loss for a box beam with 270 ksi prestressing strands is given by Equation (27):

$$(27) \quad \Delta f_p = (21.0 + 4.0 PPR - 4.0) \times 1000 \quad \text{(psi)},$$

where *Δfp* is the time dependent prestress losses from creep, shrinkage, and steel relaxation. The PPR is the partial prestress ratio given by Equation (28):

$$(28) \quad PPR = \frac{A_{ps} f_{py}}{A_{ps} f_{py} + A_s f_y}$$

where A_{ps} is the area of the prestressing strand, f_{py} is the yield strength of the prestressing strand, A_s is the area of the non-prestressed steel reinforcement, and f_y is the yield strength of the steel reinforcement. The average value of this lump sum estimate is given by Equation (29):

$$(29) \quad \Delta f_p = (19 + 4.0 PPR - 4.0) \times 1000 \quad \text{(psi)}.$$

201

To estimate the total loss of prestress the elastic shortening losses must be added to this lump sum estimate of the time dependent losses. This loss is given by AASHTO-LRFD-3 as Equation (30):

$$(30) \quad \Delta f_{pES} = \frac{E_p}{E_{ci}} f_{cgp} \quad \text{(psi)},$$

where E_p is the modulus of elasticity of the prestressing steel, E_{ci} is the modulus of elasticity of the concrete at transfer, and f_{cgp} is the total compressive stress acting at the center of gravity of the prestressing tendons at transfer. This stress includes effects from the prestressing force at transfer and the self-weight of the member. The lump sum method thus provides a rough estimate of the prestressed loss in a quick manner.

A second lump sum estimate that is given in the AASHTO-LRFD-3 specification is shown in Equation (31):

$$(31) \quad \Delta f_{LT} = 10.0 \frac{f_{pi} A_{ps}}{A_{c-Trans}} \gamma_H \gamma_{ST} + 12.0 \gamma_H \gamma_{ST} + \Delta f_{PR} \quad \text{(ksi)}$$

where f_{pi} is the initial stress applied to the strands, A_{ps} is the area of the prestressing strand and, $A_{c-Trans}$ is the non-composite, transformed area of the beam. γ_H is a correction factor for the humidity at time of casting and is given by Equation (32):

$$(32) \quad \gamma_H = 1.7 - 0.01H$$

with H = 75 for the region where this bridge was constructed. γ_{ST} accounts for the shrinkage of the concrete and is given by Equation (33):

$$(33) \quad \gamma_{ST} = \frac{5}{1 + f'_{ci}}$$

where f'_{ci} is the strength of concrete at the time of transfer. If this value is unknown it can be estimated as 80% of the 28-day compressive strength. Finally Δf_{PR} is the relaxation of the steel, which is estimated as 2,400 psi for low relaxation steel in the AASHTO-LRFD-3 specification [4].

The refined method used to predict the amount of prestress lost over time as presented in the AASHTO-LRFD-3 specification [4] calculates losses over two time intervals. The first interval is from the time the prestressing force is transferred to the concrete to the time the deck is cast in place, and the second interval is from the time the deck is cast in place until the end of the life of the bridge. For simplicity, the end of the life of the bridge is taken as infinity. This method was first reported by Tadros et. al. in "NCHRP Report 496: Prestress Losses in Pretensioned High-Strength Concrete Bridge Girders" [51] before being adopted into the AASHTO-LRFD-3 Specification [4]. In this method if transformed section properties are used then losses due to elastic shortening is already accounted for, thus they do not need to be calculated directly. Therefore, in this method all variables for area, moment of inertia, eccentricity, and neutral axis depth are assumed to be taken from the transformed section properties.

The total prestress loss calculated using the refined method is found by Equation (34):

$$(34) \quad \Delta f_{LT} = \left(\Delta f_{pSR} + \Delta f_{pCR} + \Delta f_{pR1} \right)_{id} + \left(\Delta f_{pSD} + \Delta f_{pCD} + \Delta f_{pR2} - \Delta f_{pSD} \right)_{df} \text{ (ksi)}.$$

In this equation, and throughout this method, the subscript I represents the time at transfer, the subscript d represents the time at deck casting, and the subscript f represents the final time or infinity. Thus, the interval id is from the time the prestressing force was transferred to the strand to the time the deck was cast, and the interval df is from the time

the deck was cast to the time infinity. The other variables in this equation represent the individual losses due to each time dependent factor.

The shrinkage loss from the time of transfer to the time the deck is cast, Δf_{pSR} is given by Equation (35):

$$(35) \quad \Delta f_{pSR} = \varepsilon_{bid} E_{ps} k_{id} \text{ (ksi)}.$$

ε_{bid} is the shrinkage strain from transfer to the time of deck casting and is given by Equation (36):

$$(36) \quad \varepsilon_{bid} = 480 \times 10^{-6} k_{td} k_{hs} k_s k_f$$

where, k_{td}, k_{hs}, k_s, and k_f, are factors that depend on time, humidity, shape, and concrete strength respectively. These factors are found using Equations (37) - (40) where all variables have been defined except for t which is equal to the number of days in the interval, and V/S which is equal to the volume to surface area ratio.

$$(37) \quad k_{td} = \frac{t}{61 - 4f'_{ci} + t}$$

$$(38) \quad k_f = \frac{5}{1 + f'_{ci}}$$

$$(39) \quad k_s = 1.45 - 0.13\left(V/S\right)$$

$$(40) \quad k_{hs} = 2.00 - 0.014H$$

The final variable in the shrinkage loss equation is k_{id} which is given by Equation (41):

$$(41) \quad k_{id} = \frac{1}{1 + \dfrac{E_{ps}}{E_{ci}} \dfrac{A_{ps}}{A_g}\left(1 + \dfrac{A_g e_{pg}^2}{I_g}\left[1 + 0.7\psi_{bif}\right]\right)}$$

where all variables have been previously defined except for e_{pg}, which is the eccentricity of the prestressing steel, and ψ_{bif}, which is the creep coefficient for the interval from transfer to final. This variable is found using Equation (42):

$$(42) \qquad \psi_{bif} = 1.90(k_s)(k_{hc})(k_f)(k_{td})t_i^{-0.118}$$

where t_i is the time at the beginning of the interval and k_{hc} is the humidity factor which is found using Equation (43):

$$(43) \qquad k_{hc} = 1.56 - 0.008H .$$

The loss due to concrete creep for the interval from transfer to the time the deck is cast is given by Equation (44):

$$(44) \qquad \Delta f_{pCR} = \frac{E_{ps}}{E_{ci}} f_{cgp} \psi_{bid} k_{id} \quad \text{(ksi)}$$

where f_{cgp} is the stress at the centroid of the prestressing strand, and ψ_{bid} can be found using Equation (42).

The loss of prestress due to steel relaxation for this first interval is found using Equation (45):

$$(45) \qquad \Delta f_{pR1} = \frac{f_{pi}}{k_L}\left[\frac{f_{pi}}{f_{py}} - 0.55\right] \quad \text{(ksi)},$$

where f_{pi} is the initial prestress in the strands, f_{py} is the yield strength of the prestressing strands, and k_L is equal to 30 for low relaxation steel.

The loss of prestress over the interval from the deck casting to the final time in the life of the bridge is calculated in a very similar way to the previous interval. The shrinkage loss is found using Equation (46):

$$(46) \qquad \Delta f_{pSD} = \varepsilon_{bdf} E_{ps} k_{df} \quad \text{(ksi)}.$$

205

The difference between this equation and the previous shrinkage loss equation is that the value of the shrinkage strain, ε_{bdf} is found using Equation (47):

$$(47) \qquad \varepsilon_{bdf} = \varepsilon_{bif} - \varepsilon_{bid}$$

with each variable found using Equation (36). Also, the value of k_{df} is found using Equation (48):

$$(48) \qquad k_{df} = \cfrac{1}{1 + \cfrac{E_{ps}}{E_{ci}} \cfrac{A_{ps}}{A_{comp}} \left(1 + \cfrac{A_{comp} e_{pcomp}^2}{I_{comp}} \left[1 + 0.7 \psi_{bif} \right] \right)}$$

with the only difference from the calculation of k_{id} is the use of composite transformed properties.

The loss of prestress due to concrete creep over this interval is found using Equation (49):

$$(49) \qquad \Delta f_{pCD} = \frac{E_{ps}}{E_{ci}} f_{cgp} \left[\psi_{bif} - \psi_{bid} \right] k_{df} + \frac{E_{ps}}{E_{ci}} \Delta f_{cd} \psi_{bdf} k_{df} \quad \text{(ksi)},$$

with the only new variable being the Δf_{cd} value which is the difference between the stress caused by the non composite dead loads and the composite dead loads. The loss of prestress due to steel relaxation over this interval is taken to be equal to the loss of steel relaxation over the previous interval thus Equation (50):

$$(50) \qquad \Delta f_{pR2} = \Delta f_{pR1} \quad \text{(ksi)}.$$

The final component of the prestress loss for the interval from the casting of the deck to the final time in the life of the bridge is the loss of prestress due to the shrinkage of the deck concrete. This component accounts for the fact that the deck and beam act compositely, thus any volume related material changes that occur in the deck should

affect the beam as well. The loss of prestress due to the shrinkage of the concrete in the deck is calculated using Equation (51):

$$(51) \qquad \Delta f_{pSS} = \frac{E_{ps}}{E_{ci}} \Delta f_{cdf} k_{df} \left(1 + 0.7\psi_{bdf}\right) \text{ (ksi)},$$

where the only new variable, Δf_{cdf} is found using Equation (52):

$$(52) \qquad \Delta f_{cdf} = \frac{\varepsilon_{ddf} A_{deck} E_{cd}}{1 + 0.7\psi_{ddf}} \left(\frac{1}{A_{comp}} - \frac{e_{pg}e_d}{I_{comp}}\right) \text{ (ksi)}$$

where ε_{ddf} and ψ_{ddf} are calculated using the deck properties and e_d is the eccentricity of the deck.

6.3.1.2 AASHTO-LRFD-2 [3] Provisions

The total prestressing loss for a bridge beam according to the AASHTO-LRFD-2 Specification [3] can be estimated by Equation (53):

$$(53) \qquad \Delta f_{pT} = \Delta f_{pC} + \Delta f_{pSR} + \Delta f_{pR} \qquad \text{(psi)},$$

where Δf_{pT} is the total prestressing loss, Δf_{pC} is the prestressing loss due to creep of the concrete, Δf_{pSR} is the prestressing loss due to the shrinkage of the concrete, and Δf_{pR} is the prestressing loss due to the relaxation of the prestressing steel. All of these terms are time dependent as they occur over time during the life of the bridge. The instantaneous losses are not considered explicitly in this equation. This is due to the fact that transformed section properties are used in the calculation of the losses. If gross section properties were used to calculate this loss, the instantaneous loss due to elastic shortening would have to be included.

207

The refined method of analysis of prestress losses is described in the AASHTO-LRFD-2 Specification [3]. This calculation for total prestress losses uses separate estimates of the time dependent losses. The method only applies to members that have a span of less than 250 feet, and are constructed with normal density concrete with compressive strengths greater than 3,500 psi at transfer. While this method was replaced in the AASHTO-LRFD-2 Specification [4] by the previously discussed refined method it is discussed here for comparison purposes. For purposes of identification this method will be labeled AASHTO: Old Refined Method. According to this old refined method the prestress loss due to concrete shrinkage is given by Equation (54):

$$(54) \quad \Delta f_{pSR} = (17.0 - 0.150H) \times 1000 \quad (\text{psi}),$$

where H is the average annual ambient relative humidity. The value of H depends on location and is given in the AASHTO-LRFD-2 Specification [3] as 75% for Michigan.

The prestress losses caused by creep are calculated using Equation (55):

$$(55) \quad \Delta f_{pCR} = (12.0 f_{cgp} - 7.0 \Delta f_{cdp}) \times 1000 \geq 0 \quad (\text{psi}),$$

where f_{cgp} is the stress in the concrete at the level of the prestressing strand, and Δf_{cdp} is the change in the concrete stress at the level of the prestressing strand due to the application of permanent loads except for the loads that are in place at the time of transfer. For the demonstration bridge in this project the deck and haunch are the only load that affects the Δf_{cdp}.

The final time dependent loss, the relaxation of the strands, is given in two parts as shown in Equation (56):

$$(56) \quad \Delta f_{pR} = \Delta f_{pR1} + \Delta f_{pR2} \quad (\text{psi}).$$

208

The first part is the relaxation of the strand that occurs from the time the strand is stressed until it is transferred to the concrete. This value is found using Equation (57):

$$(57) \quad \Delta f_{pR1} = \frac{\log(24t)}{40.0} \left[\frac{f_{pj}}{f_{py}} - 0.55 \right] f_{pj} \quad \text{(psi)},$$

where t is the time in days from the stressing of the strand to transfer, and f_{pj} is the stress in the strand at the end of stressing.

The second part of relaxation occurs from transfer throughout the service life of the bridge. In the AASHTO-LRFD-2 Specification [3] refined analysis this value is estimated by Equation (58):

$$(58) \quad \Delta f_{pR2} = \left(20.0 - .4\Delta f_{pES} - 0.2(\Delta f_{pSR} + \Delta f_{pCR})\right) \times 1000 \quad \text{(psi)},$$

where all variables have been described previously. Once each of the separate prestress losses are calculated the total prestress loss can be found using Equation (53).

6.3.1.3 Time Step Analysis Methods

Conducting a time step analysis to calculate the total prestressing loss is valuable for two reasons: the time step analysis allows for the prediction of the amount of prestress remaining at different stages of the construction process, and it accounts for the interdependence of the losses. As the time dependent losses occur at different rates, they affect the amount of stress remaining to affect the loss due to another source [34]. For instance, the majority of the shrinkage loss occurs at the beginning of the construction process as the free water in the concrete evaporates. This causes less stress to be applied to the concrete member at later ages, causing less creep strain to develop, and consequently reducing the amount of prestress lost due to creep. A Time step analysis

uses time dependent models to calculate the strain in the concrete due to concrete creep, and concrete shrinkage as well as the relaxation of the steel. Many models exist for this purpose. Naaman [34] presents models for these calculations in his textbook. The models he presents are taken from Prestressed Concrete Institute (PCI) and American Concrete Institute (ACI) recommendations. The model presented by Naaman [34] will be called Time Step Analysis and abbreviated TSA.

For the time step analysis transformed section properties will be used, as was the case for the AASHTO Refined Method. However, in this calculation procedure the loss due to elastic shortening will be calculated explicitly. This will be done with Equation (30).

The suggested equation for the time dependent loss of prestress due to steel relaxation comes from the PCI Committee on Prestress Losses. This loss is calculated using Equation (59):

$$(59) \qquad \Delta f_{pR}(t_i, t_j) = \frac{f_{ps}(t_i)}{45} \left(\frac{f_{ps}(t_i)}{f_{py}} - 0.55 \right) \log\left(\frac{t_j}{t_i} \right), \text{ psi,}$$

where $f_{ps}(t_i)$ is the stress in a prestressing strand at the beginning of the time interval under consideration, t_j is time at the end of the time interval, and t_i is the time at the beginning of the time interval.

For the loss of prestress due to the shrinkage and creep of concrete the TSA presents an equation that modifies the concrete strain caused by either concrete creep or concrete shrinkage by a series of correction factors that account for the shape and size of the element, the average humidity of the region, and the strength of the concrete.

The prestressing loss due to shrinkage of concrete according to the TSA is given

by Equation (60):

$$(60) \qquad \Delta f_{pS}(t_i, t_j) = E_{ps} \varepsilon_{su} K_{SH} K_{SS} \frac{b(t_j - t_i)}{(b + t_i)(b + t_j)} , \text{psi},$$

where ε_{su} is the shrinkage strain, K_{SH} is a correction factor that depends on the average

relative humidity, K_{SS} is a correction factor for the shape and size of the member, and b is

a parameter that is taken to be 35 for moist-cured concrete. According to Naaman [34],

the time function and the value b is suggested by ACI Committee 209. The shrinkage

strain depends on the amount of water in the concrete mix design and is given by

Equation (61):

$$(61) \qquad \varepsilon_{SU} = \left[2 + \frac{11}{230}(w - 220) \right] \times 10^{-4} ,$$

where w is the water content in the mix design in lb/yd^3. The correction factor K_{ss}

depends on the volume to surface ratio and can be found in the literature. For an average

humidity between 40% and 80% for moist-cured concrete, K_{SH} is calculated using

Equation (62):

$$(62) \qquad K_{SH} = 1.40 - 0.01H .$$

The loss of prestress due to concrete creep as presented by the TSA is given by

Equation (63):

$$(63) \qquad \Delta f_{pC}(t_i, t_j) = n_p C_{CU} K_{CH} K_{CA} K_{CS} f_{CGS}(t_i) [g(t_j) - g(t_i)] \quad (\text{psi})$$

where n_p is the ratio of modulus of elasticity of prestressing strand to the modulus of

elasticity of concrete, C_{CU} is the ultimate creep coefficient, K_{CH} is a correction factor

depending on average humidity, K_{CA} is a correction factor depending on the age at transfer, K_{CS} is a correction factor depending on the size and shape of the member. C_{CU} depends on the compressive strength of the concrete and varies between 2 and 3.1. K_{CH} for moist-cured concrete depends on the average humidity according to the Equation (64):

$$(64) \quad K_{CH} = 1.27 - 0.0067H \ .$$

where K_{CS} is the size and shape factor that varies depending on the volume to surface are ratio. K_{CA}, for moist-cured concrete, is given by the Equation (65):

$$(65) \quad K_{CA} = 1.25 t_A^{-0.118}$$

where t_A is the time in days to transfer. The time function $g(t)$ is given by Equation (66):

$$(66) \quad g(t) = \frac{t^{0.6}}{10 + t^{0.6}}$$

where t is in days.

As was the case with the previous methods, the total prestress loss in the time step method is the sum of each of the individual prestress losses. However, in the time step analysis methods, this total is calculated at various stages throughout the life of the bridge. Time is considered a variable and the stress is changed depending on the amount lost in each step.

6.3.2 Observations and Results

To accurately calculate the loss of prestress using the previously discussed methods the transformed section properties needed to be used. The transformed

212

properties account for the difference in stiffness between the prestressing steel and the concrete. To calculate the transformed properties the area of steel was increased by the value *n-1*. The value of *n* is found by taking the ratio of the elastic modulus of the prestressing steel to the elastic modulus of the concrete. As the modulus of the concrete varies throughout the life of the bridge as well as for the 4 concrete mix designs the transformed properties were calculated at multiple times. The transformed properties were taken at three different times. The first time was at the transfer of the prestressing force. This corresponds to event one in the previously presented Table 51. The second set of transformed properties were calculated at event two from Table 51. This was the point at which the top strands were transferred. The final time the transformed properties were calculated was at event four. This is the point at which the deck is cast making the composite section.

The transformed properties for the four instrumented beams, which each have a different concrete mix design, at the three events discussed above are shown in Table 54 through Table 57. The properties shown include cross section area, moment of inertia, and neutral axis distance from the bottom of the section. These properties account for the different concrete strengths recorded at each event.

Table 54. NCC Transformed Section Properties

Event	Area (in^2)	I (in^4)	y (in.)
1	528.57	49,277	13.22
2	526.13	49,024	13.27
4	1,390	163,376	24.61

Table 55. SCC 1 Transformed Section Properties

Event	Area (in^2)	I (in^4)	y (in.)
1	528.92	49,314	13.21
2	526.00	49,012	13.27
4	1,391	163,970	24.59

Table 56. SCC 2 Transformed Section Properties

Event	Area (in^2)	I (in^4)	y (in.)
1	528.50	49,271	13.22
2	528.33	49,253	13.22
4	1,391	164,834	24.59

Table 57. SCC 3 Transformed Section Properties

Time Step	Area (in^2)	I (in^4)	y (in.)
1	528.68	49,289	13.22
2	528.31	49,251	13.22
4	1,392	164,368	24.57

In order to accurately estimate the force in the prestressing strands using the previously described methods, several assumptions had to be made. The prestressing strands from both the top and bottom flange were assumed to act as one strand with an equivalent area to the total strand area. The assumed strand is assumed to be located at the resultant centroid of all of the strands. This centroid was calculated using the strand areas and centroid of each row of strands. There are four rows of strands in the demonstration beams: the first row is two inches from the bottom of the beam and has 10 strands, the second row is four inches from the bottom of the beam and has four strands, the third and fourth rows each have two strands, and are eight inches and 24.5 in. from the bottom of the beam respectively. At the mid span of these beams, where all of the

prestress loss analysis take place, the top two strands are debonded and thus do not affect the calculation of the centroid of the strand at this location.

The presence of debonded strands at various locations in the beams made calculating the stress throughout the cross section difficult. To account for the debonded strands the axial load and moments about the neutral axis caused by the force in the prestressing strands were calculated at several critical locations. The critical locations were places where the strand bonding condition changed. These locations are shown in Figure 102. Three prestressing conditions exist throughout the beam. The first condition is for the top strands where two strands are bonded to the concrete over the first 13 feet of the beam. This is represented from section A to section C in the figure. At section C the strands are no longer bonded to the beam. The second condition is for the bottom strands. It represents the first four feet from the end of the beam, section A to B. In this section 14 of the 16 strands are bonded to the beam. Two strands in the bottom row of prestressing strands are not bonded to the beam. The third prestressing condition occurs from section B to section D, which is the mid point of the beam. Here all 16 of the strands in the bottom flange are bonded to the beam and no top strands are bonded to the beam.

The eccentricity changes for each of the four concrete mix designs because the value relies on the transformed section properties. Thus, these values must be calculated at the same three events that the transformed properties were calculated. Table 58 through Table 61 gives the eccentricities for the three different bonding conditions. Also included in these tables are the eccentricities of the VWSG. This value is necessary to calculate the strain at the location where the strain is being measured in the beams.
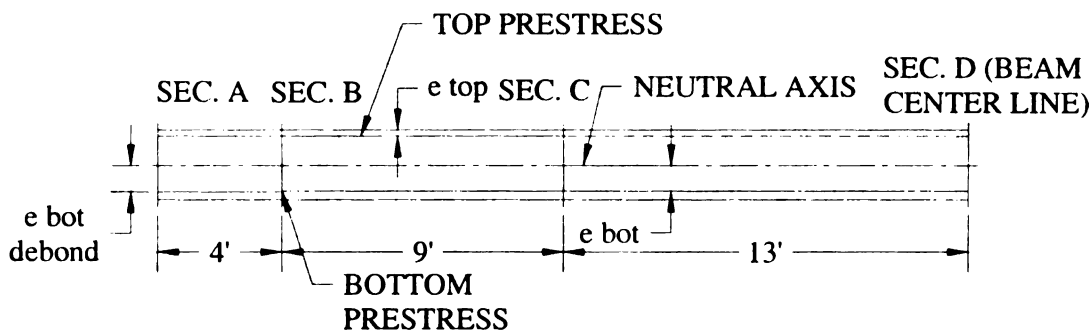
Figure 102. Prestress Strand Geometry

Table 58. NCC Transformed Strand and Instrument Eccentricities

Event	Condition 1	Condition 2	Condition 3	Top Inst. (in.)	Bot. Inst. (in.)
1	11.28	9.79	9.97	11.28	11.22
2	11.23	9.84	10.02	11.23	11.27
4	-0.11	21.18	21.36	-0.11	22.61

Table 59. SCC 1 Transformed Strand and Instrument Eccentricities

Event	Condition 1	Condition 2	Condition 3	Top Inst. (in.)	Bot. Inst. (in.)
1	11.29	9.78	9.96	11.29	11.21
2	11.23	9.84	10.02	11.23	11.27
4	-0.09	21.16	21.29	-0.09	22.59

Table 60. SCC 2 Transformed Strand and Instrument Eccentricities

Event	Condition 1	Condition 2	Condition 3	Top Inst. (in.)	Bot. Inst. (in.)
1	11.28	9.79	9.97	11.28	11.22
2	11.28	9.79	9.97	11.28	11.22
4	-0.09	21.34	21.34	-0.09	22.59

Table 61. SCC 3 Transformed Strand and Instrument Eccentricities

Event	Condition 1	Condition 2	Condition 3	Top Inst. (in.)	Bot. Inst. (in.)
1	11.28	9.79	9.97	11.28	11.22
2	11.28	9.79	9.97	11.28	11.22
4	-0.07	21.14	21.32	-0.07	22.57

The axial load and moment about the beam neutral axis due to the prestressing strand were calculated at each of the sections shown in Figure 102. The moments were found using the eccentricities from the Table 58 through Table 61. These forces were then summed to find the total axial load and moment about the neutral axis at the centerline of the beam, which was the location where the analysis was to take place. Added to this moment was the moment due to the self-weight of the beam, which acts in the opposite direction than the moment caused by the prestressing strands. Like the beam self-weight, the weight of the deck caused a moment that opposed the moment caused by the prestressing force. This moment was considered in the stress calculations after the deck was cast in place at the bridge site. The total axial load and moment were used to calculate the stress in the concrete at the level of the strand using Equation (67):

$$(67) \qquad f_{cgs} = \frac{P}{A} + \frac{Mc}{I} \qquad \text{(psi)}$$

where P is the total compressive axial load from the prestressing force, A is the area of concrete in the cross section, M is the total moment acting about the neutral axis of the beam from the prestressing force, the self-weight and deck loads at the centerline of the beam, c is the distance from the beam neutral axis to the center of gravity of the effective prestressing strand, and I is the moment of inertia for the beam.

Differences in the four concrete mix designs and the construction procedures for each day of casting affected the results of the prestressing loss calculations. The prestressing losses were affected by differences in the rate of concrete compressive strength gain through the effect that this strength had on the modulus of elasticity of the concrete. The strengths used to predict the prestress loss at the four preliminary strain measurements are shown in Table 62. The concrete compressive strength given in the table for the fourth event is the strength that is used to estimate the prestress loss for all calculations made after this time.

The difference in the age of the concrete at transfer indirectly affected the losses due to elastic shortening. The more time that elapsed between the stressing of the strands and the transfer of the strand stress to the concrete, the stiffer the concrete was and consequently, the less loss due to elastic shortening. This is evident in the NCC and SCC 2 cases where transfer occurred at 3 days after stressing because casting was done on a Friday, and transfer did not occur until the following Monday. The age of the concrete at each of the preliminary measurements are listed in Table 63.

The final effect that the mix designs had on the prestress loss calculations was the model used to predict the shrinkage strain in the time step analysis method described by Naaman [34]. This method relies on the amount of water included in the mix. Thus, mixes with greater amounts of water resulted in higher predictions for shrinkage strains. The average amount of water used in each cubic yard produced of the mix designs are listed in Table 64.

Table 62. Concrete Compressive Strengths at Construction Events (psi)

Event	NCC	SCC 1	SCC 2	SCC 3
1	6537	6338	6572	6471
2	8196	8292	6674	6685
3	8560	7549	7764	6968
4	8560	7549	7764	6968

Table 63. Concrete Age at Construction Events (days)

Event	NCC	SCC 1	SCC 2	SCC 3
1	3	0.875	3	0.917
2	36	41	36	33
3	86	94	86	83
4	97	102	97	94

Table 64. Mix Design Water Content for Shrinkage Loss Estimation (lb/yd^3)

NCC	SCC 1	SCC 2	SCC 3
218	262	276	310

The total prestress loss results from the five methods are given in Table 65 and in Figure 103. From these results it can be seen that the five methods produce results that generally agree well with each other. The TSA and AASHTO-LRFD-3 refined methods produce results that extend the range of values. With all of the methods considered the prestress loss estimates from the five methods vary only slightly, with a difference between 6,000 and 11,000 psi for each of the four mix designs.

Table 65. Total Prestress Loss (psi)

Method	NCC	SCC 1	SCC 2	SCC 3
AASHTO, Lump Sum Upper Bound [4]	35,293	35,490	35,256	35,362
AASHTO, Lump Sum Average [4]	33,293	33,490	33,256	33,362
AASHTO, Refined Method [4]	29,008	31,357	28,864	30,545
AASHTO, Estimate [4]	32,655	33,241	32,544	32,551
Time Step Analysis [34]	31,649	37,497	35,781	41,225
AASHTO, Refined Method (old) [3]	34,373	33,712	34,348	33,736
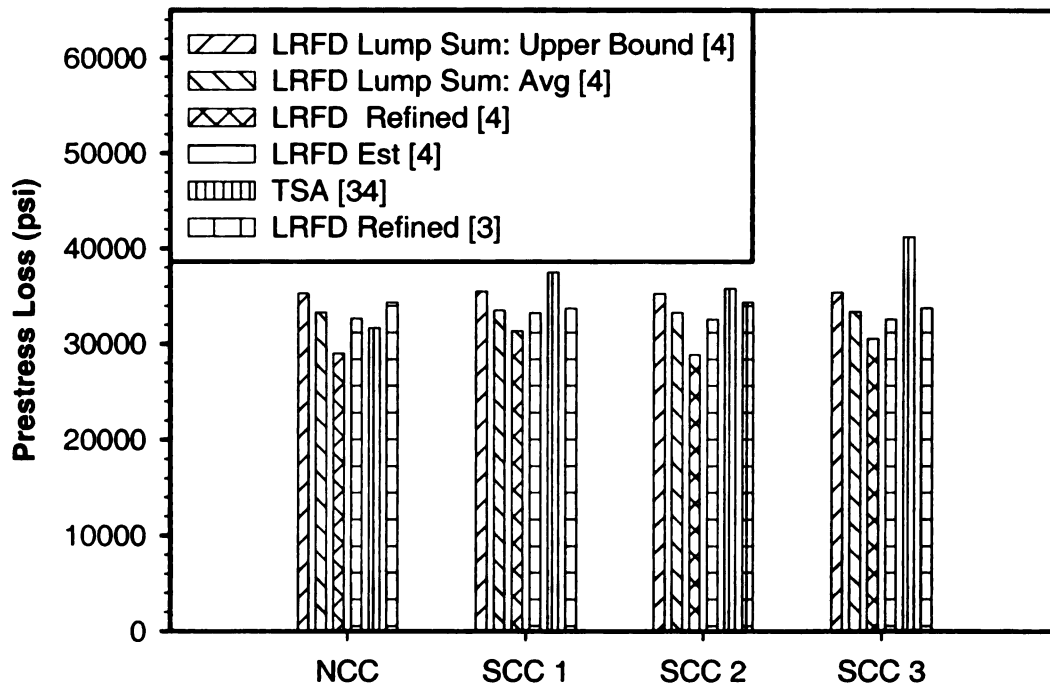
Figure 103. Total Prestress Loss for Different Calculation Methods

The difference between the results from various methods can be further analyzed by looking at the individual components of the prestress loss. As mentioned previously, the total prestress loss is made up of four components in a prestressed bridge beam. These components are: elastic shortening, concrete creep, concrete shrinkage, and steel relaxation. Figure 104 through Figure 106 show how the total prestress loss is divided into the individual components for each of the three prestress loss calculation methods that consider the time dependent loss separately.

The prestress losses for the AASHTO-LRFD-3 refined method [4] are shown in Figure 104. From this figure it is possible to see that the largest amount of loss comes from concrete creep. Due to the fact that elastic shortening is not considered independently in this method it is assumed that some of this creep loss accounts for this loss. The amount of creep loss is controlled by the stiffness of the concrete. This stiffness, the modulus of elasticity, is controlled by the concrete strength at the time the prestressing force was transferred to the concrete. Thus, the concrete with the highest strength, NCC, has the least amount of creep loss and the concrete with the least strength, SCC 1, has the highest amount of creep loss.
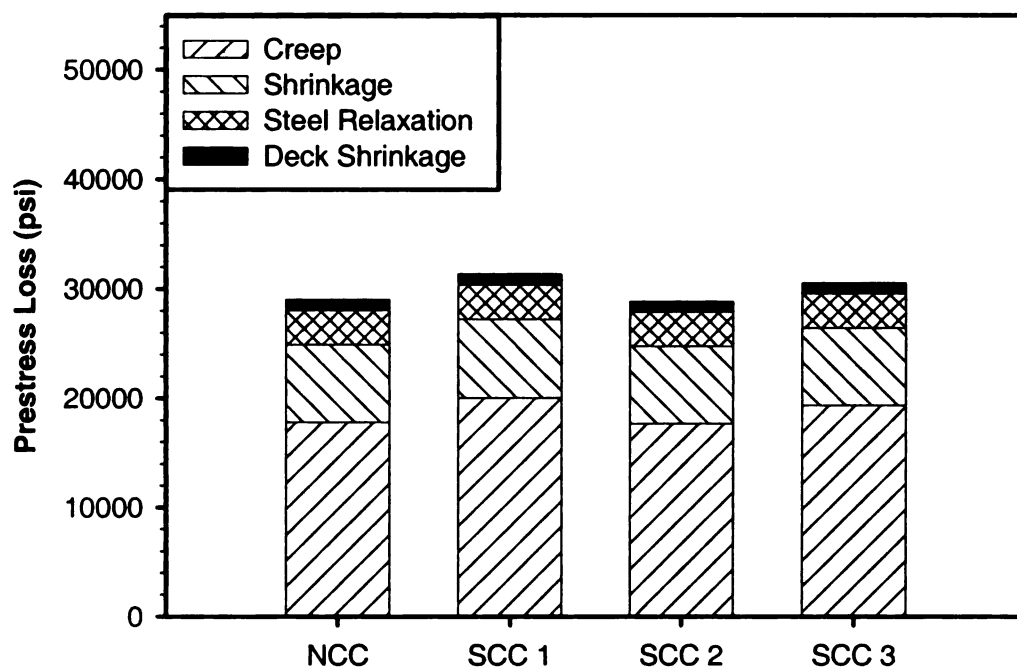
Figure 104. Prestress Loss According to AASHTO-LRFD-3 Refined Method [4]

Figure 105 shows the prestress loss for the TSA method broken down into separate components. As was the case with the previous method, the loss of prestress due to the creep of the concrete represents a large portion of the total loss. However, in the

TSA method, a significant amount of the total prestress loss is accounted for in the elastic shortening. However, it is important to note that both the creep and elastic shortening losses are very similar for all four concrete mix designs. The TSA method produced the largest range of total prestress loss values. The source for this difference lies in the calculation of the loss due do shrinkage. The material model used to calculate the shrinkage strain in the concrete depends on the amount of water used in the concrete mix design. As the SCC mix designs higher than normal amounts of water this value may not be reliable. More discussion on this shrinkage strain calculation will follow.
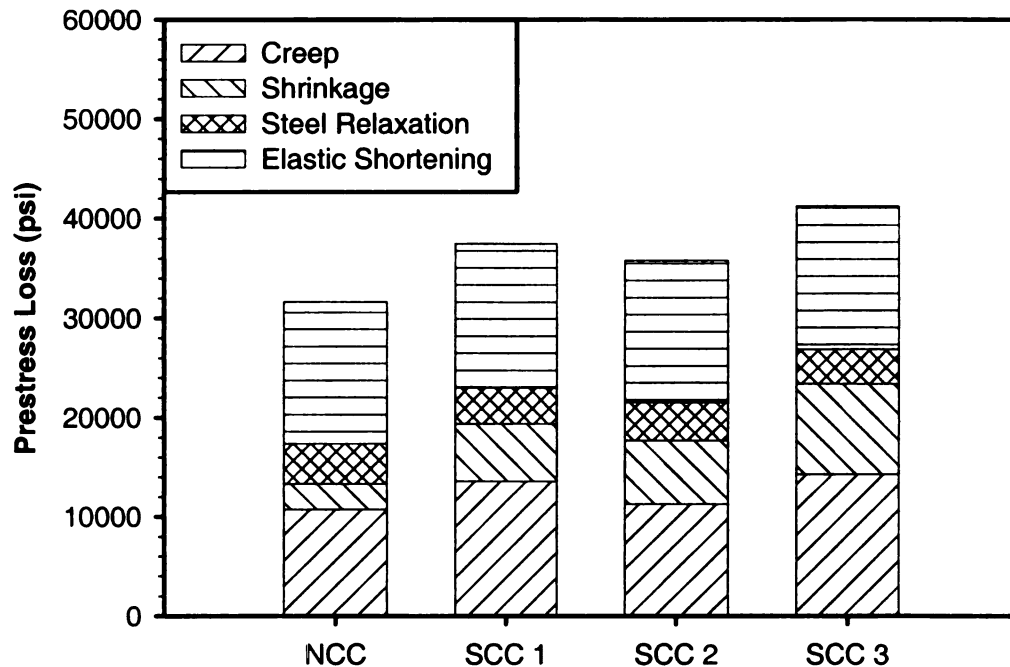
Figure 105. Prestress Loss According to Time Step Analysis [34]

Figure 106 shows the final prestress loss calculation that considered time separate losses for each time dependent component. The AASHTO-LRFD-2 refined method [3] produced the results with the least amount of variability. These results also show similar

trends to the previous methods with concrete creep being the dominant factor in the total

prestress loss.
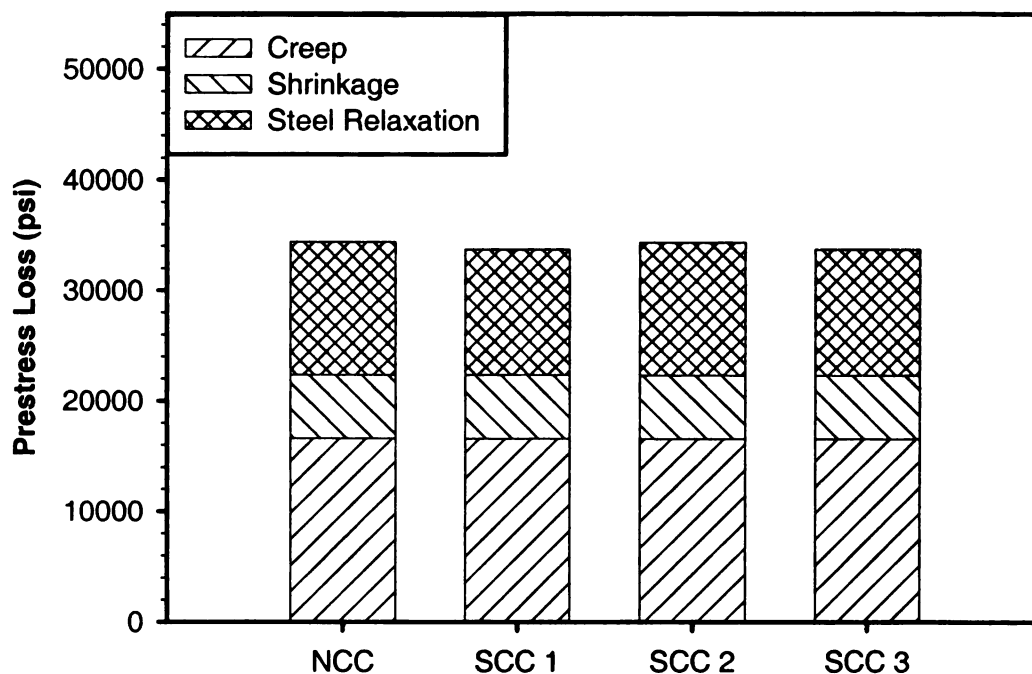
Figure 106. Prestress Loss According to AASHTO-LRFD-2 Refined Method [3]

In Table 66 the loss due to elastic shortening is shown for all methods. The development of the AASHTO-LRFD-2 methods assumes the elastic shortening is included inherently when transformed section properties are used, thus the elastic shortening is only calculated in the TSA method [51]. This fact is verified by the relatively small difference that exists in the total calculated prestress loss for the different methods considered. The main material property that affects the amount of prestress loss is the elastic modulus of the concrete at the time of transfer. This parameter is directly affected by the compressive strength of the concrete at this time. Thus, the strongest concrete, NCC, shows the least amount of elastic shortening loss. The weakest concrete, SCC 1, shows the most prestress loss due to elastic shortening. The increased strength that is seen in the NCC and SCC 2 concretes comes from the concrete age at the time of

transfer. While the stress in the strands in both the SCC 1 and SCC 3 beams was transferred less than 24 hours after casting took place, the NCC and SCC 2 beams did not under go transfer for 3 days. This difference in time has a significant affect on the amount of prestressing force lost during the life of the bridge element.

Table 66. Prestress Loss Due To Elastic Shortening (psi)

Method	NCC	SCC 1	SCC 2	SCC 3
AASHTO, Lump Sum Upper Bound [4]	0	0	0	0
AASHTO, Lump Sum Average [4]	0	0	0	0
AASHTO, Refined Method [4]	0	0	0	0
AASHTO, Estimate [4]	0	0	0	0
Time Step Analysis [34]	14,292	14,490	14,256	14,362
AASHTO, Refined Method (old) [3]	0	0	0	0

Table 67 presents the loss of prestress due to the concrete creep. The three models that predict concrete creep individually show large differences in the total value. In general, the AASHTO-LRFD-3 refined method [4] produces the highest value, with the AASHTO-LRFD-2 refined method [3] and TSA values further behind. The TSA and LRFD refined method [4] show variability through the four concrete mix designs. The AASHTO LRFD refined method (old) [3] has very little variation among the four mix designs. This results from the equations used to calculate the creep. The old refined method relied on the other loss parameters while the new refined method and the TSA method both calculate the creep using material models. The main factors in these models are the compressive strength of the concrete and time elapsed. NCC and SCC 2 have lower results because more time elapsed between casting and transfer of the strands. This increase in time also leads to an increased compressive strength. Other factors that affect this value may have to do with the interdependence of the different losses.

Table 67. Prestress Loss Due To Concrete Creep (psi)

Method	NCC	SCC 1	SCC 2	SCC 3
AASHTO, Refined Method [4]	17,823	20,049	17,710	19,356
Time Step Analysis [34]	10,733	13,600	11,285	14,307
AASHTO, Refined Method (old) [3]	16,603	16,584	16,554	16,550

Table 68 gives the prestressing loss due to concrete shrinkage. These values do not show the same range of variance as the creep values. It is also clearer as to what is governing the results. The AASHTO-LRFD-2 and AASHTO-LRFD-3 refined methods calculates the prestressing loss due to concrete shrinkage based on the average relative humidity. The TSA method, also depends on humidity, but uses a shrinkage strain model that depends on the amount of water used in the concrete. A parametric study on this equation shows that the amount of the water in the mix has a large affect on the total prestress loss through the amount of shrinkage loss. An increase in the amount of water of 10 pounds per cubic yard of concrete results in an increase in the total prestress loss of 500 psi to 700 psi. For the SCC 3 mix design that has 100 pounds of water per cubic yard of concrete more than the NCC mix this is a significant amount of loss. It is believed that the material model used to predict the shrinkage strain in the TSA method is not correct for SCC. In general a mix design with higher amounts of water will produce greater amounts of shrinkage. However, in developing SCC mix designs this is considered. In order to prevent this increase in shrinkage SCC mix designs use VMA. The affect of the VMA is not considered by this material model. The model proposed by the AASHTO LRFD refined method [4] does not have this same problem.

225

Table 68. Prestress Loss Due To Concrete Shrinkage (psi)

Method	NCC	SCC 1	SCC 2	SCC 3
AASHTO, Refined Method [4]	7,063	7,177	7,035	7,068
Time Step Analysis [34]	2,601	5,780	6,390	9,091
AASHTO, Refined Method (old) [3]	5,750	5,750	5,750	5,750

The losses due to steel relaxation are shown in Table 69. Large differences are shown between the AASHTO-LRFD-3 refined method [4] and the TSA methods and the AASHTO-LRFD-2 refined method [3]. This is because the steel relaxation loss calculated in the AASHTO-LRFD-2 method relies on the three other factors (concrete creep, elastic shortening, concrete shrinkage) where as the relaxation in the AASHTO-LRFD-3 refined method [4] and the TSA methods are calculated directly using essentially the same equation.

Table 69. Prestress Loss Due To Steel Relaxation (psi)

Method	NCC	SCC 1	SCC 2	SCC 3
AASHTO, Refined Method [4]	3,170	3,170	3,170	3,170
Time Step Analysis [34]	4,023	3,628	3,850	3,465
AASHTO, Refined Method (old) [3]	12,020	11,378	12,044	11,436

The final factor considered for prestress loss is the shrinkage of the deck concrete. This is only considered in the AASHTO-LRFD-3 refined method [4]. While the value of this loss is relatively low it is important to consider this value in bridges where the deck is cast compositely. The other methods do not explicitly consider this method.

226

Table 70. Prestress Loss Due To Shrinkage of Deck Concrete (psi)

Method	NCC	SCC 1	SCC 2	SCC 3
AASHTO, Refined Method [4]	953	960	949	951
Time Step Analysis [34]	0	0	0	0
AASHTO, Refined Method (old) [3]	0	0	0	0

6.3.3 Comparison to Measured Data

While analytical models are useful to predict well-understood phenomenon, their accuracy may be reduced when new parameters are introduced. This is the case for the prestressing loss calculations for beams produced with SCC. Even with the different ways the concrete mix designs are factored into the calculations there is no way to be certain that these predictions are accurate for beams made with SCC. Much like the case of bond between the prestressing strand and the concrete, changes made to the mix designs may affect the loss of prestress in prestressed beams. Verification of these predictions requires the use of information from the beams themselves.

6.3.3.1 Theoretical Considerations

The data recorded from the instruments in the demonstration bridge could provide information on the performance of elements cast with SCC. Differences in the concrete strain in the SCC beams could be from a difference in the prestress loss or deflection of the beam. The data recorded from the instruments in the demonstration bridge may provide information on the amount of stress remaining in the prestressing strand. During the calculation of the prestressing losses the strain in the cross section can be calculated using the well known Hooke's law for one dimensional response which is given as Equation (68):

$$(68) \quad \varepsilon = \frac{\sigma}{E},$$

where ε represents the strain in the cross section, σ is the stress in the cross section at the level of the gage, and E is the elastic modulus of the concrete for the given time step.

6.3.3.2 Discussion

A comparison of the analytical and measured strains for the bottom VWSG in the NCC beam is shown in Figure 107. From the figure it is possible to see that the measured first data point does not match the analytical data point. Possible reasons for this difference could stem from the effect of the unbonded strands in the top flange of the beam. An analysis to asses the role of these strands on this first point is on going. Further, the behavior of the measured data during the monitoring period, after December 20th, 2005, does not match the predicted behavior from analysis. The increase in measured compressive strain seen in the plot could be the result of temperature effects. From the plots of the temperature presented before it can be seen that the increase in temperature that occurs near the end of February coincides with the beginning of this compressive strain growth. Also, the minimum strain point that occurs around the 400th day after transfer of prestress force, which is in the month of September coincides with the beginning of the temperature decrease seen in the thermocouples. An analysis of the affect of temperature gradient across the composite section of these beams is on going and will be added to this discussion.
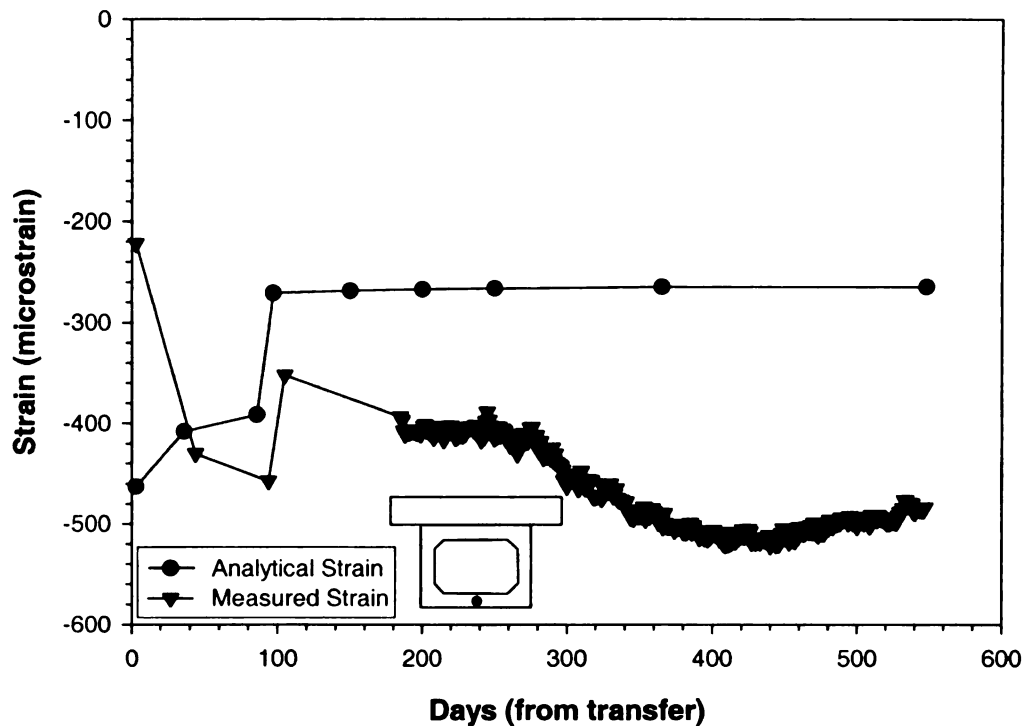
Figure 107. Strain Comparison For Bottom VWSG NCC Beam Section A

Figure 108 shows the comparison of the analytical strains and measured strains for the VWSG at the top of the NCC beam at section A. These points seem to agree well for the four initial measurement events. However, once the continuous monitoring begins, significant differences between the measured values and analytical values exist. The sudden increase in strain shown in the analytical values is caused by the inclusion of the deck in the composite beam section. Once the deck is in place on the beam the section that resists the loads is much larger. The neutral axis of this section moves up towards the top of the beam. The neutral axis for the composite section is less than 6 inches from the top gage location. Because of this, in the analysis, the stress due to the moment caused by the prestressing strand at the top location is very small. Consequently the strain is reduced. The effect of temperature may improve this plot.

229
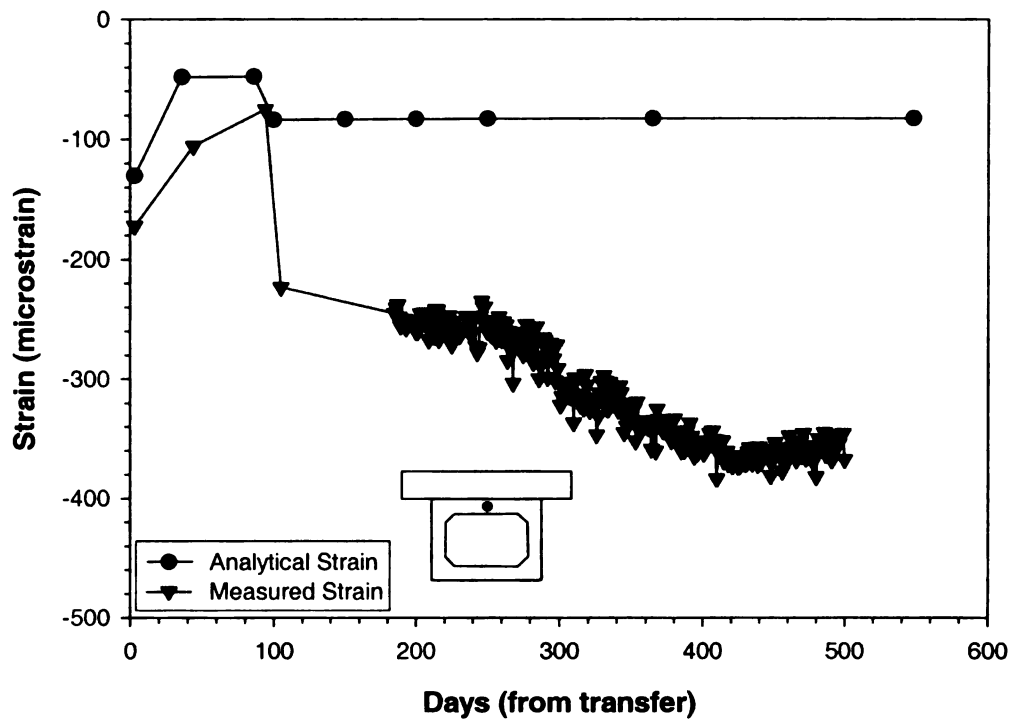
Figure 108. Strain Comparison for Top VWSG NCC Beam Section A

Figure 109 through Figure 114 display the comparisons of strains for the SCC beams. These plots are similar to the plots shown for the NCC beam. The main difference is in the plots of the comparison of strains from the top flange of the SCC girders. In the NCC plot, the analytical strains and the measured strains showed good agreement. In the SCC plots, the plots do not show the same agreement. In these plots, the shape of the curves is very similar, but the starting value is not. The difference in the values varies from 600 micro strain to 700 micro strain. However, the reason for this difference could not be determined.
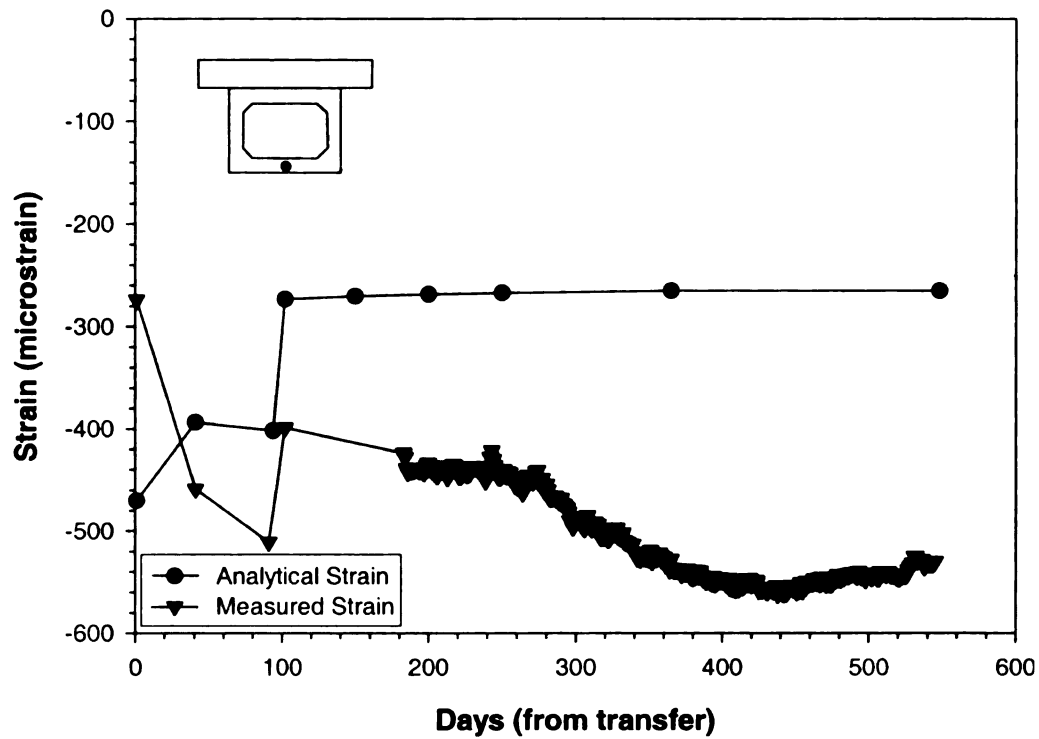
Figure 109. Strain Comparison for Bottom VWSG SCC 1 Beam Section A
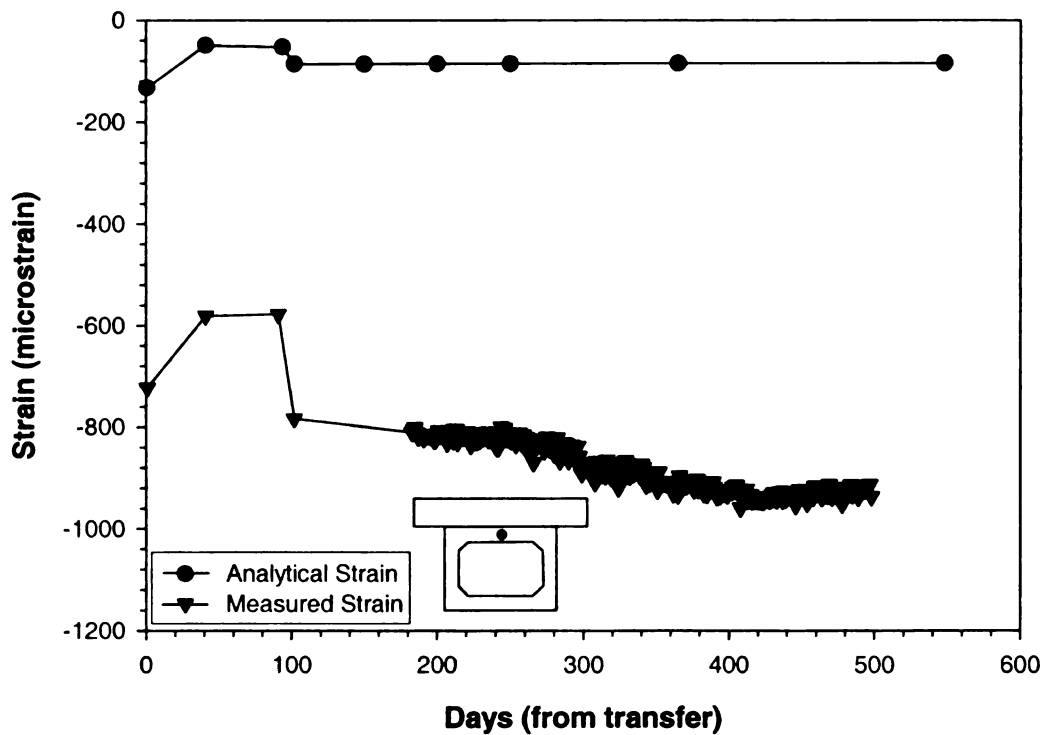
Figure 110. Strain Comparison for Top VWSG SCC 1 Beam Section A

231
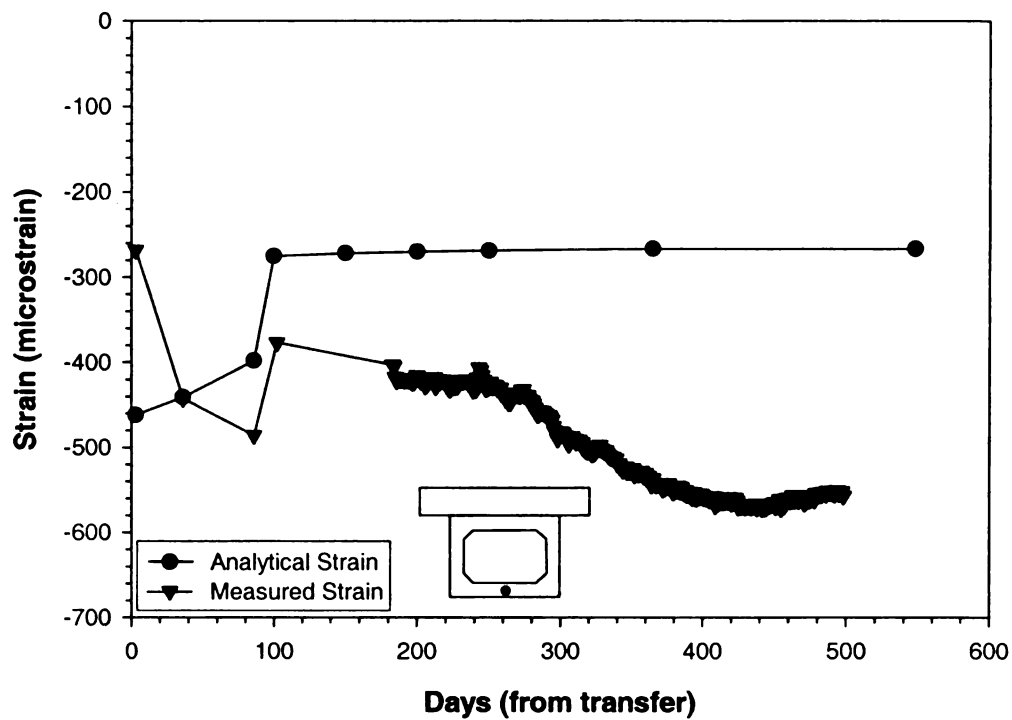
Figure 111. Strain Comparison for Bottom VWSG SCC 2 Beam Section A
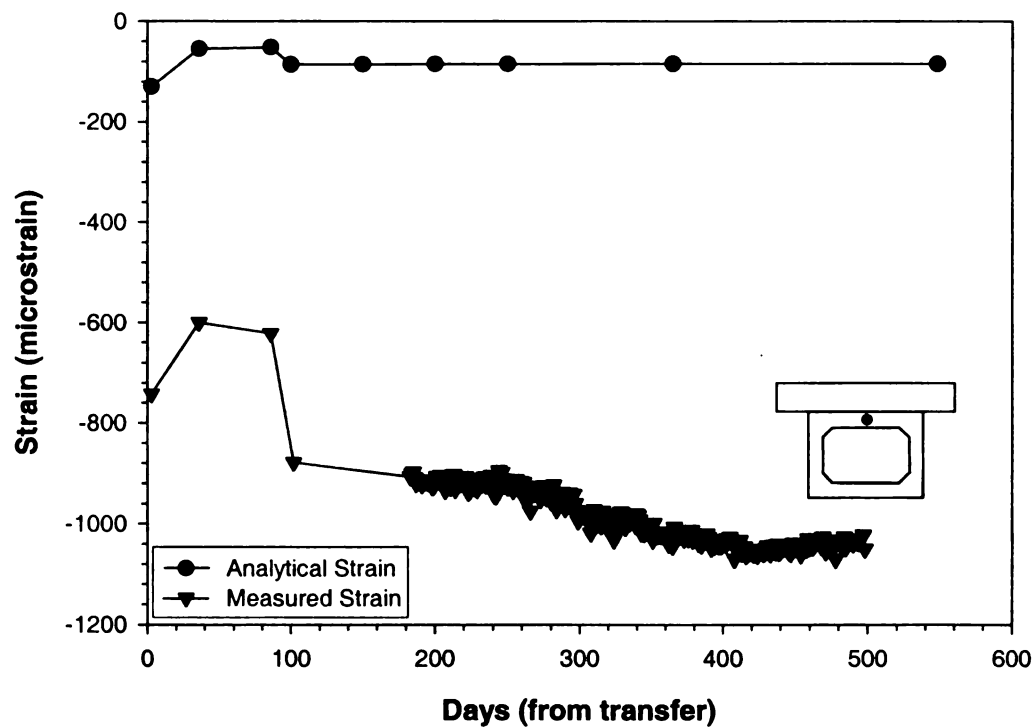
Figure 112. Comparison of Strains for Top VWSG SCC 2 Section A

232
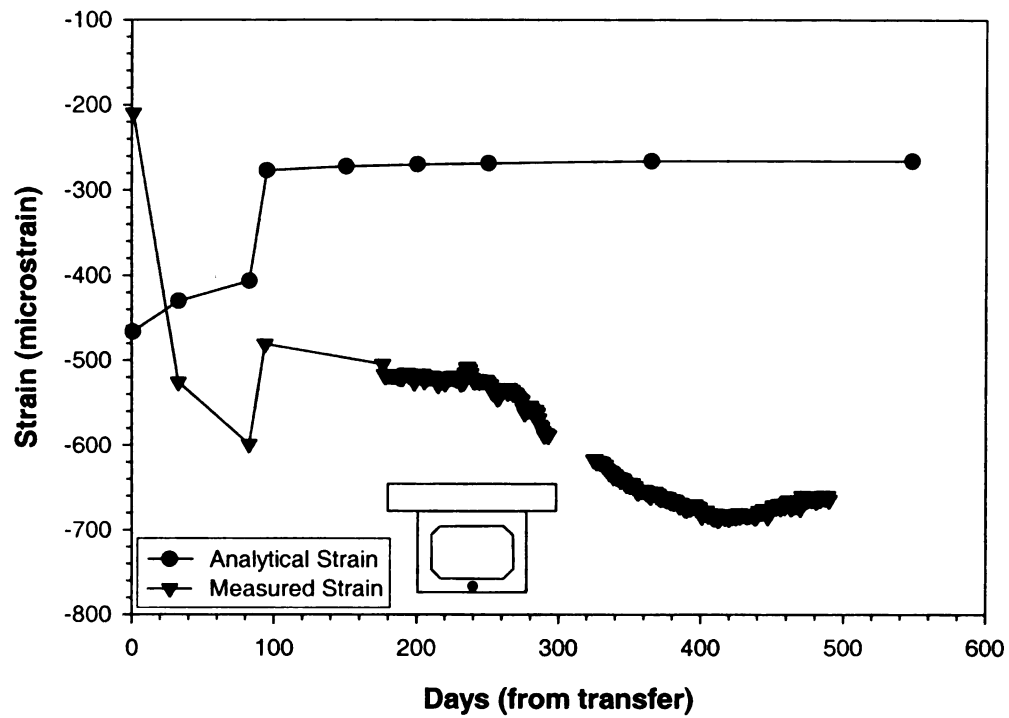
Figure 113. Comparison of Strains for Bottom VWSG SCC 3 Section A
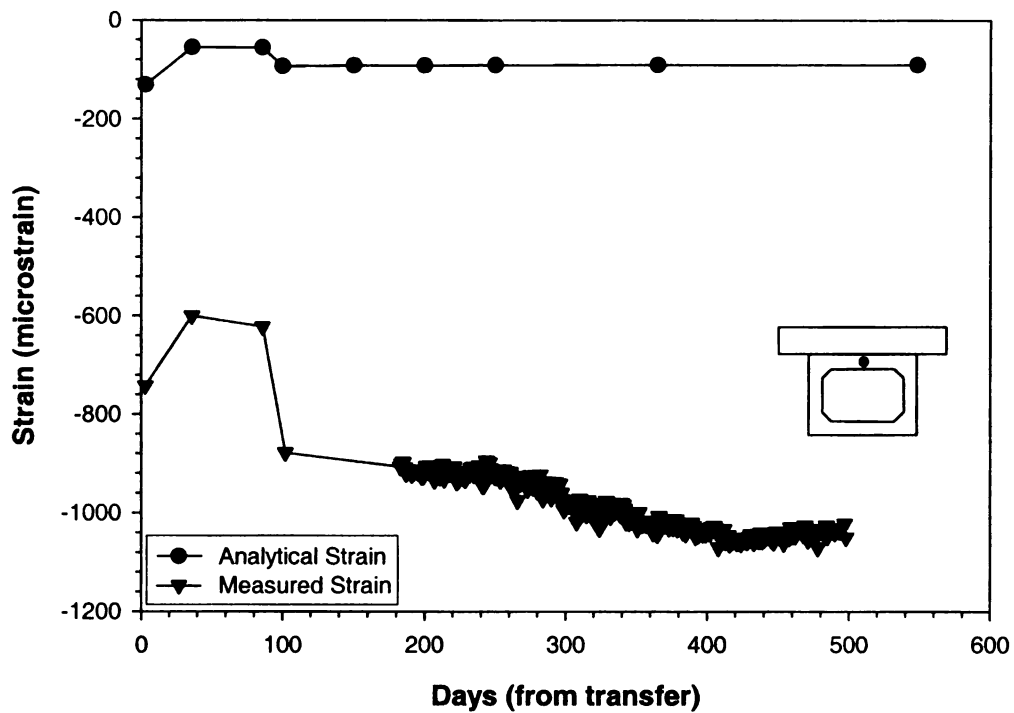
Figure 114. Comparison of Strains for Top VWSG SCC 3 Section A

233

6.4 Influence of Diaphragm on Strain in Beam

The previous plots show the comparison of the analytical or calculated strain to the measured strain at the midspan of the bridge beams or, section A. The comparisons shows some significant differences. The first is the discrepancy between the analytical and measured first point. While none of the points seem to match exactly, this point seems to have the largest difference. One possible complication that may exist at this position is the presence of an eight in. diaphragm. This solid concrete portion completely encases the 6 in. strain gage. The section properties used in the calculation of the prestress losses were the voided section properties. To see if this solid section caused inaccuracies in the comparison two methods were carried out, first the section properties at the diaphragm were used in the prestressing loss analysis, second the prestressing loss at section B, 12 in. from the midspan were calculated. Each of these methods was done for both the NCC and SCC 1 beams.

As was the case for the voided section properties, the section properties at the diaphragm needed to be transposed to account for the area of the prestressing steel. This needed to be done at multiple times throughout the bridge life and separately for each concrete mix design. Table 71 and Table 72 show the properties used to calculate the strain in the NCC beam while Table 73 and Table 74 show the properties used to calculate the strain in the SCC 1 beam.

Table 71. NCC Section Properties Without Void

Event	Area (in^2)	I (in^4)	y (in.)
1	949.60	54,143	12.80
2	983.16	58,609	13.29
4	1,847	212,862	21.81

234

Table 72. NCC Strand and Instrument Eccentricities Without Void

Event	Condition 1	Condition 2	Condition 3	Top Inst. (in.)	Bot. Inst. (in.)
1	11.70	9.37	9.55	11.70	10.80
2	11.21	9.86	10.04	11.21	11.29
4	2.69	18.38	18.56	2.69	19.81

Table 73. SCC 1 Section Properties Without Void

Event	Area (in^2)	I (in^4)	Y (in.)
1	926.79	54,073	13.04
2	962.79	58,581	13.50
4	1,827	212,814	22.01

Table 74. SCC 1 Strand and Instrument Eccentricities Without Void

Event	Condition 1	Condition 2	Condition 3	Top Inst. (in.)	Bot. Inst. (in.)
1	11.46	9.61	9.79	11.46	11.04
2	11.00	10.07	10.25	11.00	11.50
4	2.49	18.58	18.76	2.49	20.01

The results of the prestressing loss calculation using the diaphragm section properties are shown in Figure 115 and Figure 116 for the bottom and top flanges of the NCC beam. The results for the SCC beam bottom and top flanges are shown in Figure 117 and Figure 118. From these plots for the bottom flange, Figure 115 and Figure 117, it is possible to see that the first point of the analytical plot seems to be closer to the measured value, however, the following points including the continuously monitored data do not show any improvements over the plots with the voided section properties. The plots of the top flange do not show improvement over the plots with the voided section properties. From these plots it can be concluded that the use of the section properties considering the diaphragm does not cause a positive change to the strain comparison.
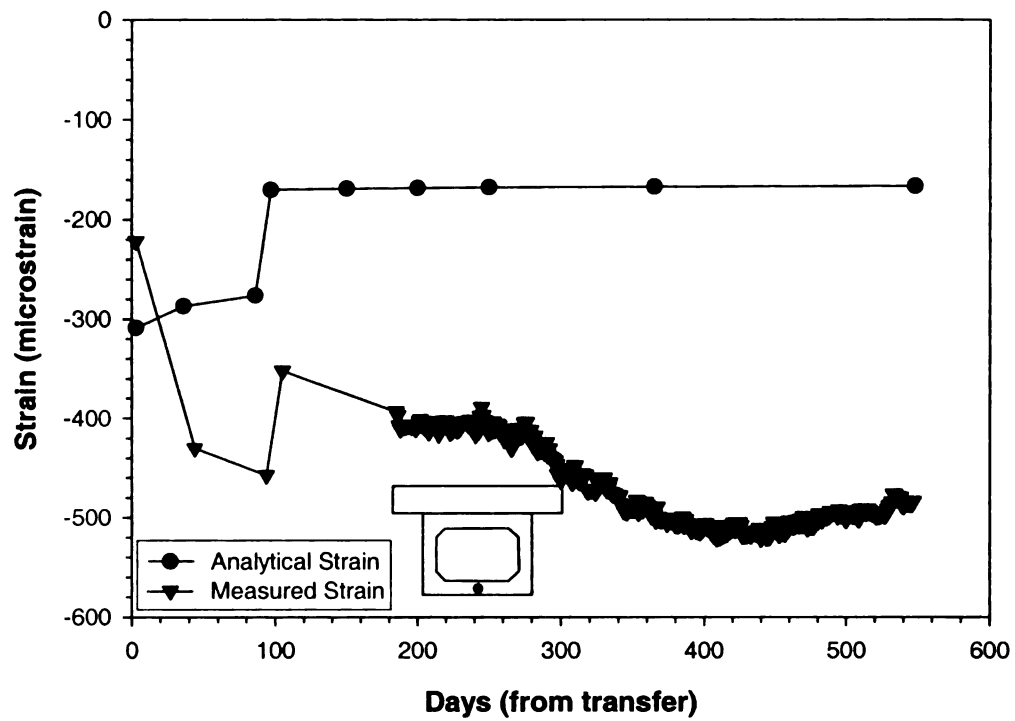
Figure 115. Bottom Strain Comparison With Diaphragm NCC Section A
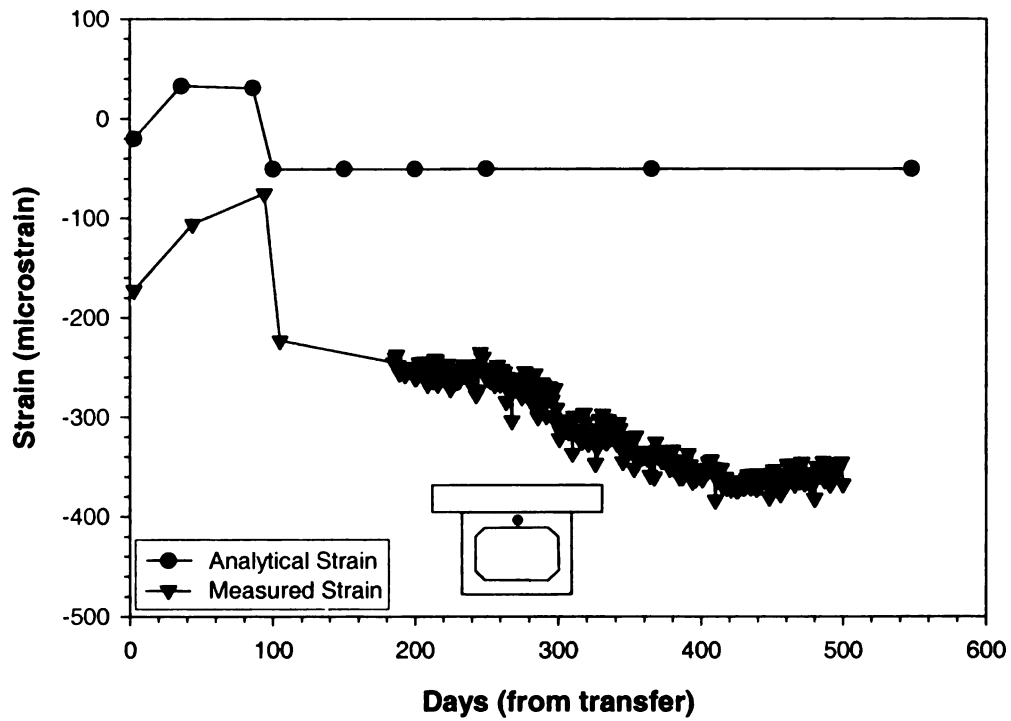
Figure 116. Top Strain Comparison With Diaphragm NCC Section A

236
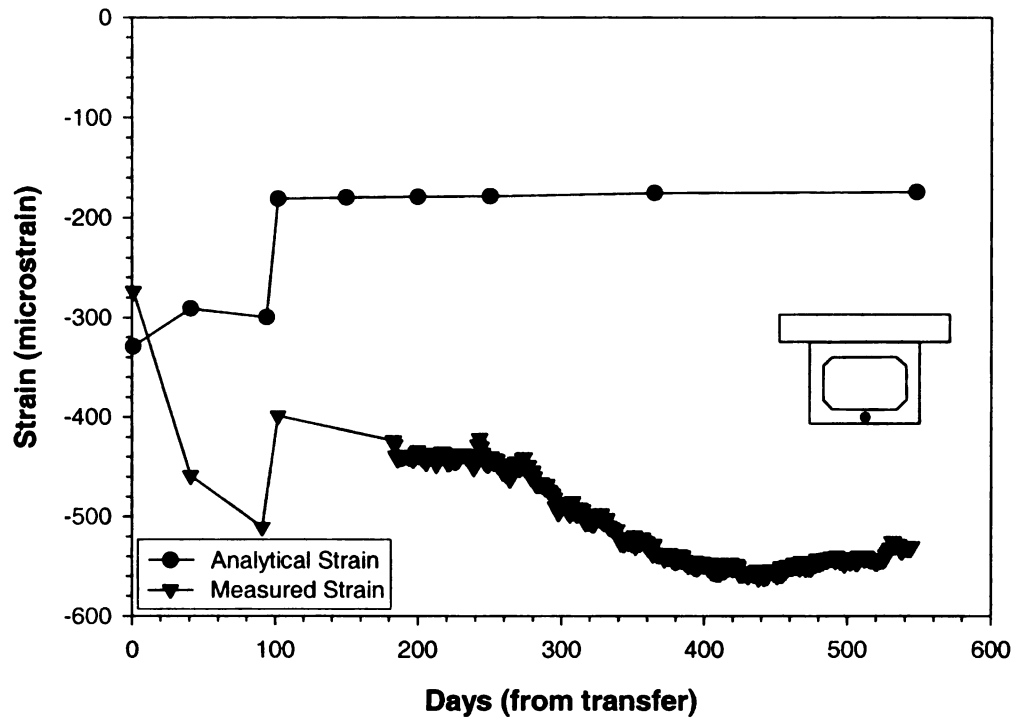
Figure 117.   Bottom Strain Comparison With Diaphragm SCC 1 Section A
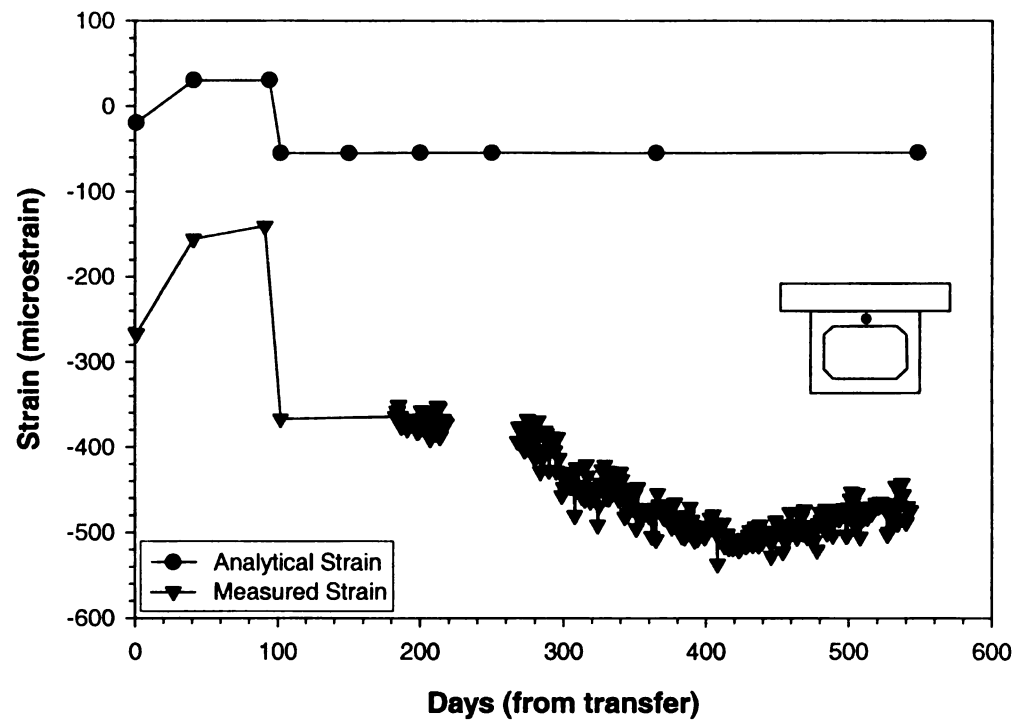
Figure 118.   Top Strain Comparison With Diaphragm SCC 1 Section A

To further investigate the influence of the diaphragm on the strain comparison the strain was predicted outside the influence of the diaphragm. The results of the prestressing loss calculations at section B are shown in Figure 119 and Figure 120 for the bottom and top flanges of the NCC beam and Figure 121 and Figure 122 for the bottom and top flanges of the SCC 1 beam. The main difference from in the calculation of the prestress loss at section A is the calculation of the moment due to the self-weight of the beam and the deck. Section A represents the maximum moment due to self-weight, thus at section B, the moment due to self-weight is slightly lower. From these plots it is possible to see that the analytical values do not match the measured data with any more accuracy than the values at Section A.
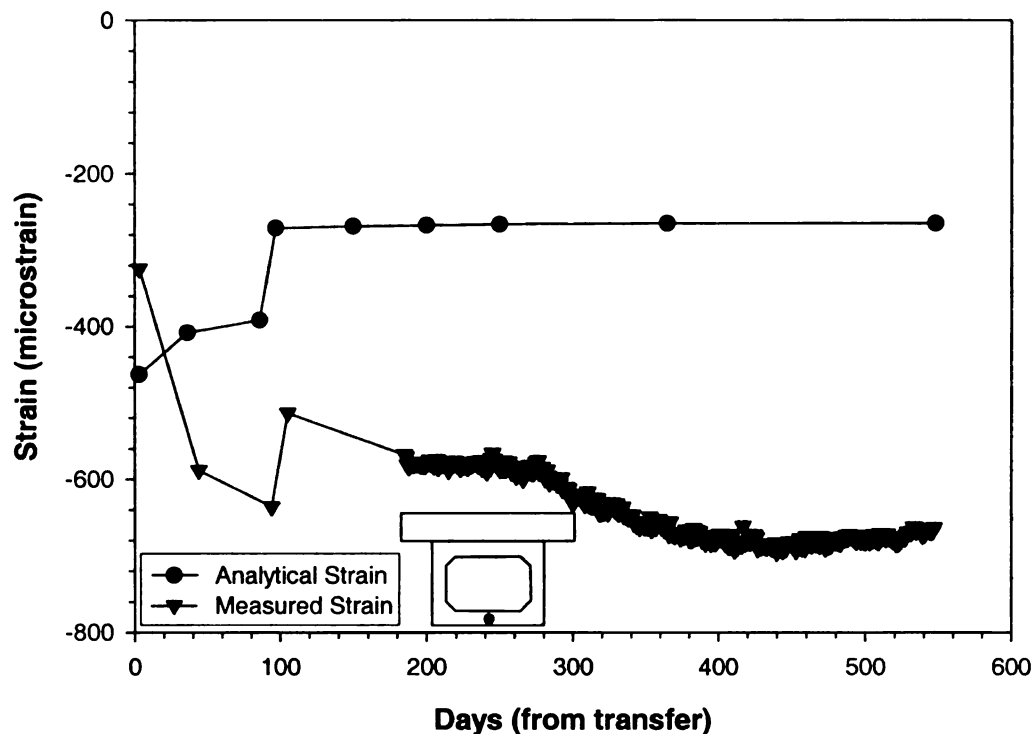
Figure 119. Bottom Strain Comparison NCC Section B
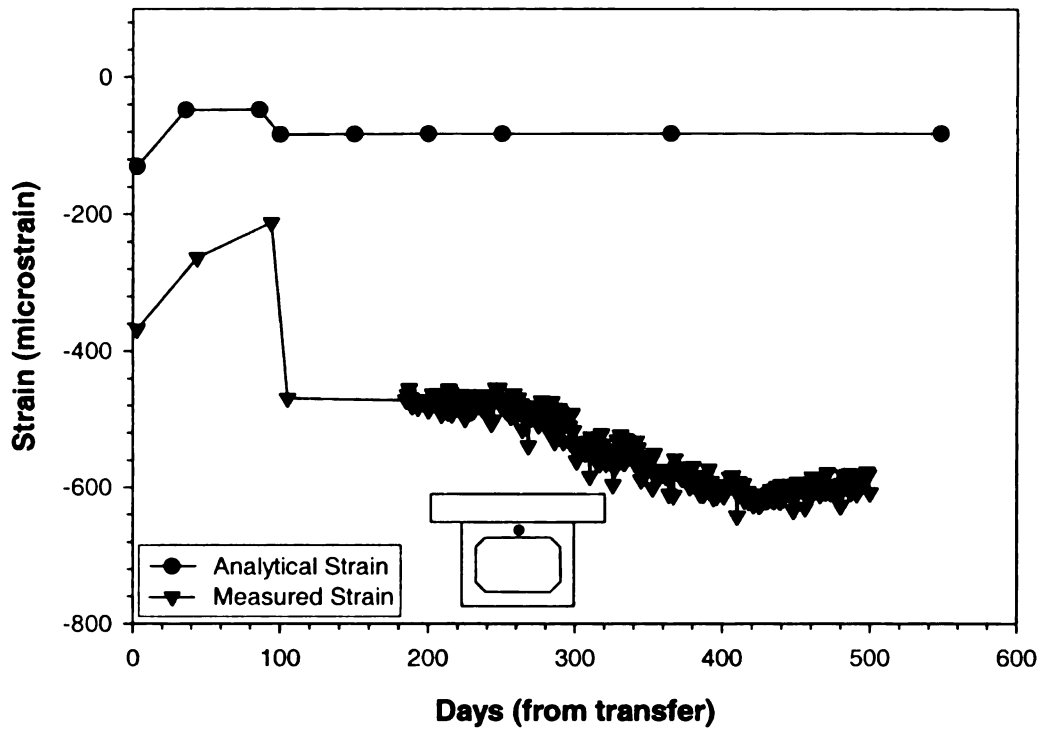
Figure 120. Top Strain Comparison NCC Section B
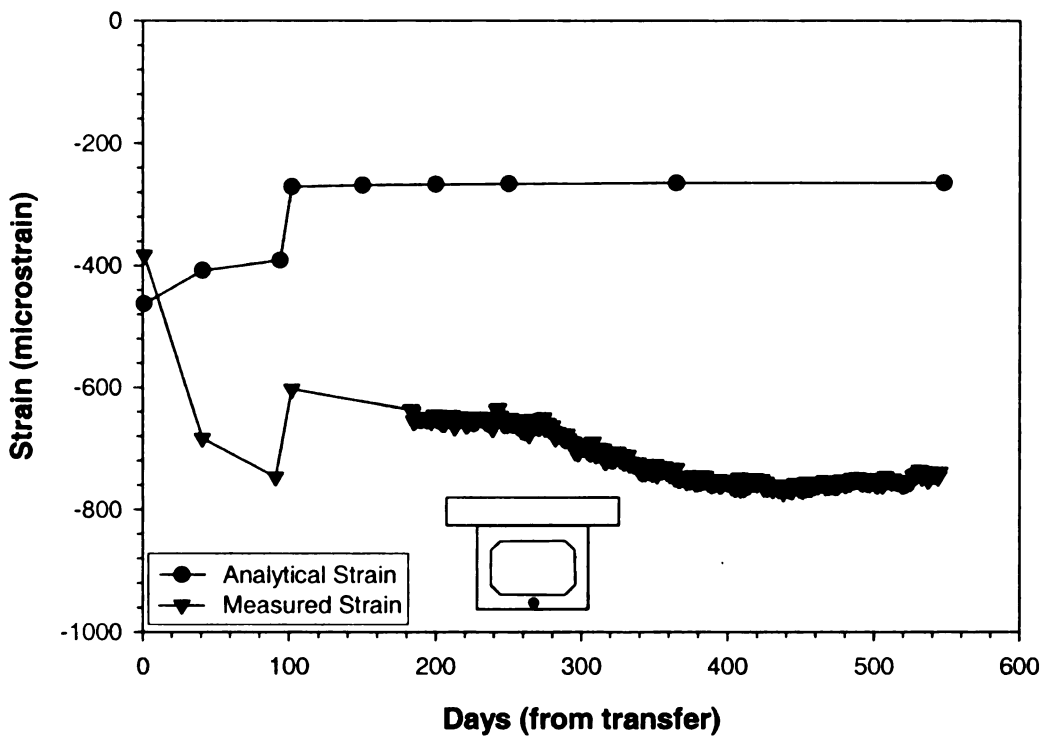
Figure 121. Bottom Strain Comparison SCC 1 Section B

239
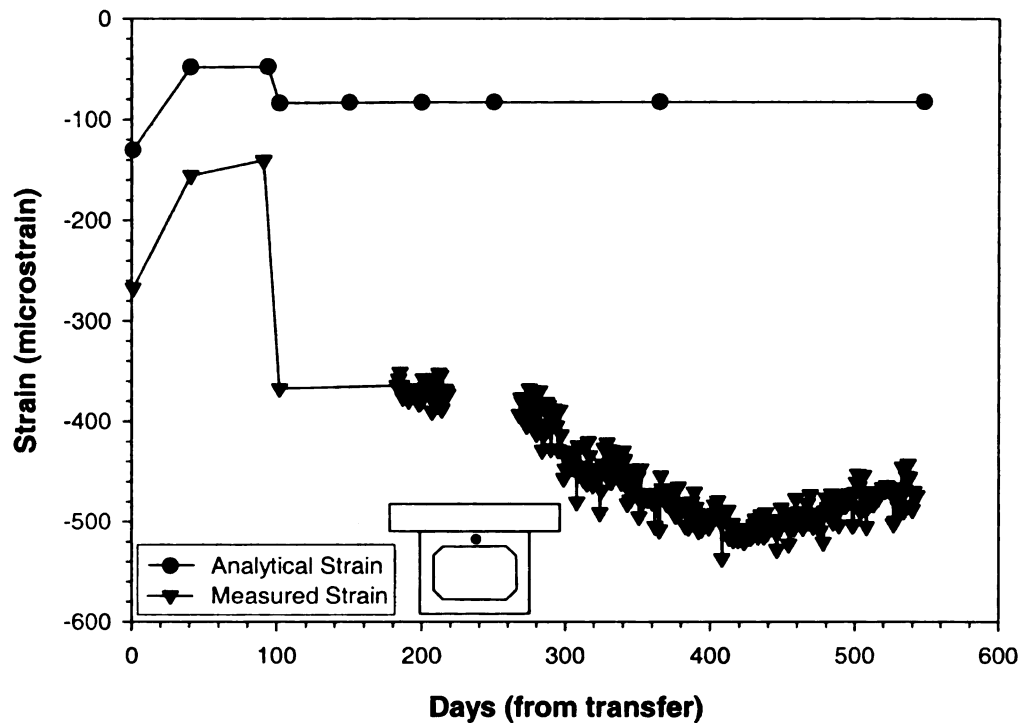
Figure 122. Top Strain Comparison SCC 1 Section B

The two methods used to account for the influence of the diaphragm on the strain comparisons did not increase the accuracy of the results. Differences between the analytical and measured values existed whether voided section properties were used or not, and at sections completely outside the diaphragm. The difference that do exist seem to be consistent through out the four mix designs. This shows that all four of the instrumented beams behave in a similar manner.

6.5 Effect of Temperature on Strain in Beam

As discussed previously, the increase in compressive strain during the warmest months of the year seem to indicate that the change in temperature of the beams affects the strain in the beams. This change in strain is significant as an increase in compressive strain would imply that the prestressing force is also increasing. This increase could cause cracking in the concrete if the change was large enough.

240

There are two ways that temperature can affect the strain in a bridge beam. The first is a temperature change that is uniform throughout the depth of the beam. The second is when the temperature change throughout the beam depth is not uniform. In reality a combination of these two events occurs.
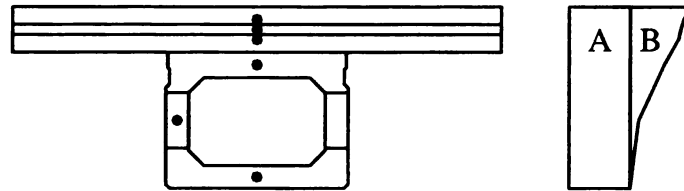
Figure 123.   Thermocouple Locations and Temperature Variation

Figure 123 shows the location of temperature readings throughout the depth of the composite beam as black dots in the cross section. The readings taken at these locations throughout time can be summarized by the assumed temperature gradient shown in the figure. In this gradient there are two parts. Part A is a uniform temperature that exists from the top to the bottom of the beam cross section. Part B is the temperature gradient that is large at the top and reaches zero at the bottom of beam. It is the combination of these two temperature change that cause the strain in the beam to change.

The bridge in this project is a simply supported beam with one end free to expand, and the other is fixed against horizontal movements. As is shown in Figure 124, both ends of the beams for the demonstration bridge rest on elastomeric bearing pads. These pads allow horizontal movements, or expansions of the beam. One end of the beam is fixed against these movements through a dowel bar that is grouted into place at the center of the bearing. This bar extends from the beam into the abutment wall and does not allow

the beam to expand. Thus all of the expansion is taken up in one end, the expansion end, of the bridge beam.
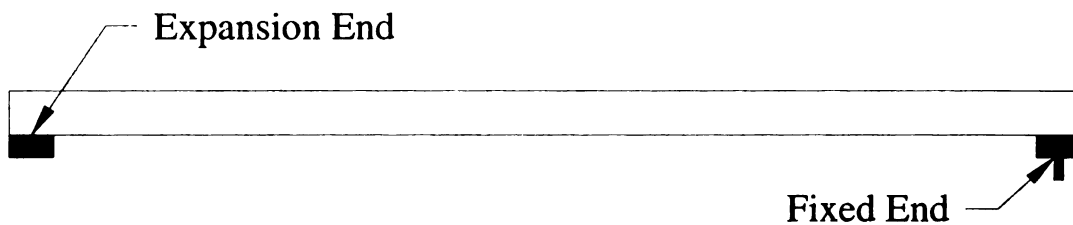
Expansion End

Figure 124. Fixed and Expansion Ends of Bridge Beams

The changes in temperature that cause changes to the strain in the beam must be referenced to the temperature at the time of bridge construction. The temperature when the beams were placed at the bridge site was approximately 50 degrees Fahrenheit. This temperature is the reference temperature for all temperature calculations.

The uniform temperature change n is shown in Figure 125. Here a positive change in temperature causes the free end of the beam to move horizontally. Because the beam elongates a VWSG located at the center of the beam should record an increase in strain. This increase should be in a positive direction as the beam lengthens causing the tension in the concrete. This result comes from the fact that the beams are free to expand under normal conditions. If the beam was not free to expand, this positive temperature change would cause an increase in compressive strain in the concrete.

$+\Delta T$
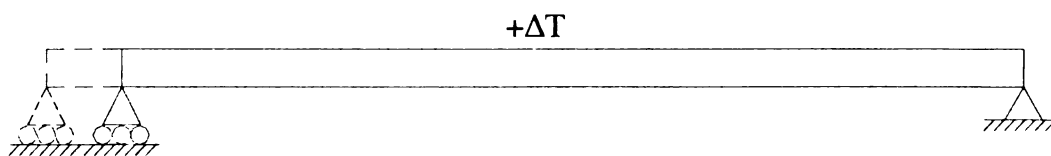
Figure 125. Expansion Due to a Uniform Positive Temperature Change

242

Because the coefficient of thermal expansion for concrete and steel are very similar the increase in strain seen in the concrete due to a temperature increase should also cause an increase in strain in the prestressing strand. This will happen because the prestressing steel and concrete should expand or contract by the same amount. The coefficient of thermal expansion as given by the AASHTO-LRFD-2 Specification [3] is 6 x 10^{-6}/°F.

The second way temperature can affect the strain in a beam is through a temperature gradient. A temperature gradient is formed when the temperature throughout the depth of the beam is not uniform. It can either be warmer at the top and cooler at the bottom or the opposite. Of interest for this analysis is the situation during the warmest months of the year. During these months, the deck, at the top of the section is generally warmer than the bottom flange of the beams. When this occurs, the top of the beam tries to expand more than the bottom of the beam. The result of this deformation is an upward curling of the beam as shown in Figure 126. This curling causes the top of the beam to be in tension and the bottom of the beam to be in compression.

+ΔT: Curvature
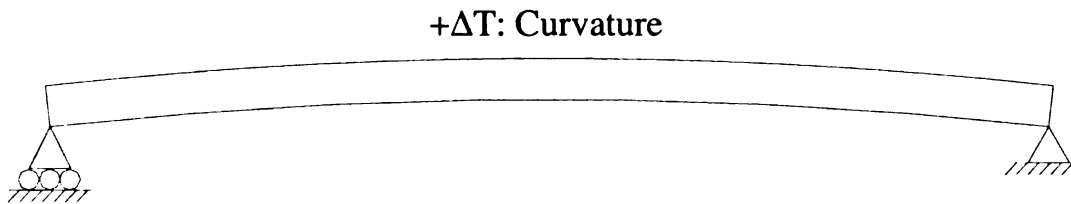
Figure 126. Deformation Caused by Temperature Gradient

The calculation of the strain induced in the beam due to a uniform temperature change is done using Equation (69),

$$(69) \qquad \varepsilon_{uniform} = \alpha \Delta T$$

243

where α is the coefficient of thermal expansion of concrete and ΔT is the difference in temperature from the time the beams were set at the bridge until the point of interest. The point of interest for this calculation is the 365th day of the prestress loss analysis. This day was chosen as it falls in the middle of the compressive strain increase for the monitored data. The actual date at this point is June 21st, 2006. The temperature data recorded by the thermocouples at 12:00 pm on this day are shown in Table 75. The six thermocouple recordings are identified by their position in the beam. The remaining temperatures were chosen to lie on the temperature profile from the thermocouples. The temperature gradient shown in the last column is the difference between the temperature at the specific height and the minimum recorded temperature.

Table 75. Recorded Temperatures for NCC Beam (6/21/06)

Location	Beam Ht (in.)	Temperature (°F)	Gradient (°F)
	36	76.1	5.1
Top of Deck	34.25	75.2	4.2
	32.5	75.2	4.2
Middle of Deck	31.5	76.0	5
	30.5	77	6
Bottom Deck	28.75	79.4	8.4
	27	77	6
Top Flange	24.5	75.5	4.5
	22	73.4	2.4
Middle of Beam	13.5	72.7	1.7
	8	71.6	0.6
Bottom Flange	2.25	71.0	0
	0	71.0	0

The minimum recorded temperature in Table 75 is 71 °F. This temperature is 21 °F higher than the temperature when the beams were set at the bridge site. Thus, this

temperature change is used to calculate the strain due to the uniform temperature change

using Equation (69). This strain is a tensile strain equal to 126 microstrain.

The calculation of the strain due to the temperature gradient is more complicated

than that for the uniform temperature change. This calculation requires the cross section

to be separated into multiple sections. The sections for the beams in this project were

chosen such that each of the six thermocouples used in the analysis lie at the centroid of a

section. The section properties for the multiple sections used in the temperature analysis

are shown in Table 76.

Table 76. Section Properties for Gradient Temperature Analysis

Section	Area (in^2)	Centroid (in.)	I (in^4)	Y (in.)	d (in.)
1	336	34.25	343	9.39	3.5
2	192	31.5	64	6.64	2
3	336	28.75	343	3.89	3.5
4	208.5	23.88	823	0.98	5
5	99	13.5	998	11.36	11
6	202	3.02	786	21.84	4.5

There are two components to the gradient temperature induced strain. The first is

an axial temperature strain. This strain is calculated using Equation (70):

$$(70) \qquad \varepsilon_{axial} = \frac{\alpha}{A} \sum T_i A_i \, , \, [3]$$

where A is the total area of the composite cross section, T_i is the temperature at the

centroid of a specific section and A_i is the area of a specific section. When the

temperature gradient and section properties for the beams are applied to this equation a

strain value of 27.5 microstain is calculated. This strain is a tensile strain as the beam is

expanding, thus, it will have a positive value.

The second component of the temperature induced strain comes from the curvature caused as the beam curls. This curvature is calculated using Equation (71):

$$(71) \qquad \psi = \frac{\alpha}{I} \sum \left[T_i y_i A_i + \frac{\Delta T_i}{d_i} I_i \right], [3]$$

where I is the moment inertia of the composite section, $155{,}789$ in^4, y_i is the distance from the neutral axis of the total section to the neutral axis of the specific section, ΔT_i is the change in temperature from the bottom of a section to the top of that section, I_i is the moment of inertia for the given section, and d_i is the depth of a given section. The calculated curvature for these beams is 1.322 in^{-1}.

This curvature can be used to find the strain induced in the beam due to the temperature gradient. First the moment caused by this curvature is calculated using Equation (72):

$$(72) \qquad M = EI\psi,$$

where E is the modulus of elasticity of the concrete. This moment can be used to calculate the stress at the top or bottom of the beam using Equation (73):

$$(73) \qquad \sigma = \frac{My}{I},$$

where y is either the distance from the neutral axis to the top of the beam or to the bottom of the beam depending on where the stress is to be found. Finally by simplifying the previous two equations and applying Hooke's Law, Equations (74) and (75) result:

$$(74) \qquad \varepsilon_{bottom} = y_b \psi,$$

$$(75) \qquad \varepsilon_{top} = y_t \psi.$$

Thus, the strain at the bottom of the section due to the temperature gradient is a compressive strain of 32.9 microstrain. While the strain at the top of the beam due to the temperature gradient is a tensile strain of 14.7 microstrain.

All three strain components, the strain due to the uniform temperature change, and the axial and curvature based strains from the gradient temperature, can be combined to find a resultant strain acting at the top and bottom of the section. If temperature is the reason for the increase in compressive strain seen in the measured plots, the strain from this analysis should be similar. Figure 127 shows the resulting strain diagrams for the temperature analysis. The total strain in the section due to the temperature is calculated to be between 100 and 200 microstrain for this time period.

+126   +27.5   +14.7   +168

$$\square \ + \ \square \ + \ \diagup \ = \ \square$$

+126   +27.5   -32.9   +121
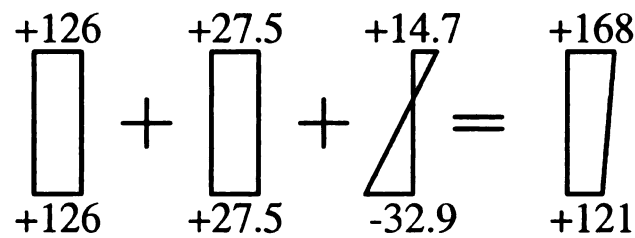
Figure 127. Strain Diagram for Temperature Analysis

The total strain in the top and bottom flange due to the temperature throughout the cross section is very close to the value of compressive strain increase seen in the measured data. However, the sign of this value which is positive for a tensile strain is opposite of what is seen in the measured data. Thus, it seems that temperature alone cannot explain the change in strain seen in the measured data.

6.6 Influence of Bridge System on Strain in Beam

While the temperature induced strain is the opposite sign of what is expected based on the measured data it may still be the reason for the compressive strain increase. The above temperature analysis is based on the assumption that the beam is completely free to expand. In reality, the elastomeric bearing pad has some stiffness that may prevent some of the expected temperature based expansion. Furthermore, other factors could influence the stiffness of the bearing. Some of these factors could include the presence of a backwall cast between the beams on the abutment wall, or the interconnectivity of the bridge system through the external diaphragm and the bridge deck. Figure 128 shows an idealized beam system. In this system the beam rests on a bearing of height e, with a roller replaced by a spring with stiffness k. This stiffness can very from zero if nothing obstructed the expansion of the beam to infinity if the beam was unable to expand at all.
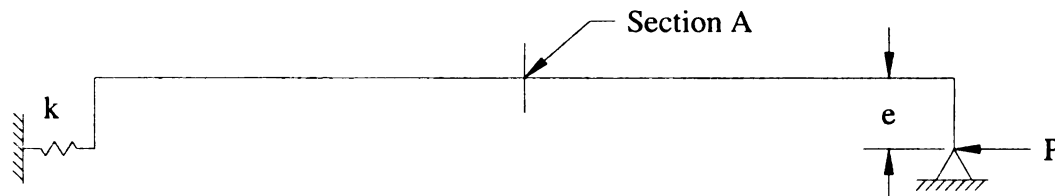
Figure 128. Assumed Beam System With Bearing Stiffness k

To see if the bearing stiffness of the beam could result in an increase of the compressive strain on the order to that seen in the measured data the worst case scenario should be analyzed. The worst-case scenario is that where the stiffness of the bearing is infinity, or the beam is pinned at both ends. This system is shown in Figure 129.

248
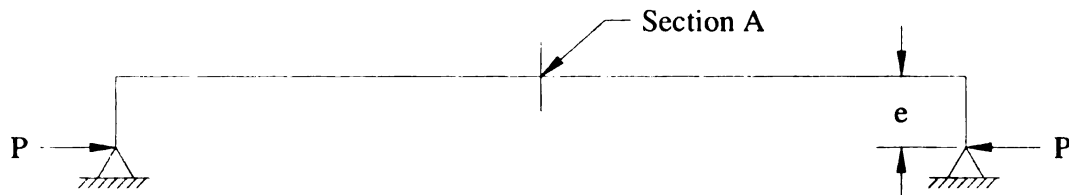
Figure 129. Idealized System With Infinite Bearing Stiffness

When a temperature increase on the same order as that seen in the temperature analysis is applied to the beam the reaction forces, P at the pins develop. This force creates a bending moment diagram as shown in Figure 130. The maximum moment that occurs uniformly across the entire length of the beam is equal to the reaction P multiplied by the height of the bearing e.
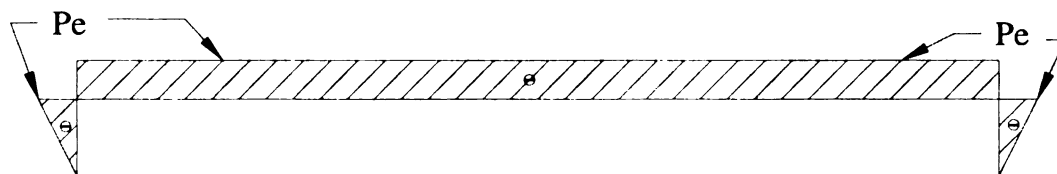
Figure 130. Bending Moment Diagram For Idealized System

To investigate the affect of the bearing stiffness could induce the increase in continuous strain that is seen in the measured data two procedures were carried out. First the idealized system described above was modeled using SAP 2000 (Computers & Structures Inc, Berkeley, California). The beam in this model was then given a temperature expansion equal to the uniform temperature expansion seen in the temperature analysis, 21 °F. The reaction at the pins was then reported by the model.

The second procedure was to back calculate the reaction caused in the idealized model based on the increase in compressive strain seen in the measured data. This was

done by calculating the stress both using Hooke's Law and the beam flexure equation shown in Equation (76):

$$(76) \quad \sigma = \frac{My}{I}.$$

The moment in Equation (76) is calculated using Equation (77):

$$(77) \quad M = Pe.$$

Combining these two equations with Hooke's law gives Equation (78):

$$(78) \quad E\varepsilon = \frac{Pey}{I},$$

which when simplified for the reaction P is Equation (79):

$$(79) \quad P = \frac{\varepsilon EI}{ey}.$$

Thus, the reaction in the pins can be calculated in two ways, first by using a computer model and the observed temperature increase of 21°F and secondly by back calculation from the observed strain increase of 100 microstrain. The results of these two procedures show that the reaction found using the computer model was 943,380 lbs, while the reaction from the strain increase was found to be 1,099,900 lbs.

These results would imply that the beam is acting as a pinned beam with no ability to expand. It is unlikely that the beam is unable to expand as this bridge is built with a common MDOT bearing detail. Yet, this lack of free expansion most likely plays a role in the explanation for the compressive strain increase in the measured strain response.

250

6.7 Data Normalization

The final discrepancy in the data is the large difference that exists between the values of the NCC and SCC beams. To remove this difference, the data was normalized by making the reference temperature and reference strain for all readings zero. In doing this, the data is essentially showing the change in strain, without regard for the starting value. The result of this for the strain response of the bottom flange is shown in Figure 131.
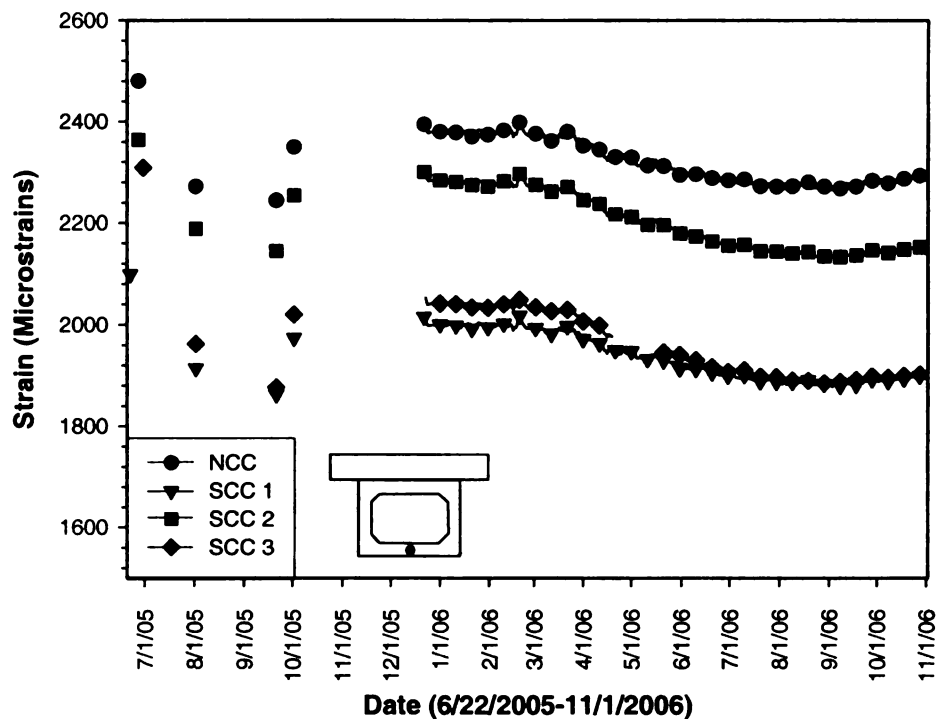
Figure 131. Normalized Strain Response for Bottom Flange Section A

From the figure it is possible to see that very little has changed from the unnormalized plot presented previously. In fact this figure is merely an upward translation of the other figure. All that has changed is the reference point is now zero

instead of what it was previously. The differences between the values of the various

beams is on the order of 100-300 microstrain.

The strain response in the top flange showed a larger difference in the previously

presented figure (Figure 95) than that of the bottom flange. The difference in this plot

was on the order of 600 microstrain. Once the data is normalized Figure 132 is the result.

In this figure the difference between the four plots is reduced to 100-300 microstrain.

Thus, by normalizing the data to a common reference point it is possible to see that the

responses of all four beams are nearly identical.
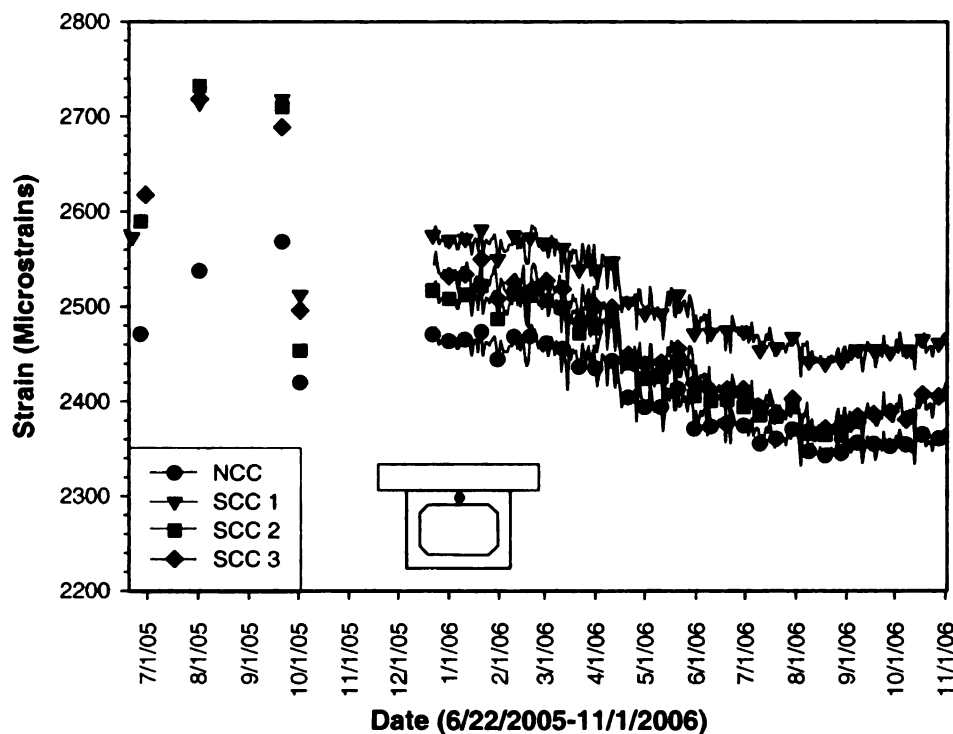
Figure 132. Normalized Strain Response for Top Flange at Section A

It is unclear why the data in the unnormalized state shows such large differences

in value. However, the scope of this thesis is limited to the differences between the four

concrete mix designs. From the normalized figures it is possible to see that the responses

of each of the beams is nearly identical and thus no significant differences in the behavior

252

of the different concrete mix designs seems to exist. To investigate further the reasons for the differences in strain values would be outside the scope of this project.

6.8 Long Term Performance Conclusions

From the results obtained from the field monitoring program it is possible to see that while the values of strain that are recorded are very different from the analytical values, the overall behavior of the beams appears to be similar. The beams show similar behaviors for all of the concrete mix designs. Additional analysis trying to explain the differences that existed in the beam were conducted but proved to be inconclusive. Multiple factors were investigated without definitive results.

It is likely that it is not a single factor that causes the differences in the measured and predicted strains, but rather a combination of many affects. It was shown that the presence of the diaphragm does not greatly influence the predicted results thus this is not likely to contribute to the inaccuracies.

The temperature analysis showed, that as expected, temperature does play a role in the discrepancies seen in the measured and predicted data. However, it can not be the temperature alone, as the temperature increase seen in the measured data should cause a tensile strain in the beam. The influence of the bearing system stiffness for the bridge could introduce a compressive strain increase on the order of what is seen in the measured data. However, the real behavior of this boundary condition is complicated and its complete analysis is beyond the scope of this thesis.

Normalization of the data allowed for the direct comparison of the SCC and NCC plots as significant differences in the values of the strain were removed. The difference

in the reference value appeared to cause the difference in the strain values that was present in the unnormalized plots. From the normalized plots it is possible to see that the response of the four beams is nearly the same.

In spite of the inconclusive evaluation just presented, the results of the long-term monitoring system show that the four concrete mix designs behaved similarly over the measurement period of one year. The strains over time show similar rates of loss of prestress and affects of temperatures. While differences do exist between the four plots, they seem to be limited to the overall bridge system and they do not dependent on the concrete material properties.

7 CONCLUSIONS AND RECOMMENDATIONS

The use of SCC to cast elements for highway bridges can lead to reductions in both the time labor required in production. For this project, casting times for SCC beams were reduced an average of 61% over NCC beams. Significant reductions in labor led were also realized. However, implementing SCC in a precast facility is not as simple as changing the concrete mix design. Extensive work is required to develop a mix design and certain modifications to current casting operations are required to use SCC effectively. Further, time is necessary to gain the experience that will allow SCC to be used most efficiently.

Multiple methodologies can be used to develop SCC mix designs that consistently produce high quality concrete. These mixes can achieve the desired SCC fresh properties using commonly available equipment and ingredients. One way to develop and refine an SCC mix design is by conducting a systematic trial and error process that revaluates the mix based on fresh property test results after each phase. Fresh property tests, either preliminary, as those proposed by PCI, or standardized, as those being developed by ASTM, can provide sufficient information to adjust mix design parameters to achieve satisfactory performance of the fresh concrete.

The use of chemical admixtures in the SCC mix designs may affect the bond performance of the concrete. Specifically the use of VMA may lead to reduced bond strengths. While some reduction in bond strength over the NCC mix was seen, the size of the structural members used in this project was not bond critical. Slightly reduced bond strength, or an increased development length would not likely lead to a compromise in either flexural or shear strength for the bridge beams.

255

The beneficial properties of SCC were realized in this project as the production of the box beams was reduced from four steps to two through the use of SCC. The most difficult part of the production process was restraining the Styrofoam block from the pressure generated by the flowing concrete as it filled the formwork. Top wood restraints bolted to the formwork were successful in restraining the Styrofoam block while not impairing the flow of concrete through the formwork.

The self-consolidating nature of SCC allows for a more complete compaction of the concrete. This, along with the superior flow behavior of SCC, led to beams being produced with higher surface quality in the SCC beams when compared to the NCC beams. Fewer and smaller surface imperfections were seen due to trapped air at the formwork concrete interface. This improved surface quality led to less work being done to patch the surface of the beams.

The decreased beam production time led to a nearly continuous batching operation. Greater amounts of concrete were produced in less time during the production of the SCC beams compared to the NCC beams. This increased production rate leads to less down time for the labor during beam production.

The constant quality control during the production of the SCC batches allowed for necessary adjustments to maintain consistent fresh property behavior throughout the beam production process. Small changes to the SCC mix design required for changing conditions of weather and material constituents were able to be made. Increased experience with SCC would lead to more accurate estimates of these necessary adjustments.

From the full-scale flexural tests the overall behavior of the SCC beams was seen to be very similar to that of the conventional beam (NCC). Cracking patterns, widths, and failure levels followed predicted responses through conventional prestressed concrete theory. While the failure of the flexure test units was explosive, the beam was not over-reinforced and the strands yielded before failure, technically defining the failure mode as ductile. Consequently, variations in concrete compressive strength did not significantly modify the beam's ultimate capacity, which were very similar for all beams. The absolute capacities of the SCC beams were marginally lower than that of the NCC beam, specifically, 1.3, 3.4, and 3.5 percent lower for the SCC1, SCC2, and SCC3 beams, respectively. However, the flexural capacities of the SCC beams exceeded the required design capacity by 6 to 9 percent.

The shear behavior of the SCC beams was also found to be adequate and very similar to that of the NCC beam. Cracking paths and widths were consistent in all beams and the failure levels closely matched analytical predictions. The shear capacities of the SCC beams were comparable to that of the NCC beam. The ratio of capacity to nominal strength for the SCC1, SCC2, and SCC3 beams as 1.22, 1.12, and 1.08, respectively, while that same ratio for the NCC beam was 1.11. The shear capacity and response of the SCC beams is thus considered adequate.

Due to the large amount of prestressing and the extension of the beam beyond the supports, failure of the critical section in shear did not result in overall member failure. Rather, the beam was able to re-distribute demands beyond the critical shear area thus allowing the beam to resist increasing loads that in two beams eventually lead to flexure-induced failures and in two others the tests were terminates. However, even though the

257

overall beam failure was not in a pure shear mode, the shear behavior and capacity provided by the beams was successfully evaluated. This was determined by studying the shear force versus shear strain response of the critical shear areas in the beam, which showed that the sections reached a peak shear force beyond which shear strains would increase rapidly in an almost elastic-perfectly-plastic response. This same behavior was supported by the moment-curvature response of this sections, which had essentially a bi-linear response with a failure at a load level much below the known flexural capacity. The reduced flexural capacity of the section is thus a consequence of the shear failure of the section. In addition, evaluation of strain profiles of the steel stirrups in the critical shear areas indicated that the transverse steel had yielded through the section depth for all beams, further supporting that sections shear failure was reached.

Overall, the performance of the SCC prestressed box beams in flexure and shear was found to be essentially equal to that of the NCC beam and their behavior was well predicted by conventional prestressed concrete theory. While additional issues pertaining to long-term behavior of SCC in prestressed elements, namely creep effects, are still to be fully evaluated, the short-term flexural and shear response evaluated through this testing program indicates that the SCC prestressed beams safely satisfy their prescribed design requirements. The results of this testing program provided sufficient evidence to believe the SCC beams could be used in the demonstration bridge as planned.

Long-term in-service performance of the SCC beams in comparison of the NCC beams is being achieved by the field monitoring of 4 beams in the demonstration bridge (3 SCC beams and one NCC beam). Performance is being measured by means of strains in selected cross sections and temperature instruments are permitting the compensation in

the strain readings as well as evaluation of temperature effects. Results to date indicate that the SCC beams are performing similarly to the NCC beam. To date, the effects of temperature on the strain measurements are dominant. An attempt has been made to compare the measured strains to predicted values by estimating the strain variations due to prestress losses as well as temperature induced effects. Differences between the predicted and measured values exist. However, the applicability of time-dependent losses due to concrete shrinkage and creep to SCC is questionable. Little information on the applicability of current code prestress loss models to SCC exists. Thus, further work is required to obtain a better comparison between predicted and measured responses.

The data measured to date indicates that while some variations exist in the initial strain levels of the girders. The variation of initial readings can be attributed to the different losses in the SCC beams caused by concrete shrinkage and elastic shortening, which are controlled by the water content in the mix and the concrete elastic modulus. Clearly, both of these parameters vary considerably for the SCC beams. Thus, further work is required to understand the reasons behind the difference in initial readings in the SCC girders.

Finally, the variation of strain once the bridge was in service seems to be very similar for all girders. This would indicate that thus far there has been no change in performance between the different beams. However, it is recognized that the monitoring process has been in place for slightly over a year. Evaluation of true long-term performance will require acquisition of data for several more years before more sound conclusions on the long-term behavior of SCC prestressed elements can be reached.

From the results obtained from the field monitoring program it is possible to see that while the values of strain that are recorded are very different from the analytical values, the overall behavior of the beams appears to be similar. The beams show similar behaviors for all of the concrete mix designs. Additional analysis trying to explain the differences that existed in the beam were conducted but proved to be inconclusive. Multiple factors were investigated without definitive results.

It is likely that it is not a single factor that causes the differences in the measured and predicted strains, but rather a combination of many affects. It was shown that the presence of the diaphragm does not greatly influence the predicted results thus this is not likely to contribute to the inaccuracies.

The temperature analysis showed, that as expected, temperature does play a role in the discrepancies seen in the measured and predicted data. However, it can not be the temperature alone, as the temperature increase seen in the measured data should cause a tensile strain in the beam. The influence of the bearing system stiffness for the bridge could introduce a compressive strain increase on the order of what is seen in the measured data. However, the real behavior of this boundary condition is complicated and its complete analysis is beyond the scope of this thesis.

Normalization of the data allowed for the direct comparison of the SCC and NCC plots as significant differences in the values of the strain were removed. The difference in the reference value appeared to cause the difference in the strain values that was present in the unnormalized plots. From the normalized plots it is possible to see that the response of the four beams is nearly the same.

In spite of the inconclusive evaluation presented in the long term monitoring section, the results of the long-term monitoring system show that the four concrete mix designs behaved similarly over the measurement period of one year. The strains over time show similar rates of loss of prestress and affects of temperatures. While differences do exist between the four plots, they seem to be limited to the overall bridge system and they do not dependent on the concrete material properties.

APPENDICES

APPENDIX A

Appendix A contains the Special Provisions for Production of Prestressed Beams With Self Consolidating Concrete. This document was written for the Michigan Department of Transportation and is included here with MDOT's permission for reference purposes only. All references and tables in this document are independent of the rest of this thesis.

MICHIGAN
DEPARTMENT OF TRANSPORTATION

SPECIAL PROVISION
FOR
**PRODUCTION OF PRESTRESSED BEAMS WITH
SELF-CONSOLIDATING CONCRETE**

a. Description. This specification describes the minimum requirements for the production of nine prestressed concrete beams with three different self-consolidating concrete (SCC) mix designs for use in a demonstration bridge. All work shall be according to Section 708 of the Standard Specifications for Construction, except as modified herein. The use of SCC for precast/prestressed elements shall follow the procedures and requirements of the PCI Interim Guidelines for the Use of Self-Consolidating Concrete in Precast/Prestressed Institute Member Plants [1], except as modified herein.

In order to place the SCC beams for the bridge, they must perform equally or better than the conventional beams. Two beams for each SCC mix design and two beams for the conventional mix design will be tested for flexural characterization. Thus, the number of conventional beams to be built will be equal to the total number of beams in the bridge plus the two test units. Similarly, for each SCC beam to be placed, two more beams are needed for testing. Thus, a total of nine SCC beams are needed (three beams for each of the three SCC mix designs).

With the above strategy, should the performance of the SCC beams be sub-standard after structural testing, the bridge project with the conventional beams will proceed

264

without delays. Further, if the SCC beams are placed, the extra conventional beams will be stored at the Michigan State University (MSU) Civil Infrastructure Laboratory in case that the field monitoring shows that they have to be replaced.

b. Materials. The materials used shall meet the requirements specified in the designated section of the Standard Specifications for Construction and as specified herein:

Portland Cement, Type I or III 901

Fine Aggregate, 2NS 902

Coarse Aggregate, 6AA or 17A .... 708 and 902

Mineral admixtures shall not be used for the production of SCC for this project.

All conventional chemical admixtures shall conform to Section 903. A trial mixture program shall be developed in consultation with Dr. Rigoberto Burgueño at MSU (Phone: 517-353-1743). The fabricator shall demonstrate satisfactory performance of the admixture relative to fluidity, stability, workability, air content, and strength under the conditions of use, particularly with respect to temperature and humidity typical of production conditions in accordance with this specification.

Chemical admixtures for SCC shall be carefully selected in consultation with the admixture supplier for compatibility with the cement and all admixtures used to ensure that they perform adequately. Admixture supplier's recommendations shall be observed.

c. Design and Proportioning of Concrete Mixtures. Three self consolidating concrete (SCC) mixtures and one normally consolidating concrete (NCC) mixtures shall be designed and proportioned meeting the following requirements.

265

The tailorable design of SCC mixes, for specific plastic (fresh) and hardened properties, complicates the selection of representative mix proportioning. In addition, SCC proportioning is highly dependent on mixing equipment, discharge methods, type of chemical admixtures, and placement procedures. Thus, the required mix designs shall be developed in coordination with the chemical admixture supplier and MSU as discussed below.

While general guidelines for the required mix designs are provided here, the specific mix designs will vary depending on the preceding variables. The proportioning of the SCC mixes shall be done by a qualified commercial laboratory or qualified precast concrete technician according to subsection 605.02D. A qualified concrete technologist experienced with SCC mix design shall establish the mix design with respect to the specifications, and concrete mixing and placing conditions. The SCC mix designs for the project need to be specifically developed and tested by the fabricator in coordination with MSU and a concrete admixtures company. The fabricator must have experience with SCC mix design and casting is required.

Three different SCC mix designs are to be developed and used for the project. The overall concept for proportioning of the SCC mixes is shown in Table 1. The key guiding parameter for the mix designs is the water cement (w/c) ratio. All mixes are to be designed for a design compressive strength at 28-days of 5500 psi using Type I or III cement, and aggregates in agreement with section 708. The level of entrained air content for all mixes shall be 6% +/- 1.5%. For research purposes, the mix designs are bounds to the approaches for SCC, that is:

• *Approach 1:* Proportioning with moderate w/c ratios (e.g., 0.45), and use of HRWR and viscosity-enhancing admixtures (VMA) to provide fluidity and increase stability, respectively. This approach corresponds to the SCC-3 mix in Table 1 and Table 2.

• *Approach 2:* Mixes without viscosity-enhancing admixture, but with lower w/c ratios (e.g., 0.33) to reduce free water content and provide stability and use of a relatively high content of HRWR to provide high-fluidity. This approach corresponds to the SCC-1 mix in Table 1 and Table 2.

The SCC-2 mix design is the reference SCC mix design for relative "amounts" noted in Table 1. The SCC-2 mix is to be obtained by using the NCC mix as a basis. Typically, this requires a decrease of the coarse aggregate content (CAC) with a corresponding increase of sand, or increase in the sand to paste ratio (S/Pt). This approach will require moderate use of HRWRs and VMAs.

The normally consolidated concrete mix (NCC) used for the conventional beam shall have a target *w/c* ratio of that normally used in production (Table 1) and use the same materials, except chemical admixtures, as the SCC mix designs.

The amounts of HRWRs and VMAs will vary depending on the source, mixing procedure, and delivery needs. Use of a set-retardant admixture may be used, particularly if using Type III cement, to maintain the SCC plastic properties during placement. The

effect of variations of charging the admixtures into the mixer shall be determined from the recommendations of the admixture supplier, MSU researchers, and by trial mixes.

MSU has experience in developing the proposed SCC mix designs and will assist the fabricator in the design and calibration of their mixes. Similar mix designs to those required in this project have been successfully developed and used in MSU research for design strengths at 28 days of 7000 psi and are listed in Table 2.

The fabricator shall demonstrate the ability to produce the mix designs described above in a consistent manner and satisfying the quality control requirements outlined in item (d). A trial batch or data from previous projects shall be used to verify the mix designs. The trial batches and previous data must use the same materials that will be used for this project. Trial batches must be repeated, at no cost to the Department, if the concrete does not meet the requirements of this specification.

Table A-1. Conceptual Mix Design Matrix

Mix Design	w/c	HRWR	VMA	CAC	S/Pt
SCC-1	0.35	More	less	less or same	more
SCC-2	0.40	Moderate	moderate	conventional	conventional
SCC-3	0.45	Less	more	more	less
NCC	regular	Regular	none	regular	regular

w/c = water/cement ratio; HRWR = high range water reducer; VMA = viscosity modifying admixture; CAC = coarse aggregate content; S/Pt = sand to paste ratio

* The guideline of "conventional" in SCC-2 refers to the usual procedure of proportioning an SCC mix from a standard NCC mix, where the coarse aggregate content is reduced with a corresponding increase in sand.

** The guidelines of "more," "less," or "same" noted in the mix content refers to relative amounts compared to the SCC-2 mix design.

Table A-2. Sample 7000 psi Mix Designs from MSU Research

	Type	SCC-1	SCC-2	SCC-3	NCC
Constituents (lbs)					
Cement	Type-III	700	700	700	700
Sand	2 NS	1519	1426	1275	1216
Coarse Aggregate	6 AA	1380	1380	1435	1580
Water		245	280	315	280
Air	6 % (target)	6%	6%	6%	6%
w/c Ratio		0.35	0.4	0.45	0.4
Admixtures (oz/cwt)					
Air Entraining	MB-AETM 90	0.5	0.5	9.08	1
HRWR	Glenium® 3200 HES	6.29	7	8	2
VMA	Rheomac® VMA 358	0	1	9	0
Set Retardant	DELVO® Stabilizer	6.14	6.69	6	6

d. Testing and Quality Control. The proportioned SCC mixes shall be tested according to subsection 604.03.B and to satisfy the SCC performance criterion of having a highly flowable and stable mix with consideration to temperature and humidity typical of production conditions.

Testing and quality control shall be done by following the procedures and apparatus in accordance with the Interim Guidelines for the use of Self-Consolidating Concrete in Precast/Prestressed Concrete Institute Member Plants by the Precast/Prestressed Concrete Institute [1]. At a minimum, the tests identified in Table 3 shall be conducted. The performance of each SCC mix shall be documented as specified in Interim Guidelines for the use of Self-Consolidating Concrete in Precast/Prestressed Concrete Institute Member Plants by the Precast/Prestressed Concrete Institute [1]. Acceptability of the mixes for each of the minimum identified methods is noted in Table 3. Acceptability criteria for other methods are to be determined by the Engineer in consultation with MSU.

Table A-3. Minimum tests to be used for evaluating SCC performance (see Ref [1])

Test Method	Description	Measurement Objective	Acceptability Criteria
Inverted Slump Flow	The lateral flow (diameter) of the concrete patty is measured when executing a traditional slump test with the slump cone in the inverted position without rodding (ASTM C192).	Evaluate self-compactibility as it relates to yield stress.	Slump flow equal to 27 in. ± 1.0 in.
Visual Stability	Visual evaluation of the SCC patty prior to placement and after the performance of the slump flow test.	Used to evaluate the relative stability of batches of the same or similar SCC mixes. It requires considerable judgment.	VSI rating equal to or less than 1
J-Ring	Used to force the SCC flow through reinforcement in conjunction with the inverted slump flow test. The 12" ring of vertical bars shall be provided with 5/8"-diam. bars spaced at even intervals along the ring diameter equal to 3 times the maximum aggregate size. Other dimensions are in given in Reference [1].	The difference between the spread with and without the ring or the height difference inside and outside the ring is measured.	J-Ring value between 0.5 in. and 0.6 in.
L- Box	Used to simulate the casting process by forcing a SCC sample to flow through a removable gate with vertical fitted reinforcement bars under static pressure. The sections of reinforcement bar shall consist of 3 #5 bars spaced at 3 times the maximum aggregate size. Other apparatus dimensions are given in Reference [1].	Provides an indication on the static and dynamic segregation resistance as well as the ability to flow through reinforcement.	L-Box ratio parameter greater than 80 (80%)

* The reader shall refer to Reference [1] for further details on the test method description, equipment dimensions, procedure, and interpretation of results.

e. Mix Design Refinement. Once an SCC mix with the required plastic properties has been developed, the mix and production process shall be refined to provide an optimum production mix that meets all of the following requirements:

- Required compressive strength and air content

- Required fresh properties (see acceptability criteria in Table 3)

- Repeatability of acceptable quality.

f. Strand Bond Confirmation Tests. Strand bond tests shall be run for all mixes to verify that the bond with SCC is equivalent or better than the conventional mix design with equal strand. Bond characteristics of strand shall be determined for all mixes in Table 1 by the Moustafa test [2] and using the "standard conventional concrete mix" that the plant uses for strand bond acceptance testing as the comparison basis. The peak pullout force (average) for the SCC mix design shall not be less than 67% of the peak pullout force (average) using the conventional concrete mix design.

g. Use of Mock-Ups in Production Qualification of Mixes. As part of the mix design qualification/development process, each SCC mix must be subject to actual production-based confirmation by the production of mock-up elements. Quality confirmation of elements fabricated with SCC shall include:

- Visual inspection. Precast concrete elements shall have a post pour inspection as per PCI MNL-116 and the fabricators' quality systems manual. Special attention should be paid to any signs of deficiency that would impair the

271

concrete performance such as segregation, sedimentation, cold joints, or other visual defects.

- Inspection and testing by saw cutting and coring. If a visual inspection of the product after form removal indicates that problem areas could exist, or if observations during the placing process identify potential areas and the element is not to be rejected, then additional verification of the concrete quality shall be undertaken. Saw cut or cored samples can be visually inspected or submitted for strength testing and/or petrographic analysis.

- Strand bond confirmation. Bond confirmation tests shall be performed by measuring strand pull-in or draw-in after strand release. The average strand draw-in shall not exceed 0.15 inches.

Test pieces can also help the qualification of placement methods. The following issues must be evaluated prior to fabrication.

- Transportation/handling techniques

- Placement methods/conditions

- Placement distance

- Free-fall distance

- Lateral flow distance from charging point

- Lift height/head pressures.

h. Equipment. The fabricator shall supply the apparatus needed to perform the SCC plastic property evaluation as specified in section (d). The test apparatus shall follow the

requirements outlined in the Interim Guidelines for the use of Self-Consolidating Concrete in Precast/Prestressed Concrete Institute Member Plants by the Precast/Prestressed Concrete Institute [1].

i. Beam Instrumentation and Data Collection. The fabricator shall coordinate the manufacturing of the SCC and NCC beams with Dr. Rigoberto Burgueño at MSU and allow for the following:

- Instrumentation of passive and prestressing reinforcement.

- Place embedded instrumentation on the beam reinforcement before stressing.

- Installation of additional instruments once the beam reinforcement and strands are placed, but before stressing.

- Data collection during stressing, after casting but before prestress release, and after prestress release.

- Sampling and testing of the SCC mix designs for information purposes.

The fabricator shall allow the MSU research team to place instrumented reinforcement and appropriately route and secure instrumentation cabling.

The fabricator shall allow for the instrumentation and monitoring of prestressing strands with strain gages and load cells during the stressing process.

j. Concrete Placement. The SCC beams shall be cast according to the following requirements:

- Batching shall be done so that the SCC mix does not loose its plastic properties.

- Plastic properties shall be evaluated for every batch.

- SCC beams shall be placed in a continuous operation from one end of the beam to the other with all internal components in place.

- The SCC mix shall not be dropped from a height of more than six feet.

- The SCC beams shall not be vibrated.

k. Laboratory Testing of Beams. The fabricator shall deliver two beams of each SCC mix design (six total), along with two beams of the normal mix design to:

Dr. Rigoberto Burgueño
c/o Mr. Siavosh (Sia) Ravanbakhsh
MSU Civil Infrastructure Laboratory
2851 Jolly Road
Okemos, Michigan 48864
Phone (Campus): 517-353-1743
Fax (Campus): 517-432-1827
Phone (Lab): 517-432-4913
Fax (Lab): 517-432-4915

Two weeks notice prior to delivery is required.

The fabricator and contractor shall allow four weeks for laboratory testing the beams to determine SCC beam performance and acceptability. If the SCC beams are acceptable, the fabricator shall ship the three remaining SCC beams to the site for erection at the locations shown on the plans and ship the remaining three normal mix design beams to the MSU Civil Laboratory. If the SCC beams are not acceptable, the fabricator shall ship

the three normal mix design beams to the site for erection at the locations shown on the plans and ship the remaining three SCC beams to the MSU Civil Laboratory.

l. Performance Monitoring. The Contractor shall coordinate their construction activities with MSU researchers and allow for the following:

- Installation of instrumentation on the demonstration bridge. This includes the installation of measuring devices at the bridge system level, routing of cables for the embedded instruments, installation of the data logger, and connection of cables to the data logger.

- Static loading through a controlled service-load prior to opening the bridge to traffic. The contractor shall provide a minimum of a 40,000 pound truck with known axle weights and axle spacing for loading.

m. Measurement and Payment.

Contract Item (Pay Item)

Pay Unit

Prestressed Concrete Box Beam, SCC, Furnished, 27 Inch..................Foot

Payment includes furnishing all the necessary materials, labor and equipment necessary for the production of the SCC beams. All testing, trial batches, coordination with researchers, and delivery is considered incidental to the pay item. Shipping the SCC beams and the normal mix beams to the MSU laboratory is considered included in the pay item for furnishing the prestressed concrete member.

Beams used for testing will also be paid for in addition to those being erected.

275

Erection of the Prestressed Concrete Box Beam, SCC, Furnished, 27 Inch will be paid

according to section 708 of the Standard Specifications for Construction.

References.

[1] Precast/Prestressed Concrete Institute (PCI), "Interim Guidelines for the use of Self-Consolidating Concrete in Precast/Prestressed Concrete Institute Member Plants," TR-6-03, Chicago, IL, 2003.

[2] Logan, D. "Acceptance Criteria for Bond Quality of Strand for Pretensioned Prestressed Concrete Applications," *PCI Journal*, March-April 1997, pp. 52-90.

APPENDIX B   NCC Production Cast 1 (6-21-05)

The information presented in the following tables is the complete list of NCC batches produced for the first cast on the 21st of June in 2005.

Table 77. NCC Mix Design Batch 1

	Target Value	Actual Value
Constituents (lbs/yd^3)		
Cement	564	562.5
Fine Aggregate	1354	1353
Coarse Aggregate	1882.5	1885.5
Total water	219	218.5
W/c	0.39	0.39
Admixture (oz/yd^3)		
Air Entraining	10.5	10
VMA	28	27.5
HRWR	64	63.5

Table 78. NCC Mix Design Batch 2

	Target Value	Actual Value
Constituents (lbs/yd^3)		
Cement	564	574
Fine Aggregate	1353	1356
Coarse Aggregate	1879	1881.5
Total water	219	219.5
W/c	0.38	0.38
Admixture (oz/yd^3)		
Air Entraining	10.5	11
VMA	28	28
HRWR	64	63.5

Table 79. NCC Mix Design Batch 3

	Target Value	Actual Value
Constituents (lbs/yd³)		
Cement	564	576.5
Fine Aggregate	1353	1350.5
Coarse Aggregate	1875	1878.5
Total water	219	219
W/c	0.38	0.38
Admixture (oz/yd³)		
Air Entraining	11.5	11
VMA	28	28
HRWR	64	63.5

Table 80. NCC Mix Design Batch 4

	Target Value	Actual Value
Constituents (lbs/yd³)		
Cement	564	562.5
Fine Aggregate	1353	1339
Coarse Aggregate	1875	1880.5
Total water	219.5	219.5
W/c	0.39	0.39
Admixture (oz/yd³)		
Air Entraining	11.5	11
VMA	28	28
HRWR	64	63.5

Table 81. NCC Mix Design Batch 5

	Target Value	Actual Value
Constituents (lbs/yd³)		
Cement	564	570.5
Fine Aggregate	1353	1340.5
Coarse Aggregate	1875	1886.5
Total water	218.5	218.5
W/c	0.38	0.38
Admixture (oz/yd³)		
Air Entraining	11.5	0
VMA	14	14
HRWR	64	63.5

Table 82. NCC Mix Design Batch 6

	Target Value	Actual Value
Constituents (lbs/yd³)		
Cement	564	561.5
Fine Aggregate	1353	1344.5
Coarse Aggregate	1875	1883.5
Total water	219	219
W/c	0.39	0.39
Admixture (oz/yd³)		
Air Entraining	11.5	11
VMA	14	13.5
HRWR	64	63.5

Table 83. NCC Mix Design Batch 7

	Target Value	Actual Value
Constituents (lbs/yd³)		
Cement	564	562
Fine Aggregate	1353	1353.5
Coarse Aggregate	1875	1871.5
Total water	211	211
W/c	0.38	0.38
Admixture (oz/yd³)		
Air Entraining	11.5	11
VMA	14	14
HRWR	64	63.5

Table 84. NCC Mix Design Batch 8

	Target Value	Actual Value
Constituents (lbs/yd³)		
Cement	564	562
Fine Aggregate	1353	1339
Coarse Aggregate	1875	1892.5
Total water	219	219
W/c	0.39	0.39
Admixture (oz/yd³)		
Air Entraining	11.5	10.5
VMA	14	13.5
HRWR	64	63.5

Table 85. NCC Mix Design Batch 9

	Target Value	Actual Value
Constituents (lbs/yd^3)		
Cement	564	562
Fine Aggregate	1352.67	1348
Coarse Aggregate	1882.67	1882
Total water	220	220
W/c	0.39	0.39
Admixture (oz/yd^3)		
Air Entraining	11	10.67
VMA	14	13.33
HRWR	64	63.33

APPENDIX C   SCC 1 Production Cast 1 (6-21-05)

The information presented in the following tables is the complete list of SCC 1 batches

produced for the first cast on the 21st of June in 2005.

Table 86. SCC 1 Mix Design Batch 1

	Target Value	Actual Value
Constituents (lbs/yd^3)		
Cement	700	714
Fine Aggregate	1655.5	1650
Coarse Aggregate	1355.5	1361
Total water	256	235.5
W/c	0.37	0.33
Admixture (oz/yd^3)		
Air Entraining	16	15.5
VMA	21	20.5
HRWR	105	118.5

Table 87. SCC 1 Mix Design Batch 2

	Target Value	Actual Value
Constituents (lbs/yd^3)		
Cement	700	695
Fine Aggregate	1656	1667
Coarse Aggregate	1350	1350
Total water	264	264
W/c	0.38	0.38
Admixture (oz/yd^3)		
Air Entraining	12	11
VMA	21	20
HRWR	105	104

Table 88. SCC 1 Mix Design Batch 3

	Target Value	Actual Value
Constituents (lbs/yd^3)		
Cement	700	713
Fine Aggregate	1655.5	1649.5
Coarse Aggregate	1350	1356.5
Total water	265	265
W/c	0.38	0.37
Admixture (oz/yd^3)		
Air Entraining	12	11.5
VMA	21	21
HRWR	105	104.5

Table 89. SCC 1 Mix Design Batch 4

	Target Value	Actual Value
Constituents (lbs/yd^3)		
Cement	700	698.5
Fine Aggregate	1655.5	1646
Coarse Aggregate	1350	1362
Total water	263.5	263.5
W/c	0.38	0.38
Admixture (oz/yd^3)		
Air Entraining	12	11.5
VMA	21	20.5
HRWR	105	104.5

Table 90. SCC 1 Mix Design Batch 5

	Target Value	Actual Value
Constituents (lbs/yd^3)		
Cement	700	700.5
Fine Aggregate	1655.5	1649.5
Coarse Aggregate	1350	1360
Total water	259.5	259
W/c	0.37	0.38
Admixture (oz/yd^3)		
Air Entraining	12	11.5
VMA	21	20.5
HRWR	105	104.5

Table 91. SCC 1 Mix Design Batch 6

	Target Value	Actual Value
Constituents (lbs/yd³)		
Cement	700	710
Fine Aggregate	1655.5	1645.5
Coarse Aggregate	1350	1360
Total water	263.5	263
W/c	0.38	0.37
Admixture (oz/yd³)		
Air Entraining	12	11.5
VMA	21	20.5
HRWR	105	104.5

Table 92. SCC 1 Mix Design Batch 7

	Target Value	Actual Value
Constituents (lbs/yd³)		
Cement	700	701
Fine Aggregate	1655.5	1646
Coarse Aggregate	1350	1359.5
Total water	264	264
W/c	0.38	0.38
Admixture (oz/yd³)		
Air Entraining	12	11.5
VMA	21	21
HRWR	105	104.5

Table 93. SCC 1 Mix Design Batch 8

	Target Value	Actual Value
Constituents (lbs/yd³)		
Cement	700	712.5
Fine Aggregate	1655.5	1645.5
Coarse Aggregate	1350	1361
Total water	264	264
W/c	0.38	0.37
Admixture (oz/yd³)		
Air Entraining	12	11.5
VMA	21	20.5
HRWR	105	104.5

Table 94. SCC 1 Mix Design Batch 9

	Target Value	Actual Value
Constituents (lbs/yd³)		
Cement	700	700.5
Fine Aggregate	1655.5	1651
Coarse Aggregate	1350	1359
Total water	265.5	265.5
W/c	0.38	0.38
Admixture (oz/yd³)		
Air Entraining	12	11.5
VMA	21	20.5
HRWR	105	104.5

Table 95. SCC 1 Mix Design Batch 10

	Target Value	Actual Value
Constituents (lbs/yd³)		
Cement	700	712.5
Fine Aggregate	1655.5	1648
Coarse Aggregate	1350	1357
Total water	264	263.5
W/c	0.38	0.38
Admixture (oz/yd³)		
Air Entraining	12	11.5
VMA	21	20.5
HRWR	105	104.5

Table 96. SCC 1 Mix Design Batch 11

	Target Value	Actual Value
Constituents (lbs/yd³)		
Cement	700	701
Fine Aggregate	1655.5	1659.5
Coarse Aggregate	1350	1345.5
Total water	267.5	260
W/c	0.38	0.37
Admixture (oz/yd³)		
Air Entraining	12	11.5
VMA	21	20.5
HRWR	105	104.5

Table 97. SCC 1 Mix Design Batch 12

	Target Value	Actual Value
Constituents (lbs/yd³)		
Cement	700	715
Fine Aggregate	1655.5	1653.5
Coarse Aggregate	1350	1354
Total water	264	264
W/c	0.38	0.37
Admixture (oz/yd³)		
Air Entraining	12	11.5
VMA	21	20.5
HRWR	105	104.5

Table 98. SCC 1 Mix Design Batch 13

	Target Value	Actual Value
Constituents (lbs/yd³)		
Cement	700	700
Fine Aggregate	1655.5	1655.5
Coarse Aggregate	1350	1355
Total water	264	264
W/c	0.38	0.38
Admixture (oz/yd³)		
Air Entraining	12	11.5
VMA	21	20.5
HRWR	105	104.5

Table 99. SCC 1 Mix Design Batch 14

	Target Value	Actual Value
Constituents (lbs/yd³)		
Cement	700	698
Fine Aggregate	1655.5	1651
Coarse Aggregate	1350	1357
Total water	265.5	265.5
W/c	0.38	0.38
Admixture (oz/yd³)		
Air Entraining	12	11.5
VMA	21	20.5
HRWR	105	104.5

285

APPENDIX D   NCC Production Cast 2 (6-24-05)

The information presented in the following tables is the complete list of NCC batches

produced for the second cast on the 24th of June in 2005.

Table 100. NCC Mix Design Batch 1

	Target Value	Actual Value
Constituents (lbs/yd^3)		
Cement	564	570
Fine Aggregate	1351.5	1353
Coarse Aggregate	1886.5	1884.5
Total water	227	227
W/c	0.40	0.40
Admixture (oz/yd^3)		
Air Entraining	11	10.5
VMA	14	13.5
HRWR	64	64

Table 101. NCC Mix Design Batch 2

	Target Value	Actual Value
Constituents (lbs/yd^3)		
Cement	564	572.5
Fine Aggregate	1351.5	1352
Coarse Aggregate	1875	1884
Total water	219.5	219
W/c	0.39	0.38
Admixture (oz/yd^3)		
Air Entraining	11	10.5
VMA	14	13.5
HRWR	64	63.5

Table 102.NCC Mix Design Batch 3

	Target Value	Actual Value
Constituents (lbs/yd^3)		
Cement	564	574
Fine Aggregate	1351.5	1342
Coarse Aggregate	1875	1883
Total water	219	218.5
W/c	0.39	0.38
Admixture (oz/yd^3)		
Air Entraining	11	10.5
VMA	14	13.5
HRWR	64	63.5

Table 103.NCC Mix Design Batch 4

	Target Value	Actual Value
Constituents (lbs/yd^3)		
Cement	564	561.5
Fine Aggregate	1351.5	1348
Coarse Aggregate	1886.5	1894
Total water	220	220
W/c	0.39	0.39
Admixture (oz/yd^3)		
Air Entraining	11	10.5
VMA	14	13.5
HRWR	64	63.5

Table 104.NCC Mix Design Batch 5

	Target Value	Actual Value
Constituents (lbs/yd^3)		
Cement	564	572
Fine Aggregate	1351.5	1343.5
Coarse Aggregate	1882.5	1891.5
Total water	219.5	219.5
W/c	0.39	0.38
Admixture (oz/yd^3)		
Air Entraining	11	10.5
VMA	14	13.5
HRWR	64	63.5

Table 105.NCC Mix Design Batch 6

	Target Value	Actual Value
Constituents (lbs/yd^3)		
Cement	564	573
Fine Aggregate	1351.5	1348
Coarse Aggregate	1882.5	1865.5
Total water	219.5	219
W/c	0.39	0.38
Admixture (oz/yd^3)		
Air Entraining	11	10.5
VMA	14	13.5
HRWR	64	63.5

Table 106.NCC Mix Design Batch 7

	Target Value	Actual Value
Constituents (lbs/yd^3)		
Cement	564	568.5
Fine Aggregate	1351.5	1350
Coarse Aggregate	1886.5	1891.5
Total water	220	220
W/c	0.39	0.39
Admixture (oz/yd^3)		
Air Entraining	10.5	10
VMA	14	13.5
HRWR	64	63.5

Table 107.NCC Mix Design Batch 8

	Target Value	Actual Value
Constituents (lbs/yd^3)		
Cement	564	566
Fine Aggregate	1351.5	1351
Coarse Aggregate	1886.5	1884.5
Total water	220	220
W/c	0.39	0.39
Admixture (oz/yd^3)		
Air Entraining	10.5	10
VMA	14	13.5
HRWR	64	63.5

Table 108.NCC Mix Design Batch 9

	Target Value	Actual Value
Constituents (lbs/yd³)		
Cement	564	566
Fine Aggregate	1351.67	1523.33
Coarse Aggregate	1886.67	1920
Total water	225	225
W/c	0.40	0.40
Admixture (oz/yd³)		
Air Entraining	10.5	10
VMA	14	13.3333
HRWR	64	63.3333

APPENDIX E   SCC 2 Production Cast 2 (6-24-05)

The information presented in the following tables is the complete list of SCC 2 batches produced for the second cast on the 24th of June in 2005.

Table 109.SCC 2 Mix Design Batch 1

	Target Value	Actual Value
Constituents (lbs/yd^3)		
Cement	700	702
Fine Aggregate	1487.5	1485.5
Coarse Aggregate	1435.5	1440.5
Total water	277.5	277.5
W/c	0.40	0.40
Admixture (oz/yd^3)		
Air Entraining	12	11.5
VMA	21	20.5
HRWR	84	83.5

Table 110.SCC 2 Mix Design Batch 2

	Target Value	Actual Value
Constituents (lbs/yd^3)		
Cement	700	724.5
Fine Aggregate	1487.5	1490.5
Coarse Aggregate	1435.5	1433.5
Total water	278.5	278.5
W/c	0.40	0.38
Admixture (oz/yd^3)		
Air Entraining	12	11
VMA	21	20.5
HRWR	84	83.5

Table 111.SCC 2 Mix Design Batch 3

	Target Value	Actual Value
Constituents (lbs/yd^3)		
Cement	700	699.5
Fine Aggregate	1487.5	1482.5
Coarse Aggregate	1435.5	1442.5
Total water	279.5	279.5
W/c	0.40	0.40
Admixture (oz/yd^3)		
Air Entraining	12	11
VMA	21	21
HRWR	84	83.5

Table 112.SCC 2 Mix Design Batch 4

	Target Value	Actual Value
Constituents (lbs/yd^3)		
Cement	700	716
Fine Aggregate	1487.5	1487.5
Coarse Aggregate	1435.5	1435.5
Total water	275	275
W/c	0.39	0.38
Admixture (oz/yd^3)		
Air Entraining	12	11
VMA	21	20.5
HRWR	84	83.5

Table 113.SCC 2 Mix Design Batch 5

	Target Value	Actual Value
Constituents (lbs/yd^3)		
Cement	700	699.5
Fine Aggregate	1487.5	1490.5
Coarse Aggregate	1435.5	1432
Total water	275	275
W/c	0.39	0.39
Admixture (oz/yd^3)		
Air Entraining	11.5	11
VMA	21	20.5
HRWR	84	83.5

Table 114.SCC 2 Mix Design Batch 6

	Target Value	Actual Value
Constituents (lbs/yd³)		
Cement	700	709
Fine Aggregate	1487.5	1483
Coarse Aggregate	1435.5	1441
Total water	274.5	274.5
W/c	0.39	0.39
Admixture (oz/yd³)		
Air Entraining	11.5	11
VMA	21	21
HRWR	84	83.5

Table 115.SCC 2 Mix Design Batch 7

	Target Value	Actual Value
Constituents (lbs/yd³)		
Cement	700	712
Fine Aggregate	1487.5	1487
Coarse Aggregate	1435.5	1438
Total water	275	275
W/c	0.39	0.39
Admixture (oz/yd³)		
Air Entraining	11.5	11
VMA	21	21
HRWR	84	83.5

Table 116.SCC 2 Mix Design Batch 8

	Target Value	Actual Value
Constituents (lbs/yd³)		
Cement	700	698
Fine Aggregate	1487.5	1477.5
Coarse Aggregate	1435.5	1443.5
Total water	274.5	274.5
W/c	0.39	0.39
Admixture (oz/yd³)		
Air Entraining	11.5	11
VMA	21	20.5
HRWR	84	83.5

Table 117.SCC 2 Mix Design Batch 9

	Target Value	Actual Value
Constituents (lbs/yd³)		
Cement	700	713.5
Fine Aggregate	1487.5	1475.5
Coarse Aggregate	1438	1446
Total water	274.5	274.5
W/c	0.39	0.38
Admixture (oz/yd³)		
Air Entraining	11.5	11
VMA	21	20.5
HRWR	84	83.5

Table 118.SCC 2 Mix Design Batch 10

	Target Value	Actual Value
Constituents (lbs/yd³)		
Cement	700	711
Fine Aggregate	1487.5	1483.5
Coarse Aggregate	1438	1446
Total water	274.5	274.5
W/c	0.39	0.39
Admixture (oz/yd³)		
Air Entraining	11.5	11
VMA	21	21
HRWR	84	83.5

Table 119.SCC 2 Mix Design Batch 11

	Target Value	Actual Value
Constituents (lbs/yd³)		
Cement	700	714
Fine Aggregate	1487.5	1475
Coarse Aggregate	1445.5	1454
Total water	274.5	274.5
W/c	0.39	0.38
Admixture (oz/yd³)		
Air Entraining	11.5	11
VMA	21	20.5
HRWR	84	83.5

Table 120.SCC 2 Mix Design Batch 12

	Target Value	Actual Value
Constituents (lbs/yd^3)		
Cement	700	714
Fine Aggregate	1487.5	1476.5
Coarse Aggregate	1445.5	1456
Total water	274.5	274.5
W/c	0.39	0.38
Admixture (oz/yd^3)		
Air Entraining	11.5	11
VMA	21	20.5
HRWR	84	83.5

APPENDIX F   NCC Production Cast 3 (6-29-05)

The information presented in the following tables is the complete list of NCC batches

produced for the third cast on the 29th of June in 2005.

Table 121.NCC Mix Design Batch 1

	Target Value	Actual Value
Constituents (lbs/yd³)		
Cement	564	569
Fine Aggregate	1354	1346.5
Coarse Aggregate	1884.5	1887
Total water	219.5	226.5
W/c	0.39	0.40
Admixture (oz/yd³)		
Air Entraining	9	8.5
VMA	11	11
HRWR	64	63.5

Table 122.NCC Mix Design Batch 2

	Target Value	Actual Value
Constituents (lbs/yd³)		
Cement	564	565.5
Fine Aggregate	1354	1344.5
Coarse Aggregate	1884.5	1891.5
Total water	219.5	219
W/c	0.39	0.39
Admixture (oz/yd³)		
Air Entraining	8.5	8
VMA	11	10.5
HRWR	64	63.5

Table 123.NCC Mix Design Batch 3

	Target Value	Actual Value
Constituents (lbs/yd^3)		
Cement	564	561.5
Fine Aggregate	1354	1342.5
Coarse Aggregate	1884.5	1892
Total water	220	220
W/c	0.39	0.39
Admixture (oz/yd^3)		
Air Entraining	8.5	8
VMA	0	0
HRWR	64	63.5

Table 124.NCC Mix Design Batch 4

	Target Value	Actual Value
Constituents (lbs/yd^3)		
Cement	564	564.5
Fine Aggregate	1354	1344
Coarse Aggregate	1884.5	1895.5
Total water	220	219.5
W/c	0.39	0.39
Admixture (oz/yd^3)		
Air Entraining	8.5	8
VMA	0	0
HRWR	64	63.5

Table 125.NCC Mix Design Batch 5

	Target Value	Actual Value
Constituents (lbs/yd^3)		
Cement	564	573.5
Fine Aggregate	1354	1344.5
Coarse Aggregate	1884.5	1890
Total water	219.5	219.5
W/c	0.39	0.38
Admixture (oz/yd^3)		
Air Entraining	8.5	8
VMA	11	10.5
HRWR	64	63.5

Table 126.NCC Mix Design Batch 6

	Target Value	Actual Value
Constituents (lbs/yd³)		
Cement	564	570.5
Fine Aggregate	1354	1347.5
Coarse Aggregate	1884.5	1888
Total water	219.5	219.5
W/c	0.39	0.38
Admixture (oz/yd³)		
Air Entraining	8.5	8
VMA	11	10.5
HRWR	64	63.5

Table 127.NCC Mix Design Batch 7

	Target Value	Actual Value
Constituents (lbs/yd³)		
Cement	564	574.5
Fine Aggregate	1354	1359.5
Coarse Aggregate	1884.5	1882
Total water	220.5	220.5
W/c	0.39	0.38
Admixture (oz/yd³)		
Air Entraining	8.5	8
VMA	0	0
HRWR	64	63.5

Table 128.NCC Mix Design Batch 8

	Target Value	Actual Value
Constituents (lbs/yd³)		
Cement	564	563.5
Fine Aggregate	1354	1357
Coarse Aggregate	1884.5	1881
Total water	220.5	220.5
W/c	0.39	0.39
Admixture (oz/yd³)		
Air Entraining	8.5	8
VMA	0	0
HRWR	64	63.5

Table 129.NCC Mix Design Batch 9

	Target Value	Actual Value
Constituents (lbs/yd^3)		
Cement	564	562
Fine Aggregate	1354	1353.5
Coarse Aggregate	1884.5	1889
Total water	220	220
W/c	0.39	0.39
Admixture (oz/yd^3)		
Air Entraining	8.5	8
VMA	0	0
HRWR	64	63.5

APPENDIX G   SCC 3 Production Cast 3 (6-29-05)

The information presented in the following tables is the complete list of SCC 3 batches

produced for the third cast on the 29th of June in 2005.

Table 130.SCC 3 Mix Design Batch 1

	Target Value	Actual Value
Constituents (lbs/yd^3)		
Cement	700	705.5
Fine Aggregate	1373.5	1361
Coarse Aggregate	1457.5	1466
Total water	309.5	311.5
W/c	0.44	0.44
Admixture (oz/yd^3)		
Air Entraining	10	9.5
VMA	21	20.5
HRWR	49	48.5

Table 131.SCC 3 Mix Design Batch 2

	Target Value	Actual Value
Constituents (lbs/yd^3)		
Cement	700	709.5
Fine Aggregate	1373.5	1375.5
Coarse Aggregate	1457.5	1454
Total water	310	312.5
W/c	0.44	0.44
Admixture (oz/yd^3)		
Air Entraining	8.5	8
VMA	21	21
HRWR	56	55.5

Table 132. SCC 3 Mix Design Batch 3

	Target Value	Actual Value
Constituents (lbs/yd³)		
Cement	700	711.5
Fine Aggregate	1373.5	1367
Coarse Aggregate	1457.5	1466
Total water	309.5	312
W/c	0.44	0.44
Admixture (oz/yd³)		
Air Entraining	8	7.5
VMA	21	21
HRWR	56	55.5

Table 133. SCC 3 Mix Design Batch 4

	Target Value	Actual Value
Constituents (lbs/yd³)		
Cement	700	709
Fine Aggregate	1373.5	1361.5
Coarse Aggregate	1457.5	1465
Total water	309.5	312.5
W/c	0.44	0.44
Admixture (oz/yd³)		
Air Entraining	8	7.5
VMA	21	20.5
HRWR	56	55.5

Table 134. SCC 3 Mix Design Batch 5

	Target Value	Actual Value
Constituents (lbs/yd³)		
Cement	700	708
Fine Aggregate	1373.5	1365
Coarse Aggregate	1457.5	1463
Total water	309.5	312.5
W/c	0.44	0.44
Admixture (oz/yd³)		
Air Entraining	8	7.5
VMA	21	20.5
HRWR	56	55.5

Table 135. SCC 3 Mix Design Batch 6

	Target Value	Actual Value
Constituents (lbs/yd^3)		
Cement	700	712.5
Fine Aggregate	1373.5	1371
Coarse Aggregate	1457.5	1462.5
Total water	311	313.5
W/c	0.44	0.44
Admixture (oz/yd^3)		
Air Entraining	8	7.5
VMA	21	21
HRWR	56	55.5

Table 136. SCC 3 Mix Design Batch 7

	Target Value	Actual Value
Constituents (lbs/yd^3)		
Cement	700	712
Fine Aggregate	1373.5	1367.5
Coarse Aggregate	1457.5	1461.5
Total water	310.5	313
W/c	0.44	0.44
Admixture (oz/yd^3)		
Air Entraining	8	7.5
VMA	21	20.5
HRWR	56	55.5

Table 137. SCC 3 Mix Design Batch 8

	Target Value	Actual Value
Constituents (lbs/yd^3)		
Cement	700	713
Fine Aggregate	1373.5	1380.5
Coarse Aggregate	1457.5	1455
Total water	310.5	313
W/c	0.44	0.44
Admixture (oz/yd^3)		
Air Entraining	8	7.5
VMA	21	20.5
HRWR	56	55.5

Table 138. SCC 3 Mix Design Batch 9

	Target Value	Actual Value
Constituents (lbs/yd³)		
Cement	700	709.5
Fine Aggregate	1373.5	1368.5
Coarse Aggregate	1457.5	1464.5
Total water	310.5	313
W/c	0.44	0.44
Admixture (oz/yd³)		
Air Entraining	8	7.5
VMA	21	20.5
HRWR	56	55.5

Table 139. SCC 3 Mix Design Batch 10

	Target Value	Actual Value
Constituents (lbs/yd³)		
Cement	700	709.5
Fine Aggregate	1373.5	1369.5
Coarse Aggregate	1457.5	1460
Total water	310.5	313.5
W/c	0.44	0.44
Admixture (oz/yd³)		
Air Entraining	8	7.5
VMA	21	20.5
HRWR	56	55.5

Table 140. SCC 3 Mix Design Batch 11

	Target Value	Actual Value
Constituents (lbs/yd³)		
Cement	700	697.5
Fine Aggregate	1373.5	1379
Coarse Aggregate	1457.5	1454.5
Total water	310.5	314.5
W/c	0.44	0.45
Admixture (oz/yd³)		
Air Entraining	8	7.5
VMA	21	20.5
HRWR	56	55.5

Table 141. SCC 3 Mix Design Batch 12

	Target Value	Actual Value
Constituents (lbs/yd^3)		
Cement	700	699
Fine Aggregate	1373.5	1376.5
Coarse Aggregate	1457.5	1454.5
Total water	311	315
W/c	0.44	0.45
Admixture (oz/yd^3)		
Air Entraining	8	7.5
VMA	21	21
HRWR	56	55.5

Table 142. SCC 3 Mix Design Batch 13

	Target Value	Actual Value
Constituents (lbs/yd^3)		
Cement	700	711
Fine Aggregate	1373.5	1363.5
Coarse Aggregate	1457.5	1464.5
Total water	311	314
W/c	0.44	0.44
Admixture (oz/yd^3)		
Air Entraining	8	7.5
VMA	21	20.5
HRWR	56	55.5

Table 143. SCC 3 Mix Design Batch 14

	Target Value	Actual Value
Constituents (lbs/yd^3)		
Cement	700	712
Fine Aggregate	1373.5	1363.5
Coarse Aggregate	1457.5	1466.5
Total water	311	313
W/c	0.44	0.44
Admixture (oz/yd^3)		
Air Entraining	8	7.5
VMA	21	20.5
HRWR	56	55.5

APPENDIX H   NCC Production Cast 4 (7-1-05)

The information presented in the following tables is the complete list of NCC batches produced for the fourth cast on the 1st of July in 2005.

Table 144. NCC Mix Design Batch 1

	Target Value	Actual Value
Constituents (lbs/yd^3)		
Cement	564	561.5
Fine Aggregate	1354	1347
Coarse Aggregate	1875	1876
Total water	219.5	219.5
W/c	0.39	0.39
Admixture (oz/yd^3)		
Air Entraining	7.5	7
VMA	11	11
HRWR	64	63.5

Table 145. NCC Mix Design Batch 2

	Target Value	Actual Value
Constituents (lbs/yd^3)		
Cement	564	562
Fine Aggregate	1354	1333
Coarse Aggregate	1884	1807
Total water	219	219
W/c	0.39	0.39
Admixture (oz/yd^3)		
Air Entraining	7.5	7
VMA	11	11
HRWR	64	63

Table 146. NCC Mix Design Batch 3

	Target Value	Actual Value
Constituents (lbs/yd^3)		
Cement	564	561.5
Fine Aggregate	1354	1352
Coarse Aggregate	1884.5	1889.5
Total water	219	218.5
W/c	0.39	0.39
Admixture (oz/yd^3)		
Air Entraining	7.5	7
VMA	0	0
HRWR	64	63.5

Table 147. NCC Mix Design Batch 4

	Target Value	Actual Value
Constituents (lbs/yd^3)		
Cement	564	562
Fine Aggregate	1354	1360
Coarse Aggregate	1884.5	1879.5
Total water	219.5	220
W/c	0.39	0.39
Admixture (oz/yd^3)		
Air Entraining	7.5	7
VMA	0	0
HRWR	64	63.5

Table 148. NCC Mix Design Batch 5

	Target Value	Actual Value
Constituents (lbs/yd^3)		
Cement	564	562
Fine Aggregate	1353	1339
Coarse Aggregate	1892	1909
Total water	220	220
W/c	0.39	0.39
Admixture (oz/yd^3)		
Air Entraining	7.5	7
VMA	11	11
HRWR	64	63

Table 149. NCC Mix Design Batch 6

	Target Value	Actual Value
Constituents (lbs/yd^3)		
Cement	564	579
Fine Aggregate	1354	1337.5
Coarse Aggregate	1894	1900
Total water	219	219
W/c	0.39	0.38
Admixture (oz/yd^3)		
Air Entraining	7.5	7
VMA	11	10.5
HRWR	64	63.5

Table 150. NCC Mix Design Batch 7

	Target Value	Actual Value
Constituents (lbs/yd^3)		
Cement	564	571
Fine Aggregate	1353	1359
Coarse Aggregate	1894	1896
Total water	220	221
W/c	0.39	0.39
Admixture (oz/yd^3)		
Air Entraining	7	6
VMA	11	11
HRWR	64	63

Table 151. NCC Mix Design Batch 8

	Target Value	Actual Value
Constituents (lbs/yd^3)		
Cement	564	579
Fine Aggregate	1354	1364
Coarse Aggregate	1894	1889.5
Total water	220	220
W/c	0.39	0.38
Admixture (oz/yd^3)		
Air Entraining	7	6.5
VMA	0	0
HRWR	64	63.5

Table 152. NCC Mix Design Batch 9

	Target Value	Actual Value
Constituents (lbs/yd³)		
Cement	564	577
Fine Aggregate	1353	1348
Coarse Aggregate	1894	1900.5
Total water	219.5	219
W/c	0.39	0.38
Admixture (oz/yd³)		
Air Entraining	7	6.5
VMA	0	0
HRWR	64	63.5

Table 153. NCC Mix Design Batch 10

	Target Value	Actual Value
Constituents (lbs/yd³)		
Cement	564	560
Fine Aggregate	1353	1338
Coarse Aggregate	1894	1914
Total water	219	219
W/c	0.39	0.39
Admixture (oz/yd³)		
Air Entraining	7	6
VMA	0	0
HRWR	64	63

Table 154. NCC Mix Design Batch 11

	Target Value	Actual Value
Constituents (lbs/yd³)		
Cement	563	617
Fine Aggregate	1353	1478
Coarse Aggregate	1893	1898
Total water	225	225
W/c	0.40	0.36
Admixture (oz/yd³)		
Air Entraining	7	7
VMA	0	0
HRWR	64	63

REFERENCES

[1] ACI Committee 318, "Building Code Requirements for Structural Concrete (ACI 318-05) and Commentary (ACI 318R-05)," American Concrete Institute, Farmington Hills, MI, 1995.

[2] American Association of Highway Transportation Officials (AASHTO), <u>AASHTO Bridge Design Specifications – 17th Edition</u>, Washington DC, 2002.

[3] American Association of Highway Transportation Officials (AASHTO), <u>AASHTO-LRFD Bridge Design Specifications – 2nd Edition</u>, Washington DC, 1998.

[4] American Association of Highway Transportation Officials (AASHTO), <u>AASHTO-LRFD Bridge Design Specifications – 3rd Edition</u>, Washington DC, 2007.

[5] Bendert, D. A. "Experimental Evaluation and Field Monitoring of Self-Consolidating Concrete Prestressed Box Beams Implemented in a Demonstration Bridge." Masters Thesis, Department of Civil and Environmental Engineering, Michigan State University, East Lansing, MI, December 2006.

[6] Bendert, D. A., and Burgueño, R., "Report on the Experimental Evaluation of Prestressed Box beams for SCC Demonstration Bridge." Research Report CEE-RR-2006-01, Department of Civil and Environmental Engineering, Michigan State University, East Lansing, MI, December 2006.

[7] Bendert, D. A., and Burgueño, R., "Report on the Production of Prestressed Box beams for SCC Demonstration Bridge." Research Report CEE-RR-2006-02, Department of Civil and Environmental Engineering, Michigan State University, East Lansing, MI, December 2006.

[8] Bentz, E.C., and Collins, M.P., Response-2000 – Reinforced Concrete Section Analysis Program using the Modified Compression Field Theory, v. 1.0.5, University of Toronto, 2000.

[9] Bonen, D, Shah, S., "Fresh and Hardened Properties of Self-Consolidating Concrete," *Progress in Structural Engineering and Materials*, V. 7 No. 1, January-March, 2005, pp. 14-26.

[10] Burgueño, R. and Haq, M., "Transfer and Development Length of Prestressing Strands in Precast/Prestressed Girders Using Self-Consolidating Concrete." Proceedings Second North American Conference on the Design and Use of Self-Consolidating Concrete and the Fourth International RILEM Symposium on Self-Compacting Concrete, (CD-ROM), Chicago, Illinois, October, 2005.

[11] Burgueño, R., and Till, R., "Special Provision for Production of Prestressed Beams with Self-Consolidating Concrete," *Internal Report, Michigan Department of Transportation*, Lansing, MI, January 2005.

[12] Choulli, Y. Mari, A.R., "Shear Behaviour of full scale prestressed I beams made with Self Compacting Concrete," Proceedings Second North American Conference on the Design and Use of Self-Consolidating Concrete and the Fourth International RILEM Symposium on Self-Compacting Concrete, (CD-ROM), Chicago, Illinois, October, 2005.

[13] Collins, M.P., and Mitchell, D., Prestressed Concrete Structures, Response Publications, Canada, 1997.

[14] Daczko, J., and Vachon, M., "Self Consolidating Concrete (SCC)," Significance of Tests and Properties of Concrete and Concrete-Making Materials STP 169D. ASTM International West Conshohocken, PA. May 2006 pp. 637-645.

[15] Das, D, Kaushik, S.K., Gupta V.K., "Shear Resistance of Self-Compacting concrete," Proceedings Second North American Conference on the Design and Use of Self-Consolidating Concrete and the Fourth International RILEM Symposium on Self-Compacting Concrete, (CD-ROM), Chicago, Illinois, October, 2005.

[16] Domone, P.L., "Self-Compacting Concrete: An analysis of 11 years of case studies," Cement and Concrete Composites. V. 28. 2006 pp. 197-208

[17] Fernandez, P. Luciano, J. Constantiner, D., "Successful Implementation of SCC In a Precast Operation," Proceedings Second North American Conference on the Design and Use of Self-Consolidating Concrete and the Fourth International RILEM Symposium on Self-Compacting Concrete, (CD-ROM), Chicago, Illinois, October, 2005.

[18] Goodier, C.I., "Development of Self-Compacting Concrete." Proceedings of the Institution of Civil Engineers, Structures and Buildings. V 156. November 2003 Issue SB4 pp. 405-414.

[19] Haq, M., and Burgueño, R., "Effect of Self-Compacting Concrete Mix Design on Strand Bond Performance Parameters in Prestressed Beams," Research Report CEE-RR-2006-03, Department of Civil and Environmental Engineering, Michigan State University, East Lansing, MI, December 2006.

[20] Harrison, T., Concrete. V. 40 n. 7 August 2006 pp. 15.

[21] Hegger, J. Kommer, B., "Pretensioning in Self Consolidating Concrete (SCC)," *Proceedings Second North American Conference on the Design and Use of Self-Consolidating Concrete and the Fourth International RILEM Symposium on Self-Compacting Concrete*, (CD-ROM), Chicago, Illinois, October, 2005.

[22] Hsu, T.T.C., <u>Unified Theory of Reinforced Concrete</u>, CRC Press, Boca Raton, FL, 1993.

[23] "Interim Guidelines for the Use of Self-Consolidating Concrete In PCI Member Plants" TR-6-03 Precast/Prestressed Concrete Institute, Chicago, Illinois, April, 2003, 88 pp.

[24] Juvas, K., "The European Experience of Working With Self-Compacting Concrete In the Precast Concrete Industry," *Proceedings Second North American Conference on the Design and Use of Self-Consolidating Concrete and the Fourth International RILEM Symposium on Self-Compacting Concrete*, (CD-ROM), Chicago, Illinois, October, 2005.

[25] Khayat, K., "Use of Viscosity-Modifying Admixtures to Reduce Top_bar Effect of Anchored Bars Cast with Fluid Concrete," ACI Materials Journal, March-April 1998 pp. 158-167.

[26] Khayat, K., "Workability, Testing, and Performance of Self-Consolidating Concrete," *ACI Materials Journal*, V. 96 No. 3, May-June, 1999, pp. 346-353.

[27] Lachemi, M., Hossain, K.M.A., Lombros, V., "Shear Resistance of Self-Consolidating Concrete Beams – Experimental Investigation," Canadian Journal of Civil Engineering. V. 32. no. 6 December, 2005 pp. 1103-1113.

[28] Lachemi, M., Hossain, K.M.A., Labros, V., Nkinamubanzi, P.-C., Bouzoubaa, N., "Self-Consolidating Concrete Incorporating New Viscosity Modifying Admixtures," Cement and Concrete Research. V 34 2004 pp. 917-926.

[29] Larson, K.H., Peterman, R.J., Esmaeily, A., "Determining the Time-Dependent and Bond Characteristics of an SCC Mix for Kansas Prestressed Concrete Bridge Girders." Proceedings Second North American Conference on the Design and Use of Self-Consolidating Concrete and the Fourth International RILEM Symposium on Self-Compacting Concrete, (CD-ROM), Chicago, Illinois, October 2005.

[30] Larson, K.H., Peterman, R.J., Esmaeily, A., "Determining the Time-Dependent Deformations of Pretensioned Bridge Girders Cast with Self-Consolidating Concrete," Proceedings 2006 Concrete Bridge Conference. Dallas Texas, October 2006 (CD-ROM).

[31] Logan, D., "Acceptance Criteria for Bond Quality of Strand for Pretensioned Prestressed Concrete Applications," *PCI Journal*, V. 42, No. 2, March-April, 1997, pp. 52-90.

[32] Mindess, S. Young, F. Darwin, D., *Concrete Second Edition*, Prentice Hall, Upper Saddle River, NJ, 2003, 644 pp.

[33] Morgan Girgis, A.F, Tuan,C.Y., "Bond Strength and Transfer Length of Pretensioned Bridge Girders Cast with Self-Consolidating Concrete," *PCI Journal* V. 50, No. 6, November-December 2005, pp. 72-87.

[34] Naaman, A., Prestressed Concrete Analysis and Design, McGraw-Hill, Inc. New York, NY, 1982.

[35] Naito, C. Hoover, M. "Applicability of Self Consolidating Concrete for Use in Precast Bridge Beam Construction." Proceedings Second North American Conference on the Design and Use of Self-Consolidating Concrete and the Fourth International RILEM Symposium on Self-Compacting Concrete, (CD-ROM), Chicago, Illinois, October 2005.

[36] Nasvik, J., "The ABC's of SCC," Concrete Construction. March 2003. pp. 40-47.

[37] Okamura, H. "Self-Compacting High-Performance Concrete," Concrete International. July 1997. pp. 50-54.

[38] Okamura, H Ouchi, M., "Self-Compacting Concrete. Development, Present Use and Future," *Proceedings 1st International RILEM Symposium on Self-Compacting Concrete*, Stockholm, Sweden, September 1999, pp. 3-14.

[39] Okamura, H. Ozawa, K., "Mix Design for Self-Compacting Concrete," *Concrete Library of Japanese Society of Civil Engineers*, No. 25, June 1995, pp. 107-120.

[40] Ouchi, M, Nakamura, S, Osterberg, T, Hallberg, S, Lwin, M., "Applications of Self-Compacting Concrete in Japan, Europe, and The United States," US Federal Highway Administration Office of Bridge Technology. 2003 ISHPC. Available from http://www.fhwa.dot.gov/bridge/scc.pdf.

[41] Ozyildirim, C., "VDOT Early Experience With Self-Consolidating Concrete," Transportation Research Record, Journal of the Transportation Research Board. Transportation Research Board of National Academies, Washington D.C., N 1914 2005, pp. 81-84.

[42] Ozyildirim, C., Lane, D.S., "Final Report: Evaluation of Self-Consolidating Concrete," Virginia Transportation Research Council, Charlottesville, Virginia, June 2003.

[43] Ramsburg, P. Ludirdja, D. Masek, O., "Utilizing SCC in Double Cycling Production of Double Tee Beams," Proceedings Second North American Conference on the Design and Use of Self-Consolidating Concrete and the Fourth International RILEM Symposium on Self-Compacting Concrete, (CD-ROM), Chicago, Illinois, October 2005.

[44] Seible, F., and Igarashi, A., "Full Scale Testing of Masonry Structures Under Simulated Seismic Loadings," *Experimental and Numerical Methods in Earthquake Engineering,*J. Donea and P.M. Jones (Eds.), ECSC, EEC, EAEC, Brussels and Luxemburg, Netherlands, 1991, pp. 119-148

[45] Sonebi, M. Taminmi, A.K., Bartos, P.J.M., "Performance of Cracking Behavior of Reinforced Beams Cast with Self-Consolidating Concrete," *ACI Materials Journal,* V. 100 n. 6 November-December, 2003, pp. 492-500.

[46] "Standard Testing Method for Compressive Strength of Cylindrical Concrete Specimen (C39-05)," Annual Book of ASTM Standards, V 4.02 2006.

[47] "Standard Testing Method for Splitting Tensile Strength of Cylindrical Concrete Specimen (C496-04)," Annual Book of ASTM Standards, V 4.02 2006.

[48] "Standard Testing Method for Passing Ability of Self-Consolidating Concrete by J-Ring (C 1621-06)," Annual Book of ASTM Standards, V 4.02 2006.

[49] "Standard Testing Method of Slump Flow of Self-Consolidating Concrete (C1611-05)," Annual Book of ASTM Standards, V 4.02 2006.

[50] Su, N., Hsu, K.C., Chai, H.W., "A Simple Mix Design Method for Self-Compacting Concrete," Cement and Concrete Research, V 31 2001 pp. 1799-1807.

[51] Tadros, M.K., Al-Omaishi, N., Seguirant, S.J., Gallt, J.G. "NCHRP Report 496: Prestress Losses in Pretensioned High-Strength Concrete Bridge Girders," Transportation Research Board, Washington D.C., 2003, 63 pgs.

[52] Umehara, H. Hamada, D., Yamamuro, H., Oka, S. "Development and Usage of Self-Compacting Concrete in Precast Concrete Field," *Proceedings 1st International RILEM Symposium on Self-Compacting Concrete*, Stockholm, Sweden, September 1999, pp. 705-716.

[53] Wilson, N.D. Kiousis, P., "High-Strength SCC in Shear" Proceedings Second North American Conference on the Design and Use of Self-Consolidating Concrete and the Fourth International RILEM Symposium on Self-Compacting Concrete, (CD-ROM), Chicago, Illinois, October 2005.

[54] Yelton, R., "Flowing smoothly: Superintendent uses SCC to assist Milwaukee motorists," *The Concrete Producer,* V. 23, No. 11, November, 2005, pp. 46-49.